Mitochondrial DNA Double-Strand Breaks: In Replication and In Repair

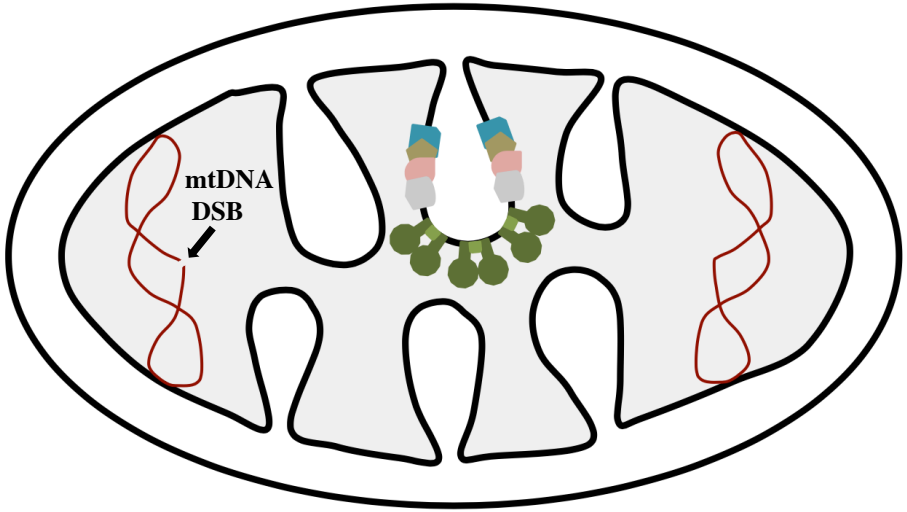

Kanchanjunga Prasai, Ph.D.
Department of Molecular and Cellular Physiology
LSU Health-Shreveport, USA
kjprasai@gmail.com

MITOCHONDRIAL DNA DOUBLE-STRAND BREAKS: IN REPLICATION AND IN REPAIR

A Dissertation

Submitted to the Graduate Faculty of the Health Sciences Center of
Louisiana State University and
Agricultural and Mechanical College
In partial fulfillment of the
Requirements for the degree of
Doctor of Philosophy

in

The Department of Molecular and Cellular Physiology

by

Kanchanjunga Prasai
M.Sc., Hemwati Nandan Bahuguna Garhwal University, 2007
May 2017

This dissertation is dedicated to my grandmother, Bhagiratha Prasai (1919-2012), whose eternal blessings have enabled me to become a person that I am today.

ACKNOWLEDGEMENTS

I would like to sincerely acknowledge the lead person behind my Ph.D., my mentor Dr. Lynn Harrison, for her continual guidance, support, and suggestions. I became interested in her work during my rotation in her lab and soon after joining her lab, my fascination for the "mighty mitochondria" emerged. Not only she believed in me and my work, but also provided a decent scientific environment that enabled me to think critically. I am grateful to her for allowing me to design and execute experiments independently, and also for her supervision, which helped me to stay on the right track. Overall, I thank Dr. Harrison for everything that she has done for me during my life as a graduate student, but most importantly for arousing my interest in mitochondria and for guiding me to a Ph.D. degree.

My heartfelt gratitude also extends to Dr. Kelly Tatchell and Dr. Lucy Robinson, without whom my graduate student life would have been extremely difficult. These wonderful scientists not only taught me yeast techniques, but also provided me yeast strains, lab space, reagents, and protocols. Because of a pleasant ambiance, I felt homey in their labs, and I really enjoyed the time I spent with them. Dr. Tatchell, a member of my dissertation advisory committee, was more like a mentor, and his genuine care and supportive attitude have helped me cruise through several tormenting hurdles. Dr. Robinson also played a significant role during my career as a graduate student. Even though she was not on my committee, Dr. Robinson helped me with my experiments, and more importantly, read and edited my manuscripts and other scientific writings without the slightest hesitation.

I genuinely thank the rest of my dissertation advisory committee: Dr. Diana Cruz-Topete, Dr. Norman Harris, Dr. Chris Pattillo and Dr. Yunfeng Zhao for their critical insights on all aspects of my dissertation. I am also indebted to Dr. Rona Scott, Dr. David Gross, and Dr. Anandhakumar Jayamani for their assistance with various experimental techniques. I thank Feist-Weiller Cancer Center for providing me a Carroll Feist Predoctoral Fellowship, which supported me financially from 2013-16. My sincere appreciation also extends to all the members of the Department of Molecular and Cellular Physiology as well as the School of Graduate Studies for making my 'graduate student life' a pleasant journey.

After successfully defending my Ph.D., the most rewarding words came from my father, who said, "son, you have made my life worthwhile". These words are engraved in my heart and I hope I could make him and my family even prouder in future. I thank my father, my role model, for his unconditional love and my mother for her everlasting prayers and blessings. I also thank my beloved wife, Priya, for supporting and encouraging me throughout. In fact, Priya is the 'prime spark' behind my Ph.D. as she is the one who encouraged me to take a GRE and apply for Ph.D. programs in the US universities. Moreover, I thank Priya with all my heart for giving me the best gift of my life, Prakriti, our 'little miracle'.

Finally, I thank God, my grandmother, and all the departed souls for their countless blessings, without which I could have never come this far.

Thank you all!!!

TABLE OF CONTENTS

ACKNOWLEDGEMENTS iii

LIST OF TABLES x

LIST OF FIGURES xi

ABSTRACT xiv

INTRODUCTION 1

CHAPTER I: REVIEW OF LITERATURE 3

1. Mitochondrial structure, protein import, and function 4

Mitochondria: A historical perspective 4

Mitochondrial structure 5

Mitochondrial protein import 10

Presequence pathway 12

Internal targeting signal pathway 16

Biological roles of mitochondria 23

Roles in lipid metabolism, ketogenesis, and the Krebs cycle 24

Roles in synthesis of heme and Fe-S clusters 27

Role in thermogenesis 29

Role in Ca^{2+} homeostasis 29

Role in innate immunity 30

Role in apoptosis 31

Role in ATP synthesis 33

Complex I 35

Complex II 36

Complex III 37
Complex IV 40
Complex V 42
Mitochondria as sources of reactive oxygen species (ROS) 45
2. Mitochondrial DNA replication and inheritance 50
Mitochondrial DNA (mtDNA): An introduction 50
mtDNA in budding yeast 52
Organization and topology 52
mtDNA nucleoids 55
Rho mutants 57
mtDNA replication models in yeast 59
Recombination-dependent rolling circle replication 63
Mitochondrial homologous recombinase (Mhr1) 66
mtDNA inheritance in yeast 67
mtDNA in human 69
Organization and topology 69
mtDNA nucleoids 73
mtDNA replication models in human 75
3. DNA damage 79
Nuclear and mtDNA damage by ROS 79
Nuclear and mtDNA damage by ionizing radiation 83
Nuclear and mtDNA damage by chemotherapeutic agents 86
DNA damage by restriction endonucleases 89

Restriction endonuclease XhoI 91
4. DNA repair 93
Types of nuclear DNA repair 93
Base excision repair (BER) 93
Nucleotide excision repair (NER) 97
Mismatch repair (MMR) 100
Double-strand break (DSB) repair 103
Homologous recombination (HR) 104
Non-homologous end joining (NHEJ) 107
Classical NHEJ (C-NHEJ) 107
Alternative NHEJ (A-NHEJ) 110
Human Ku complex 112
Yeast Ku (Yku) complex 115
NHEJ in prokaryotes 116
Ku proteins in *Mycobacterium tuberculosis* and *Mycobacterium marinum* 119
5. mtDNA repair 124
Introduction 124
Types of mtDNA repair 126
BER 126
MMR 128
Sanitation of premutagenic free nucleotides 129
mtDNA degradation 130
mtDNA DSB repair in mammals 131

mtDNA DSB repair in yeast 134

6. Yeast as a model system for studying mtDNA metabolism 136

References 139

CHAPTER II: EVIDENCE FOR DOUBLE-STRAND BREAK MEDIATED MITOCHONDRIAL DNA REPLICATION IN *SACCHAROMYCES CEREVISIAE* 176

Abstract 177

Introduction 178

Materials and methods 182

Results 196

Discussion 220

Acknowledgements 226

References 227

CHAPTER III: *IN VIVO* EVIDENCE FOR MHR1, BUT NOT YKU80, AS A GENERAL MITOCHONDRIAL DNA DOUBLE-STRAND BREAK REPAIR FACTOR IN *SACCHAROMYCES CEREVISIAE* 237

Abstract 238

Introduction 239

Materials and methods 243

Results 253

Discussion 265

Conclusions 268

Acknowledgements 269

References 270

SUMMARY AND FUTURE PROSPECTS 278

References 284

CURRICULUM VITAE 286

LIST OF TABLES

Table 1. Oligonucleotides used in the study (Chapter II) 182

Table 2. Quantitation of MmKu and Cox4 in total cell extracts 205

Table 3. Mitochondrial-targeted MmKu induces ρ^0 formation 207

Table 4. Oligonucleotides used in the study (Chapter III) 243

Table 5. Yeast strains used in the study (Chapter III) 245

LIST OF FIGURES

Figure 1. Structure of a mitochondrion 7

Figure 2. The presequence pathway 15

Figure 3. The internal targeting signal pathways for MOM proteins 18

Figure 4. The internal targeting signal pathway for MIM proteins 20

Figure 5. The internal targeting signal pathway for IMS proteins 22

Figure 6. The OXPHOS system 34

Figure 7. Mechanism of the Q-cycle 39

Figure 8. Human mitochondrial complex V 44

Figure 9. Schematic representation of *S. cerevisiae* mitochondrial genome 54

Figure 10. Model for transcription-dependent mtDNA replication initiation in *S. cerevisiae* 62

Figure 11. Model for recombination-dependent rolling circle replication of mtDNA in *S. cerevisiae* 65

Figure 12. Model for mtDNA inheritance in *S. cerevisiae* 68

Figure 13. Schematic representation of human mitochondrial genome 72

Figure 14. Two predominant models of human mtDNA replication 78

Figure 15. Structures of normal and oxidized DNA bases of guanine and thymine 81

Figure 16. Schematic representation of the mechanism of SP-BER and LP-BER 96

Figure 17. Schematic representation of the mechanism of GG-NER and TC-NER 99

Figure 18. Schematic representation of the mechanism of MMR 102

Figure 19. Schematic representation of the mechanism of DSB repair via HR 106

Figure 20. Schematic representation of the mechanism of DSB repair via C-NHEJ 109

Figure 21. Model for DSB repair via A-NHEJ 111

Figure 22. Domain organization of eukaryotic and prokaryotic Ku proteins 114

Figure 23. Two-component repair system of bacterial NHEJ 118

Figure 24. Operons for mycobacterial NHEJ proteins in chromosomes of *M. tuberculosis* and *M. marinum* 121

Figure 25. Regions in MtKu and MmKu proteins 123

Figure 26. Galactose-inducible expression of mitochondrial-targeted proteins 197

Figure 27. Mitochondrial-targeted MmKu impairs mitochondrial respiration 199

Figure 28. Mitochondrial-targeted MmKu decreases mtDNA content in yeast cells 202

Figure 29. Comparison of mtDNA content in cells containing pGalSu9RFP grown in Raff or Gal 203

Figure 30. Mitochondrial-targeted MmKu triggers mtDNA depletion 204

Figure 31. Verification for the lack of mtDNA in ρ^0 cells generated following MmKu expression 208

Figure 32. MmKu binds preferentially to *ori5* in the yeast mitochondrial genome 209

Figure 33. Comparison of the percentage of ρ^+ colonies between KT1112 and KT1112/Δ*ntg1* 211

Figure 34. PCR from KT1112 and KT1112/Δ*ntg1* DNA using primers encompassing the region where DSBs are induced in *ori5* 212

Figure 35. Expression and activity of mitochondrial-targeted MmKu from KT1112 pRS305MmKu 214

Figure 36. Pedigree analyses indicate that MmKu expression inhibits mtDNA segregation into daughter cells 215

Figure 37. Expression of mitochondrial-targeted bKu proteins in human MCF7 cell lines 217

Figure 38. Mitochondrial-targeted bKu proteins do not induce mtDNA depletion in human MCF7 cells 218

Figure 39. Determination of relative mtDNA copy number of human MCF7 cells grown in ρ^0 medium 219

Figure 40. A model explaining the effect of MmKu on *S. cerevisiae* mtDNA 223

Figure 41. Schematic representation of the galactose-inducible system for expression of mitochondrial-targeted proteins 253

Figure 42. Expression and activity of mitoXhoI in KT1357 256

Figure 43. Expression of mitoXhoI in KJP1976 and KJP2011 259

Figure 44. XhoI restriction sites in KJP1976 and KJP2038 are cleaved only following induction of mitoXhoI expression 261

Figure 45. Following induction of mitoXhoI expression, Mhr1 has increased binding to mtDNA near the XhoI restriction sites 264

ABSTRACT

Mitochondria are essential eukaryotic organelles containing multiple copies of mitochondrial DNA (mtDNA), which encodes protein subunits of the oxidative phosphorylation (OXPHOS) machinery. In addition to producing the majority of a cell's ATP, the OXPHOS system can also generate reactive oxygen species (ROS), which are known to damage mtDNA molecules. Such ROS-induced mtDNA damage generally comprises strand breaks, base loss, and base modifications. Because of its complexity, a double-strand break (DSB) in the mitochondrial genome is regarded as the most deleterious form of mtDNA lesion. However, site-specific mtDNA DSBs can also be beneficial depending on the type of eukaryotic cell under consideration.

Studies in the budding yeast *Saccharomyces cerevisiae* have revealed that mtDNA DSBs at the replication origin *ori5* initiate mtDNA recombination dependent rolling circle replication (RDR) in respiratory deficient petite (ρ^-) mutants. However, it was not certain if respiratory competent wild-type (ρ^+) cells also employed a similar replication mechanism for propagating their mitochondrial genome. To understand this, the DSB binding property of an evolutionarily conserved protein was utilized. Ku, a central protein involved in DSB repair via non-homologous end joining, is found across different domains of life and contains a conserved 'core' domain dedicated for DNA end binding. Eukaryotic Ku, unlike bacterial Ku (bKu), also possesses additional N- and C-terminal domains required for communicating with downstream eukaryotic repair proteins. With this knowledge, I hypothesized that expression of mitochondrial-targeted bacterial Ku in ρ^+ yeast cells would bind to mtDNA DSBs and prevent mtDNA replication or repair due to lack of communication with eukaryotic factors. Results

revealed that mitochondrial-targeted bKu bound to *ori5* in ρ^+ mtDNA and inducible expression of bKu triggered petite formation preferentially in daughter cells. In addition, bKu expression induced mtDNA depletion, which occurred to such an extent that cells devoid of mtDNA (ρ^0 cells) were identified. These observations supported the idea that mtDNA replication in ρ^+ yeast cells is initiated by a DSB since binding of bKu to DSB at *ori5* not only triggered mtDNA depletion but also interfered with mtDNA segregation into daughter cells. Expression of mitochondrial-targeted bKu, however, did not decrease mtDNA content in human breast cancer MCF7 cells. This is in agreement with the knowledge that human mtDNA replication, typically, is not initiated by a DSB. Collectively, the study provided a direct evidence for DSB-mediated replication as the predominant, and probably the only, form of mtDNA replication in ρ^+ yeast cells.

DSB-mediated mtDNA replication is a rare instance of the beneficial aspect of mtDNA DSBs, as these lesions are generally considered detrimental. By disrupting mtDNA integrity, mtDNA DSBs can compromise the function of the OXPHOS system and this in turn can prove disastrous to a cell. Fortunately, eukaryotic cells have evolved with a mtDNA DSB repair system, which is dedicated to restore the integrity of the mitochondrial genome. However, factors mediating mtDNA DSB repair are not well characterized and only a few proteins have been identified as *bona fide* mtDNA DSB repair factors in the entire Eukaryota domain. To identify mtDNA DSB repair factors, *S. cerevisiae* was utilized as a eukaryotic model system in which two putative proteins were selected: Mhr1 (mitochondrial homologous recombinase) and yeast Ku80 (Yku80). Utilizing mitochondrial-targeted restriction endonuclease XhoI (mitoXhoI), Mhr1 was shown to bind near mitoXhoI-induced DSBs *in vivo*. This observation, together with the

preexisting knowledge of its homologous pairing activity *in vitro*, bolstered my hypothesis that Mhr1 is a general mtDNA DSB repair factor. Yku80, on the other hand, could not be detected in the yeast mitochondrial extracts. In addition, the level of Mhr1 binding near mitoXhoI-induced DSBs was comparable between the wild-type strain and isogenic *yku80* null mutant, suggesting that *YKU80* gene product did not compete with Mhr1 for binding to mtDNA DSBs. These observations indicated that Yku80, most likely, is not involved in repairing mtDNA DSBs. Hence, I concluded that Mhr1, but not Yku80, is a general mtDNA DSB repair factor in yeast.

Taken together, this study has expanded our knowledge on mtDNA DSBs in replication and in repair. If explored comprehensively, the knowledge of mtDNA replication and repair can open new avenues to identifying potential therapeutic targets against different human diseases.

INTRODUCTION

Statement of problem

Our current knowledge of the mechanism of mtDNA replication in yeast has been derived from respiratory deficient petite (ρ^-) mutants. Evidence indicates that ρ^- mutants employ mtDNA DSB-mediated recombination dependent rolling circle replication (RDR) as a mechanism for propagating their mitochondrial genome. Even though the mtDNA topology of respiratory competent wild-type (ρ^+) cells also favored DSB-mediated RDR as a potential replication mechanism, the exact mode of mtDNA replication in ρ^+ cells was unknown.

The involvement of DSBs in the initiation of mtDNA replication, for example in yeast cells, is an unusual instance in which a damaged DNA molecule is utilized for the benefit of the organism. DSBs are typically considered deleterious and therefore have to be dealt with effectively to avoid adverse cellular consequences. Even though mtDNA DSB repair activities and repair products have been identified in various eukaryotic systems, merely a handful of proteins have been identified as genuine mtDNA DSB repair factors, and the pursuit of additional factors is an area of active research.

Significance

Mitochondria are essential eukaryotic organelles that play central roles in determining if cells live or die. Because mtDNA is essential for human cell survival, a comprehensive understanding of mtDNA biology is necessary for identifying novel drugs that may destroy harmful cells while rescuing or protecting normal ones to preserve tissue integrity. Certain human cells/tissues have been hypothesized to replicate their

mitochondrial genome in DSB-mediated manner. If this idea holds true, the knowledge can be exploited to enhance mtDNA replication in such cells/tissues. This approach may prove valuable in cases where there is a requirement for a high mtDNA copy number, as in the tissues of patients with mtDNA depletion syndrome. Similarly, a comprehensive knowledge on mtDNA DSB repair is equally important. To understand the repair process, identification of the participating proteins is a prerequisite. As DNA repair pathways are highly conserved from yeast to humans, the knowledge of mtDNA DSB repair in a simple eukaryote can shed light on the repair process in complex eukaryotes like human beings.

Objectives

The major objectives of this dissertation are: (i) to understand if ρ^+ yeast cells replicate mtDNA in DSB-mediated manner; and (ii) to identify proteins involved in mtDNA DSB repair utilizing yeast as a model system.

CHAPTER I

REVIEW OF LITERATURE

1. MITOCHONDRIAL STRUCTURE, PROTEIN IMPORT, AND FUNCTION

1.1 Mitochondria: A historical perspective

About 2 billion years ago, when the Earth's atmosphere started to become oxygen-rich, a primordial eukaryotic cell incapable of using oxygen engulfed aerobic bacteria. Evading digestion, these bacteria developed an endosymbiotic relationship with the engulfing cell: the bacteria acquired shelter and nourishment from the host and in return supplied energy to the host to meet its bioenergetic demands [1]. The engulfed bacteria were eventually named mitochondria by a German physician Carl Benda in 1898; the word derives from the Greek "mitos" (thread) and "chondros" (granule), descriptive of the appearance of these entities during spermatogenesis [2]. The endosymbiotic theory of the origin of mitochondria is now universally accepted [3]; the theory is reinforced not only by the fact that these organelles contain their own genetic material but also from the observation that they harbor their own protein-synthesizing machinery dedicated to translate mitochondrial genes [4]. Moreover, close homology of bacterial and mitochondrial respiratory chain complexes [5] and other membrane proteins [6, 7] together with the ability of mitochondria to divide further provide evidence in support of the theory. Endosymbiosis is now regarded as a crucial force that steered eukaryotic evolution [8]. Indeed, the acquisition of mitochondria by a proto-eukaryote is believed to have provided energy necessary for expansion of the nuclear genome, and this, with time, enabled evolution of complex organisms.

1.2 Mitochondrial structure

Mitochondria are essential organelles present in almost all eukaryotic cells [9]. Those eukaryotes that do not contain mitochondria once possessed the organelle and eventually lost them [10]. These ancient organelles exhibit a remarkable heterogeneity in their shape, size, number and location in various cell types [9]. Since they constantly undergo fission and fusion [11], mitochondria do not have fixed shape and size [3]. However, in cells like hepatocytes and fibroblasts, they appear like sausage-shaped organelles of ~1 μm diameter and 3-4 μm length [3]. Most eukaryotic cells harbor multiple mitochondria, which collectively may occupy a substantial portion of the cytoplasmic volume [12]. Different cell types vary considerably in number/volume of mitochondria they possess [3]; in general, the number/volume of mitochondria per cell is regulated to match its bioenergetic demand [12, 13]. For example, ~35% of the volume of ventricular cardiomyocytes is occupied by mitochondria, which are located predominantly between individual myofibrils [14, 15]. In contrast, hepatocytes, which have lower bioenergetic needs, contain about 1000-2000 mitochondria dispersed throughout the cytosol that constitute ~20% of the cell's volume [1, 16]. This vast range of mitochondrial number in a given cell type is because of ongoing fission and fusion events [9]. Not surprisingly, the number of mitochondria also differs significantly between different species. For example, the giant amoeba *Chaos chaos* has been reported to harbor ~500,000 mitochondria [3], whereas the budding yeast *Saccharomyces cerevisiae* during log phase growth contain up to 10 elongated reticular mitochondria [9, 17, 18]. In the budding yeast, the shape, size and number of mitochondria vary considerably under different growth conditions. For example, under anaerobic conditions, these organelles form tiny entities called

promitochondria; however, mitochondria become large and appear like interconnected tubules when grown in the presence of oxygen. This reticular network of yeast mitochondria observed during vegetative growth epitomizes mitochondrial structure in many different eukaryotic cell types [9].

With the invention of the electron microscope, a comprehensive morphological analysis of mitochondria became feasible. Early studies revealed a peculiar architecture of the organelle, comprising a double membrane system, viz., an outer membrane and an inner membrane [3, 19] (Figure 1). The mitochondrial outer membrane (MOM) encloses the organelle and is the gateway for exchange of a variety of molecules with its immediate environment [19]. In regard to its composition, the MOM is fairly homogeneous, consisting about 1.0-1.5 μg proteins per μg phospholipids [20, 21]. Phosphatidylcholine and phosphatidylethanolamine are the most abundant lipid constituents of the MOM [22], whereas the mitochondrial signature phospholipid cardiolipin is present in minute quantity [23]. The MOM is characterized by the presence of a large number of porins, also referred as voltage-dependent anion channels (VDACs) [7]. These pore-forming proteins render the membrane freely permeable to all ions and molecules of 5000 Daltons or less [1, 12]. Larger molecules, however, pass through the MOM via special translocases [5]. Apart from VDAC, other major protein components of MOM include those involved in mitochondrial protein import (TOM complex), mitochondrial lipid transport (TSPO), intrinsic apoptotic pathway (Bak), and mitochondrial fission (Mff) and fusion (Mfn1) [1, 20, 22]. Thus, the MOM plays a vital role in biogenesis, dynamic behavior and morphology of the organelle [20].

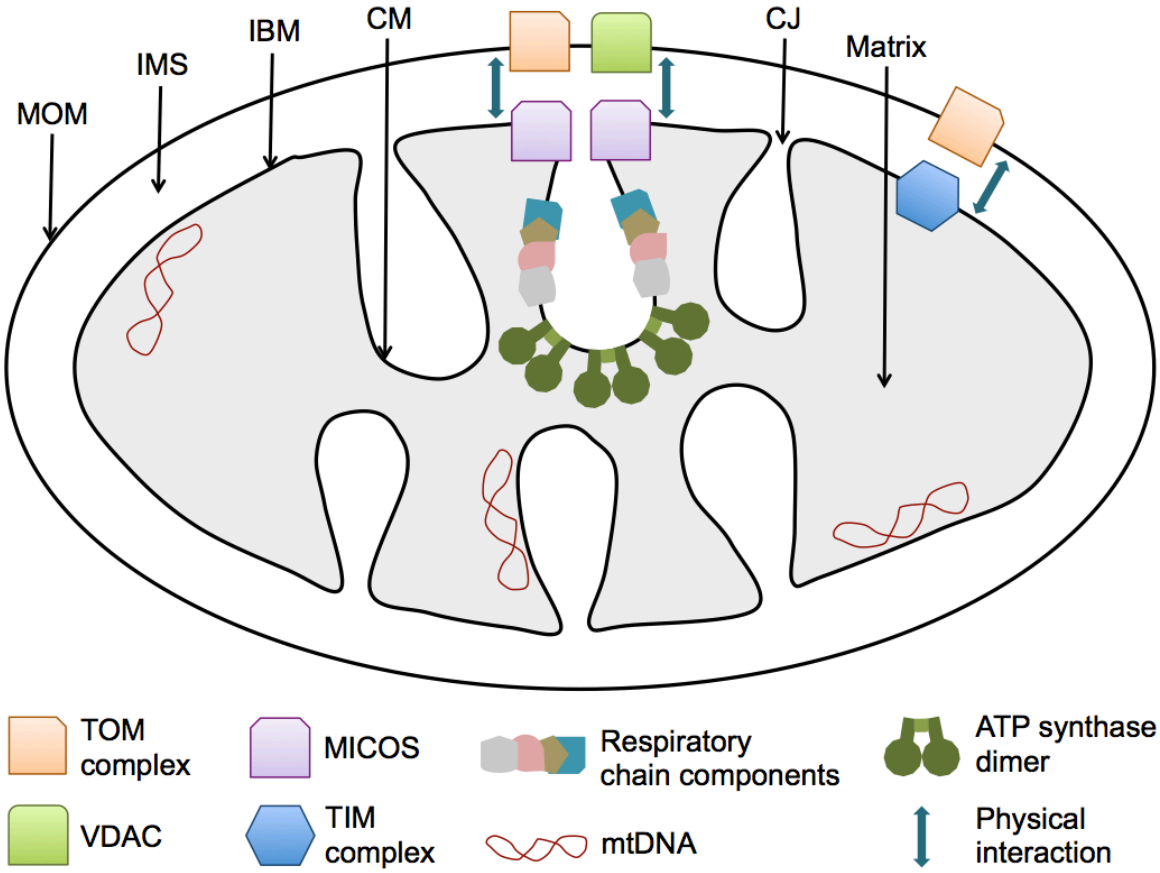

Figure 1. Structure of a mitochondrion. A highly specialized double membrane encloses the mitochondrion. The MOM is enriched with VDAC and components of the protein import machinery (TOM complex). The IMS contains soluble proteins involved in different biological processes. The MIM is comprised of IBM and CM, which are connected via CJ. In addition to forming the structural basis of CJs, MICOS also connects cristae with protein components of the MOM at contact sites. Moreover, physical interaction between the TOM and the TIM complexes also occurs at contact sites. The IBM contains a large number of protein translocases (TIM complex), whereas the CM is enriched in respiratory chain components and ATP synthase. Several copies of mtDNA are localized in the protein-rich mitochondrial matrix. CJ, crista junction; CM, cristae membrane; IBM, inner boundary membrane; IMS, intermembrane space; MICOS, mitochondrial contact site and cristae organizing system; MOM, mitochondrial outer membrane; mtDNA, mitochondrial DNA; TIM, translocase of the inner membrane; TOM, translocase of the outer membrane; VDAC, voltage-dependent anion channel (Adapted from van der Laan *et al.* [19]).

Between the MOM and the inner membrane that is juxtaposed to the MOM, a gap of ~20 nm exists [24]. This smallest sub-compartment of mitochondria, known as the intermembrane space (IMS), acts as the hub of molecular transport between the cytosol and the mitochondrial matrix [25]. Because of the abundance of porins on MOM, the biochemical composition of the IMS was believed to be the same as the cytosol [1]. However, recent studies have provided evidence for several distinct physiochemical properties of the IMS compared to the cytosol. For example, the H^+ concentration was found to be higher in the IMS than in the cytosol, the difference in pH being 0.2 to 0.7 units [25, 26]. Moreover, composition of glutathione redox buffer is also different such that the buffer is in more oxidized state in the IMS than in the cytosol [27]. In regard to the protein content, the IMS is predicted to harbor more than 100 different proteins. These soluble factors have diverse biological functions, which include electron transport (cytochrome *c*), mitochondrial fusion (OPA1), nucleotide metabolism (adenylate kinase), redox control (Cu-Zn superoxide dismutase), apoptosis (Smac/DIABLO), and signaling (Sirt5) [25].

Unlike the MOM, the mitochondrial inner membrane (MIM) represents a tight diffusion barrier and is permeable only to small uncharged molecules of 100-150 Daltons or less [2]. The vast majority of molecules cross the MIM with the help of specific membrane transport proteins, which are selective for the ions or molecules they ferry [2, 5]. Accordingly, the MIM is literally packed with proteins [3], which constitute ~76% of the total mass of the MIM. This represents the highest protein content of any cellular membranes [12]. As for the MOM, phosphatidylcholine and phosphatidylethanolamine predominate in the MIM [22]; however, this internal lipid bilayer is also enriched with

the diglycerophospholipid cardiolipin, which is critical for MIM organization as well as for its barrier function [1, 19]. The barrier activity of the MIM favors the establishment and maintenance of a mitochondrial membrane potential across the membrane, with the IMS side being positively charged [5].

Early morphological studies on mitochondria also revealed that the surface area of the MIM is several-fold larger than that of the MOM [19], with the MIM containing many finger-like projections, cristae, protruding into the matrix [2]. Accordingly, the inner membrane is divided into two domains: the inner boundary membrane (IBM), which is closely apposed to the MOM, and the folded cristae membranes (CM), which form invaginations of different shape and size [19]. The presence of numerous cristae increases the surface area of the MIM, which has been positively correlated with respiratory activity [2]. Indeed, extensively folded, lamellar cristae are typically present in muscle cells, reflecting their greater ATP demand [3], whereas tissues like liver have less densely stacked cristae [5]. Interestingly, the protein composition differs between the IBM and the CM [28, 29]. Apart from the protein translocases (TIM complexes) that import nuclear encoded preproteins into the mitochondria [19], the IBM is also enriched with numerous carrier proteins that transport ions, nucleotides and small metabolites between the cytosol and the matrix [5]. In contrast, the respiratory chain complexes and the F_1F_0-ATP synthase are preferentially localized in the CM [19]. Indeed, rows of F_1F_0-ATP synthase dimers are present along the edges and tips of cristae and this arrangement generates a high membrane curvature, providing cristae their characteristic shape [30]. An apparent difference in protein localization between two adjacent regions of MIM has been attributed to the presence of crista junctions (CJs) [5], narrow neck-like structures

that connect the CM with the IBM [19]. In contrast to the variation in cristae morphology between different cell types, CJs are homogenous structures that are formed by protein subunits of the mitochondrial contact site and cristae organizing system (MICOS) [19]. The barrier activity of CJs separates the peripheral region of the IMS and cristae lumen, which has been proposed to represent an ideal environment for chemiosmotic coupling [31-33]. Intriguingly, cristae lumen harbors a substantial amount of small soluble electron transport protein cytochrome *c*, and during apoptosis opening of the CJs allows escape of this proapoptotic factor from the mitochondria [34-36].

Enclosed by the MIM is the innermost compartment, termed the mitochondrial matrix. This protein-dense region contains a high concentration of hundreds of enzymes that are involved in substrate metabolism, including those essential for fatty acid oxidation and the citric acid cycle. The matrix also harbors multiple copies of mitochondrial DNA (mtDNA), and is the site for mtDNA replication and gene expression [1]. Another striking feature of the matrix is the high pH (~7.9) compared to the IMS (~6.9). This pH gradient drives ATP synthesis via electron transport chain (ETC) and oxidative phosphorylation (OXPHOS) in the membranes of cristae [5, 26, 37].

1.3 Mitochondrial protein import

Mitochondria are protein-rich organelles. Proteomic analyses have provided an estimate of ~1000 distinct proteins in yeast mitochondria and even more (~1500 proteins) in mammalian mitochondria [38-40]. Distribution of these proteins in different mitochondrial regions is asymmetric: for example, in the liver, ~67% of the total

mitochondrial protein is localized in the matrix, ~21% in the MIM, and ~6% each in the MOM and the IMS [1]. In spite of the existence of a complete genetic system in the matrix, the mitochondrial genome encodes only about 1% of the total mitochondrial proteome; the remaining ~99% are encoded by nuclear genes [6, 41]. The nuclear-encoded mitochondrial proteins are synthesized as precursor proteins on cytosolic ribosomes. The vast majority of these precursor proteins are imported following completion of their synthesis on ribosomes (post-translational import), and for this process, cytosolic chaperones play a vital role in guiding the preproteins to the MOM [6]. Nonetheless, cytosolic ribosomes are also known to associate with the mitochondrial surface, and translocation of numerous precursor proteins into mitochondria is initiated co-translationally as their C-termini are still being synthesized [42]. Irrespective of these import modes, the precursor proteins possess targeting signals that direct them to the correct mitochondrial subcompartment [7, 42]. Indeed, both the MOM and MIM harbor specialized machineries for precursor recognition, translocation, and membrane insertion [6]. These protein import machineries are indispensible for cell viability and the basic principles of mitochondrial protein import are well conserved from yeast to human [43].

Depending on the location of targeting signals, mitochondrial precursor proteins can be distinguished into two major groups. The first group consists of proteins with amino-terminal cleavable extensions, called presequences, which are the classical mitochondrial targeting signals (MTS). The second group of precursor proteins lacks cleavable extensions but harbors multiple internal targeting signals that persist in the mature protein [6, 7]. Accordingly, the mitochondrial protein import pathways can be broadly classified into the presequence pathway and the internal targeting signal pathway.

1.3.1 Presequence pathway

This classical route of mitochondrial protein import is utilized by the majority of mitochondrial proteins [43], including virtually all matrix proteins and a considerable fraction of MIM and IMS proteins [6, 7]. Presequences are located at the amino termini of proteins and typically consists of ~10-60 amino acid residues [41]. Rich in positively charged amino acids, these presequences also contain significant amount of hydrophobic residues, and assume an amphipathic α-helical conformation, with positively charged residues on one side and hydrophobic residues on the other [12]. Import of a precursor protein begins when the presequence interacts with the import machinery of the MOM, the translocase of the outer membrane (TOM complex), which is the central entry gate for all preproteins of the presequence pathway (Figure 2). The TOM is a multimeric protein complex comprising of the central channel-forming protein Tom40, three preprotein receptors, Tom20, Tom22 and Tom70, and three small Tom proteins, Tom5, Tom6, and Tom7 [44-46]. The receptors Tom20 and Tom22 bind to distinct segments of the incoming presequence: the hydrophopic surface of the amphipathic α-helix is recognized by Tom20 [47], whereas Tom22 associates with the positively charged residues [48]. The preproteins are then translocated through the import channel formed by Tom40 [44], following which the protruding presequence interacts with the IMS domain of Tom22 [6, 49, 50]. Subsequently, the presequence is translocated through the MIM via the TIM23 complex, also known as the presequence translocase [7]. As the channels formed by the TOM and TIM23 complexes are too narrow for folded proteins to pass through, the preproteins are transported in an unfolded conformation [42]. Like the TOM complex, the TIM23 complex is also a multimeric protein complex, with Tim50

and Tim23 playing major roles in the translocation process. The IMS domain of Tim50 first binds to the emerging preprotein, and guides it to the import channel formed by Tim23 [6, 51]. Moreover, the IMS domain of Tim50 induces channel closure in the absence of preprotein in transit [52], thereby acting to gate the Tim23 channel. However, on arrival of a presequence, Tim50 releases the blockade and allows preproteins to enter through Tim23. This mechanism prevents ion leakage across the MIM and ensures maintenance of mitochondrial membrane potential ($\Delta\Psi$) [7]. In addition to its role in ATP production during OXPHOS, the $\Delta\Psi$ is crucial for preprotein translocation through the Tim23 channel. $\Delta\Psi$ induces opening of the channel and also exerts an electrophoretic effect on the positively charged presequences, pulling them to the matrix side [51, 53-55]. Interestingly, the passage of presequence-containing preproteins through the MOM and MIM occurs at the contact sites formed by physical interaction between the membrane proteins. Indeed, several components of the TOM and TIM complexes, including the IMS domains of Tom22, Tom40, Tim50 and Tim23, participate in formation of a major translocation contact site that facilitates transfer of preproteins to their final destination [42].

Following translocation of the presequences across the MIM, the preproteins are either completely imported into the matrix or are laterally released into the MIM [7]. Hydrophilic preproteins enter the matrix with the help of the presequence translocase-associated motor (PAM) [56-59], whereas preproteins containing a hydrophobic sorting signal following the presequence become embedded into the MIM [60, 61]. The matrix heat shock protein 70 (mtHsp70) is the central motor component of the PAM and plays a critical role in driving protein import. Upon exit from the Tim23 channel, the preproteins

are bound by mtHsp70, which is believed to trap and pull the preproteins into the matrix in an ATP-powered manner [6, 42]. Mitochondrial processing peptidase (MPP), a heterodimeric metallopeptidase, cleaves off presequence from most preproteins arriving in the matrix [62, 63]. Moreover, several preproteins are also subjected to a second processing by additional matrix-localized peptidases [7] before folding to their native conformation with the help of matrix-localized molecular chaperones [6, 12]. On the other hand, preproteins containing a hydrophobic sorting signal following a positively charged presequence are typically arrested in the TIM23 complex by the hydrophobic sequence and are then laterally discharged into the lipid phase of the membrane [60, 61]. This process operates independently of ATP-driven import by PAM and the energy for this process is obtained from $\Delta\Psi$ [6, 64]. As with the matrix-translocated preproteins, the presequences of MIM-sorted preproteins are also proteolytically removed by the MPP [42, 62, 63]. In addition, sorting of some preproteins into the IMS can also occur via this pathway. After being embedded into the MIM, the hydrophobic transmembrane segment is cleaved by the inner membrane peptidase (IMP) located in the MIM facing the IMS, thereby releasing the mature protein into the IMS [7, 12]. Intriguingly, translocation of some preproteins bearing presequences and internal hydrophobic domains does not stop in the MIM, but are completely or partially imported into the matrix via the TIM23-PAM complexes [42]. Following removal of the presequence by MPP, the resulting proteins are rerouted into the MIM for insertion by the cytochrome oxidase activity (OXA) export machinery. mtDNA-encoded proteins synthesized on mitochondrial ribosomes also utilize the OXA machinery for their insertion into the MIM [42, 65-67].

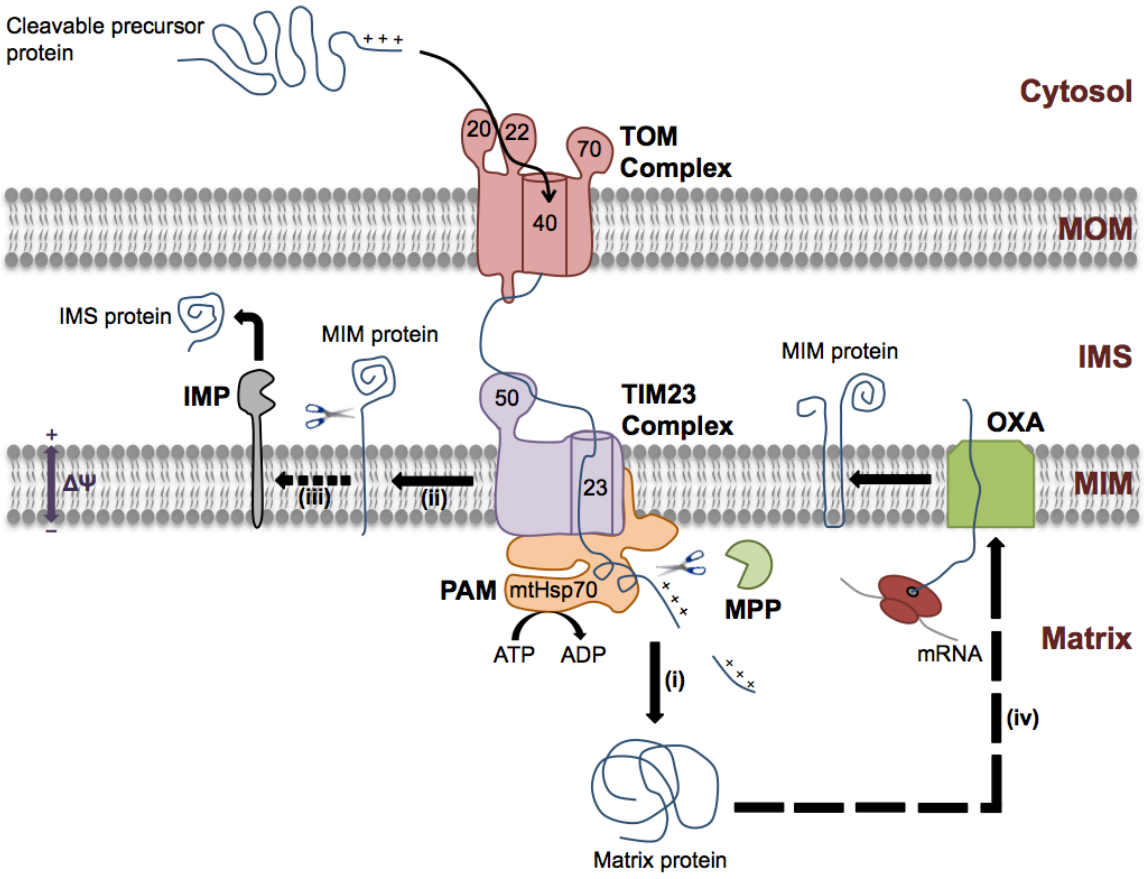

Figure 2. The presequence pathway. Preproteins containing presequences are transferred to the central entry gate of mitochondria, the TOM complex, from where they are directed to the TIM23 complex. After exiting through the Tim23 channel, presequences are cleaved by the MPP in the matrix. Preproteins traversing through the TIM23 complex can take one of several different routes to reach their destined subcompartments. (**i**) Hydrophilic preproteins are pulled into the matrix with the help of the PAM, whose central motor component, mtHsp70, utilizes ATP to drive the process. (**ii**) Preproteins carrying a hydrophobic sorting signal following the presequence are released laterally into the lipid phase of the MIM. (**iii**) The IMP cleaves the hydrophobic sorting signal of some preproteins embedded in the MIM, thereby releasing them into the IMS. (**iv**) Some precursor proteins with bipartite signals (presequence followed by hydrophobic sorting signal) are first transported towards the matrix, following which they are eventually inserted into the MIM via the OXA machinery. The OXA machinery also catalyzes incorporation of proteins synthesized by mitochondrial ribosomes into the MIM. ΔΨ, mitochondrial membrane potential; IMP, inner membrane peptidase; IMS, intermembrane space; MIM, mitochondrial inner membrane; MOM, mitochondrial outer membrane; MPP, mitochondrial processing peptidase; mtHsp70, matrix heat shock protein 70; OXA, cytochrome oxidase activity machinery; PAM, presequence translocase-associated motor; TIM, translocase of the inner membrane; TOM, translocase of the outer membrane (Adapted from Horvath *et al.* [42] and Becker *et al.* [41]).

1.3.2 Internal targeting signal pathway

The precursor proteins adopting this pathway generally harbor multiple internal targeting sequences, which remain part of their biologically active form. All MOM proteins along with a substantial number of MIM and IMS proteins take this pathway [6]. In the MOM, two types of transmembrane proteins exist: pore forming β-barrel proteins (VDAC, Tom40, etc.) and membrane-anchored proteins with one or more α-helical transmembrane segments (Tom20, Tom22, Tom70, etc.). Intriguingly, β-barrel proteins localize only in the outer membranes of bacteria, mitochondria and chloroplasts [7], further bolstering endosymbiotic theory of the origin of mitochondria. The precursors for β-barrel proteins are initially recognized and translocated by the TOM complex into the IMS [68] (Figure 3). These preproteins then bind IMS-localized small Tim chaperones, which reroute them to the sorting and assembly machinery (SAM) present in the MOM [6, 69, 70]. A β-strand at the C-terminal end of the preprotein acts as a sorting signal that directs insertion into the multisubunit SAM complex [71], which subsequently facilitates release of the preproteins into the lipid phase of the MOM [72]. In contrast to β-barrel proteins, insertion of α-helical proteins in the MOM involves multiple pathways that are only partly characterized [42]. The membrane anchor transmembrane segments, which typically function as targeting signals, can be located in N-terminal, middle or C-terminal regions of the preproteins [7]. Even though the majority of preproteins enter mitochondria via the TOM complex, some α-helical MOM proteins have been known to bypass it [43]. Examples of preproteins bypassing the TOM complex include N-terminally anchored proteins (Tom20, Tom70, etc.), which directly use mitochondrial import complex (MIMC) for membrane insertion [73-75] [7, 20]. On the contrary,

proteins containing a transmembrane segment in the middle region (Tom22, etc.) exploit TOM receptors for mitochondrial targeting and the SAM complex for membrane insertion [76]. C-terminal membrane anchor proteins (Bcl-X_L, Fis1, Tom6 etc.), on the other hand, can use various pathways for membrane insertion [20]. Some of these proteins use MIMC complex [77], whereas insertion of other proteins seems to be independent of any of the known outer membrane machineries. Proteins in the latter category are either directly embedded into the lipid phase of the membrane or may use an unidentified insertase to facilitate the insertion process. Efficient insertion of these proteins is believed to depend on the membrane lipid composition, as the C-terminal membrane anchor domain appears to have increased affinity for certain lipid components [7, 20, 78, 79].

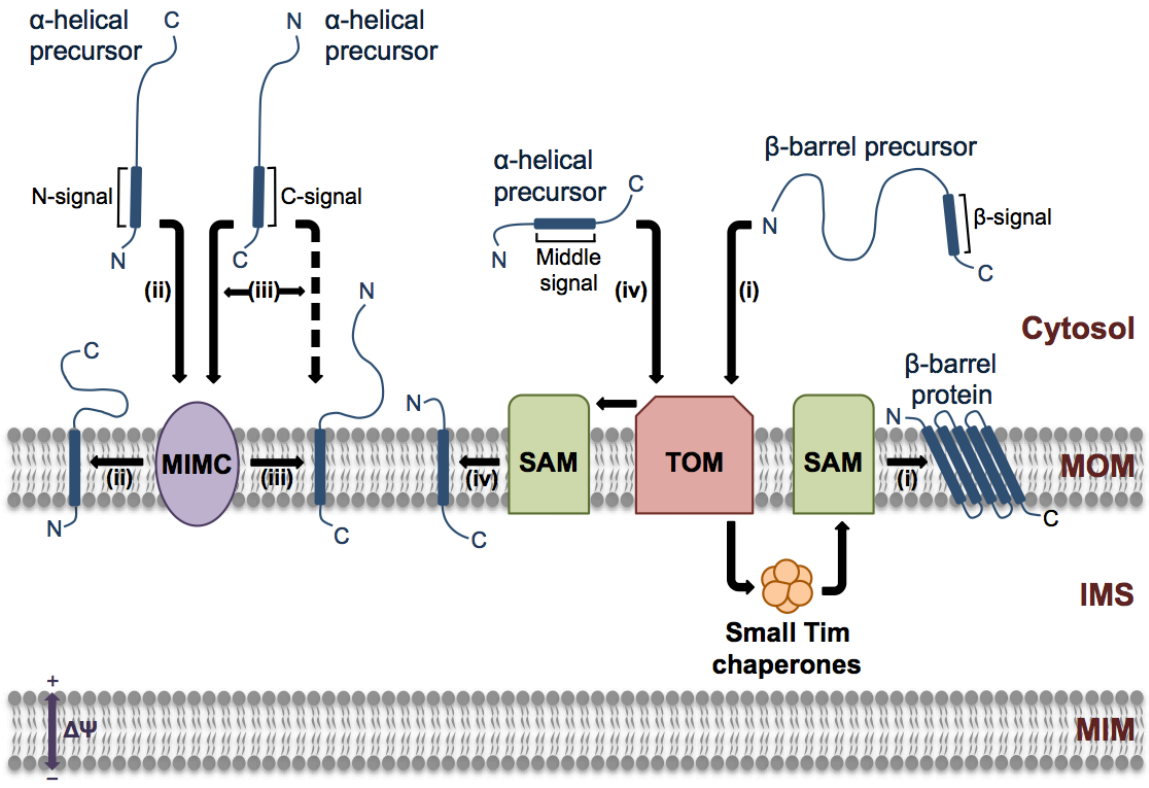

Figure 3. The internal targeting signal pathways for MOM proteins. (**i**) The precursors of β-barrel proteins are translocated through the TOM complex in the MOM, following which small Tim chaperone complexes in the IMS ferry the precursors to the SAM complex present in the MOM for membrane insertion. (**ii**) N-terminal signal containing precursors use the MIMC complex for membrane insertion. (**iii**) C-terminal membrane anchor proteins can either use the MIMC complex or be directly integrated into the lipid phase of the MOM. (**iv**) Preproteins with transmembrane segments in the middle region use TOM receptors before being relayed to the SAM complex, which then mediates membrane insertion. ΔΨ, mitochondrial membrane potential; IMS, intermembrane space; MIM, mitochondrial inner membrane; MIMC, mitochondrial import complex; MOM, mitochondrial outer membrane; SAM, sorting and assembly machinery; TOM, translocase of the outer membrane (Adapted from Schmidt *et al.* [7] and Horvath *et al.* [42]).

Unlike the MOM, the MIM harbors only α-helical membrane proteins. The internal targeting signal pathway has been extensively studied for these proteins. The major substrates of this pathway include multiple transmembrane spanning hydrophobic carrier proteins such as the ADP/ATP carrier, and the phosphate carrier that mediate the transport of metabolites between the matrix and the IMS. For this reason, this protein import route is commonly referred as the carrier pathway. The number of internal targeting elements present in a carrier protein can vary from three to six, which are dispersed in different regions and have only been partially characterized [7]. Initially, the hydrophobic carrier precursors are bound by cytosolic chaperones, which not only prevent their aggregation in the cytosol but also interact with the Tom70 receptor that allows their delivery to the MOM [80-82] (Figure 4). Tom20 and Tom22 receptors located in the vicinity also assist in inserting the precursors into the Tom40 channel. In contrast to preproteins with presequence, hydrophobic carrier precursors do not traverse as linear chains but translocate the MOM in a loop structure [83]. The preproteins subsequently enter the IMS, where they are bound by small soluble Tim chaperones. Apart from preventing aggregation of the hydrophobic precursors in the aqueous IMS milieu, these small Tim chaperones specifically dock to the TIM22 complex in the MIM [84-86]. Also known as the carrier translocase, the TIM22 complex consists of a channel-forming protein, Tim22, through which the precursor proteins traverse. Like the presequence translocase, the Tim22 channel is also activated by the $\Delta\Psi$, which provides energy for both the initial insertion of the precursors into the translocase and their ultimate release into the lipid phase of the MIM [6, 7, 42, 43].

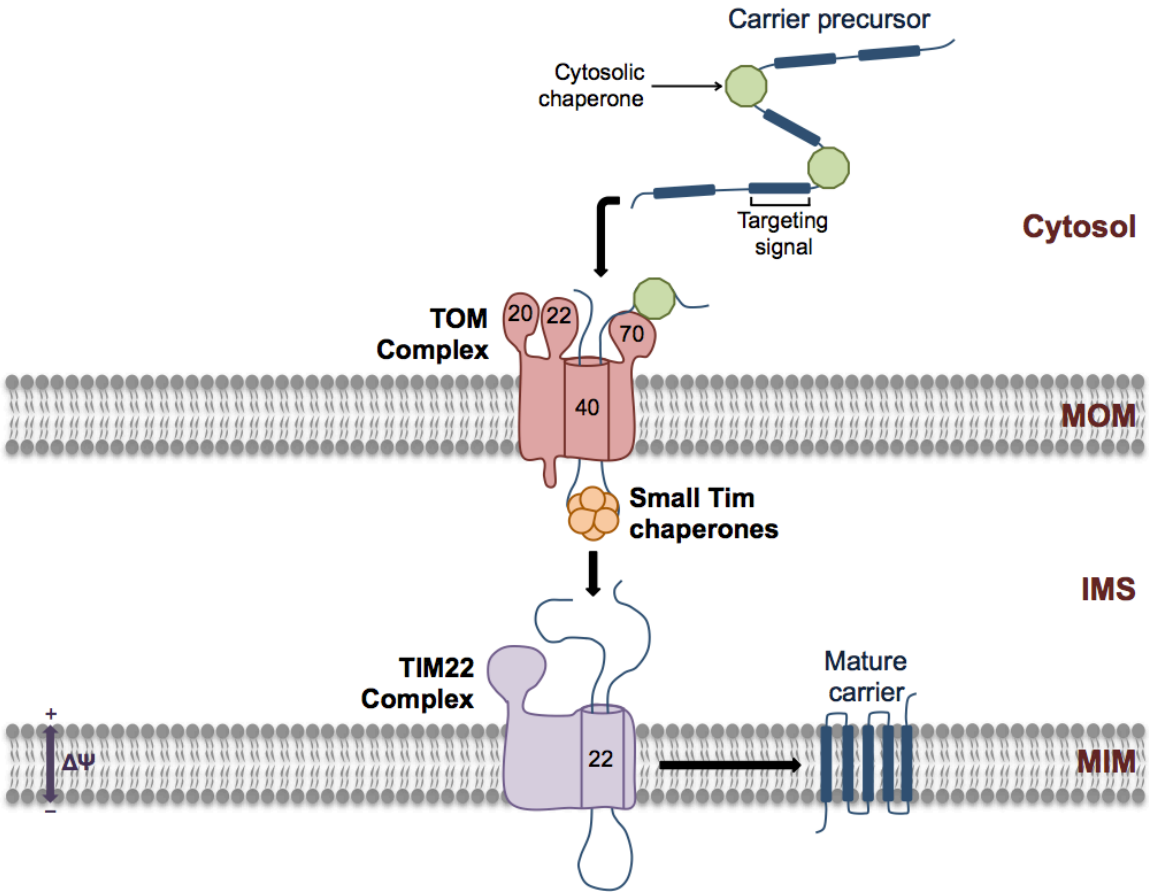

Figure 4. The internal targeting signal pathway for MIM proteins. Cytosolic chaperones bind and direct carrier precursors to the Tom70 receptor, following which they are translocated through the Tom40 channel. IMS-localized small Tim chaperones bind the incoming precursors and guide them to the TIM22 complex, which drives their membrane insertion in a ΔΨ-dependent mechanism. ΔΨ, mitochondrial membrane potential; IMS, intermembrane space; MIM, mitochondrial inner membrane; MOM, mitochondrial outer membrane; TIM, translocase of the inner membrane; TOM, translocase of the outer membrane (Adapted from Schmidt *et al.* [7]).

In addition to all MOM and numerous MIM proteins, a considerable fraction of IMS proteins also possess internal targeting signals. The IMS, like the cytosol, was initially assumed to possess a reducing environment, so the oxidation of proteins in this mitochondrial sub-compartment was believed to be disfavored [7]. However, this long-standing misperception was rectified by the identification of an oxidative protein import and folding system in the IMS, which led to the discovery that a vast number of IMS proteins are in the oxidized state [42]. The apparatus responsible for this phenomenon, the mitochondrial intermembrane space import and assembly (MIA) machinery, consists of two essential components, Mia40 and Erv1 (essential for respiration and viability) (Figure 5). Mia40 is the core component of the MIA machinery and acts as a receptor on the IMS side of the MOM. It recognizes cysteine-containing internal targeting signals in IMS precursors, which are translocated through the Tom40 channel in a reduced, unfolded state. By transiently forming a disulfide bond with the incoming precursor, Mia40 acts as a disulfide carrier that relays multiple disulfide bonds into the preprotein, thereby promoting their oxidation. This not only facilitates protein folding to the mature form, but also prevents their retrotranslocation into the cytosol. Finally, the sulfhydryl oxidase Erv1 transfers a disulfide bond to Mia40, reverting the latter to its initial state, thus ensuring the feasibility of additional rounds of precursor import and oxidation. The electrons that are removed during the formation of disulfides flow from the imported proteins via Mia40 to Erv1, and eventually to the cytochrome *c* oxidase via cytochrome *c* [87-92].

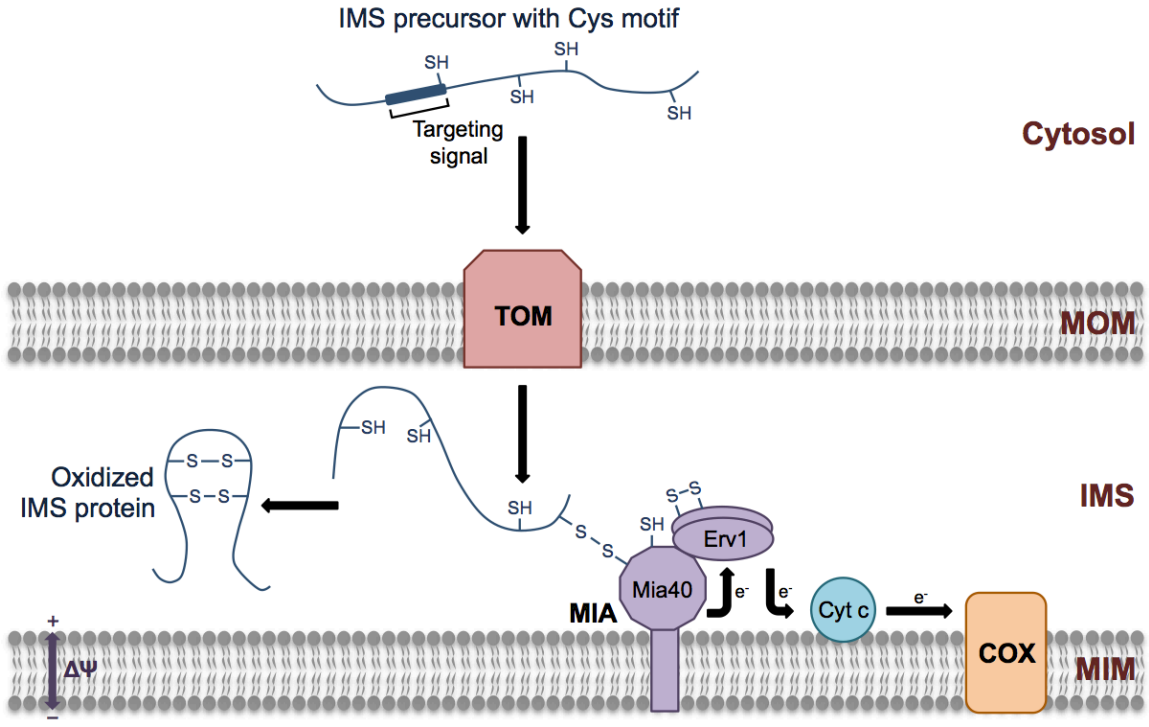

Figure 5. The internal targeting signal pathway for IMS proteins. IMS precursors containing characteristic Cys motifs traverse through the TOM complex. Mia40 binds the incoming precursor via a transient disulfide bond, which is subsequently transferred to the precursor. Erv1 then reoxidizes Mia40, and is reduced in the process. Electrons removed during protein oxidation flow from the precursor via Mia40 to Erv1 and finally to the respiratory chain through cytochrome *c*. ΔΨ, mitochondrial membrane potential; COX, cytochrome *c* oxidase; Cyt *c*, cytochrome *c*; Erv1, essential for respiration and viability; IMS, intermembrane space; MIA, mitochondrial intermembrane space import and assembly machinery; MIM, mitochondrial inner membrane; MOM, mitochondrial outer membrane; TOM, translocase of the outer membrane (Adapted from Becker *et al.* [41]).

It is important to note that membrane contact sites, in addition to playing an important role in passage of presequence-containing preproteins, also promote translocation of preproteins containing internal targeting signals. In the latter instance, MICOS bears particular importance as mitochondria deficient in this complex exhibit impaired protein import into the IMS and MOM. Indeed, physical contacts between MICOS and MOM proteins (e.g., TOM and SAM complexes) have been shown to facilitate efficient membrane insertion of proteins via MIA and β-barrel pathways. Thus, mitochondria employ a variety of MOM and MIM protein complexes to form multiple dynamic and transient contact sites, which allow import of distinct classes of precursor proteins [42].

1.4 Biological roles of mitochondria

Executing diverse yet interconnected functions, mitochondria are the 'yin and yang' organelles that, in addition to supporting cell's life by producing key biomolecules, can also mediate cell death under stress conditions [93]. The fact that we must breathe to stay alive is the consequence of our mitochondria demanding oxygen, an instance signifying the importance of mitochondria in our lives [94]. These cellular power houses supply energy necessary for performing almost all cellular activities [94], including force generation (e.g., during muscle contraction and cell division), synthesis, folding and degradation of proteins, and generation and maintenance of membrane potentials [5]. Moreover, mitochondria house enzymes involved in synthesis of lipids, ketone bodies, heme, iron-sulfur (Fe-S) clusters, etc., while concurrently facilitating degradation of

biomolecules via processes like fatty acid β-oxidation and the Krebs cycle. Furthermore, their central roles in thermogenesis, Ca^{2+} homeostasis, innate immunity and apoptosis further exemplify the essential duty they perform in almost all aspects of eukaryotic life [93]. The following section briefly discusses some crucial functions performed by mitochondria.

1.4.1 Roles in lipid metabolism, ketogenesis, and the Krebs cycle

The unique lipid composition of mitochondrial membranes is indispensible for maintaining the architecture and functioning of the organelle. Even though the majority of cellular lipid synthesis occurs in the endoplasmic reticulum (ER), mitochondria play an essential role in the biosynthesis of phospholipids, viz., phosphatidylethanolamine, phosphatidylglycerol and cardiolipin, which occurs in the MIM [95]. Among these, cardiolipin is regarded as the signature phospholipid of mitochondria that localizes predominantly in the MIM [3]. This unique mitochondrial lipid has been shown to interact with a wide range of MIM proteins, including electron transport chain complexes and the ADP/ATP carrier. Indeed, cardiolipin is required for optimal activity of complexes I, III, IV and V [96], and has been known to exert a stabilizing effect on respiratory chain supercomplexes [3]. Moreover, the functions of cardiolipin have also been extended to mitochondrial protein import, maintenance of inner membrane architecture and cytochrome *c* mediated apoptosis [3].

Apart from phospholipid synthesis, mitochondria are also responsible for generating a membrane lipid ubiquinone (coenzyme Q), which is an essential electron carrier in the respiratory chain [95]. Ubiquinone has an isoprenoid tail that makes it

highly hydrophobic, such that it can diffuse freely in the hydrophobic core of the MIM [97]. Operating in either one or two electron transfer reactions [97], ubiquinone emerges from complexes I and II in fully reduced form, ubiquinol, which is subsequently reoxidized to the initial form by complex III [95]. Another important class of lipids synthesized in mitochondria are the fatty acids. Interestingly, the enzymes involved in mitochondrial fatty acid synthesis share homology with the bacterial system, signifying the conservation of fatty acid biosynthetic machinery in the endosymbiont. Distinct from the cytosolic counterpart, mitochondrial fatty acid synthesis is essential for formation of lipoic acid, a cofactor that acts as a prosthetic group in α-ketoacid dehydrogenases [95], including pyruvate dehydrogenase and α-ketoglutarate dehydrogenase complexes [98]. The importance of mitochondrial fatty acid synthesis in cell physiology is revealed from the observation that yeast cells lacking this pathway have small mitochondria and a respiratory-deficient phenotype [99].

As an opposing phenomenon, the degradation of lipids, specifically of fatty acids, also operates in mitochondria. This phenomenon, fatty acid β-oxidation, was one of the first metabolic pathways discovered in the mitochondrial compartment. Subsequent identification of the Krebs cycle enzymes in the same organelle allowed the integration of these two important metabolic pathways via acetyl-CoA, as acetyl-CoA molecules generated during fatty acid oxidation typically feed into the Krebs cycle [3]. β-oxidation of fatty acids also directly produces reducing equivalents NADH and $FADH_2$, which donate electrons to the respiratory chain for energy generation. The oxidation of fatty acids serves as a central energy-yielding pathway in many organisms and tissues. For example, β-oxidation of fatty acids supplies ~80% of the energetic needs to mammalian

heart and liver under all physiological circumstances [98]. Fatty acid oxidation becomes even more important during fasting, when glucose supply becomes limited. Under such a situation, fatty acids can be directly used to generate energy by most tissues in our body, except the brain. Moreover, acetyl-CoA produced during fatty acid oxidation can be converted into ketone bodies in liver mitochondria by a process known as ketogenesis. Ketone bodies are an important energy source that can be used by all tissues in our body, including the brain [100]. The utilization of ketone bodies by the brain becomes particularly important during starvation, when glucose is unavailable. Under such conditions, ketone bodies are produced in copious amounts, and being water soluble, they travel readily via blood to peripheral tissues including the brain, where they are used as fuel [101].

The Krebs cycle, also known as citric acid cycle or tricarboxylic acid (TCA) cycle, occurs completely in the mitochondria in the vicinity of respiratory chain complexes [101]. It is an integral part of cellular respiration, a molecular process by which cells consume oxygen and release CO_2, the ultimate goal of which is generation of energy in the form of ATP [98]. As the final common metabolic pathway, the Krebs cycle constitutes enzymes that oxidize the acetyl group of acetyl-CoA produced from degradation of organic fuels (glucose, fatty acids and some amino acids) to two molecules of CO_2 with concomitant release of reducing equivalents, NADH and $FADH_2$, which in turn become substrates for the respiratory chain. Moreover, the Krebs cycle also generates numerous biosynthetic precursors (like succinyl-CoA for heme synthesis, α-ketoglutarate for glutamate synthesis, etc.) and hence is acknowledged as an amphibolic pathway [102].

1.4.2 Roles in synthesis of heme and Fe-S clusters

Heme is a biologically important iron containing compound present in hemoglobin, myoglobin and the cytochromes [103]. Its synthesis begins in the mitochondria by condensation of glycine and succinyl-CoA, latter being a Krebs cycle intermediate present only in this organelle. The condensed product is then decarboxylated to form δ-aminolevulinic acid [104], which is exported to the cytoplasm and transformed in a series of reactions to the ring-structured compound coproporphyrinogen III [3]. This compound then shuttles back into the mitochondrial matrix, where synthesis of heme is completed with conjugation of an iron to the center of the porphyrin ring [3]. Iron, being a transition metal, can readily accept and donate electrons, allowing it to act as an oxidant or reductant in a variety of biochemical reactions. In mammals, for example, iron in the heme is required for oxygen transport by hemoglobin, for deoxyribonucleotide synthesis as a component of ribonucleotide reductase, and as an electron acceptor/donor in the cytochromes during electron transport [105].

Fe-S clusters also are synthesized in the mitochondria. Comprised of iron and inorganic sulfur, Fe-S clusters are ancient, ubiquitous cofactors that serve as prosthetic groups of several proteins of prime biological importance [106]. Since they can bind electron-rich substrates, accept or donate single electron, and stabilize native protein conformation, Fe-S clusters play critical roles in facilitating enzyme activities in all forms of life [107]. Examples of proteins that require Fe-S clusters for their function include enzymes involved in DNA replication (helicases, primases), DNA repair (DNA glycosylase, Xeroderma pigmentosum group D protein, etc), ribosome assembly (Rli1/ABCE1), iron storage (ferredoxins), iron-sensing (cytoplasmic aconitase),

metabolism (mitochondrial aconitase), and electron transport (complexes I-III) [3, 106]. It is important to note that mitochondria are crucially involved in biogenesis of both mitochondrial and extra-mitochondrial (cytosolic and nuclear) Fe-S proteins. As some of the extra-mitochondrial Fe-S proteins (e.g., Rli1/ABCE1) are essential for cell viability [108], the indispensability of mitochondria in eukaryotic life can be linked to their involvement in Fe-S proteins biogenesis and assembly.

The enzymes responsible for biogenesis of Fe-S clusters are highly conserved in all kingdoms of life [106]. Indeed, iron-sulfur cluster machinery that generates the majority of cellular Fe-S proteins in bacteria has been inherited by eukaryotic cells from their endosymbionts [3]. Mitochondrial biogenesis of Fe-S clusters is a multistep complex process involving several dedicated protein complexes. In regard to mitochondrial proteins, Fe-S cluster biogenesis is essential for incorporation of Fe-S clusters into the Krebs cycle enzymes aconitase and succinate dehydrogenase, and into respiratory chain complexes I-III. Commonly found in the rhomboid [Fe_2–S_2], the cuboidal [Fe_3–S_4], and the cubane [Fe_4–S_4] forms, Fe-S clusters are generally attached to cysteine residues of the polypeptide chain; however, other amino acids like histidine may also participate in the interaction. For example, in the Rieske protein of respiratory chain complex III, two cysteines and two histidines coordinate the [Fe_2–S_2] cluster [106]. In yeast, Fe-S cluster biogenesis proteins have been known to reside exclusively in the mitochondrial compartment; however, growing evidence indicates that several key Fe-S cluster biosynthetic enzymes also localize in cytosol and/or nucleus in mammalian cells [107].

1.4.3 Role in thermogenesis

The proton gradient that is established across the MIM as a result of electron transport can be dissipated either through complex V with concomitant ATP production or by proton leakage without ATP production. The latter mechanism is adopted by brown adipose tissues for thermogenesis. This process utilizes an uncoupling protein, UCP1 (thermogenin) that accounts for ~6-14% of total MIM proteins in brown adipocytes [3]. When activated by long chain fatty acids [109], UCP1 acts as a proton transporter that abolishes the proton gradient, thereby stimulating respiratory chain activity. In effect, the free energy stored in the form of proton gradient is dissipated as heat, which is dispersed to the rest of the body via the circulatory system [110]. Because of its essential role in thermogenesis, UCP1 gene expression increases following a decrease in environmental temperature [111, 112]. Unlike brown adipose tissues, the white adipose tissues are best known for fat storage; however, cells within white adipose tissues can be induced (for example by cold or β3-adrenergic agonists) to develop into cells bearing characteristics of brown adipocytes. These cells, called beige cells, have high mitochondrial content with UCP1 clusters and hence possess thermogenic capacity. Indeed, brown adipocytes together with beige cells have been implicated in inducing weight loss and counteracting metabolic diseases, including obesity and type 2 diabetes [110, 113].

1.4.4 Role in Ca^{2+} homeostasis

Mitochondria buffer Ca^{2+} flux from plasma membrane and endoplasmic reticulum to maintain Ca^{2+} homeostasis [93], and the driving force for mitochondrial Ca^{2+} influx is $\Delta\Psi$ [94]. Ca^{2+} influx occurs primarily through VDAC in the MOM and the mitochondrial

calcium uniporter (MCU) complex in the MIM. The accumulated matrix Ca^{2+} is eventually removed through the actions of the Na^{+}/Ca^{2+} exchanger and H^{+}/Ca^{2+} antiporter [114]. The principal role of intramitochondrial Ca^{2+} rise is agreed to be the activation of the Krebs cycle [94]. Enzymes of the Krebs cycle, specifically α-ketoglutarate dehydrogenase and isocitrate dehydrogenase, are allosterically activated by Ca^{2+} binding [115]. Moreover, a Ca^{2+}-dependent phosphatase activates pyruvate dehydrogenase [116], the enzyme required for conversion of pyruvate to acetyl-CoA, the central substrate of the Krebs cycle. Conceptually, increased Krebs cycle activity results in increased ATP production. This elegant mechanism ensures tight coordination between energy supply with demand, as calcium signals are generally associated with work (contraction, secretion, etc.) [94]. However, mitochondrial Ca^{2+} overload, especially when accompanied by oxidative stress, can cause mitochondrial injury leading to cell death. This calcium overload-induced cell pathology occurs due to sustained opening of the mitochondrial permeability transition pore (mPTP), a large non-specific pore in the MIM that enables free passage of molecules up to 1.5 kDa. This results in dissipation of $\Delta\Psi$ across the MIM, diminishing oxidative phosphorylation and ATP synthesis. Moreover, high colloid-osmotic pressure in the matrix pulls water inside, resulting in matrix swelling, cristae unfolding, and MOM rupture. Cell death soon ensues through apoptosis and/or necrosis, depending on the level of cellular ATP [94, 117, 118].

1.4.5 Role in innate immunity

In 2005, an unexpected role of mitochondria in defense against RNA viruses was revealed. This mitochondrial-mediated antiviral immunity, occurring particularly in mammals, requires participation of an integral protein located in the MOM called the

mitochondrial antiviral signaling (MAVS) protein [119]. The invading viral double-stranded RNA in host cell cytoplasm can be detected by receptors like retinoic acid-inducible gene I (RIG-I) and melanoma differentiation-associated gene 5 (MDA-5) [120, 121]. The RNA-bound receptors then interact with MAVS, which acts as an adaptor between the receptors and various effectors, including tumor necrosis factor receptor-associated factors (TRAF2, TRAF3 and TRAF6). An intracellular signaling cascade is triggered that subsequently activates transcription factors nuclear factor κB (NF-κB) and interferon regulatory factor 3 (IRF-3). Activation of these transcription factors in turn causes rapid production of type I interferons (IFN-α and -β) and other proinflammatory cytokines, which together facilitate the subsequent development of adaptive antiviral immunity [122]. The importance of mitochondria in antiviral innate immunity is underscored by the observations that silencing the expression of MAVS abolishes NF-κB and IRF-3 activation by viruses, thus allowing viral replication. Conversely, MAVS overexpression induces activation of NF-κB and IRF-3, thereby boosting antiviral immunity [119]. In essence, mitochondria serve as a platform for antiviral defense and this phenomenon epitomizes a crucial role these organelles perform in signal transduction pathways [122].

1.4.6 Role in apoptosis

The mitochondrial apoptotic pathway is regulated by members of a protein family that share homology with the protein B-cell CLL/lymphoma 2 (Bcl-2). Possessing one or more Bcl-2 homology (BH) domains, Bcl-2 family members are divided into two groups on the basis of proapoptotic and antiapoptotic functions [123]. Antiapoptotic proteins like Bcl-2 and Bcl-X_L contain four BH domains (BH1-4) [124], whereas proapototic proteins

contain up to four BH domains and are classified into two subgroups on the basis the number of BH domains they possess [123]. Like the antiapoptotic counterparts, multidomain proapoptotic proteins (e.g., Bax, Bak and Bok) harbor four BH domains [124]. The remaining proapoptotic proteins (e.g., Bid, Bad, Bim, Puma, Noxa, etc.) possess only the third BH domain and hence are referred as BH3-only proteins. These proapoptotic and antiapoptotic members of Bcl-2 family control the mitochondrial apoptotic pathway by regulating the integrity of the MOM. Upon exposure to apoptotic stimuli (e.g., oxidative stress, UV-radiation, growth factor deprivation, etc.), BH3-only proteins are activated [123]. Once activated, the BH3-only proteins act either as activators (Bid, Bim, etc.) that directly activate Bax/Bak, or sensitizers (e.g., Bad, Noxa, etc.) that neutralize the prosurvival effects of antiapototic Bcl-2 proteins [125]. Under normal physiological conditions, Bax predominantly localizes in the cytosol, with a small fraction loosely attached to the MOM, whereas Bak is constitutively embedded in the MOM. However, following activation, Bax translocates from the cytosol to the MOM for membrane integration and homo-oligomerization [124]. Moreover, activated Bak also homo-oligomerizes within the MOM, and homo-oligomers of Bax and Bak participate in pore formation in the MOM, a process commonly referred as mitochondrial outer membrane permeabilization (MOMP) [123]. MOMP then acts as an exit for small proapoptotic molecules, including cytochrome *c* [126], Smac/Diablo [127], Omi/HtrA2 [128], AIF [129], and EndoG [130] to the cytosol. Among these, cytochrome *c* is considered as the prime culprit for apoptotic cell death because of its ability to initiate caspase cascade. Following its entry into the cytosol, cytochrome *c* binds to the adapter molecule APAF-1, causing its oligomerization and resulting in formation of a structure

called the apoptosome. The apoptosome recruits procaspase-9 and activates it, which in turn activates the executioner caspases-3 and -7. As their names suggest, these executioner caspases execute cell death by catalyzing cleavage of multiple cellular substrates. In addition, Smac/Diablo and Omi/HtrA2 promote caspase activity by antagonizing the activity of an endogenous inhibitor of caspase called XIAP [125]. Furthermore, EndoG and AIF released from mitochondria appear to participate in apoptosis by degrading nuclear DNA; however, their roles as essential apoptotic factors are still controversial [131].

1.4.7 Role in ATP synthesis

Inarguably, one of the most important functions of mitochondria is generation of ATP by cooperative activities of respiratory chain complexes and ATP synthase, in the process of oxidative phosphorylation or OXPHOS (Figure 6). The enzymes of the OXPHOS system are huge multi-subunit protein assemblies that include NADH:ubiquinone oxidoreductase (complex I), succinate:ubiquinone oxidoreductase (complex II), ubiquinone:cytochrome *c* oxidoreductase (complex III), cytochrome *c* oxidase (complex IV), and ATP synthase (complex V). Among these, complexes I, III and IV serve as proton pumps to transport protons from the matrix to the IMS, utilizing energy harnessed from electron transfer reactions. An electrochemical proton gradient is thus generated across the MIM and the energy of protons flowing back into the matrix via complex V is utilized to produce ATP from ADP and inorganic phosphate [132-134].

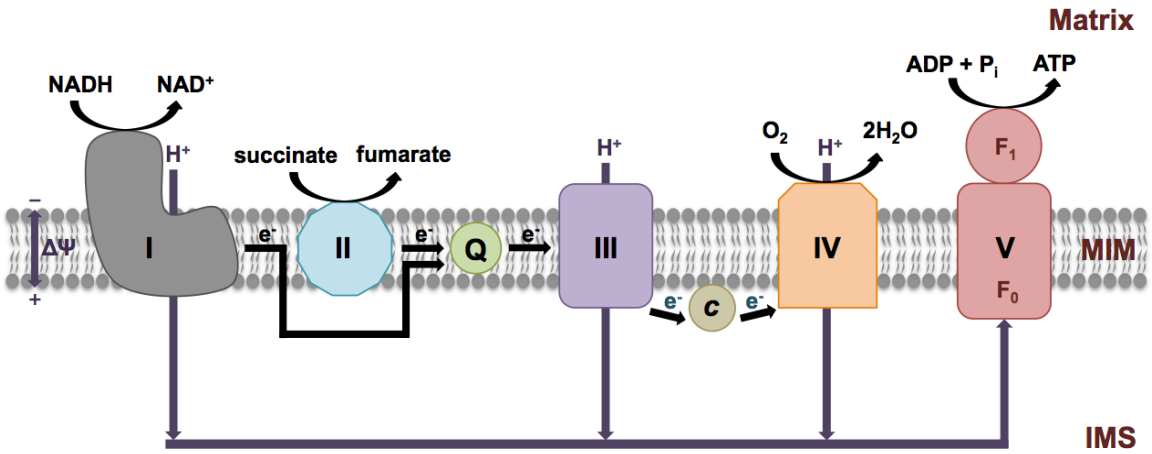

Figure 6. The OXPHOS system. The mitochondrial OXPHOS machinery includes proton-pumping complexes (I, III, and IV), which generate electrochemical proton gradient that in turn drives complex V for ATP synthesis. Complex I is the entry point for electrons donated by NADH, whereas complex II receives electrons from succinate oxidation. Membrane-integrated ubiquinone and soluble cytochrome *c* mediate electron transfer between different complexes. Electrons are finally donated to molecular oxygen to form water in a reaction catalyzed by complex IV. ΔΨ, mitochondrial membrane potential; *c*, cytochrome *c*; IMS, intermembrane space; MIM, mitochondrial inner membrane; Q, ubiquinone (Adapted from Schon *et al.* [135]).

The respiratory chain complexes I-IV harbor many redox cofactors that facilitate intra-protein electron transfer; however, electron transport between individual complexes is facilitated by mobile carriers, viz., membrane-integrated ubiquinone and soluble protein cytochrome *c*. Since the redox potentials of electron donors and acceptors gradually increase, free energy is liberated at each step along the chain [132]. This free energy is harnessed by proton pumps (particularly complexes I and IV) to undergo conformational changes, which in turn facilitate unidirectional flow of protons across the MIM [134]. In the following subsections, the stepwise flow of electrons through each respiratory chain complex, the associated proton translocation, and the mechanism of ATP generation are briefly discussed.

1.4.7.1 Complex I (NADH:ubiquinone oxidoreductase/ NADH dehydrogenase)

The first proton pump in the respiratory chain, complex I, is a gigantic enzyme through which the majority of electrons enter the respiratory chain [134]. Bovine complex I, for example, consists of 45 distinct subunits with a combined molecular weight of ~980 kDa [136]. Electron microscopy of complex I revealed an L-shaped structure with one arm embedded within the MIM (hydrophobic arm) and the other arm protruding into the matrix (hydrophilic arm). In mammals, the mtDNA encodes seven core subunits of complex I that are localized in the hydrophobic arm, and the remaining subunits are encoded by the nuclear genome [137].

The reducing equivalent NADH, produced during glycolysis, β-oxidation of fatty acids, and the Krebs cycle, is an electron-rich substrate that transfers two electrons to membrane-embedded ubiquinone in a reaction catalyzed by complex I. This complex

contains a non-covalently bound flavin mononucleotide (FMN), up to nine Fe-S clusters and at least two binding sites for ubiquinone. Electrons are transferred from NADH to FMN and then through a linear series of Fe-S centers to N-2 (an Fe-S protein), which donates electrons to ubiquinone (Q), reducing it to ubiquinol (QH_2). Mathematically, transfer of each electron from NADH to ubiquinone is coupled with translocation of two protons through the protein [134]; thus, a total of four protons are pumped from the matrix to the IMS. The overall reaction [98] can be written as:

$$NADH + 5\ H^+_N + Q \rightarrow NAD^+ + QH_2 + 4\ H^+_P$$

where N and P denote negative side (matrix) and positive side (IMS), respectively. Finally, ubiquinol (QH_2) diffuses across the lipid bilayer to donate electrons to complex III.

1.4.7.2 Complex II (succinate:ubiquinone oxidoreductase/ succinate dehydrogenase)

This complex catalyzes oxidation of succinate to fumarate, and two electrons released during the oxidation reaction are transferred to ubiquinone according to the equation [134]:

$$Succinate + Q \rightarrow Fumarate + QH_2$$

Mammalian complex II consists of four subunits with a combined molecular weight of 125 kDa [134]. Extending into the matrix, the hydrophilic subunits A and B are anchored to the membrane-spanning hydrophobic subunits C and D. Subunit A is a flavoprotein that, in addition to containing a covalently linked flavin adenine dinucleotide (FAD), possesses the binding site for succinate, whereas subunit B consists of a chain of

Fe-S centers [137]. Subunits C and D contain a heme group, heme *b*, and a ubiquinone binding site [98]. During succinate oxidation, electrons are transported from succinate to FAD, and then through Fe-S centers to ubiquinone. Heme *b* does not take part in the electron transfer process but is believed to play a structural role, stabilizing the assembly of the matrix-localized subunits and the transmembrane subunits [137]. Moreover, the presence of heme *b* has also been proposed to reduce the frequency of electron leak during succinate oxidation, thereby reducing the production of reactive oxygen species (ROS) in the process [98, 137].

Complex II has unique features that distinguish it from the rest of the respiratory chain complexes. First, all protein subunits of mammalian complex II are nuclear encoded, whereas a number of protein subunits of other respiratory chain complexes are encoded by the mtDNA. Second, complex II operates both in the respiratory chain and the Krebs cycle. Finally, it is the only complex in the respiratory chain in which electron transfer through the complex is not coupled with translocation of protons across the MIM [137].

1.4.7.3 Complex III (ubiquinone: cytochrome *c* oxidoreductase/ cytochrome bc_1 complex)

Complex III exists functionally as a homodimer. Each monomer is composed of eleven subunits with a molecular weight of 240 kDa. The catalytic core of the protein, however, consists only of three subunits: cytochrome *b*, cytochrome c_1 and an Fe-S protein (the Rieske Fe-S protein) [134]. Cytochrome *b*, the largest of the three core subunits, is encoded by mtDNA in all eukaryotes [137]. It consists of two ubiquinol/ubiquinone

binding sites, the Q_P and Q_N sites, and two heme *b* prosthetic groups, designated as b_L and b_H. Cytochrome c_1 houses a heme *c*, whereas the Fe-S protein contains a [Fe_2-S_2] cluster [134].

Ubiquinol produced from complexes I and II can diffuse along and across the MIM to complex III, where it is oxidized back to ubiquinone. The electrons released from the oxidation reaction are subsequently transferred to soluble cytochrome *c* in the IMS [137]. Even though this mechanism seems straightforward, complex III operates in a complicated fashion such that both oxidation of ubiquinol and reduction of ubiquinone are catalyzed during the same reaction cycle [134] (Figure 7). Commonly known as the Q-cycle, this phenomenon is a part of proton-translocating apparatus that substantially augments proton buildup in the IMS [134, 137]. The Q-cycle begins when the Q_P site in cytochrome *b* is occupied by ubiquinol, which then undergoes oxidation. Two protons released during the oxidation are expelled into the IMS, whereas two liberated electrons take different paths. One electron is passed to the [Fe_2-S_2] cluster that eventually transfers the electron to cytochrome *c* via cytochrome c_1. The second electron travels in series via b_L and b_H to the Q_N site where a molecule of ubiquinone is reduced to ubisemiquinone ($Q^{\bullet}$) [134]. The reaction equation for the first phase of Q-cycle is:

$$QH_2 + \text{cyt } c \text{ (oxidized)} \rightarrow \quad Q^{\bullet} + \text{cyt } c \text{ (reduced)} + 2\ H^{+}_{P}$$

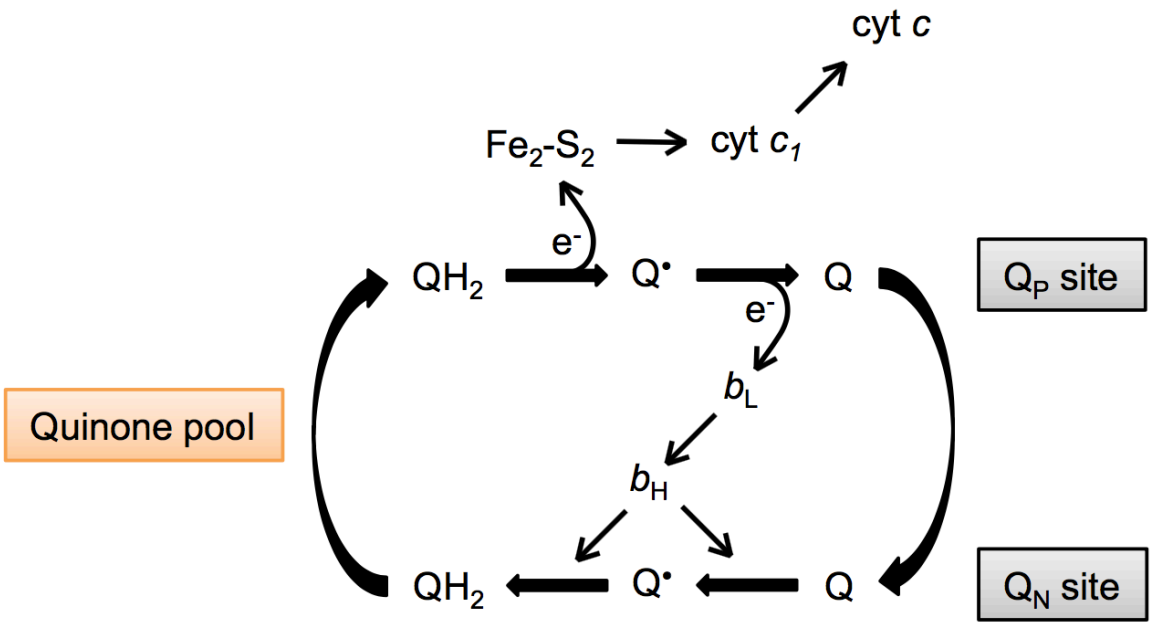

Figure 7. Mechanism of the Q-cycle. In the figure, thick arrows represent substrate transformation or movement, whereas thin arrows represent electron transfer. cyt *c*, cytochrome *c*; cyt c_1, cytochrome c_1; Q, ubiquinone; Q$^{\bullet}$, ubisemiquinone; QH_2, ubiquinol; Q_N and Q_P, ubiquinone and ubiquinol binding sites in cytochrome *b* located at the negative (matrix) and positive (IMS) sides, respectively (Redrawn from Schultz and Chan [134]).

In the second phase of the Q-cycle, another molecule of ubiquinol is oxidized at the Q_P site. The electrons and protons thus released follow the same routes as described above for the first phase except that the second electron is used to reduce ubisemiquinone present at the Q_N site that was formed during the first phase. This process results in formation of ubiquinol with a concomitant uptake of two protons from the matrix [134]. The reaction equation for the second phase is:

$$QH_2 + Q^{\bullet} + 2\ H^+_N + \text{cyt } c \text{ (oxidized)} \rightarrow \quad QH_2 + Q + \text{cyt } c \text{ (reduced)} + 2\ H^+_P$$

Therefore, four protons are liberated in the IMS for every two molecules of cytochrome *c* reduced, and the overall equation [98] for the Q-cycle is:

$$QH_2 + 2\ H^+_N + 2\ \text{cyt } c \text{ (oxidized)} \rightarrow \quad Q + 2\ \text{cyt } c \text{ (reduced)} + 4\ H^+_P$$

Cytochrome *c* is a water-soluble IMS protein that associates loosely with a leaflet of MIM facing towards the cytosol. Like ubiquinone, cytochrome *c* is a mobile electron carrier [97]. It has a single heme that accepts an electron from complex III, following which it travels along the membrane surface to complex IV to donate the electron [98].

1.4.7.4 Complex IV (cytochrome *c* oxidase)

Catalyzing the terminal step of respiration, complex IV transfers electrons from reduced cytochrome *c* to molecular oxygen, which is converted to water [134]. Reduction of molecular oxygen to two molecules of water requires four electrons from cytochrome *c* and four protons, which are withdrawn from the matrix [137]. Moreover, for each electron transfer, the complex pumps a proton from the matrix to the IMS [98]. Unlike complex III, which utilizes ubiquinone to transport protons across the MIM, complex IV

relies on conformational changes of its transmembrane ion channels to pump protons. In total, eight protons are extracted from the matrix, which boost the electrochemical gradient across the MIM [134]. Thus, the overall reaction [98] catalyzed by complex IV is:

$$4 \text{ cyt } c \text{ (reduced)} + 8\ H^{+}_{N} + O_2 \ \rightarrow \ 4 \text{ cyt } c \text{ (oxidized)} + 4\ H^{+}_{P} + 2H_2O$$

Complex IV consists of thirteen subunits with a combined molecular weight of 200 kDa [134]. The functional core of the complex is composed of subunits I-III, which are encoded by the mtDNA, while the remaining subunits are encoded by the nuclear genome. Subunits I and II facilitate electron and proton transfer reactions, whereas subunit III is believed to provide a channel for diffusion of oxygen to the site where it is reduced to water [137]. In addition to possessing a binding site for cytochrome *c*, subunit II contains a binuclear copper (two copper ions), Cu_A [137] that accepts electrons from cytochrome *c* [134]. Subunit I, on the other hand, possesses mononuclear copper ion (Cu_B) and two heme groups, viz., heme *a* and heme a_3 [98]. Heme a_3 and Cu_B participate to form a binuclear site where oxygen binds and is reduced to water [134]. Electron transfer through complex IV occurs in series from reduced cytochrome *c* to Cu_A, to heme *a*, then to heme a_3−Cu_B center and finally to the ultimate electron acceptor, molecular oxygen. Reduction of molecular oxygen requires four electrons; however, redox centers (Cu_A, heme *a*, and heme a_3−Cu_B) of complex IV carry only one electron at a time. The intermediates formed during the individual electron transfer reaction remain tightly bound to the complex, until conversion into water is completed [98].

1.4.7.5 Complex V (F_1F_0-ATPase/ ATP synthase)

The electrochemical proton gradient established as a result of proton pumping activities of complexes I, III and IV is utilized by complex V to generate ATP by the phosphorylation of ADP, according to the following equation [98]:

$ADP + P_i + n\ H^+_P \rightarrow ATP + H_2O + n\ H^+_N$ where n is in the range of 3-4 [134]. Complex V can, however, work in a reversible fashion and hence can pump protons to the IMS by utilizing energy from ATP hydrolysis under conditions of high [ATP]/[ADP] ratio and low $\Delta\Psi$. This complex consists of a membrane-embedded subcomplex F_0 and a matrix-residing subcomplex, F_1 [134] (Figure 8). The F_0 subcomplex forms a transmembrane channel through which protons traverse to drive ATP synthesis, catalyzed by the F_1 subcomplex [97]. The mammalian F_0 subcomplex consists of ten different subunits: a, b, c, d, e, f, g, A6L, F_6, and OSCP, in which eight copies of c-subunit form a ring structure that act as a conduit for proton translocation. In contrast to the c-subunit, single copies of subunits a, b, d, f, A6L, F_6, and OSCP are present in the subcomplex, while the stoichiometry of the remaining two subunits (e and g) has not yet been determined [138]. The F_1 subcomplex, on the other hand, is composed of five distinct subunits with the stoichiometry $\alpha_3\beta_3\gamma\delta\varepsilon$ and has a combined molecular weight of 371 kDa [134]. Alternating with α-subunits like the sections of an orange, each of the three β-subunits possesses a catalytic site for ATP synthesis [98]. The F_0 and F_1 subcomplexes are connected via central and peripheral stalks, whose formation requires participation of both subcomplexes [134]. The F_1 subunits γ, δ, and ε comprise the central stalk, which is attached to the c-ring, whereas the F_0 subunits b, d, F_6, and OSCP constitute the peripheral stalk, which lies to one side of the complex and holds the $\alpha_3\beta_3$ hexamer when

the central stalk rotates during proton translocation. In essence, complex V can be mechanically divided into a rotor component, which comprises c-ring along with γ, δ, and ε subunits, and a stator component consisting of $\alpha_3\beta_3$, a, b, d, F_6, OSCP subunits [138].

The passage of protons through the c-ring of the F_0 subcomplex triggers rotation of the ring and the attached central stalk [138]. The γ-subunit of the central stalk acts as a functional link between F_0 and F_1 subcomplexes such that, during its complete rotation with respect to $\alpha_3\beta_3$ hexamer, conformational changes occur in each three β-subunits, which drives ATP synthesis from ADP and inorganic phosphate. Thus, with each turn, three molecules of ATP are synthesized [97].

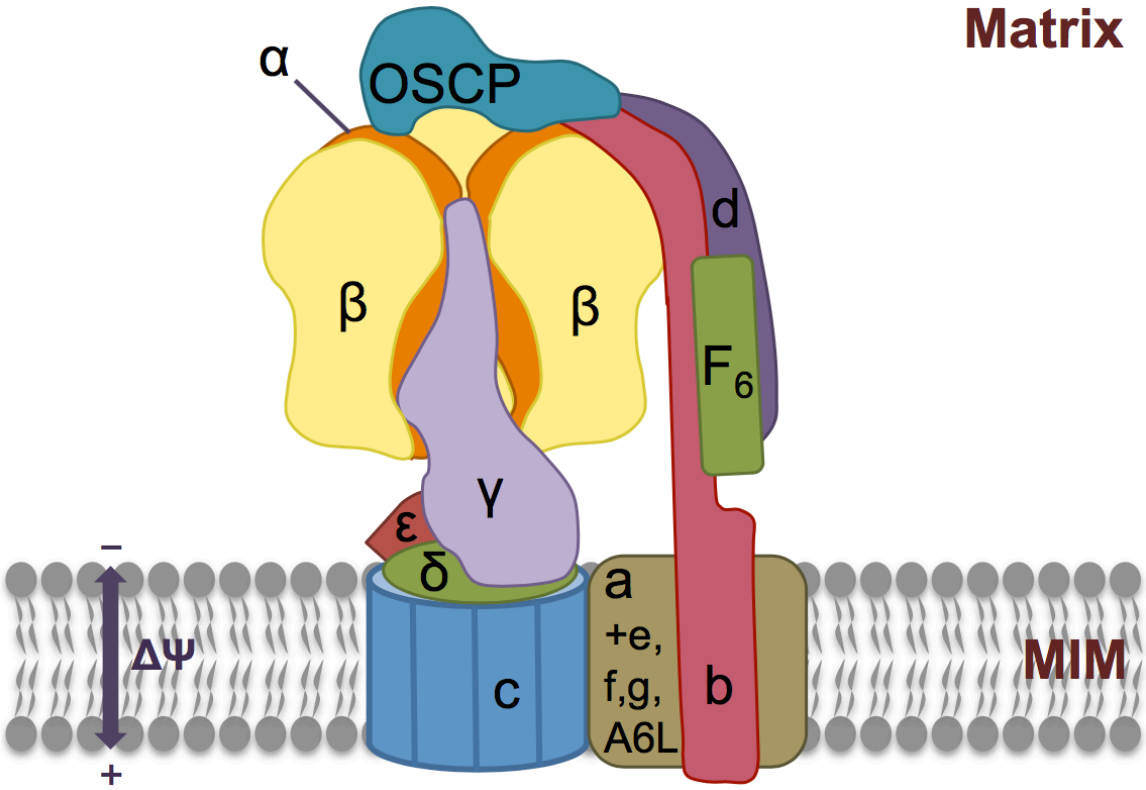

Figure 8. Human mitochondrial complex V. Complex V consists of two functional units, F_1 and F_0. F_1 is situated in the matrix and consists of five distinct subunits, whereas F_0 is integrated in the MIM and is composed of ten different subunits. F_1 subunits γ, δ, and ε form the central stalk, while the peripheral stalk is made up of F_0 subunits b, d, F_6 and OSCP. In the figure, one α-subunit is omitted to visualize the central stalk. ΔΨ, mitochondrial membrane potential; MIM, mitochondrial inner membrane (Redrawn from Jonckheere *et al.* [138]).

1.5 Mitochondria as sources of reactive oxygen species

Reactive oxygen species (ROS) is a broad term that collectively includes molecular oxygen-derived free radicals like superoxide anion radicals ($^{\bullet}O_2^-$) and hydroxyl radicals ($HO^{\bullet}$), as well as non-radical species such as hydrogen peroxide (H_2O_2) [139]. Single electron reduction of molecular oxygen produces $^{\bullet}O_2^-$, which is widely considered as a progenitor ROS, as it leads to formation of other reactive species such as $HO^{\bullet}$ and H_2O_2. Together, these molecules have the potential to impair cellular functions by inflicting oxidative damages to DNA, proteins and lipids [140-142].

In most cell types, mitochondria are the major intracellular source of ROS [140, 142], which is expected considering that ~1-2% of total oxygen consumed by mitochondria ends up in producing ROS [139]. These organelles possess various redox carriers through which single electrons can escape to incompletely reduce molecular oxygen so as to produce $^{\bullet}O_2^-$ [143], which in turn can be converted to H_2O_2 either spontaneously or by the action of mitochondrial superoxide dismutases (SOD) [144], according to the equation:

$$^{\bullet}O_2^- + {}^{\bullet}O_2^- + 2H^+ \rightarrow H_2O_2 + O_2$$

As mitochondrial proteins are loaded with metal cofactors such as hemes and Fe-S clusters, H_2O_2 can be converted to $HO^{\bullet}$ via the Fe^{2+}-dependent Fenton reaction [144], according to the following equation:

$H_2O_2 + Fe^{2+} \rightarrow Fe^{3+} + HO^- + HO^{\bullet}$ (where HO^- is a hydroxide ion)

The most potent species of its kind, $HO^{\bullet}$ is largely responsible for the cytotoxic effects of ROS [145]. It can also be produced from H_2O_2 and $^{\bullet}O_2^-$ via the Fe^{3+}-catalyzed Haber-Weiss mechanism [144], according to the equation:

$$H_2O_2 + {}^{\bullet}O_2^- \rightarrow O_2 + HO^- + HO^{\bullet}$$

A multitude of mitochondrial factors contribute to ROS generation, including components of the respiratory chain, pyruvate dehydrogenase complex, α-ketoglutarate dehydrogenase complex, monoamine oxidase, glycerol-3-phosphate dehydrogenase, dihydroorotate dehydrogenase and the electrochemical gradient across the MIM [139, 143]. Among these, a vast majority of mitochondrial ROS originate from respiratory chain complexes [140, 142], particularly at the level of complex III and complex I [139]. Indeed, complex III is regarded as the major ROS producer in mitochondria [146], as single electrons escaping from autooxidation of ubisemiquinone (at the Q_P site; Figure 7) and reduced cytochrome b_L substantially contribute to overall $^{\bullet}O_2^-$ production [144]. With respect to complex I, $^{\bullet}O_2^-$ production has been associated with the FMN prosthetic group and the ubiquinone-binding site located in the hydrophilic and hydrophobic arms, respectively [146]. In addition to these complexes, several lines of evidence also implicate two regions of complex II for $^{\bullet}O_2^-$ production, one located on the FAD cofactor and the other on the ubiquinone-binding site. Finally, complex IV does not seem to be involved in ROS generation under normal physiological conditions; however, hyperphosphorylation of complex IV during ischemic conditions has been known to facilitate electron slippage and $^{\bullet}O_2^-$ release [147]. The factors that regulate ROS generation from the ETC *in vivo* are largely vague; nonetheless, the redox status of the ETC clearly appears to be one of the major culprits. A reduced state of the electron

carriers, for example due to inhibition, increases their propensity to produce $^{\bullet}O_2^{-}$. Another important factor associated with ROS production is the electrochemical gradient across the MIM, which is composed of an electrical gradient (mitochondrial membrane potential; $\Delta\Psi$) and chemical gradient (ΔpH) [141]. A slight increase in the electrochemical gradient enhances mitochondrial ROS production; conversely, with a slight decrease, the opposite effect is observed [146]. In agreement with these observations, dissipation of the electrochemical gradient via proton ionophores have been linked with reduction of mitochondrial-mediated $^{\bullet}O_2^{-}$ production. From a physiological standpoint, proton leak through uncoupling proteins (UCP2 and UCP3), which are expressed in a wide variety of tissues, has been known to decrease generation of mitochondrial ROS [146].

When produced in excessive amounts, ROS can indiscriminately react with and damage a variety of biomolecules; their major victims being *bis*-allylic double bonds in lipids, cysteine and methionine residues in proteins, and the C8 position on deoxyguanosine [146]. Because mitochondria generate the majority of ROS in a typical eukaryotic cell, mitochondrial macromolecules such as mtDNA, proteins and lipids are believed to be primary targets of oxidative damage [140]. This notion is reinforced by the observation that mtDNA molecules, which are generally present in the immediate vicinity of respiratory chain complexes, experience a higher degree of oxidative damage than does nuclear DNA (nDNA) [142]. As mtDNA encodes indispensible components of the OXPHOS system as well as mitochondrial protein synthesizing machinery, oxidative insults that induce mtDNA mutation can impair either assembly and/or function of the respiratory chain, which in turn precipitates further ROS production. This positive

feedback loop leads to a vicious cycle resulting in severe energy depletion and eventually cell death [140]. Accordingly, excessive ROS accumulation and the accompanied oxidative stress have been correlated not only with tissue aging, but also with a multitude of pathological conditions, including cancer, neurodegenerative disorders, and metabolic diseases like obesity and type 2 diabetes [141, 146].

As persistent accumulation of ROS can elicit detrimental effects on cellular health, mitochondria employ a variety of mechanisms for their detoxification [146]. These antioxidant defense mechanisms include enzymatic as well as non-enzymatic components [143]. The non-enzymatic ROS detoxifying system mainly comprises glutathione (GSH), which, in addition to scavenging ROS directly, also donates electrons to several antioxidant enzymes. An additional non-enzymatic antioxidant component is α-tocopherol, which reduces lipid radicals and so protects membrane lipids from peroxidation. The enzymatic antioxidant system, on the other hand, includes, but is not limited to: (i) matrix-localized manganese SOD and IMS-localized copper-zinc SOD (both of which catalyze conversion of $^{\bullet}O_2^-$ to H_2O_2); (ii) catalase (reduces H_2O_2 to water) (iii) glutathione peroxidase (reduces H_2O_2 to water in the presence of GSH); (iv) glutathione reductase (converts oxidized glutathione (GSSG) back to its reduced form, i.e., GSH); (v) glutathione-S-transferase (adds GSH to toxic oxidized products like lipid peroxides); (vi) peroxiredoxins (Prx3 and Prx5; reduce H_2O_2 and lipid hydroperoxides); (vii) thioredoxin (Trx2; regenerate active Prx3 and Prx5); (viii) thioredoxin reductase (TrxR2; reduces oxidized Trx2); and (ix) glutaredoxin (reduces both protein disulfides and mixed disulfides with GSH) [143, 148, 149]. Moreover, the IMS-localized soluble protein cytochrome *c* has been found to accept electrons from $^{\bullet}O_2^-$ to facilitate its

removal [143]. Thus, under normal circumstances, a balance between ROS production and their detoxification ensures maintenance of intracellular ROS in a low, narrow range [140].

ROS were originally pictured as toxic waste of metabolism that participate only in cellular damage; however, a growing body of evidence now supports their role as chemical messengers in cell signaling [146]. In this context, H_2O_2 is widely considered as the prime candidate for a signaling molecule, because, in addition to being the most stable and abundant ROS, it is also membrane permeable and hence can diffuse within a cell [140, 146]. To act as a chemical messenger, the level of ROS in a cell seems to be important. Low to moderate increases in ROS have been shown to affect the activities of different redox-sensitive transcription factors. For example, a moderate increase in ROS activates NF-κB [150], a transcription factor that responds to cellular stresses. Interestingly, ROS-activated NF-κB has been shown to induce a variety of antioxidant genes, which in turn inhibit further ROS production to promote cell survival [145]. Another important transcription factor activated by mitochondrial-derived ROS is HIF-1α [151-153]. Following activation, this transcription factor upregulates expression of a wide array of genes, which eventually allows cells to adapt to and survive in hypoxic milieu [154]. Moreover, mitochondrial-derived ROS have been shown to activate other signaling pathways, including JNK1 [155] and p53 [156]. Thus, when generated in controlled fashion, mitochondrial ROS act as signaling molecules that facilitate communication between mitochondrial function and other cellular processes to sustain homeostasis and boost adaptation to stress [141]; on the contrary, high levels of ROS can massively impair cellular activities and trigger cell death [145].

2. MITOCHONDRIAL DNA REPLICATION AND INHERITENCE

2.1 Mitochondrial DNA: An introduction

Mitochondrial DNA (mtDNA) is a fossil molecule and its residence in the mitochondrial matrix substantiates the idea that endosysmbiosis did occur [157]. It is assumed that the mitochondrial genome, at the time of endosymbiotic event, was as large as those of the modern α-proteobacteria [158], the closest contemporary relative of the ancestral eubacterial symbiont [159]. During evolution, however, the majority of the genetic material of the α-proteobacterium progenitor was either lost or transferred to the nuclear genome, and this phenomenon is believed to be a part of the process for acquiring new functions by mitochondria [160]. Modern day mitochondria, thus, harbor remnants of the bacterial genome, which, in general, contains genes for multiple mitochondrial proteins together with components of the protein synthesizing machinery [158]. The ~16.6 kb human mtDNA, for example, encodes 13 protein components of the OXPHOS system along with 22 tRNAs and 2 rRNAs [158, 160]. Different eukaryotic species, however, display striking heterogeneity in size, physical form, and coding capacity of their mtDNA. The human malarial parasite *Plasmodium falciparum*, for instance, possesses the smallest known mitochondrial genome of ~6 kb that harbors 2 rRNA genes and 3 protein encoding genes [4]. Another interesting feature of this organism is linearity of its mtDNA, a topology found in a wide variety of organisms including *Saccharomyces cerevisiae* (fungi), *Euglena gracilis* (single-celled flagellate), and *Chenopodium album* (plant) [161]. In contrast to the mtDNA of *P. falciparum*, a flowering plant *Silene conica* contains the largest known mitochondrial genome of ~11.3 Mb, which exceeds the size of most bacterial genomes and even some nuclear genomes; nonetheless, it contains only 30

genes − 25 for proteins, 3 for rRNAs and 2 for tRNAs [162]. Intriguingly, mtDNA in *S. conica* has fragmented into dozens of 'chromosomes' (multichromosomal structure), comprising at least 128 circular mapping (circular monomeric) units that range from 44 to 163 kb in size [162]. Even though mitochondrial genome is typically perceived to comprise of a single 'chromosome', cases of multiple mapping mtDNA molecules have been reported in a variety of species. For example, the mitochondrial genome in a fungus *Spizellomyecs punctatus* consists of three distinct circular mapping molecules, whereas a protist *Amoebidium parasiticum* has several hundred distinct types of linear mtDNA molecules [159].

With respect to the coding capacity of mtDNA, the freshwater protozoan *Reclinomonas americana* is a remarkable example, which contains the largest compendium of mitochondrial genes identified so far in any eukaryotic species. Harboring 97 genes, its ~69 kb circular mitochondrial genome encodes not only for components of OXPHOS system and protein translational machinery, but also for those involved in protein import, protein maturation and mtDNA transcription [163]. A number of these genes are either completely absent or very rare in mtDNA from other species, but exist in bacterial genomes [164]. Its mtDNA also exhibit other striking features of bacterial genome, including operon-like gene clusters and putative Shine-Dalgarno motifs upstream of protein-coding genes [4]. Because of its marked resemblance to a typical bacterial genome, *R. Americana* mtDNA has been referred as "a eubacterial genome in miniature" [4].

2.2 mtDNA in budding yeast

2.2.1 Organization and topology

In 1963, a groundbreaking experiment using chick embryos led to the first clear identification of mtDNA, and a year later, budding yeast mitochondria were also revealed to possess their own genome. Soon after, mtDNA from some vertebrate species were isolated, and these extranuclear DNA molecules were shown to exist in a closed circular duplex form. Reinforcing the idea that mitochondria had originated from bacteria, which, in general, were known to possess circular genomes, the scientific community worldwide assumed that yeast mtDNA also had circular topology. This false belief persisted until 1991 when pulsed-field gel technology, for the first time, demonstrated that yeast mitochondrial genome predominantly existed in linear form [161]. These linear molecules are of variable sizes and occur as head-to-tail multimers (concatemers) of several genomic units [165-167]. Moreover, yeast mitochondria also possess a small number circular monomeric mtDNA molecules, which are believed to serve as templates for replication by rolling-circle mechanism to produce polydisperse linear tandem arrays of the genome (Section 2.3.1) [165]. Interestingly, concatemers constitute the major species of mtDNA in mother cells and non-dividing cells, whereas monomeric circles predominate in growing buds [168]. It is not clear, however, if circles are the functional units and the linear species act as replication intermediates only [169] or whether both structures are crucial for mitochondrial function.

The budding yeast mitochondrial genome accounts for ~15% of total cellular DNA, which is equivalent to ~50 monomeric copies per haploid cell [161]. The 85,779

bp monomer [170] measures over 25 μm [171] and is characterized by low gene density with only 8 protein encoding genes, namely for cytochrome *c* oxidase subunits I, II and III (*COX1*, *COX2* and *COX3* genes, respectively), ATP synthase subunits 6, 8 and 9 (*ATP6*, *ATP8* and *ATP9* genes, respectively), apocytochrome *b* (*COB* gene), and a ribosomal protein Var1 (*VAR1* gene; Figure 9) [170]. In addition, the mitochondrial genome contains genes for 2 rRNAs (15S and 21S), 24 tRNAs, the 9S RNA component of RNase P (involved in processing of mitochondrial tRNA precursors) and 8 replication-origin (*ori*) like elements (*ori* 1-8), of which four are believed to be active (*ori* 1, 2, 3, and 5) [170, 172]. Furthermore, the genome sequence contains several dispensable open reading frames and up to 13 introns; the latter are distributed among three different genes, viz., *COX1*, *COB*, and 21S rRNA. Several of these introns encode open reading frames that are translated to produce maturases, reverse transcriptases or site-specific endonucleases, and these dispensable proteins are involved in events like intron splicing and intron mobility in mitochondria [173].

Characterized by low GC content (~17%), yeast mtDNA contains a substantial amount of intergenic regions, which accounts for ~62% of the genome [174, 175]. Interestingly, the AT and GC base pairs are highly clustered in yeast mtDNA. The AT-rich sequences, which range from 150-1500 bp, comprise ~50% of the entire mtDNA sequence. On the other hand, the GC-rich sequences, commomly referred as GC-clusters, are ~50-80 bp long and constitute ~2-3% of the total mtDNA. These GC clusters are dispersed throughout the mtDNA, but are particularly enriched in the intergenic regions, and have been recognized as the preferential site of recombination in yeast mtDNA [172].

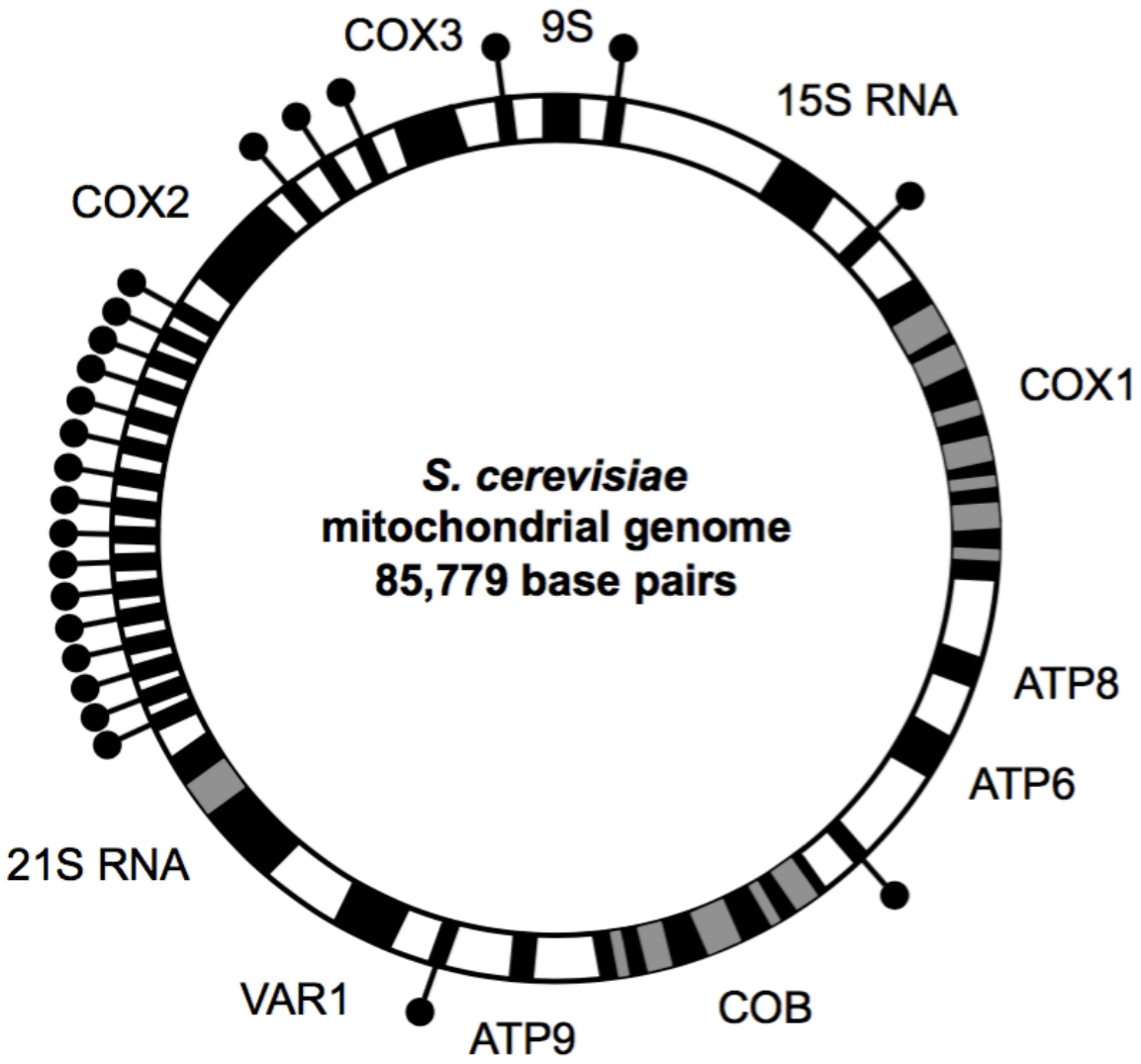

Figure 9. Schematic representation of *S. cerevisiae* mitochondrial genome. The circular monomeric mtDNA map reveals the locations of all genes, which are represented as black boxes. Intronic regions within *COX1*, *COB*, and 21S rRNA genes are indicated by grey boxes. Locations of tRNA genes are represented as sticks with filled circles (Redrawn from Ricchetti *et al.* [176]). Conceptually, the yeast mitochondrial genome is circular without fixed 5' and 3' ends. However, the majority of the yeast mtDNA molecules exist as linear concatemers because of the mode of replication it employs to propagate its mitochondrial genome (Section 2.3.1).

2.2.2 mtDNA nucleoids

Cellular DNA molecules do not occur as 'naked', but are rather shielded by a variety of proteins in intricate DNA-protein complexes. mtDNA molecules are no exception to this rule, as they are organized in nucleoprotein particles called nucleoids, a term used in analogous to DNA-organizing structures in bacteria. Each eukaryotic organism appears to have a distinct set of nucleoid-associated proteins that condense, protect, and regulate activities of mtDNA molecules. In most organisms, nucleoids contain 25 or more proteins, most of which are involved in nucleoid organization, mtDNA transactions (replication, transcription, repair, and recombination), protein quality control and metabolism [171]. The fact that proteins involved in mtDNA transactions occur in a nucleoid structure substantiates a notion that mitochondrial nucleoids are units of mtDNA inheritance that are transmitted to daughter cells with high fidelity [175].

In *S. cerevisiae*, nucleoids appear to be evenly spaced along the mitochondrial reticulum, tethered to the MIM [165]. Each yeast cell can contain ~10-40 nucleoids [165], with each nucleoid comprising of ~30 proteins that can shelter up to four mtDNA molecules [171, 175]. Moreover, each nucleoprotein particle appears somewhat spherical with a diameter of ~400 nm, supporting the idea that yeast mtDNA (which is >25 μm long) is massively condensed when packaged by nucleoid proteins [171]. This high degree of compaction is facilitated largely by Abf2, a *bona fide* mtDNA packaging protein [177] that is present at a ratio of ~1 molecule per every 15-30 bp of mtDNA [178]. Abf2 binds the majority of mtDNA, but preferentially at GC-rich sequences [177], and this interaction introduces sharp-angle curves (~78°) to mtDNA molecules [171]. This non-histone, high mobility group (HMG) protein displays homology to the DNA-

binding HMG proteins of nuclear chromatin [178]; however, unlike the nuclear counterparts which are known to regulate transcription and maintenance of DNA architecture, Abf2 lacks role a in mtDNA transcription and seems to be involved specifically in mtDNA packaging and protection [171, 177]. Indeed, Abf2 deficient yeast cells have less protected mtDNA, as evinced by increased sensitivity to nuclease attack, chemical damage and oxidative stress [171, 177]. Moreover, Abf2 has also been shown to bind and stabilize mtDNA-recombination intermediates, further highlighting the importance of this protective protein in overall mtDNA metabolism [171]. In addition to Abf2, a multitude of other nucleoid-associated proteins exist in yeast mitochondria, including those involved in mtDNA transactions (Rim1, Rpo41, Mip1, Pif1, etc.), mitochondrial protein quality control (Hsp60, Ssc1, Mdj1, Mge1, etc.), and metabolism (Aco1, Atp1, Idh1, Ilv5, etc.) [171]. Interestingly, the majority of identified nucleoid-associated proteins appear to be bifunctional: for example, aconitase (Aco1) and Ilv5, in addition to participating in carbohydrate and amino acid metabolism, respectively, also play an important role in maintenance of mtDNA as nucleoid components [171, 177].

Initially, nucleoids were believed to be static; however, evidence is now accumulating in favor of their dynamic behavior, and this dynamicity has been generally linked to metabolic status of yeast cells. For example, when cells are grown under respiring conditions (with glycerol as a carbon source), the ratio of Abf2 to mtDNA decreases and nucleoids attain more open structure. On the contrary, when respiration is repressed (with glucose as carbon source), nucleoids become more compact with a concomitant increase in Abf2 to mtDNA ratio. Thus, the abundance of Abf2 in nucleoids appears to determine the extent of nucleoid compaction [177]. As respiring growth

medium necessitates functioning of OXPHOS system, components of which are encoded by mtDNA, it seems plausible that loosening of nucleoids under such conditions favors mitochondrial gene expression, which in turn is expected to enhance respiratory activity.

2.2.3 Rho mutants

As a typical facultative anaerobe, budding yeast is able to fulfill its energy requirements with ATP produced via fermentation. Even in the presence of oxygen, yeast cells generate the majority of ATP via glycolysis with ethanol as a fermentative end product. Thus, the mitochondrial genome and the OXPHOS system in yeast become dispensable as long as the growth medium contains fermentable carbon sources (glucose, galactose, raffinose, etc.). However, the presence of an intact mitochondrial genome and functional OXPHOS system become essential when yeast cells are grown on non-fermentable carbon sources (acetate, ethanol, glycerol, etc.). Accordingly, yeast strains with dysfunctional OXPHOS system lack the ability to grow on medium containing non-fermentable carbon. These respiratory-deficient mutants are called petites, a term depicting their slow growth and small colony size when grown on medium containing limiting amounts of fermentable carbon sources [165, 179]. Petite mutants can arise spontaneously from wild-type cells, often at a frequency of ~1% per generation [180]. Because the factors governing the fitness of the mitochondrial respiratory system are encoded by nuclear as well as mtDNA, petite mutation can occur due to aberrations in either genome [179]. Respiratory-deficient strains that arise due to mutations in the nuclear genes are called nuclear petites or pet mutants, whereas mutants associated with abnormality in the mitochondrial genome are referred as cytoplasmic petites [165].

The budding yeast mitochondrial genome, also known as the *rho* factor (ρ), exists in a 'normal' state in wild-type cells, which are commonly referred as ρ^+ cells [161]. Because of their functional OXPHOS system, ρ^+ cells respire normally and form large colonies, a phenotype that led to another name – grandes. On the other hand, rho mutants are respiratory-deficient cytoplasmic petites, which are distinguished into two classes (ρ^0 and ρ^-) depending on the status of their mitochondrial genome. ρ^0 cells completely lack mtDNA [161], whereas ρ^- cells possess extensively deleted portion of ρ^+ mtDNA that is amplified and organized as oligomeric repeats [175]. Amplification of the residual ρ^+ mtDNA in ρ^- cells occurs to such an extent that the mass of ρ^- mtDNA is almost the same as that of ρ^+ mtDNA [169]. Even though replication and transcription of mtDNA persist in ρ^- strains, there is a lack of mitochondrial protein synthesis, which renders their OXPHOS system completely dysfunctional [173]. Once formed, ρ^0 and ρ^- cells do not revert to ρ^+ state indicating the irreversibility of cytoplasmic petite mutations. Interestingly, crosses of cytoplasmic petites with ρ^+ cells exhibit non-Mendelian segregation of the mutation, such that the progeny are either exclusively ρ^+ or mixture of ρ^+ and petite mutants in different proportions [181]. Accordingly, these petite mutants are divided into three major classes: neutral, suppressive and hypersuppressive [175]. If the mtDNA from petites is not transmitted to the progeny, such mutants are called neutral petites [181]. ρ^0 cells are neutral petites as they exclusively give rise to ρ^+ progeny after mating with ρ^+ cells. Crosses between ρ^- and ρ^+ cells can produce a moderate proportion of progeny containing ρ^- mtDNA, and such ρ^- mutants are called suppressive petites. In case when almost 100% of the progeny possesses ρ^- mtDNA, such mutants are called hypersuppressive (HS) petites [175]. The mitochondrial genome of HS petites harbors

tandem repeats of a short DNA fragment containing one of the active *ori* sequences [172]. It is believed that the reiteration of active *ori* sequence in HS ρ^- mtDNA provides it with a replication advantage over ρ^+ mtDNA, such that during crosses between HS petites and grandes, the mtDNA of the former out-replicates that of the latter to predominate in the zygotic progeny thereby resulting in hypersuppressiveness [161].

2.3 mtDNA replication models in yeast

S. cerevisiae mitochondrial genome is replicated by a dedicated mitochondrial polymerase, Mip1. Yeast strains devoid of *MIP1* gene immediately lose their mtDNA and become ρ^0, indicating the essential nature of its product in mtDNA maintenance. In addition to its 5′→3′ DNA polymerase activity, Mip1 is also endowed with 3′→5′ exonuclease activity and 5′-deoxyribose phosphate (5′-dRP) lyase activity, which are critical for ensuring the fidelity of mtDNA replication and for removal of the dRP moiety during short-patch base excision repair (Section 5.2.1), respectively. This highly processive DNA polymerase possesses a potent strand-displacement activity and operates as a single subunit, a feature that contrasts with the hetero-oligomeric nature of mitochondrial polymerase from most other eukaryotes [167]. Apart from the identity of Mip1, not much is known about mtDNA replication in *S. cerevisiae* with absolute certainty [167, 173]. Majority of this uncertainty is attributable to the initial belief of circular topology of its mitochondrial genome. Indeed, the erroneous theory, which lasted for almost 3 decades, has severely hindered our progress on understanding the

mechanism by which budding yeast replicates its mtDNA because the topology of the DNA molecule provides a crucial clue to its mode of replication [161].

The foremost question regarding mtDNA replication in *S. cerevisiae* is how it is initiated [173]. Till date, experimental evidences point towards two alternative, non-exclusive mechanisms for initiation: (i) transcription-dependent initiation in active *ori* mediated by the mitochondrial RNA polymerase Rpo41 (Figure 10), and (ii) recombination-dependent rolling-circle replication mediated primarily by the mitochondrial homologous recombinase, Mhr1 (Figure 11) [167]. Initially, the belief in the circularity of yeast mtDNA prompted scientists to search for transcription-dependent mitochondrial *ori* [173]. Successful in their quest, up to 8 *ori* were identified, of which 4 are believed to be active [170, 172, 173]. These *ori* are ~300 bp long and have a constant pattern as they contain 3 GC clusters (named A, B, and C; Figure 10) with AT stretches separating them. In the active *ori* (*ori* 1, 2, 3, and 5), a transcription initiation site (promoter), designated *r*, contains the consensus sequence for Rpo41 binding, which is always present upstream of the GC cluster C. The transcription-dependent replication is largely hypothetical and is limited to the initiation steps [169]. Even though evidences indicate that Rpo41 recognizes the transcription start site (*r*) to produce transcripts that are further processed to generate primers for replication, the necessity of Rpo41 in the initiation of mtDNA replication in ρ^+ strains is quite doubtful. This is because, *rpo41*-null strains are unable to maintain ρ^+ mitochondrial genomes, and their ρ^- mtDNA are still replicated. The ρ^- status of *rpo41*-null strains is most likely due to the loss of mtDNA transcription that disrupts mitochondrial protein synthesis, which in turn has been recognized as a causative factor for mtDNA instability [167, 173]. In sum, available

evidences indicate that mtDNA replication in *S. cerevisiae* is initiated, at least in some cases, in a transcription-dependent manner; however, the requirement of this pathway for propagation of the yeast mitochondrial genome is still an open question.

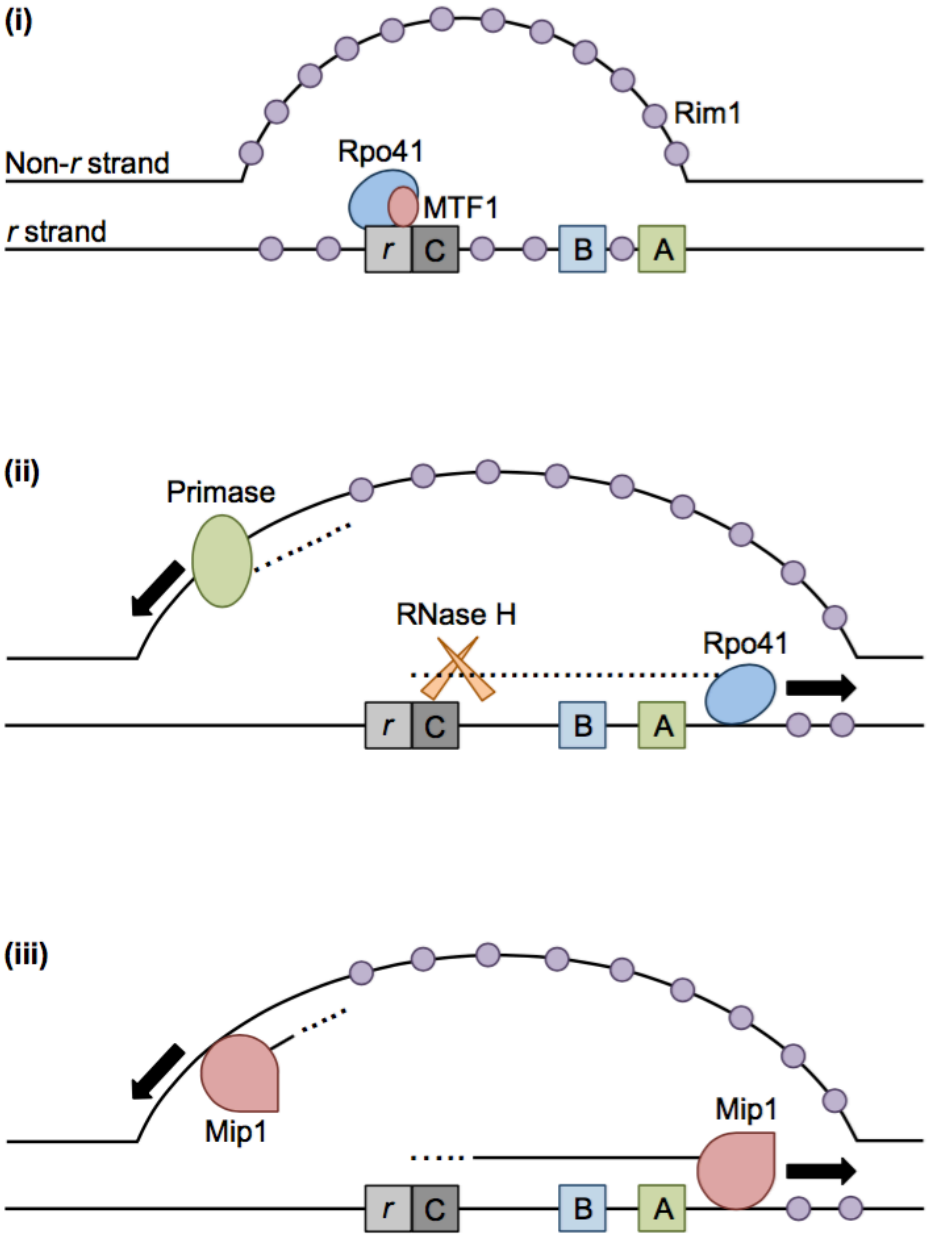

Figure 10. Model for transcription-dependent mtDNA replication initiation in *S. cerevisiae*. (**i**) Active *ori* are believed to be bidirectional that possess a promoter *r* in one of the DNA strands just upstream of a GC cluster C. MTF1, a mitochondrial RNA polymerase specificity factor, assists Rpo41 for binding to the promoter. (**ii**) Rpo41 extends a new RNA chain that is cleaved by an RNase H-like activity to generate a short RNA primer. On the non-*r* strand, RNA primer is believed to be synthesized by a primase upstream of the promoter *r*. (**iii**) Mip1 recognizes RNA primers and elongates them to new DNA chains. Rim1, a single-stranded DNA (ssDNA) binding protein, is believed to stabilize ssDNA formed during the process. In the figure, dotted line denotes RNA, continuous line represents DNA and black arrows show direction of replication (Redrawn from Lecrenier and Foury [169]).

2.3.1 Recombination-dependent rolling circle replication

The revelation that yeast mtDNA predominantly exists in linear concatemeric form, along with electron microscopic observation of lariat-shaped mtDNA molecules led to a hypothesis that yeast mtDNA replicates via a rolling-circle mechanism [173]. Indeed, a growing number of evidence supports this hypothesis with recombination between mtDNA molecules initiating rolling-circle replication, a phenomenon henceforth referred to as recombination-dependent rolling circle replication (RDRCR). As described later in the Section 2.4, this mode of replication also explains the finding that the major form of mtDNA in mother cells is concatemers, whereas circular monomers prevail in growing buds [167]. In general, DNA recombination is initiated by a double-strand break (DSB) that is processed to generate a single-stranded tail, to which a homologous DNA pairing protein binds [175]. The resulting nucleoprotein filament then invades a homologous double-stranded DNA (dsDNA), following which an intermolecular double strand, also known as heteroduplex joint, is formed between the single-stranded DNA and its complementary sequence in the dsDNA [182]. During this process, the invading single-stranded tail displaces one of the strands in the template dsDNA to produce a displacement loop, often referred as D-loop [166].

The mechanism of RDRCR has been primarily studied in hypersuppressive (HS) petites containing tandem repeats of *ori5*, which is believed to be the most active mtDNA replication origin [166]. *Ori5* possesses an atypical structure with an exposed single-stranded region, much like a bubble structure (Figure 11), as evinced by its sensitivity to ssDNA specific S1 nuclease and resistance to dsDNA specific restriction endonucleases [183]. Since they are more exposed in the ssDNA compared to dsDNA, the nucleobases

are preferentially modified by ROS in either strand of *ori5* region. Ntg1, a bifunctional enzyme with DNA glycosylase and apurinic/apyrimidinic (AP) lyase activities, recognizes oxidized pyrimidine bases at *ori5* [183]. Its DNA glycosylase activity removes the oxidized base, thus leaving an abasic site, which in turn becomes substrate for its AP lyase activity that introduces a single-strand break (nick) in dsDNA [184]. When two or more pyrimidine base lesions are closely apposed in opposite DNA strands, DNA glycosylase/ AP lyase can introduce double-strand breaks (DSBs) [185]. Accordingly, Ntg1 catalyzes a DSB specifically at *ori5* as base oxidation occurs in both strands of the replication origin [183]. A double-stranded DNA exonuclease, Din7, processes the DSB in the 5′→3′ direction to generate a 3′-single stranded tail [186], which is then coated by Mhr1, a homologous DNA pairing protein. Formation of a heteroduplex joint ensues as the resultant nucleoprotein filament invades a circular mtDNA molecule. Utilizing the latter as a template, the 3′-tail acts as a primer to initiate rolling-circle replication, which generates concatemers, thereby increasing mtDNA copy number [168, 183, 187]. It is believed that *ori5*, rather than being an orthodox replication origin, facilitates RDRCR by acting as a hot spot for recombination [161]. Even though the majority of these results were derived from strains with HS *ori5* ρ^- mtDNA, chronic exposure of ρ^+ cells to low levels of H_2O_2 has been positively correlated with an increase in mtDNA copy number, which strictly depended on the activity of Ntg1 as well as Mhr1. In essence, ROS appears to regulate mtDNA copy number via the Mhr1-dependent initiation of RDRCR facilitated by Ntg1-induced DSB in the single-stranded regions at *ori5* [183].

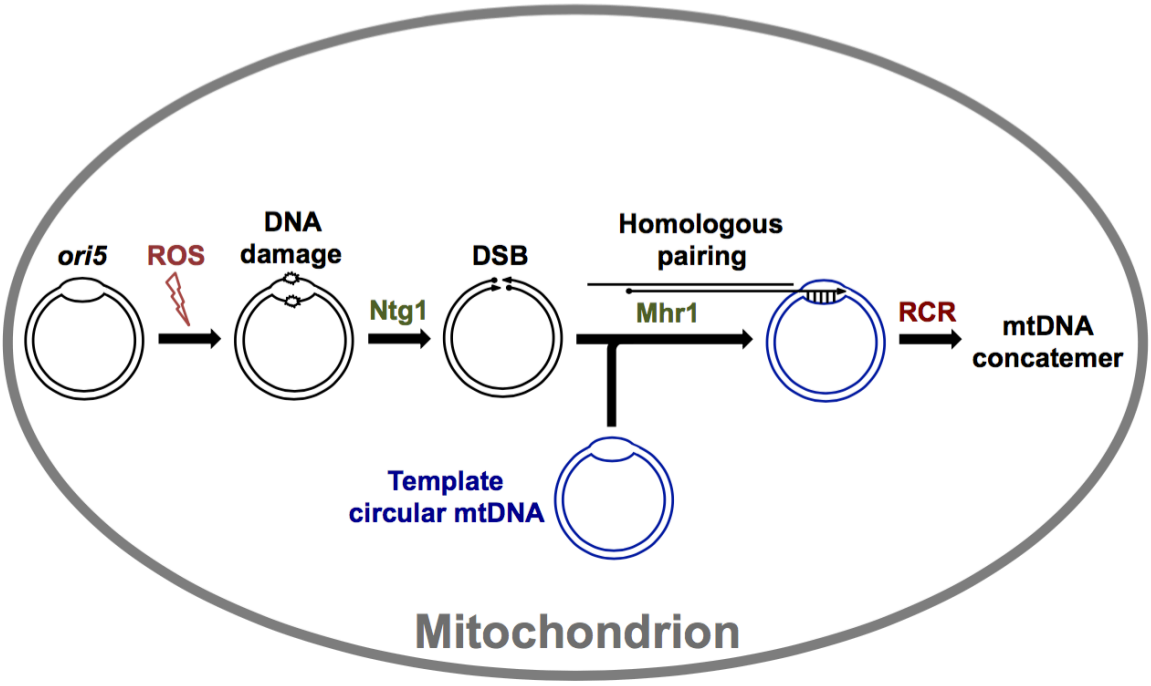

Figure 11. Model for recombination-dependent rolling circle replication of mtDNA in *S. cerevisiae*. ROS damage bases at an active mtDNA replication origin *ori5*, which has single-stranded character. Ntg1 recognizes these modifications and introduces a DSB. The 5′-ends of the DSB is processed to produce 3′ tails, to which Mhr1 binds and mediates invasion into a template circular mtDNA to form a heteroduplex joint. This is followed by the initiation of rolling circle replication resulting in formation of mtDNA concatemers. *ori5*, origin of replication 5; ROS, reactive oxygen species; DSB, double-stranded break; RCR, rolling circle replication (Adapted from Hori *et al*. [183]).

2.3.1.1 Mitochondrial homologous recombinase (Mhr1)

MHR1 was first identified as a gene required for mitochondrial genetic recombination that occurred after mating between yeast cells harboring different sets of mitochondrial alleles [166, 182]. This nuclear gene encodes Mhr1, a mitochondrial-matrix protein comprising of 226 amino acids residues with a molecular weight of 26.9 kDa [182]. Mhr1 facilitates heteroduplex joint formation *in vitro* in an ATP-independent manner [173, 175], a feature in contrast to the ATP-requiring activities of orthodox homologous pairing proteins such as RecA in prokaryotes and Rad51 in eukaryotes [166, 182]. The indispensability of Mhr1 in maintenance of ρ^+ mtDNA [173] is evident from the observation that mutation in its gene evokes mtDNA abnormality. For example, *mhr1-1* mutation, which is a single base mutation in the open reading frame of *MHR1*, results in replacement of an amino acid residue [188] that elicits temperature sensitivity to the maintenance of mtDNA [189]. When cultured at non-permissive temperature, some *mhr1-1* cells become ρ^0, whereas some show ρ^- phenotype [182]. This mutation abolishes homologous pairing activity of the protein *in vitro* and causes deficiency in mtDNA recombination after mating *in vivo* [182]. Moreover, *mhr1-1* mutation causes reduction in the amount of mtDNA concatemers whereas an opposite effect is witnessed following Mhr1 overexpression. These observations inarguably reinforce the central role of this protein in RDRCR [182]. Furthermore, *mhr1-1* cells also exhibit temperature-dependent delay in mtDNA segregation from mother cells into daughter cells during mitosis indicating that the protein also plays an important role in mtDNA partitioning [182]. Apart from its role in RDRCR, Mhr1 is also believed to be involved in repairing oxidative damages in mtDNA as its deficiency has been correlated with increased

mtDNA lesions [188]. Indeed, the multifunctional role of Mhr1 in mitochondrial biology of budding yeast is evinced from its presence not only in mitochondrial nucleoids [182] but also as a component of the large subunit of mitochondrial ribosome [190].

2.4 mtDNA inheritance in yeast

One of the traits of *S. cerevisiae* is its tendency to maintain a state of homoplasmy [173], a genetic condition of mitochondria in which all mtDNA molecules within a cell have identical nucleotide sequence [182]. Another interesting characteristics of this organism is biparental inheritance of mtDNA following mating between ρ^+ strains, a procedure that results in mtDNA heterogeneity. However, the resultant heteroplasmic state of the zygote is transient and homoplasmic cells arise within 20 mitotic cell divisions (vegetative segregation) [175, 182]. To explain this phenomenon, a segregative model has been proposed (Figure 12) in which concatemers determine the formation of homoplasmic cells from heteroplasmic zygotes. According to this model, a few circular mtDNA molecules are randomly chosen as templates for RDRCR to form concatemers that are selectively transmitted to daughter cells, where the concatemers are processed into circular monomeric mtDNA molecules [175]. Indeed, pulse chase experiments with [methyl-^{14}C] thymidine to label mtDNA have revealed that the concatemeric mtDNA in mother cells is the immediate precursor of mtDNA monomers in buds [187]. As mtDNA concatemers formed as a result of RDRCR consist of multiple monomeric mtDNA molecules whose nucleotide sequence are identical to the template mtDNA, the selective partitioning of mtDNA concatemers clearly explains quick segregation of homoplasmic

cells from heteroplasmic ones. Mhr1, a key protein involved in RDRCR, is at the center stage of this model, as its activity has been positively correlated not only with formation of mtDNA concatemers but also with the rate of segregation of homoplasmic cells [182].

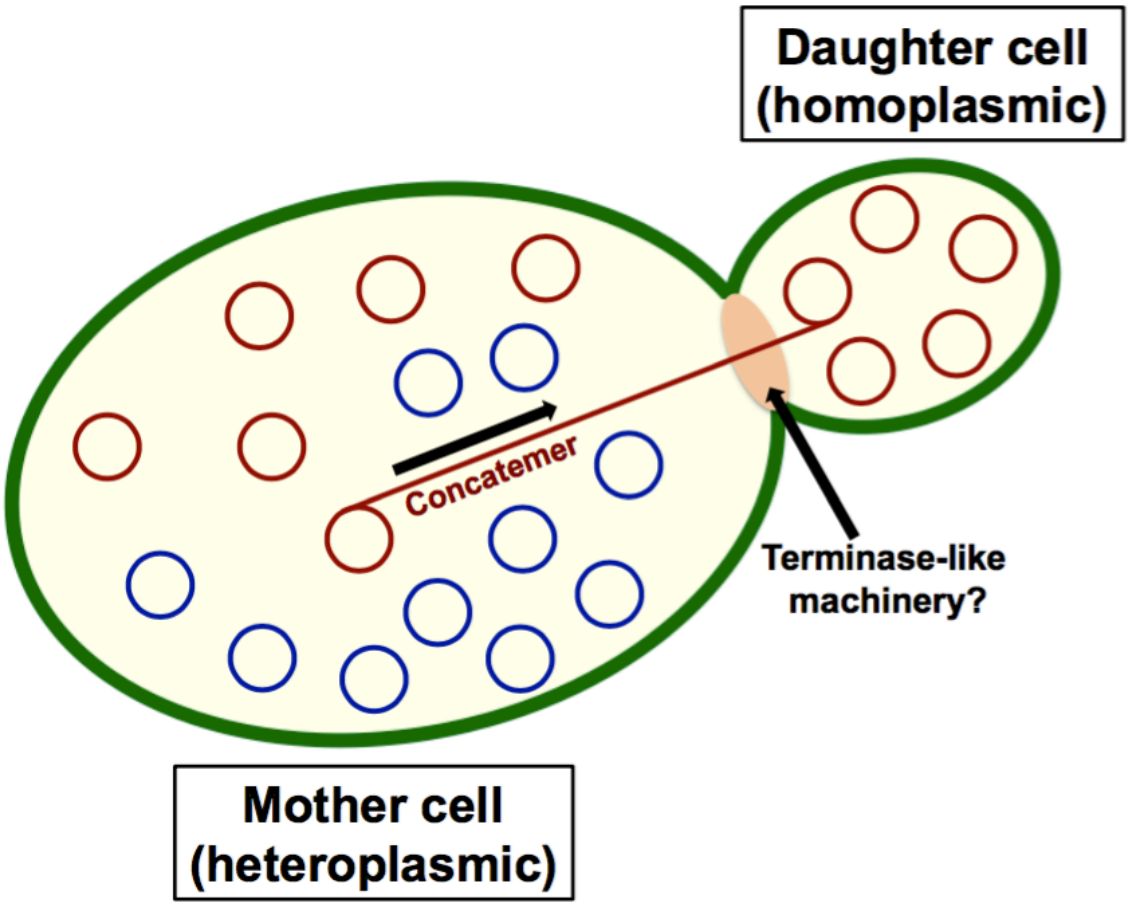

Figure 12. Model for mtDNA inheritance in *S. cerevisiae*. A template circular mtDNA (red circle) is randomly selected in the heteroplasmic mother cell to produce concatemers. These linear multimers of mtDNA are selectively transmitted to a daughter cell, where they are processed into circular monomers resulting in a homoplasmic state. Features analogous to these are also observed in the late phase of DNA replication and packaging in *Escherichia coli* lambda phage, in which concatemers formed as a result of a recombination-dependent mechanism are selectively packaged as a single genome unit into phage capsid with the help of an ATP dependent motor protein called terminase. Such terminase-like proteins are hypothesized to be involved in processing of mtDNA concatemers into circular monomers in daughter cells. In the figure, red and blue circles represent monomeric circular mtDNA molecules whereas the red line represents a mtDNA concatemer (Redrawn from Ling *et al*. [166]).

2.5 mtDNA in humans

2.5.1 Organization and topology

Following strict inheritance through the maternal lineage [191], the human mitochondrial genome typically forms 5 μm double-stranded, closed-circles of one genome length consisting of 16569 bp (Figure 13) [192]. Unlike in yeast, human mtDNA exhibits remarkable economy of organization as the genes lack introns, and intergenic sequences are either absent or reduced to a few nucleotides [193, 194]. This gene-dense molecule harbors 37 genes, 13 of which encode essential components of the OXPHOS system and include seven subunits of complex I (ND1, 2, 3, 4, 4L, 5 and 6), one subunit of complex III (Cyt *b*), three subunits of complex IV (COX I, II and III), and two subunits of complex V (A6 and A8). The remaining 24 genes specify the RNA elements required for translation of those 13 polypeptides and include two rRNAs (12S rRNA and 16S rRNA) and 22 tRNAs [135].

The human mitochondrial genome constitutes ~1% of total cellular DNA [194] and is typically maintained at a high copy number [195]; however, the copy number can vary tremendously among different cell types [196]. For example, a sperm cell can contain as little as 100 copies whereas an unfertilized oocyte can harbor hundreds of thousands of mtDNA molecules [196]. Interestingly, the content of guanosine plus thymine in one strand of the duplex of mammalian mtDNA differs from the other strand. This difference is largest in human mtDNA, and decreases gradually down the evolutionary tree. Because of this bias in nucleotide composition, the two strands of mammalian mtDNA display different buoyant densities in denaturating caesium chloride

gradient such that they can be physically separated as the 'heavy' (H) and 'light' (L) strands [197]. The vast majority of the genetic information is localized in the H-strand that contains 28 genes (for 2 rRNAs, 14 tRNAs, and 12 polypeptides), with the L-strand possessing the remaining 9 genes (for 8 tRNAs and a single polypeptide) [193]. Regulatory elements in human mtDNA are localized in two noncoding regions [194]: a small noncoding region of 30 bp harbors an origin of L-strand synthesis (O_L), whereas the major noncoding region, also known as NCR, spans just over a kilobase and concentrates almost all the noncoding DNA [192, 194]. An essential control region of mtDNA, NCR harbors the H-strand origin of replication (O_H), a single L-strand promoter (LSP), and one of two promoters of the H-strand (HSP1) [192]; a second H-strand promoter (HSP2) is positioned downstream of HSP1 and lies within the $tRNA^{Phe}$ gene (Figure 13) [195]. In the majority of vertebrate mtDNA duplexes much of the NCR is occupied by a short three-stranded structure, called the displacement loop or D-loop, so named because a short DNA molecule of 650 nucleotides displaces the H-strand and becomes complementary to the L-strand [192, 193, 198]. The importance of the NCR in maintenance of human mitochondrial genome can be validated from the observation that all partially deleted human mtDNA molecules that have been characterized retain this regulatory element; even though, about a quarter of D-loop region seems to be expendable [192].

Human mtDNA is generally depicted as single genome-sized circles; however, its topology can vary in some cell types. As an example, mitochondria of HEK cells contain catenanes of two or more interconnected circles, which constitute up to 30% of mtDNA molecules. Another striking example is observed in mtDNA from adult human heart,

which is partially organized in large catenated molecules with dozens of genome units containing abundant recombination and replication junctions. Such complex forms of mtDNA seen in human heart exhibit age dependency as they are absent in newborns and are progressively acquired in early childhood [198]. Moreover, this unusual mtDNA structure seems to be specific only for adult human hearts, as hearts from mouse, rabbit and pigs are devoid of such topological variation [199].

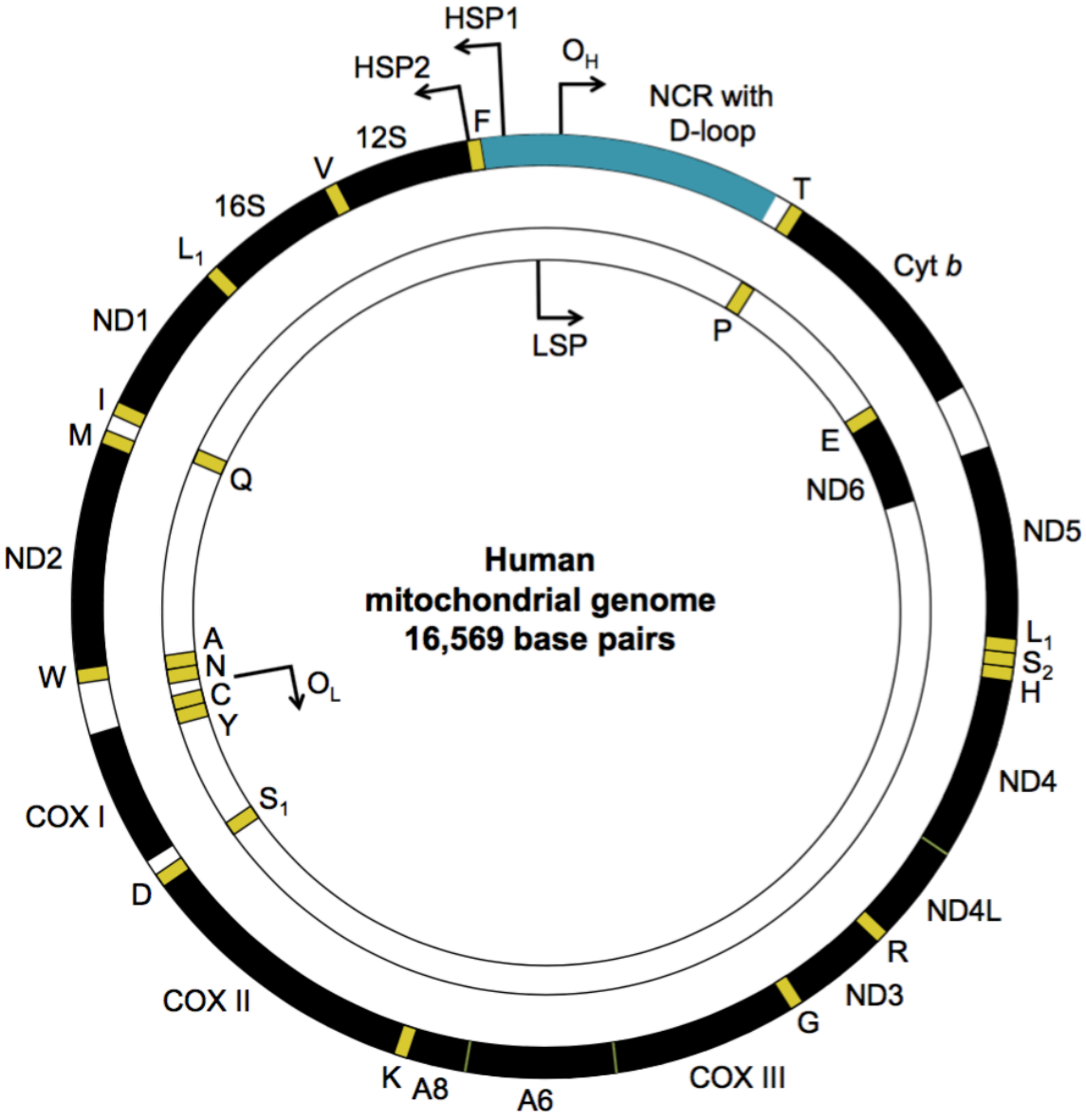

Figure 13. Schematic representation of human mitochondrial genome. In general, the human mtDNA is a closed-circular, double helix in which the outer and inner circles designate the H-strand and L-strand, respectively. It encodes essential protein components of the OXPHOS machinery as well as RNA elements that are required for translation those proteins. In the figure, black boxes depict the genes encoding 13 polypeptides and 2 rRNAs (12S and 16S), whereas yellow boxes designate the genes coding for 22 tRNAs (labeled as one-letter amino acid symbol). NCR containing D-loop region is shown as a blue box, while the arrows indicate the origins of replication and promoters for transcription (Adapted from Schon *et al*. [135], and Stewart and Chinnery [196]).

2.5.2 mtDNA nucleoids

Analogous to yeast, mtDNA molecules in humans are packaged by a variety of mtDNA-binding proteins [171] to form nucleoprotein complexes that are primarily inner membrane associated [195] and dispersed throughout the mitochondrial network [200]. Human cells can contain as many as 800 nucleoids [171], which appear roughly spherical [171, 200] with an average diameter of ~100 nm [200]. What is still an unsettled issue in the field of nucleoid biology is the number of mtDNA present in each nucleoid [201]; nonetheless, the majority of available evidence implies that one nucleoid can shelter up to 10 mtDNA molecules [171]. With respect to the protein components, TFAM (transcription factor A, mitochondrial) is undoubtedly the most prominent nucleoid-associated protein in human cells [198]. Like its yeast counterpart Abf2, TFAM is a member of the HMG family of proteins that plays a crucial role in structural organization of nucleoids [198]. In addition to actively packaging DNA, TFAM exhibits cooperativity in DNA binding as its affinity for DNA increases by previously bound TFAM [202]. When attached, TFAM induces a 180° bend to the mtDNA, causing a dramatic U-turn and this feature substantially contributes to a high degree of mtDNA compaction as observed in human nucleoids [200]. Possessing the ability to bind to any DNA sequence, TFAM is believed to fully coat human mtDNA [200], which is expected given the fact that one TFAM molecule can interact with ~20-30 bp of mtDNA [200]. However, the amount of mtDNA-associated TFAM might vary considerably depending on the cell type [178]. For example, the ratio of TFAM to mtDNA was found to be as high as 1700:1 in HeLa cells and as low as 50:1 in HEK293 cells [171]. In addition to its role in packaging and maintenance of mtDNA, TFAM is also critical for mitochondrial transcription and

replication, features that are completely absent in its yeast homologue Abf2 [200]. In fact, TFAM was originally identified as a transcription factor involved in the assembly and promoter recognition of the mitochondrial transcription machinery [178]. Because initiation of human mtDNA replication depends on an RNA primer formed by transcription (Section 2.6), the role of TFAM in mtDNA replication is also quite apparent [200]. Therefore, it is not surprising that, in spite of its ability to bind to most of the human mitochondrial genome [171], TFAM preferentially associates with regions upstream of mtDNA transcriptional promoters [200].

Apart from TFAM, the human mitochondrial nucleoid is composed of an array of additional proteins with diverse function, ranging from mtDNA transaction (mitochondrial ssDNA binding protein, polymerase γ, Twinkle helicase, mitochondrial RNA polymerase, etc.) to factors involved in protein quality control (Lon protease, HSP60, HSP70, etc.), metabolism (aspartate aminotransferase, adenosine nucleotide transferase, carbamoyl phosphate synthetase, ATPase β subunit, etc.), cellular architecture (actin and vimentin) and signal transduction (prohibitin 1, prohibitin 2, etc.) [171, 202]. Apparently, some of these nucleoid-associated proteins do not directly interact with mtDNA, and as an explanation, a 'layered' structure of human mitochondrial nucleoid has been proposed. In this model, nucleoid-associated proteins are classified into core components that directly bind to mtDNA, and peripheral components that do not interact with mtDNA but associate with the core components via protein-protein interaction. The core nucleoid proteins include those involved in mtDNA packaging, replication and transcription (such as TFAM, polymerase γ, mitochondrial RNA polymerase, etc.) whereas the peripheral proteins include those involve in

translation and complex assembly (including ATAD3, prohibitin 1, prohibitin 2, etc.) [200-202]. Because some of these peripheral proteins are components of the nucleoids as well as the inner membrane, they are believed to serve as anchors that tether nucleoids to the MIM thereby ensuring even distribution of mitochondrial genetic material throughout cell's mitochondria [201, 202].

2.6 mtDNA replication models in humans

The human mitochondrial genome is replicated by DNA polymerase γ (pol γ) in concert with additional replisome components that include Twinkle helicase, mitochondrial RNA polymerase (POLRMT), mitochondrial single-stranded DNA binding protein (mtSSB), topoisomerase, RNaseH1, and mitochondrial DNA ligase III [196, 203]. Among these, pol γ, Twinkle helicase, POLRMT, and mtSSB are believed to be the core factors that drive mtDNA replication as the process can be reconstituted *in vitro* with these proteins [204]. The human pol γ, which is essential for maintenance of mtDNA, is a 195 kDa heterotrimer consisting of a catalytic subunit (p140) and a homodimeric processivity subunit (p55). The p140 subunit possesses catalytic sites for 5′→3′ DNA polymerase, 3′→5′ exonuclease, and 5′-deoxyribose phosphate (5′-dRP) lyase activities, whereas the p55 accessory subunit is responsible for enhancing the binding affinity of the holoenzyme to the template mtDNA [203, 205].

In animal cells, replication of the mitochondrial genome is a complex and slow process, taking about an hour to synthesize both daughter strands [203]. Even though the majority of critical factors responsible for efficient mtDNA replication have been

identified [204], the exact mechanism of human mtDNA replication has not been completely delineated and two predominant theories exist: the strand-displacement model (SDM) and the ribonucleotide incorporation throughout the lagging strand (RITOLS) model (Figure 14) [206]. According to the SDM, the leading and lagging strands (complementary to the parental L and H-strands, respectively) are synthesized asynchronously and unidirectionally from two distinct replication origins: O_H and O_L. Initially, POLRMT generates a ~100 nucleotide RNA primer from LSP located within the NCR and this abortive transcript initiates leading strand synthesis at O_H. The mitochondrial replisome then starts extending the primer continuously around the circular genome. Because of template unwinding an extensive region of the H-strand is displaced and becomes single-stranded, which is believed to be bound and stabilized by mtSSB. The mtSSB not only protects the ssDNA but also prevents nonspecific priming of the lagging strand by POLRMT. After about two-thirds of the leading strand is synthesized, the passing replication fork unwinds and reveals O_L, which then assumes a stem-loop structure. This unusual topology of O_L prevents mtSSB binding, but facilitates recruitment of POLRMT for synthesis of an RNA primer [204, 207]. After polymerization of ~25 nucleotides, pol γ replaces POLRMT at the 3′ end of the primer and initiates lagging strand DNA synthesis, which proceeds in the opposite direction in a continuous manner [208]. The ultimate result is the duplication of the entire genome, with the synthesis of the lagging strand completing after the leading strand [204].

Evidence also exists for RITOLS model, an alternative replication mode that actually agrees with SDM for the most part. The real contention between the SDM and RITOLS models occurs on the mode by which the displaced ssDNA resulting from the

asynchronous replication is protected [206]. According to RITOLS, formation of the single-stranded region during mtDNA replication is prevented as processed RNA transcripts are laid down in a 3′→5′ direction complementary to the displaced H-strand (Figure 14) [203]. In support of this model, some mtDNA replication intermediates have been found to be predominantly double-stranded containing RNA-DNA hybrids. Because RNAs were present in every region of the parental H-strand (the lagging strand template) tested, a theory that ribonucleotides are incorporated throughout the lagging strand was proposed. Furthermore, the RNA transcripts are postulated to remain 'threaded' on to its template until they are displaced, degraded or further processed during lagging strand DNA synthesis [209]. The RITOLS model argues that formation of extensive ssDNA tracts is highly unlikely, because these tracts, even if coated with proteins would be fragile, which would cause potential disaster for genome stability [209] and reasons that the template H-strand would be more protected from base damage or single-strand breaks when duplexed with mitochondrial RNA [203]. Moreover, RITOLS challenges the validity of SDM with a conjecture that the large stretches of ssDNA as observed in SDM may have occurred due to RNase contamination during the mtDNA isolation process [204]. Of the two models, however, there is probably stronger evidence in favor of SDM. Indeed, results from very recent experiments with mitochondria obtained from HeLa cells revealed adequate amount of mtSSB *in vivo* to envelop the displaced parental H-strand during mtDNA replication. Moreover, utilizing immunoprecipitation and DNA sequencing, mtSSB was shown to bind exclusively to the H-strand and there was a gradient of mtSSB occupancy from high to low immediately downstream of O_H towards

O_L, in a clockwise direction. These observations firmly corroborate the idea that mtSSB stabilizes the displaced H-strand during mtDNA replication [208].

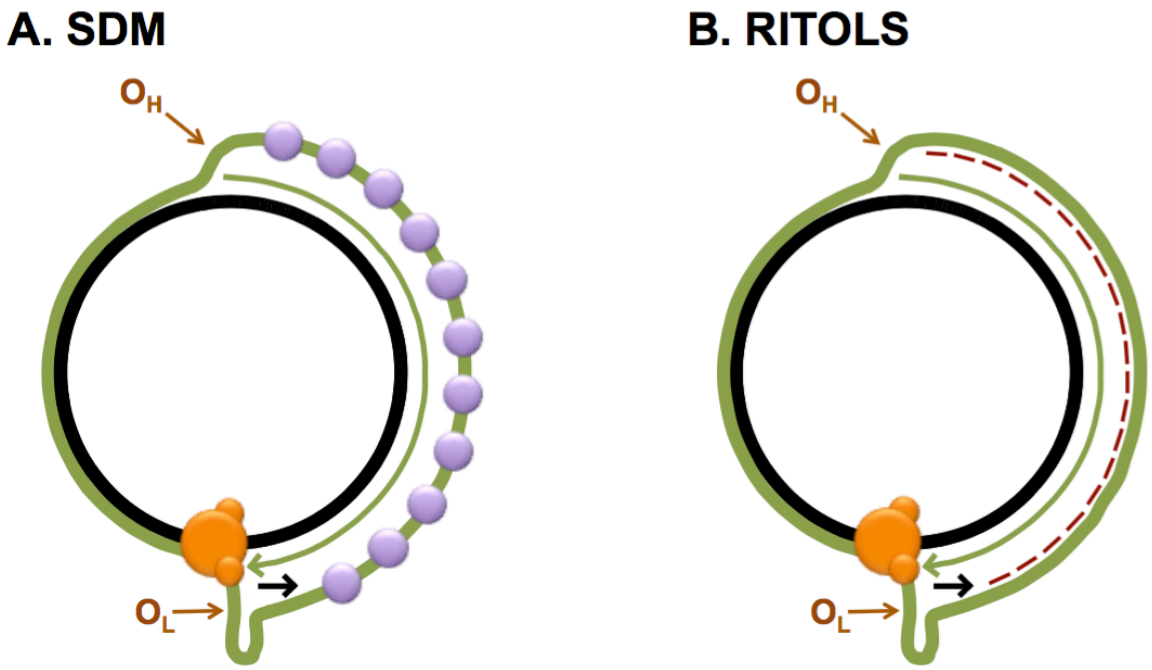

Figure 14. Two predominant models of human mtDNA replication. The exact mode of human mtDNA replication is still debated and two predominant theories prevail: (**A**) SDM and (**B**) RITOLS model. Both models concur with the existence of two primary replication origins, O_H and O_L, located at different loci that mediate asynchronous replication. Both models also agree with the idea that mtDNA replication begins with the displacement of parental H-strand (thick green structure) at the O_H following which pol γ (orange heterotrimer) synthesizes the leading strand (thin green semi-circular curve) that is complementary to the parental L-strand (thick black circle). The synthesis of lagging strand (black arrow) initiates when O_L is revealed after parental H-strand is displaced two-thirds of the way through the mitochondrial genome. The dispute between the SDM and RITOLS models arises on the mechanism by which the displaced H-strand is protected. According to SDM, the displaced H-strand is coated with mtSSB (purple spheres; panel A), which are later dislodged as the lagging strand synthesis proceeds. In contrast, RITOLS proposes that the exposed H-strand is covered with complementary RNA (thin brown lines; panel B) produced as a result of mtDNA transcription. Despite tremendous efforts, the contention as to how the parental H-strand is exactly protected has not been settled till date (Adapted from Vega *et al*. [206]).

3. DNA DAMAGE

3.1 Nuclear and mtDNA damage by ROS

Despite being a stable, well-protected molecule, cellular DNA can be attacked by ROS and the ensuing oxidative damage represents a major form of DNA damage confronted by aerobic organisms [194]. ROS have been known to instigate several types of DNA lesions including base modifications, loss of bases, damage to the deoxyribose sugar, single- and double-strand breaks, inter- and intra-strand crosslinks, and DNA-protein crosslinks [210, 211]. These abnormalities can trigger gross structural changes in the genome that have been implicated in a plethora of diseases including cancer [211]. In addition to DNA, ROS can also attack other cellular macromolecules, such as lipids and proteins, to generate reactive intermediates that can in turn attack DNA [212]. In this regard, the polyunsaturated fatty acid residues of the phospholipid bilayer are particularly vulnerable. Following assault by ROS, these unsaturated fatty acids initially produce lipid hydroperoxides, which can in turn react with metals to produce a variety of mutagenic products including malondialdehyde and 4-hydroxynonenal [212].

Different ROS have varying degree of reactivity to the DNA [213], with $HO^{\bullet}$ being the most reactive and has been largely implicated for the majority of oxidative lesions [210]. $HO^{\bullet}$ reacts with DNA by incorporating into the double bonds of bases, as well as by removing a hydrogen atom from the methyl group of thymine and the C-H bonds of deoxyribose [212, 214]. Because of its great reactivity, $HO^{\bullet}$ cannot diffuse from one cellular compartment to the other, and hence in order to oxidize DNA, it must be generated in the immediate vicinity to the nucleic acid molecule [212]. Other species

such as $^{\bullet}O_2^-$ and H_2O_2 do not seem to damage DNA at physiological concentrations [210]; however, these less reactive species can be converted to the highly reactive $HO^{\bullet}$ (Section 1.5), which can readily assault DNA. Moreover, $^{\bullet}O_2^-$ can also combine with nitric oxide resulting in the production of peroxynitrite (ONO_2^-), an extremely potent oxidant capable of directly oxidizing DNA molecules [212].

Perhaps the most common form of DNA damage inflicted by ROS is base damage. Till date more than 20 distinct oxidized base lesions have been documented that include 8-oxoguanine (8-oxoG; Figure 15B), 2,6-diamino-4-hydroxy-5-formamido-pyrimidine (FapyG), 8-hydroxyadenine, 5-hydroxycytosine, 5-hydroxyuracil, and thymine glycol (Figure 15D) [215]. Because of its high electron density and low oxidation potential, guanine, among all DNA bases, is most frequently targeted by ROS resulting in the generation of multitude of toxic products [211, 215], of which 8-oxoG has the highest prevalence in living cells [211]. For this reason 8-oxoG is widely accepted as the biomarker for oxidative DNA damage [215]. While damages to DNA can occur following its interaction with ROS, oxidation of free deoxyribonucleotides in the nucleotide pool also accounts for the oxidative damage. These oxidized deoxyribonucleotides can be incorporated into the genome by various replicating and repair DNA polymerases [216]. Most oxidative base lesions are mutagenic, regardless of whether they are generated in situ or occur by misincorporation from deoxyribonucleotide pool [214]. As an instance, 8-oxoG formed in situ can results in guanine to thymine transversion following DNA replication, whereas misincorporation of 8-oxo-dGTP opposite to adenine can produce adenine to cytosine transversion [214].

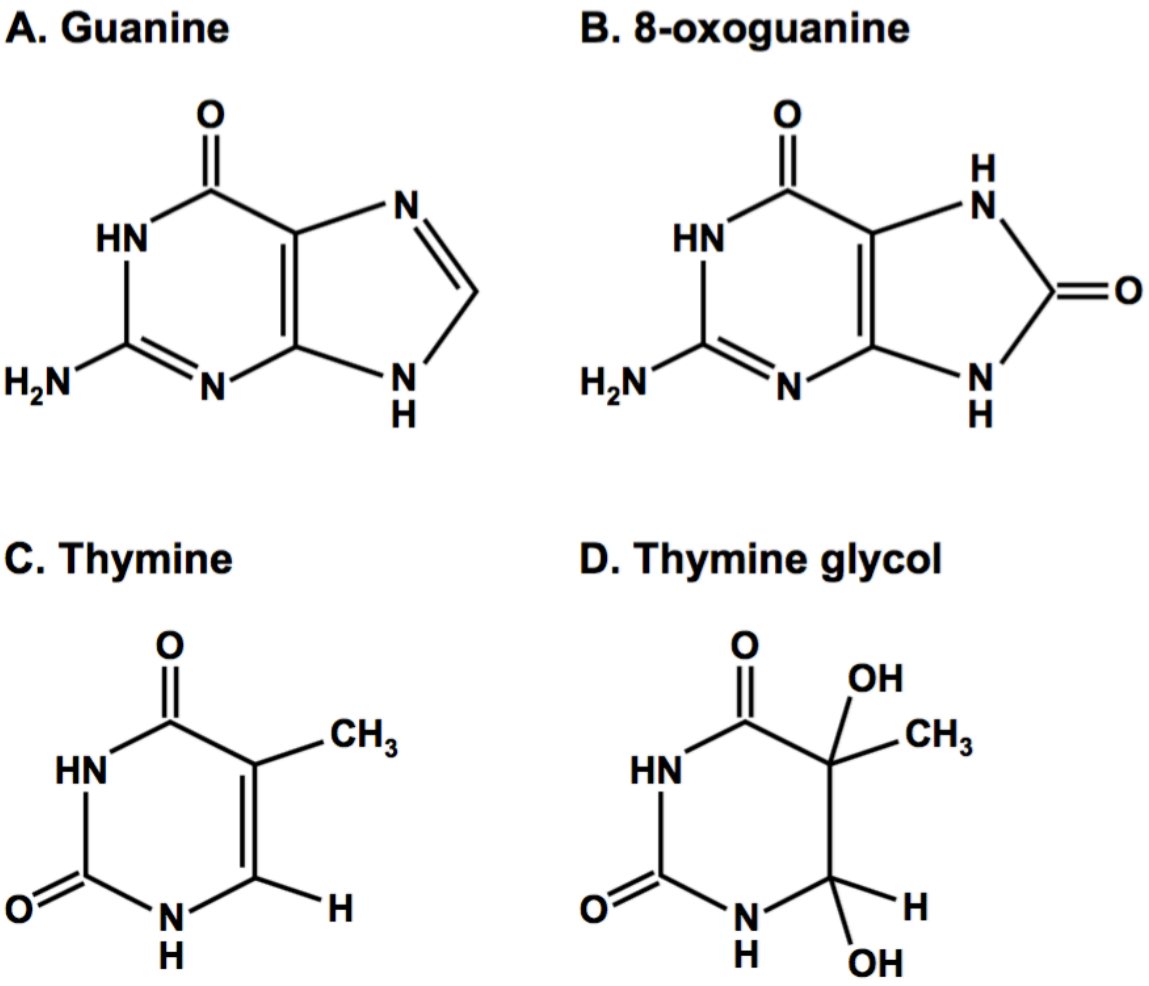

Figure 15. Structures of normal and oxidized DNA bases of guanine and thymine. (Redrawn from Marnett [212]).

Damage to DNA by ROS occurs naturally as low steady-state levels of oxidative base lesions have been identified *in vivo* both in nuclear DNA (nDNA) as well as in mtDNA [213]. In the nucleus, ROS induced oxidative DNA damage can lead to base pair mutations, deletions, insertions, rearrangements, sister chromatid exchange and translocation [213, 215]. These genome abnormalities can result in altered protein expression, or can even participate in the inactivation or loss of a wild-type allele of a gene [213, 215]. Moreover, oxidative damage in nDNA has also been known to block DNA replication and the prime candidate involved this aberrant phenomenon is thymine glycol [214]. Apart from oxidative modifications, ROS can also induce loss of DNA bases, giving rise to abasic sites, and such mutagenic lesions have also been implicated in DNA replication as well as transcription blockade [217].

In the context of the mitochondrial genome, the primary products of ROS induced DNA damage are 8-oxoG among purines and thymine glycols among pyrimidines (Figure 15) [218]. Moreover, strand breaks and deletions (due to misrepair of breaks or damage) are additional consequences of oxidative damage to mtDNA [213, 219]. Such alterations can be detrimental to cells as persistent damage to mtDNA has been known to impair mitochondrial function, induce permanent growth arrest, and commit cells to apoptosis [219]. It is interesting to note that oxidative base damage in mtDNA occurs at a several-fold higher rate than nDNA [213]. Indeed, numerous studies have revealed that base lesions such as 8-oxoG are elevated significantly in mtDNA compared to nDNA [219]. The increased vulnerability of mtDNA to ROS could be due to several factors, including: (i) close proximity of mtDNA to the electron transport chain, a major ROS generating factory; (ii) lack of complex chromatin organization; (iii) reduced complement

of DNA repair pathways; and (iv) prevalence of localized metal ions (such as Fe^{2+}) in the mitochondrial compartment that may serve as a catalyst for ROS generation (Section 1.5) [219]. Moreover, the association of mtDNA molecules with the inner membrane is also believed to contribute to the overall damage as reactive intermediates formed during membrane lipid peroxidation are known to insult the mitochondrial genome [213]. Interestingly, a recent study has demonstrated that, upon oxidative stress, mtDNA molecules have increased propensity for formation of strand breaks and abasic sites, with lower frequency of occurrence of base damages. Thus, the higher inclination of ROS to induce mtDNA strand breaks and abasic sites as opposed to mutagenic base lesions may be a novel mechanism adopted by mitochondria to maintain genomic integrity since higher degree of lesions to the sugar-phosphate backbone facilitates degradation of mtDNA, thereby avoiding the accumulation of mutagenic base lesions [218].

3.2 Nuclear and mtDNA damage by ionizing radiation

Ionizing radiation (IR) is one of the major cancer treatment regimens that kills cells in the exposed tumor tissues primarily by introducing DNA damage [220]. The effect of IR on macromolecules can be either direct or indirect. It has been estimated that about one-third of DNA damage results from its direct effect [221] that occurs when IR deposits energy directly into the biomolecule [221, 222]. This results in disruption of the atomic structure of the biomolecule, initiating a chain of events that drives chemical and biological alterations [221, 222]. Alternatively, IR can also act indirectly via radiolysis of water, a phenomenon responsible for the remaining two-thirds of DNA damage [221]. The

absorption of energy by water, an abundant cellular constituent, results in its excitation as well as ionization that culminates in generation of excessive ROS [221]. In an aerobic cellular environment, the major ROS produced by the indirect effect include $HO^{\bullet}$, $^{\bullet}O_2^-$ and H_2O_2 [221]. It was initially thought that the biochemical changes that occur during or immediately following irradiation were, by and large, responsible for the adverse effects of the IR. However, oxidative modifications may transpire even after days and months following the initial IR exposure, and this phenomenon is now believed to contribute significantly to the deleterious effects of IR [221]. Therefore, it is not surprising that exposure to IR results in DNA lesions that are chemically very similar to those generated by ROS, with base damages being most prevalent, followed by single-strand breaks (SSBs) and double-strand breaks (DSBs) [220]. Estimates have revealed that one gray of γ-radiation induces about 850 pyrimidine lesions (predominantly thymine glycols), 450 purine lesions (predominantly FapyG and 8-oxoG), 1000 SSBs and 20-40 DSBs per mammalian cell [220]. Because of its cytotoxicity, the most deleterious lesion instigated by IR is believed to be the DSB, which consists of a break in the phosphodiester backbone of both DNA strands. The level of DSBs is directly proportional to the radiation dose; in addition, the yield of DSBs increases in DNA that are more relaxed (e.g. transcriptionally active region) compared to those that are extensively packaged [220]. Moreover, IR is also renowned for instigating clustered damage, which contains two or more lesions within one or two helical turns of DNA [220]. Indeed, cluster lesions are widely considered as the hallmark of IR induced damage, which is in contrast to endogenously induced lesions that are more isolated and tend to be distributed randomly in the DNA [220]. As with DSBs, the energy deposited by IR is directly proportional to

complexity as well as yield of clustered lesions [220]. Because clustered damaged sites, particularly those comprising DSBs, are structurally and chemically complex, these lesions have reduced reparability compared to individual isolated lesions, and this is believed to be one of the main reasons why IR is more effective in killing tumor cells [220].

Experimental results have deduced that damage to nDNA is the primary cause of the deleterious effects of IR [223]. Nonetheless, a variety of lesions similar to those found in nDNA have also been identified in mtDNA following IR exposure [223]. In fact, mtDNA molecules are believed to suffer more from IR-induced DNA lesions compared to the nuclear counterparts, a phenomenon analogous to the increased vulnerability of the mitochondrial genome to chemically induced oxidative stress [223]. Apart from the aforementioned lesions encountered by either genome, the human mtDNA is also known to undergo the so-called "common deletion" following IR exposure that involves loss of 4977 base pairs from mtDNA. Because it includes genes encoding essential components of mitochondrial ETC, the common deletion can result in ineffective mitochondrial metabolism with concomitant increase in mitochondrial ROS production [221]. These observations indicate that mtDNA may play a significant role in translating radiotoxic effects of IR, an idea greatly substantiated from the fact that human ρ^0 cells are more resistant to radiation-induced cell killing compared to the ρ^+ counterparts [221]. Furthermore, IR is also known to damage a multitude of mitochondrial proteins that can in turn trigger alterations of mitochondrial function, escalation of mitochondrial oxidative stress, and induction of apoptosis. In fact, mitochondria have been reported to be the

primary target for radiation-induced apoptosis [223]. Taken together, it would not be irrational to proclaim that mitochondria are major targets of IR besides the cell nucleus.

3.3 Nuclear and mtDNA damage by chemotherapeutic agents

Chemotherapeutic drugs represent another major component of anticancer therapy that are being extensively exploited to eliminate cancer cells, diminish tumor growth, and alleviate pain. DNA damaging chemotherapeutic agents react chemically with DNA to alter DNA bases, intercalate between DNA bases, or induce DNA crosslinks. As an example, nitrogen mustard derivatives (e.g. cyclophosphamide) act by directly alkylating purine bases [224], which can subsequently result in the formation of guanine-guanine and guanine-adenine interstrand adducts within the DNA double helix [225]. Nitrosureas (e.g. carmustine) are another type of DNA-alkylator that, like nitrogen mustards, alkylate DNA bases and induce interstrand crosslink [224]. Likewise, certain antitumor antibiotics like mitomycin C also have similar dual effects [224, 225]. Base alkylation is known to block replication fork progression, which can also be triggered by DNA crosslinks. Thus, the presence of both types of lesions is believed to have more potent effect on cancer cells compared to a single type of damage, and such lesions, if not repaired, can lead to cell death via apoptosis [224]. Anthracycline antibiotics (e.g. doxorubicin), another type of antineoplastic agent, exhibits multiple mechanisms of action apart from the ability to alkylate bases and induce DNA crosslinks. These include the ability to intercalate into DNA, produce free radicals, and inhibit helicase and topoisomerase thereby making these drugs extremely cytotoxic [224]. Other DNA damaging chemotherapeutic agents with

substantial impact against cancer cells include alkylating-like platinum agents (e.g. cisplatin) [224] and glycopeptide antibiotics such as bleomycin [226]. In fact, cisplatin is regarded as one of the most important anticancer drugs ever developed. Following its entry into the cell, cisplatin is hydrated to produce a positively charged species that can interact with nDNA as well as other nucleophilic biomolecules within the intracellular milieu [227]. Cisplatin, an inorganic molecule containing a platinum core, binds to purine bases, particularly to guanine, resulting in formation of monofunctional adducts [224]. When two platinum adducts form on nearby bases, either on the same strand or opposite strands, formation of intra- or interstrand crosslinks ensues [224, 225]; however, intrastrand crosslinks between adjacent guanines has been regarded as the most prevalent form of DNA damage induced by cisplatin [225]. These adduct and crosslinks, in addition to their propensity in inducing strand breaks, can impair template function of DNA thereby massively impeding DNA replication as well as RNA transcription [225]. The genotoxicity induced by cisplatin has been attributed to its ability to produce inter- and intrastrand crosslinks in the nDNA. However, estimates suggests that only ~1% of intracellular platinum is bound to nDNA, with the vast majority of the drug available for interaction with other intracellular nucleophilic sites including mtDNA molecules [227]. Indeed, studies have demonstrated that cisplatin accumulates excessively in mitochondria. Owing to the electrochemical gradient across the MIM, the mitochondrial matrix acquires negative charge, which is thought to be responsible for the accumulation of the positively charged cisplatin [228]. In agreement with this concept, studies have indicated that mtDNA-cisplatin adducts occur more frequently than nDNA-cisplatin adducts in the same cell line treated with the same concentration of cisplatin [227]. For

example, treatment of cisplatin to head and neck squamous cell carcinoma (HNSCC) cell lines revealed at least two orders of magnitude higher level of platinum adducts in mtDNA than in nDNA. Interestingly, when HNSCC cytoplasts (viable and functional cell bodies lacking nuclei) were treated with cisplatin, they retained dose dependent cisplatin sensitivity similar to the parental cells. On the other hand, HNSCC ρ^0 cells were substantially resistant to cisplatin-induced cell death compared to parental wild-type cell. Moreover, cisplatin also triggered rapid release of cytochrome *c* from mitochondria and induced marked mitochondrial disruption characteristics of permeability transition pore opening [229]. These observations indeed corroborate the idea that mitochondria are one of the major targets of cisplatin in cancer cells [228].

Bleomycin is another important anticancer drug that is believed to participate in damaging both nuclear as well as mtDNA. Bleomycin requires specific cofactors (a transition metal, oxygen, and a one-electron reductant) to generate 'activated' bleomycin, which can oxidize lipids, hydrolyze proteins, and induce strand breaks in both DNA as well as RNA. The activated bleomycin can decompose to produce $HO^{\bullet}$, which can rapidly react with any biomolecule it encounters. Nonetheless, a wide array of experimental evidence indicates that the cytotoxicity of bleomycin is principally due to its DNA damaging activity. Bleomycin is a positively charged molecule and hence can bind to DNA electrostatically [226]. Recently, experiments with acute myeloid leukemia (AML) cells have demonstrated that bleomycin preferentially damages mtDNA compared to nDNA, and this was accompanied by a concomitant reduction in mitochondrial function as well as basal oxygen consumption. Moreover, experiments with cytoplasts revealed that these nuclei-lacking cell bodies were almost equally

sensitive to the same concentrations of bleomycin as whole cells, whereas ρ^0 cells were substantially resistant to bleomycin compared to the wild-type counterparts [230]. Likewise, experiments with human alveolar epithelial cells also revealed that bleomycin induced more damage to mtDNA compared to nDNA and ρ^0 human alveolar epithelial cells were more resistant to bleomycin-induced apoptosis compared to the isogenic parental wild-type cells. Thus, it seems very likely that bleomycin-induced cytotoxicity occurs, at least in part, because of its effect on mtDNA [231].

3.4 DNA damage by restriction endonucleases

Restriction endonucleases (REases) are enzymes that digest the sugar-phosphate back bone of dsDNA to generate 5′-phosphate and 3′-hydroxyl termini on each strand. These breaks can be staggered, forming 5′-phosphate overhangs or 3′-hydroxyl overhangs, or alternatively, when breaks are apposed on each strand, 'blunt' ends are generated [232]. REases occur exclusively in unicellular microbes, particularly in bacteria and archea, and are believed to protect these cells from invading DNA (e.g. viruses), thereby performing a host defense function [233].

REases are generally classified into 4 major types (Type I through Type IV) [234] on the basis of subunit composition, cofactor requirement, recognition sequence, and cleavage position. For example, Type I REases, the most complex among 4 classes, contain three different types of subunits and require Mg^{2+}, ATP, and *S*-adenosylmethionine in order to cleave DNA. Moreover, their recognition sites are also complex and DNA cleavage occurs at non-specific sites about 400-7000 bp away from

the recognition site. On the other hand, Type II system contains only one type of subunit, and requires only Mg^{2+} for DNA cleavage [232]. Each Type II REase recognizes short sequences of 4-8 bp with extreme accuracy and cleave DNA within or just adjacent to the recognition element [235]. Because of these features, Type II REases have become very useful for molecular biology [232] and are the only class of REase that is utilized in the laboratory for routine DNA analysis and gene cloning [236]. The orthodox Type II enzymes, such as HindIII and XhoI, exist as homodimers that recognize palindromic recognition sites. These enzymes are capable of binding with DNA in non-specific manner that involves interaction only with DNA backbone but not with DNA bases. Such interaction is prerequisite for locating the target site as the enzyme slides along the DNA strands in search of recognition elements. After it encounters the target sequence, specific binding between the protein and DNA ensues that involves interaction with the bases as well as with DNA backbone. This recognition process elicits large conformational changes to the enzyme as well as DNA, leading to the activation of catalytic center, which in turn cleaves two strands resulting in DNA fragments with 3′-hydroxyl and 5′-phosphate groups. Finally, the release of the enzyme following DNA cleavage allows it to perform another cycle of catalysis [235]. It is important to note that restriction endonucleases introduce DSBs that are readily ligatable since the DNA ends possess ligation compatible 3′-hydroxyl and 5′-phosphate groups. This feature is in stark contrast to ROS, IR, or chemotherapeutic agents (e.g. bleomycin) induced DSBs in which the DNA ends often harbor non-ligatable 3′- and/or 5′-blocking lesions.

3.4.1 Restriction endonuclease XhoI

Belonging to the Type II system, the REase XhoI recognizes the palindromic sequence 5′-CTCGAG-3′ in the dsDNA and cleaves after the first cytosine, resulting in the production of staggered breaks with 5′-phosphate overhangs. For commercial use, the gene encoding XhoI is derived from a proteobacterium *Xanthomonas holcicola* that produces a highly efficient DNA cleaving machinery of 246 amino acid residues with a molecular weight of ~26 kDa. Owing to the large sizes of the nuclear genome, XhoI has numerous recognition sites in nDNA of humans as well as *S. cerevisiae*. As an instance, it has been estimated that ~42 XhoI restriction sites exist per megabase sequence of the human nuclear genome [236]. However, only a limited number of XhoI sites are found in the mitochondrial genomes of either aforementioned species. Precisely, the ~16.6 kb human mtDNA has a single XhoI restriction site at 14955 bp, which is located within the cytochrome *b* locus. With respect to the budding yeast, the ~85.8 kb mitochondrial genome harbors two XhoI restriction sites at 23224 bp and 51370 bp, which are located within the cytochrome *c* oxidase subunit I and an open reading frame (ORF10; unknown function) loci, respectively. Thus, cleavage at both XhoI sites in the budding yeast mtDNA can result in a deletion of ~28.1 kb DNA fragment, which comprises genes essential for operation of mitochondrial ETC and OXPHOS.

Mitochondrial-targeted restriction endonucleases have been exploited for more than a decade to induce DSBs specifically in the mitochondrial genome. For mitochondrial localization, these restriction endonucleases are fused with a mitochondrial-targeting signal (MTS) that direct them into the matrix where they can access mtDNA and induce site specific DSBs. Mitochondrial-targeted REases have been

extensively explored to mimic models of mtDNA-derived OXPHOS dysfunction that occurs in a variety of conditions including neurodegenerative disorders and the aging process [237]. Moreover, the use of mitochondrial-targeted REases has also been extended to generate ρ^0 mammalian cells, which are highly valuable tools in studying, for example, the response of mtDNA to different drugs [238]. Finally, by inducing DSBs to a specific region of mtDNA, different molecular players involved in sealing the breaks can be identified. If exploited, this procedure could help unravel the mechanism(s) of mtDNA DSB repair, a field advancing through its toddlerhood that requires extensive exploration to understand the role of mtDNA both in health and in disease states.

4. DNA REPAIR

4.1 Types of nuclear DNA repair

The genomic integrity of an organism is persistently being challenged by insults arising from exogenous agents, including ionizing radiation, as well as endogenous sources such as ROS [239]. As discussed in Section 3, these insults can instigate a variety of lesions including base damage, SSBs, and DSBs. Estimates indicate that each cell within the human body experiences tens of thousands of DNA-damaging events per day [240]. It is extremely crucial to deal with these environmentally or endogenously induced DNA damage, as inability to repair these lesions leads to mutations and can eventually result in cellular dysfunction including uncontrolled cell proliferation [241]. Moreover, some lesions can be potent enough to induce permanent growth arrest and cell death. Hence, in order to preserve the integrity of the genome, cells have evolved an intricate network of DNA repair pathways [241], which are broadly categorized into four major classes depending on the type of DNA lesions they rectify. These repair pathways include base excision repair (BER), nucleotide excision repair (NER), mismatch repair (MMR), and double-strand break (DSB) repair [240].

4.1.1 Base excision repair (BER)

As its name implies, BER is the predominant mechanism dedicated to deal with damaged DNA bases that do not significantly distort the overall structure of the DNA double helix [240]. These lesions inflicted to individual bases include oxidation, methylation, depurination, and deamination [241]. BER represents the epitome of a coordinated pathway consisting of consecutive enzymatic events that is initiated when lesion-specific

DNA glycosylases recognize and remove damaged DNA bases by excising the N-glycosidic bond between the base and its corresponding deoxyribose (Figure 16) [240]. Till date, at least 12 DNA glycosylases have been identified in humans, all of which utilize base-flipping mechanism in which the damaged base is 'flipped' to an extrahelical position for removal. Following base excision, an abasic site (also known as apurinic/apyrimidinic site or AP site) is generated that typically becomes substrate for apurinic/apyrimidinic endonuclease (e.g. APE1), an enzyme catalyzing the hydrolysis of the phosphodiester linkage immediately 5′ to the AP site, thereby generating a single-strand break (SSB) [240, 241]. Alternatively, some bifunctional DNA glycosylases also possess intrinsic AP lyase activity, which is able to cleave phosphodiester bond that is immediately 3′ to the AP site [240, 241]. For example, Ogg1, a typical bifunctional glycosylase, excises 8-oxoG paired opposite to cytosine, following which a phosphodiester linkage that is 3′ to the resultant AP site is cleaved [241]. Irrespective of how the AP site is split, the scission of the phosphodiester backbone produces a strand break harboring 3′- and/or 5′-blocking lesions (e.g. 3′-phosphate, 5′-deoxyribose phosphate or 5′-dRP, etc.). A variety of DNA-end processing enzymes such as polynucleotide kinase 3′-phosphatase (removes 3′-phosphate), DNA polymerase β (removes 5′-dRP via its associated dRP lyase activity), etc. convert these blocking lesions into conventional 3′-hydroxyl and 5′-phosphate termini, a process that is indispensible for the repair process to proceed. Subsequent DNA polymerization and ligation steps can occur via short-patch BER (SP-BER) or long-patch BER (LP-BER) mechanisms depending on whether single or multiple nucleotides are incorporated at the strand break site. SP-BER constitutes ~80-90% of total BER that involves removal of 5′-dRP

following which DNA polymerase β fills a single nucleotide gap (Figure 16, pathway A). The DNA ends are then ligated by either by DNA ligase I or by the complex of DNA ligase III and XRCC1. LP-BER, on the other hand, is normally initiated when 5′-blocking lesions become refractory to the lyase activity of DNA polymerase β. This pathway incorporates several proteins involved in DNA replication that include DNA polymerase δ or ε, proliferating cell nuclear antigen (PCNA), flap endonuclease 1 (FEN1), and DNA ligase I. Specifically, DNA polymerase β, δ or ε together with PCNA elongate the 3′-hydroxyl group, and during this process the 5′-blocking lesion is displaced as a 'flap' oligonucleotide (Figure 16, pathway B). FEN1 then removes the flap structure following which DNA ligase I seals the remaining nick to complete LP-BER pathway [240]. It is interesting to note that various intrinsic and extrinsic insults instigate SSBs, which are also generated during the processing of damaged bases during BER. Hence, SSBs inflicted under diverse circumstances are processed and repaired by many of the same enzymes that participate during the later stages of BER [240].

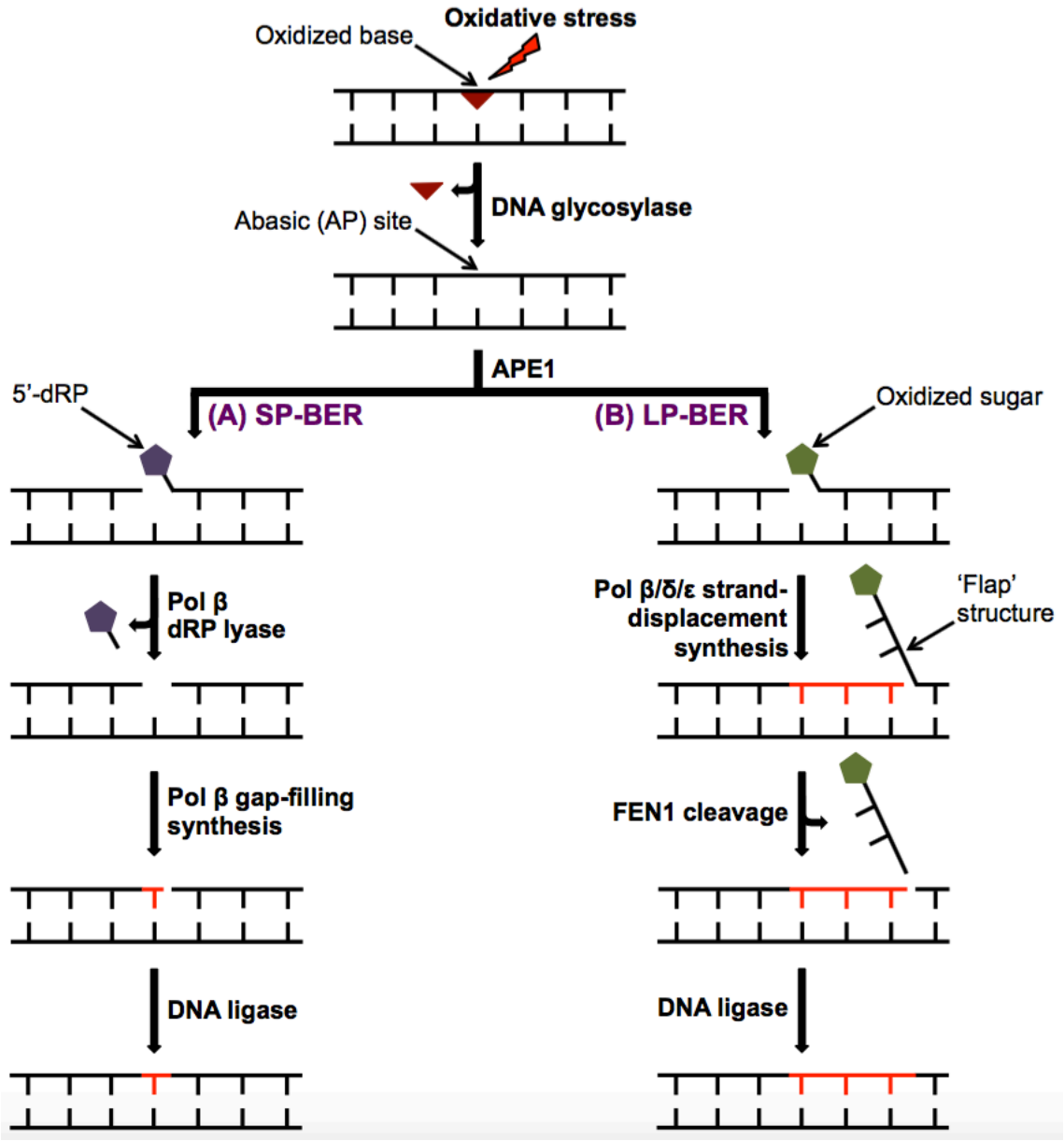

Figure 16. Schematic representation of the mechanism of SP-BER and LP-BER. Oxidative stress may produce oxidized base lesion and/ or oxidized abasic site. DNA glycosylase removes an oxidized base and leaves an AP site. APE1 then cleaves at the 5′-side of the AP site, leaving either a 5′-dRP or an oxidized sugar phosphate (the latter results, for example, when APE1 acts on the oxidized AP site). (**A**) During SP-BER, the dRP lyase activity of DNA polymerase β removes 5′-dRP following which the DNA polymerase fills the gap. The nicked DNA intermediate that remains is subsequently ligated. (**B**) When the 5′-blocking lesion is resistant to dRP lyase activity of DNA polymerase β, LP-BER proceeds during which DNA polymerase β or DNA polymerase δ/ε mediate strand displacement synthesis. A flap oligonucleotide that is produced during the process is cleaved by FEN1 and finally DNA ligase I seals the nick (Redrawn from Liu and Wilson [242]).

4.1.2 Nucleotide excision repair (NER)

NER, a highly versatile DNA repair pathway, deals with a wide variety of bulky lesions that provoke structural deformity to the DNA helix [240, 241]. A typical example of such lesions includes pyrimidine dimers such as cyclobutane pyrimidine dimers and 6-4 photoproducts generated by the UV component of sunlight [240]. Interestingly, cisplatin-intrastrand crosslinks also represent important substrates of NER. Even though mechanistically very similar to BER, NER is comparatively more complex that requires participation of a large number of proteins to mediate a 'cut-and-patch' like mechanism [240]. *In vitro* reconstitution experiments have revealed that mammalian NER requires at least 25 distinct proteins, including 7 factors (XPA through XPG) involved in the human disease Xeroderma Pigmentosum and two proteins (CSA and CSB) associated with Cockayne syndrome [241]. Accordingly, defects in NER results in several human genetic disorders, including those mentioned above, which are generally characterized by extreme sensitivity to sunlight, in addition to other symptoms associated with immunological dysfunction, neurological defects, and premature aging [240].

The NER system is divided into two sub-pathways, viz., global genome NER (GG-NER) and transcription coupled NER (TC-NER) (Figure 17). As their names suggest, GG-NER is involved in removing DNA lesions from the entire genome, whereas TC-NER preferentially removes lesions located on the coding strand of actively transcribing genes. Apart from the initial lesion recognition step, both pathways follow the same subsequent steps that involve unwinding of the DNA helix flanking the lesion, removal of a short ssDNA segment spanning the lesion, and finally repair synthesis followed by strand ligation [240]. Initially in GG-NER, XPC/HR23B/CEN2 (xeroderma

pigmentosum complementation group C/ human homolog of yeast Rad23/ Centrin-2) complex recognizes helix-distorting DNA lesions. In contrast, TC-NER is initiated after arrest of elongating RNA polymerase II (RNAPII) at the damage site, following which two TC-NER specific proteins, CSA and CSB, are believed to displace the stalled RNAPII that permits the downstream NER proteins to access the lesion. After damage recognition, both GG-NER and TC-NER pathways converge to a common 'core' NER mechanism [240, 241]. The XPC/HR23B/CEN2 complex in GG-NER, or presumably CSA and CSB proteins in TC-NER recruit the basal transcription factor TFIIH to the damage site [240, 241]. Association of TFIIH allows either sequential assembly of NER complex or spontaneous assembly of preformed holocomplex [241]. Regardless of how the NER complex is assembled, the helicase subunits (XPB and XPD) of TFIIH holocomplex unwind DNA thereby allowing the XPA-RPA heterodimer to bind directly to the lesion, and simultaneously, depending on the pathway, XPC/HR23B/CEN2 or CSA/CSB complex get evicted [241]. XPA verifies the initial damage by recognizing the presence of a chemically altered base [240, 241], whereas RPA stabilizes ssDNA that arise due to helix unwinding [240]. Subsequently, two structure-specific endonucleases, viz., XPG and XPF/ERCC1, excise DNA at 3′ and 5′ positions, respectively, resulting in the removal of a lesion containing ~30 nucleotides [240]. Most of the NER complex leave the repair site after incision, apart from RPA which protects and stabilizes the remaining ssDNA tract [241]. DNA polymerase δ or ε then catalyzes resynthesis of the resulting gap by utilizing the undamaged strand as a template, and finally DNA ligase seals the nick at the end of DNA polymerization to complete the NER process [240].

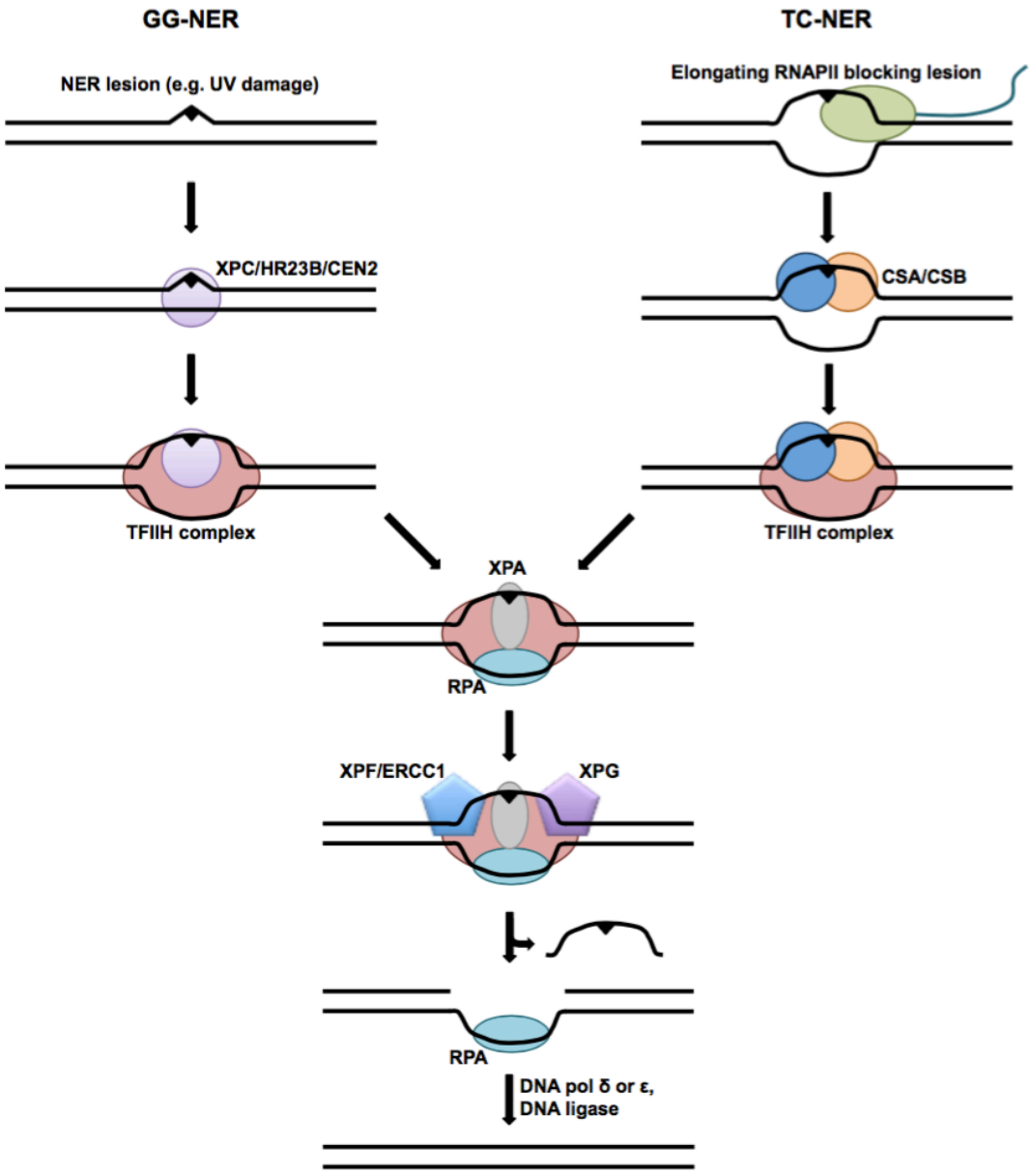

Figure 17. Schematic representation of the mechanism of GG-NER and TC-NER. During GG-NER (left pathway), DNA lesions are recognized by XPC/HR23B/CEN2 complex, which then recruits TFIIH complex. TC-NER (right pathway), on the other hand, is commenced following arrest of the elongating RNAPII at a lesion on the coding strand. CSA and CSB are then recruited that displace the stalled RNAPII, following which TFIIH complex arrives at the damaged site. After these initial lesion recognition steps, both NER sub-pathways follow same steps that include recruitment of XPA-RPA heterodimer, and depending on the sub-pathway, either XPC/HR23B/CEN2 complex or CSA/CSB complex gets dislodged. XPG and XPF/ERCC1 endonucleases then excise DNA at 3′ and 5′ ends, respectively, resulting in the removal of a DNA segment containing the lesion. Finally, DNA polymerase δ or ε fills the gap and a DNA ligase seals the ultimate nick (Adapted from de Laat *et al*. [243]).

4.1.3 Mismatch repair (MMR)

Highly conserved from bacteria to humans, the MMR is an important post-replication repair mechanism dedicated to rectify misincorporation of bases that have eluded the proofreading activity of replication polymerases. Moreover, polymerase slippage during replication of repetitive DNA sequences are known to create insertion/deletion loops (IDLs), which are also effectively removed by proteins involved in MMR [240]. Accordingly, MMR pathway contributes to the fidelity of replication as it targets the newly synthesized DNA strand for repair [244]. The biological significance of this pathway is underscored from the observation that cells lacking MMR activity are said to exhibit a mutator phenotype, which is characterized by increased mutation frequency and microsatellite instability. Moreover, germline mutation in MMR genes has been known to predispose individuals to a variety of cancers, including heredity non-polyposis colorectal cancer [240].

The MMR pathway can be broadly divided into three major steps: a recognition step in which mispaired bases are identified, an excision step in which the strand harboring the erroneous nucleotide is degraded resulting in a gap that is filled in the final repair-synthesis step (Figure 18) [240]. In humans, MMR pathway is driven by two major protein complexes, viz. MutS and MutL, based on their homology to the MMR proteins from *E.coli*. In essence, MutS is responsible for the initial mismatch recognition, while MutL links MutS-mediated recognition of mispaired bases to the downstream MMR events. In mammals, two MutS complexes (MutSα and MutSβ) exist, each of which functions as a heterodimer. The MutSα heterodimer preferentially recognizes base-base mismatches and IDLs of one or two nucleotides, whereas the MutSβ heterodimer detects

larger IDLs [240]. After recognizing and binding to its substrate, MutS undergoes an ATP-driven conformational change and recruits MutL heterodimer, the major downstream MMR protein complex [244]. Among three MutL heterodimers (MutLα, MutLβ, and MutLγ) identified so far, MutLα possesses the primary MutL activity that mediates repair initiated by both MutSα and MutSβ [240]. The MutS-MutL complex so formed can translocate in either direction along the DNA until a strand discontinuity is encountered, for example a gap between Okazaki fragments in the lagging strand. Alternatively, the endonucleolytic activity of MutLα can introduce a nick on the leading strand containing the mismatch [244]. In either case, the strand discontinuity marks the entry point for Exo1 (exonuclease 1) that catalyzes the degradation of the error-containing strand via its 5′→3′ exonucleolytic activity [240], a process that terminates past the mismatch [244]. After removal of the mismatch containing sequence, the single stranded region of the template strand is bound and stabilized by RPA [241]. The substantial gap created by Exo1 activity is then filled by DNA polymerase δ and finally DNA ligase I seals the remaining nick to complete MMR [240].

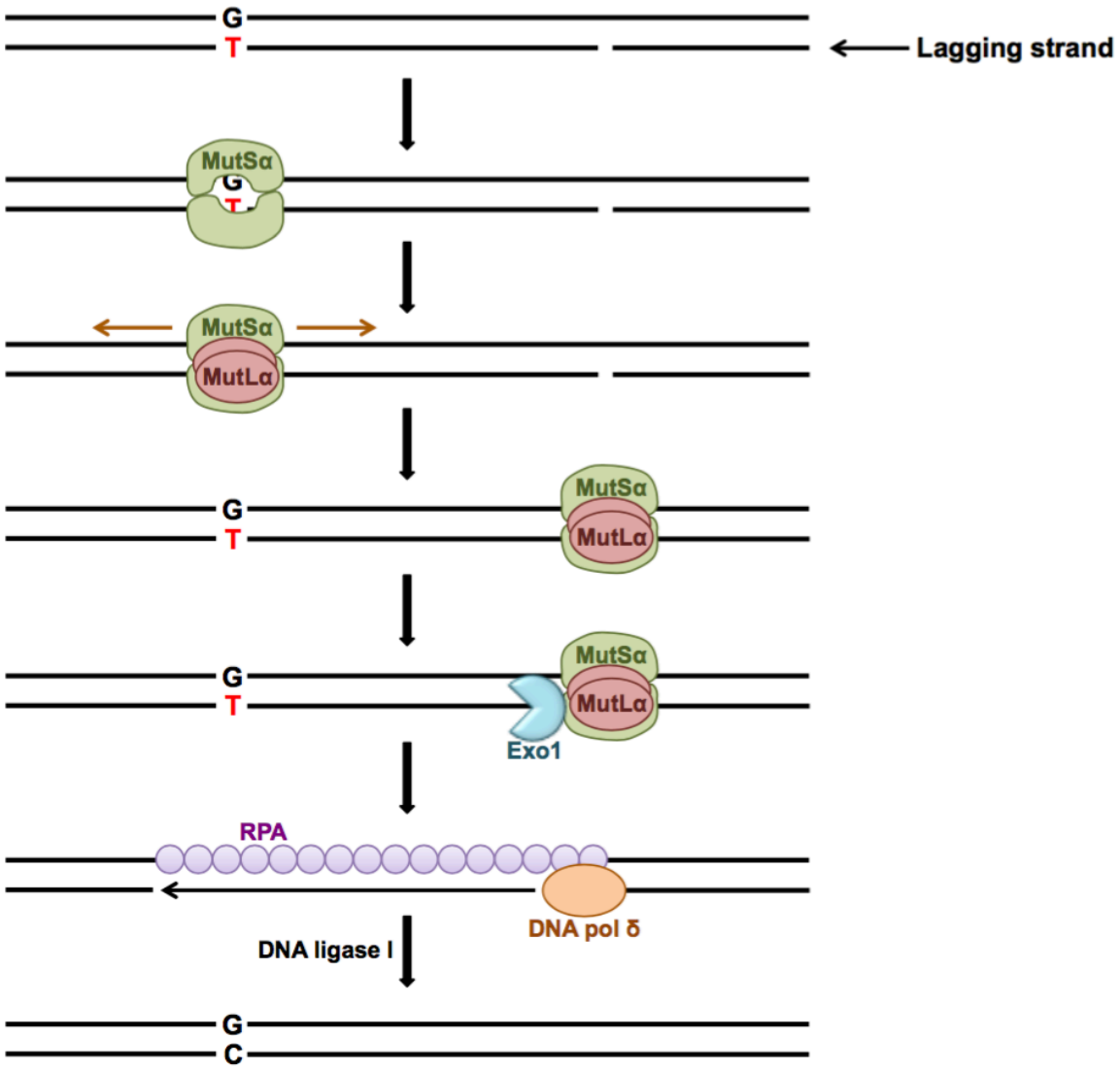

Figure 18. Schematic representation of the mechanism of MMR. The MMR commences by MutSα heterodimer binding to a mismatch (G/T in this example, that has to be corrected to G/C). The MutSα heterodimer then recruits MutLα following which the ternary complex translocates along the DNA until it encounters a strand discontinuity (e.g. a gap between Okazaki fragments), which marks loading of Exo1. The exonuclease catalyzes degradation of the nicked strand and the single-stranded region of the template strand so produced is stabilized by RPA. DNA polymerase δ fills the gap created by Exo1 and the ultimate nick is sealed by DNA ligase I (Adapted from Stojic *et al*. [245]).

4.2 Double-strand break (DSB) repair

The gravity of DSBs in a cell is revealed from the fact that a single unrepaired DSB can trigger permanent growth arrest and cell death. Moreover, inaccurate repair of DSBs can lead to deletions or chromosomal aberrations conducive to the establishment of many diseases including cancer. For this reason, DSBs are considered one of the most deleterious DNA lesions, repair of which is crucial not only for maintenance of genome integrity and cellular homeostasis, but also for cell viability [239, 240].

In one complete cell cycle, a human cell can accumulate up to 50 DSBs [246]. To tackle these lethal lesions, mammalian cells utilize two predominant pathways: homologous recombination (HR) and non-homologous end joining (NHEJ). These pathways basically differ in their requirement for a homologous DNA template as well as in the fidelity of repair. HR, as its name suggests, repairs DSBs by utilizing the undamaged sister chromatid as a template to restore the lost genetic information, and for this reason it is, by and large, an error-free mechanism. On the other hand, NHEJ eliminates DSBs by direct ligation of broken ends due to which it is normally considered error-prone [240]. Moreover, NHEJ does not require a homologous sister chromatid to initiate repair, so it is not restricted to any particular phase of the cell cycle, whereas HR is largely constrained during the late S and G2 phases when the homologous DNA template is available in the form of a sister chromatid [240, 247]. Information regarding basic mechanisms and factors participating in these pathways are concisely presented below.

4.2.1 Homologous recombination (HR)

HR is an evolutionarily conserved process that is found in all forms of life. Conceptually, this pathway can be divided into three distinct phases, viz. presynapsis, synapsis, and postsynapsis (Figure 19). During presynapsis, DNA ends near the DSB are recognized and processed to produce single-stranded tails ending with 3′-hydroxyl groups [240, 248]. This step involves trimming of nucleotides from 5′ ends (i.e. 5′→3′ end resection) on either side of DSB to generate short 3′-overhangs of ssDNA and is carried out by the heterotrimeric MRN (Mre11-Rad50-Nbs1) complex together with CtIP. End resection thus initiated is followed by extensive resection that is believed to be performed by the cooperative action of BLM helicase and Exo1 exonuclease. The stretch of ssDNA so produced then becomes substrate for RPA, a ssDNA binding protein, that removes any disruptive secondary DNA structure [240]. Subsequently, RPA is replaced by Rad51 recombinase, a process that is substantially facilitated by other mediator proteins including Rad52, BRCA1, BRCA2, and Rad51 paralogs (RAD51B, RAD51C, RAD51D, etc.) [240, 248]. During synapsis, the Rad51 coated ssDNA tail, also known as Rad51 nucleoprotein filament, sets out in search of a homologous sequence in a template dsDNA, which marks a key step in HR. Following identification of the complementary DNA sequence, Rad51 facilitates the nucleoprotein filament invasion into the template duplex to generate a displacement loop (D-loop), following which a heteroduplex joint is formed [240, 248]. During post-synapsis, DNA polymerase η utilizes the 3′-hydroxy group of the invading strand for DNA synthesis and the ultimate nick that remains at the end of DNA polymerization is sealed by DNA ligase I [240]. Similarly, the second 3′-ssDNA tail generated during presynapsis anneals with the displaced DNA strand in the

D-loop, which serves as a template for the second strand synthesis [248]. The entire process yields two Holliday junctions, which are eventually resolved to produce two intact dsDNA, thus concluding rectification of the original DSB in an error-free fashion [240, 248].

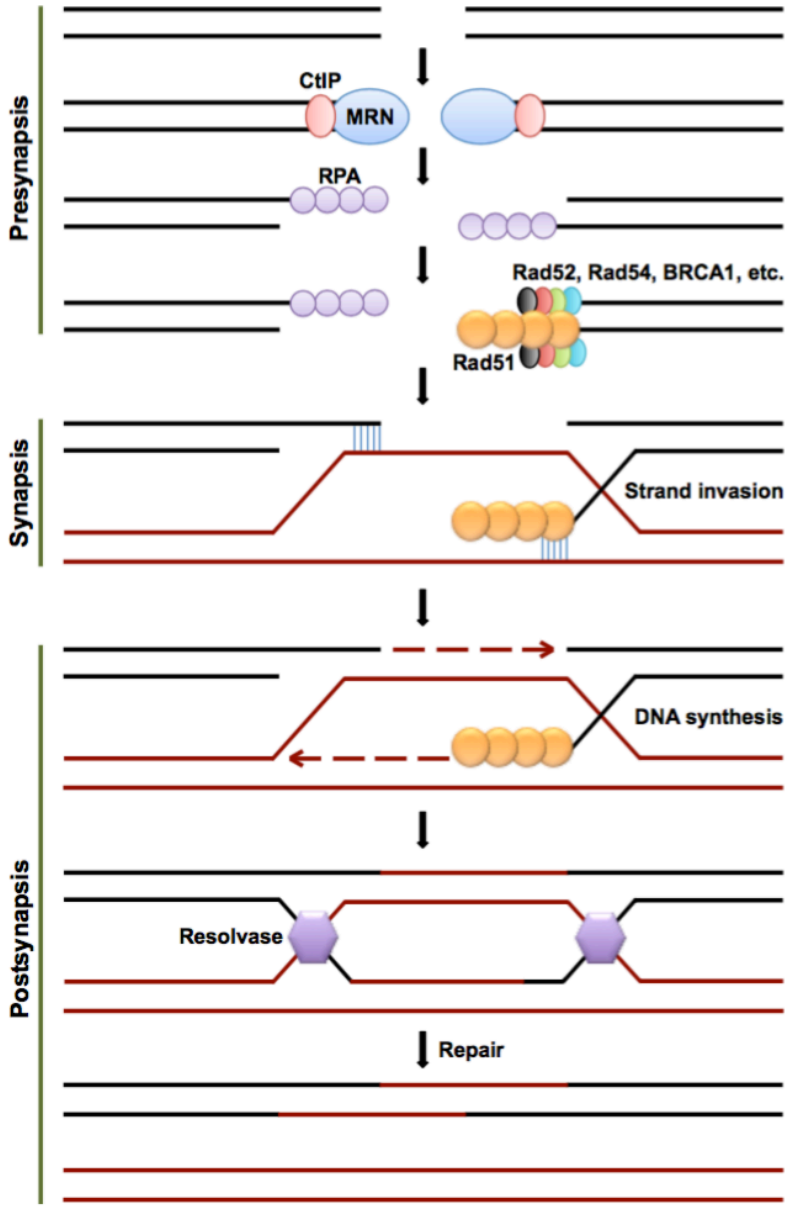

Figure 19. Schematic representation of the mechanism of DSB repair via HR. In the late S and G2 phases of the cell cycle, when a homologous dsDNA template is available, DSBs are repaired primarily via HR. Initially, the cooperative action of MRN complex and CtIP commence DNA end resection, which is followed by a more processive resection catalyzed by Exo1 (not shown). The ssDNA so formed is bound by RPA, which is subsequently displaced by Rad51, a process markedly facilitated by other proteins like Rad52, Rad54, etc. The Rad51 recombinase mediates homology search and strand invasion, which is followed by heteroduplex joint formation. The DNA polymerase η then catalyzes DNA synthesis utilizing the genetic information from the homologous DNA template and DNA ligase I seals the ultimate nick. The process eventually results in the formation of Holliday junctions, which are resolved and the original DSB is repaired in an error-free manner (Redrawn from Renodon-Cornière *et al*. [248].)

4.2.2 Non-homologous end joining (NHEJ)

NHEJ repair pathways are categorized into well-defined classical NHEJ (C-NHEJ) pathway and comparatively less characterized alternative NHEJ (A-NHEJ) pathway, both of which are discussed in the following sections.

4.2.2.1 Classical NHEJ (C-NHEJ)

C-NHEJ depicts an uncomplicated mechanism to heal DSBs and reestablish chromosome integrity [249]. Because it has the potential to rejoin any type of DNA ends, C-NHEJ is the primary form of DSB repair pathway in humans and other higher eukaryotes [240, 247, 250]. In contrast to the large number of proteins involved in repairing DSB via HR, C-NHEJ is mediated by a comparatively small number of factors that are recruited sequentially to the DSB sites. The core proteins and general mechanism of C-NHEJ exhibit remarkable conservation across eukaryotes [249]. During C-NHEJ, the exposed DNA termini of the DSBs are recognized and bound by Ku70/Ku80 heterodimer (Figure 20). This Ku complex forms a ring shaped structure that wraps around DNA ends [240] and protects DNA ends from being processed nonspecifically [247]. The Ku-DNA complex then recruits the catalytic subunit of DNA-dependent protein kinase (DNA-PKcs), resulting in the formation of DNA-PK holoenzyme that consists of the Ku heterodimer and DNA-PKcs. Following the recruitment of DNA-PKcs, the Ku complex translocates inwardly along the DNA that allows DNA-PKcs to interact directly with DNA termini. The presence of DNA-PKcs on the opposite DNA termini not only promotes tethering of two DNA molecules [240, 247], but also stimulates its kinase activity [247, 251], which, in addition to phosphorylating itself, also phosphorylates

different downstream targets that mediate DSB repair [251]. Depending on the type and complexity of the DSB, modifications of the DNA ends may be required before the broken ends can be rejoined. As an instance, DNA termini with single-stranded overhangs can either be filled-in or resected to make them ligatable. The filling-in of missing nucleotides during C-NHEJ is executed by DNA polymerases μ and λ, whereas excision of single-stranded overhangs is generally performed by C-NHEJ specific nuclease Artemis. Moreover, DNA termini can also possess 3′- and/or 5′-blocking lesions (as in IR or ROS instigated DSBs) and in such cases several end-processing proteins involved in BER (e.g. polynucleotide kinase 3′-phosphatase) as well as enzymes involved in other DNA repair pathways (e.g. Exo1) may participate in 'cleaning' the DNA ends to produce ligation compatible 3′-hydroxyl and 5′-phosphate groups. Because the end processing may involve gain or loss of nucleotides, the error-prone nature of C-NHEJ has been attributed specifically to enzymes participating in the DNA end modification step. Following the processing of the DNA termini, the DNA ends are ligated by DNA ligase IV in association with its binding partner XRCC4 [240]. Moreover, XLF interacts with XRCC4-DNA ligase IV complex to enhance DNA ligation [240] and it is believed that XLF stimulates ligase IV activity particularly towards blunt (non-cohesive) DNA ends [247].

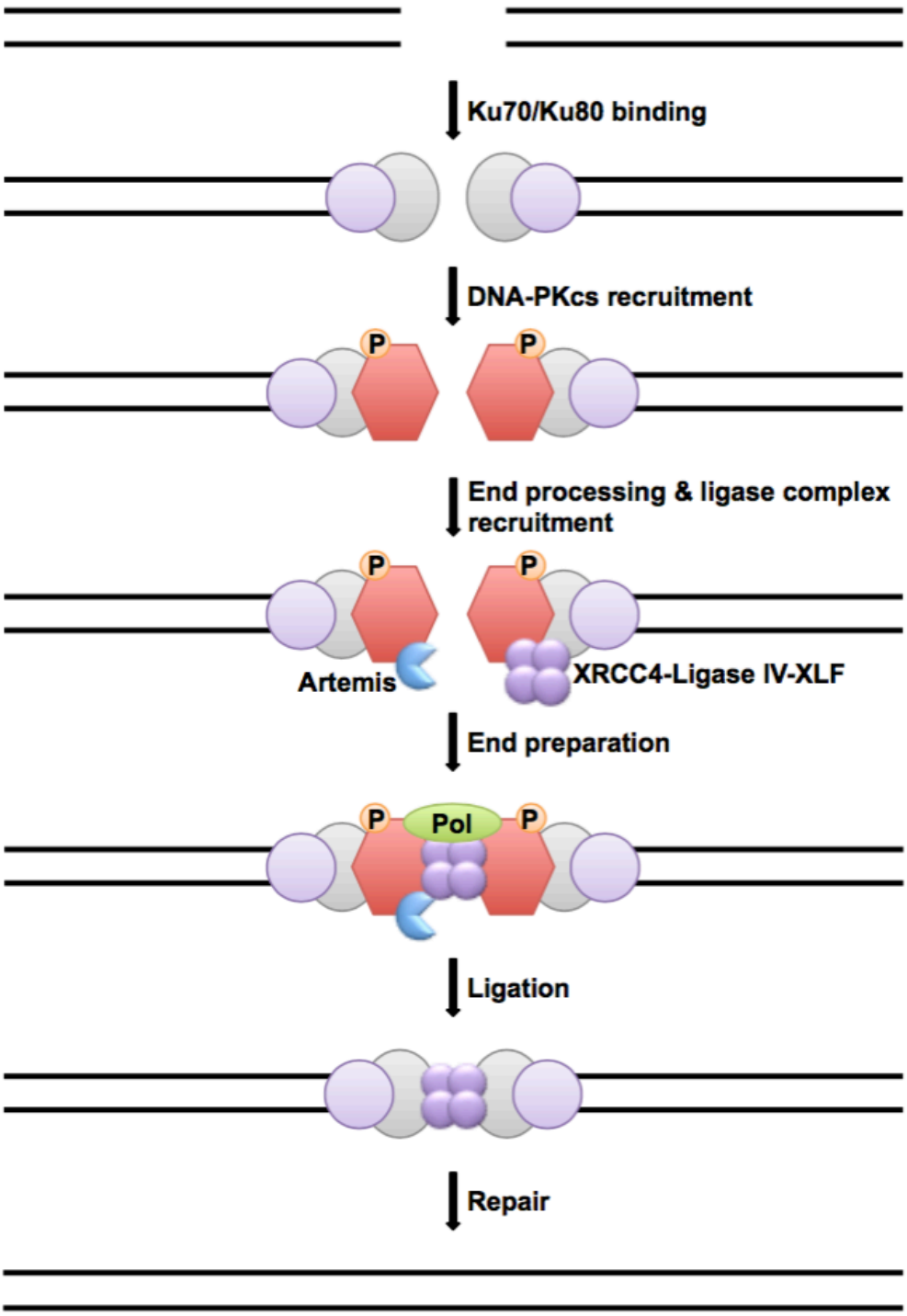

Figure 20. Schematic representation of the mechanism of DSB repair via C-NHEJ. During C-NHEJ, broken DNA ends are bound and stabilized by Ku70/Ku80 heterodimer, which in turn recruits DNA-PKcs resulting in the formation and activation of DNA-PK holoenzyme. Recruitment of downstream factors involved in end processing and ligation ensue that eventually carry out the final rejoining reaction (Redrawn from Renodon-Cornière *et al*. [248].)

4.2.2.2 Alternative NHEJ (A-NHEJ)

A-NHEJ, also known as microhomology-mediated end joining (MMEJ), is a Ku-independent end-joining pathway that, like C-NHEJ, can be active throughout the cell cycle [250]. Since deletion of essential C-NHEJ components led to the identification of A-NHEJ, this pathway is believed to be secondary to C-NHEJ [250]. In accordance with this belief, it has been revealed that A-NHEJ predominates in cells with deficiencies in C-NHEJ [250, 252]; nonetheless, A-NHEJ also operates in C-NHEJ proficient cells [252]. When compared to C-NHEJ, A-NHEJ is more mutagenic since it frequently utilizes complementary microhomologies located away from the DSBs. Such microhomologies are revealed by extensive resection of DNA from the DSBs, and as a result large deletions often occur at the repair junction [250, 252, 253].

The factors that mediate A-NHEJ and the underlying mechanisms are still not completely understood [252, 254]; nonetheless, PARP-1 has been implicated in the initiation process (Figure 21) [253], which is believed to mediate bridging of DNA ends, a process commonly referred as DNA synapsis [254]. Moreover, PARP-1 may also act as a scaffold to directly or indirectly recruit downstream A-NHEJ factors [254]. A-NHEJ generally involves exposure of up to 25 bp regions of microhomologies between the DNA strands [250]. Such complementary microhomologies are revealed by nucleolytic degradation of DNA from DSB ends, a phenomenon facilitated by nucleases Mre11 (a component of MRN complex) and CtIP [252-254]. Following alignment of the regions of microhomologies, polymerase β or θ fills the gap [250, 255] and finally DNA ligase III/XRCC1 complex, which is probably the major A-NHEJ ligase complex, catalyzes the

strand ligation [250, 253, 254]; moreover, evidence also exists in favor of DNA ligase I as a factor involved in the ligation step [252, 254].

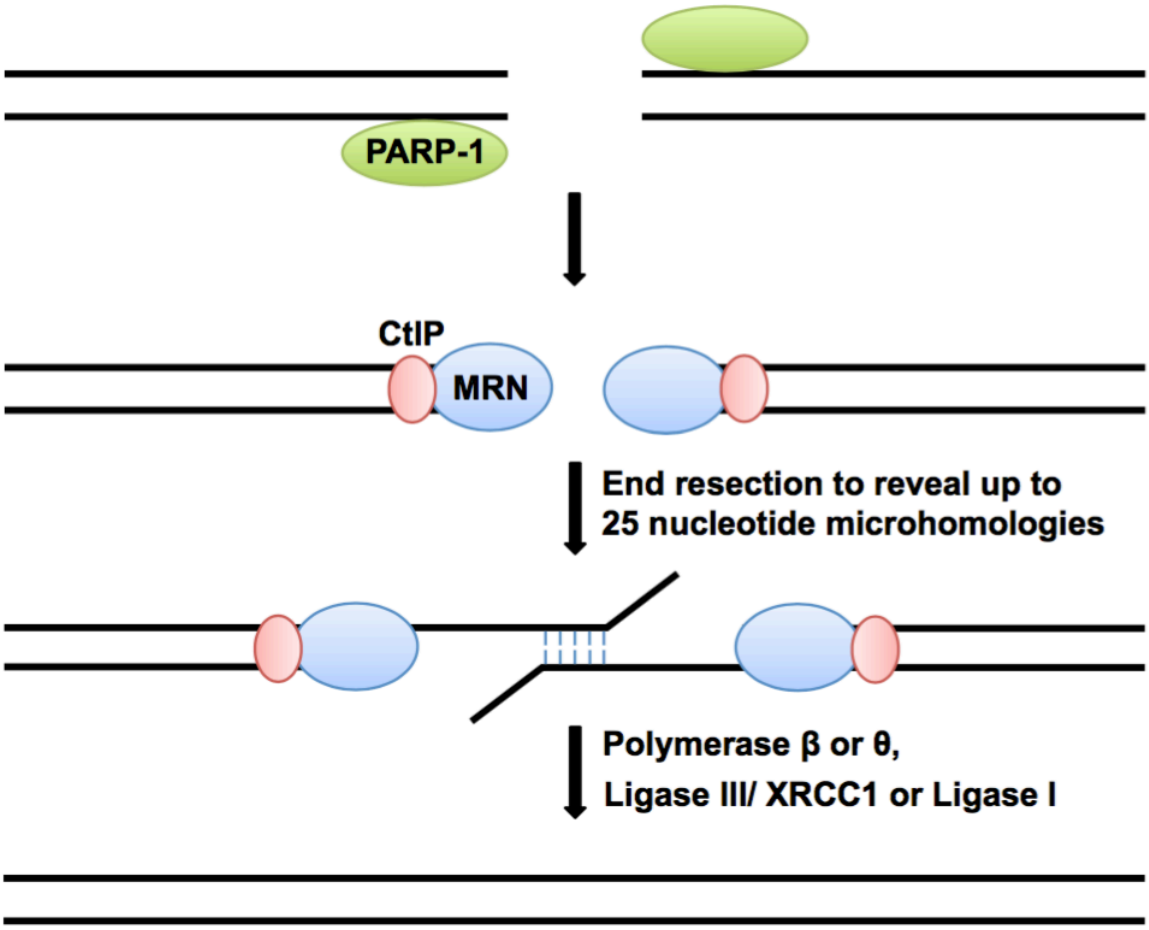

Figure 21. Model for DSB repair via A-NHEJ. The molecular players and events underlying A-NHEJ are still unclear; nonetheless, a number of factors involved in the process have been discovered. PARP-1 is believed to be involved in DNA synapsis and may also act as a scaffold to recruit downstream A-NHEJ proteins. MRN complex and CtIP have been implicated in nucleolytic degradation of DNA that exposes regions of microhomologies between DNA strands. After alignment of complementary regions, DNA polymerase β or θ fills the gap and the final nick is sealed by DNA ligase III/ XRCC1 complex or by DNA ligase I (Adapted from Fell and Schild-Poulter [250], and Deriano and Roth [252]).

4.2.2.3 Human Ku complex

Conserved from bacteria to humans, Ku is probably the most important C-NHEJ core component that is strictly required for DSB repair via C-NHEJ [256]. The eukaryotic Ku exists as a heterodimer with the individual monomer encoded by duplicate copies of an ancestral gene present in prokaryotes [249, 256]. Originally identified as an autoantigenic protein from a scleroderma patient with the initials K.U., Ku is an abundant protein (in humans, ~500,000 molecules per cell) that localizes primarily in the nucleus. In eukaryotic cells, most Ku is present as highly stable heterodimeric Ku70/Ku80 (~70 and ~80 kDa, respectively) complex, and the vast majority of data suggests that Ku functions primarily as a heterodimer [251]. The crystal structure of human Ku heterodimer revealed that the two subunits fold to assume an asymmetric ring shaped structure containing an aperture that is large enough to allow dsDNA through it [257]. Moreover, this conserved β-barrel ring structure binds avidly to DNA termini in a sequence independent manner [249]. The Ku heterodimer exhibits a high degree of versatility in recognizing and interacting with DNA ends as it is able to bind to blunt ended DSBs, DSBs with 3′ or 5′ overhangs, as well as with IR induced DSBs [251]. Once bound, the Ku complex protects DNA termini from non-specific degradation as evinced from the observation that Ku-deficient cells exhibit nucleolytic processing at DSB ends. Because it prevents the resection initiation at the DNA ends, binding of the Ku complex to DSBs has an inhibitory effect on HR as well as A-NHEJ [250].

Each Ku subunit is composed of three regions, viz., an amino terminal von Willebrand A (vWA) domain, a central ‘core’ domain, and a divergent carboxy-terminal region (Figure 22). The vWA domain of Ku70/Ku80 enables the Ku complex to recruit

downstream NHEJ factors to the DSB site [258]; moreover, this domain may also be required for heterodimerization of the Ku subunits [251, 257]. The core of Ku is conserved among all Ku orthologs and is required for dimerization as well as for formation of ring structure that binds to dsDNA ends [257]. The carboxy-terminal of Ku70 contains a SAP domain that is believed to possess a DNA binding activity [251, 257, 258], which may prevent Ku from translocating away from the dsDNA ends [258]. On the other hand, Ku80 contains a longer carboxy-terminal domain and in humans (and other higher eukaryotes), this domain contains a region (PK) to which DNA-PKcs can interact (Figure 22A) [251, 257]. Indeed, Ku in vertebrates is regarded as a component of DNA-PK holoenzyme that is made up of the Ku heterodimer and DNA-PKcs [251], both of which are essential for effective DSB repair via C-NHEJ. Even though primarily known for its role in DSB repair, human Ku is also known to participate in numerous additional cellular processes, including antigen receptor gene rearrangement, telomere maintenance, apoptosis and transcription [251].

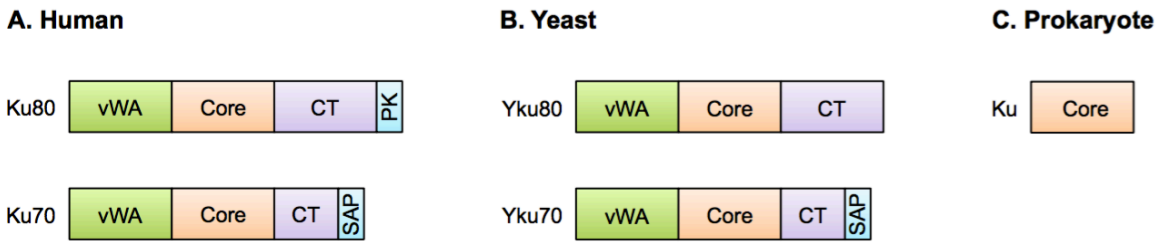

Figure 22. Domain organization of eukaryotic and prokaryotic Ku proteins. (**A** and **B**) Eukaryotic Ku proteins consist of an amino-terminal vWA domain, a central core domain, and a diverged carboxy-terminal (CT) domain. Ku70 and Yku70 (Ku70 in yeast) possess SAP domain in their carboxy-terminal region. (**A**) In humans and other higher eukaryotes, Ku80 has a longer CT domain that harbors a region (PK) to which the DNA-PKcs can bind. (**B**) In *S. cerevisiae*, heterodimeric Ku subunits are referred as Yku70 and Yku80. The tripartite organization of human Ku80 persists in Yku80; however, in contrast to human Ku80, the C-terminal domain of Yku80 is devoid of the DNA-PKcs binding motif. (**C**) In prokaryotes, only one Ku species generally exists that typically contains just the central core domain (Redrawn from Downs and Jackson [251]).

4.2.2.4 Yeast Ku (Yku) complex

In *S. cerevisiae*, the Ku complex is commonly referred as Yku [249] and the heterodimeric subunits are called Yku70 and Yku80, even though each subunit is ~70 kDa [256]. Analogous to the human Ku, binding of Yku complex to DSBs not only protects DNA ends from degradation, but also impedes the onset of resection, thus offering a window of opportunity for repair via C-NHEJ [239]. As shown in Figure 22, the domain organization of Yku70 is identical to that of human Ku70; however, the structure of Yku80 differs from human Ku80 in that the C-terminal domain of the former lacks PK region [251], which is in accordance with the observation that yeast cells are devoid of DNA-PKcs [256].

Like human Ku, Yku is a multifunctional protein that is involved in genome stability not only by mediating DSB repair, but also by participating in telomere maintenance [249, 256, 257]. Indeed, the role of Yku in C-NHEJ is genetically separable from its involvement in telomere function [249]. In Yku70/Yku80 heterodimer, the C-terminus of Yku80 is oriented towards the DSB end that consistently interacts with Dnl4 (a DNA ligase required for C-NHEJ) [256]. Thus, the C-terminus of Yku80 is essential for its role in C-NHEJ as evinced from the observation that mutation in its C-terminus selectively impairs C-NHEJ [249]. On the other hand, the C-terminus of Yku70, which is oriented inward on the DNA helix in a direction opposite to DSBs, is indispensible for telomere stability [249, 256].

4.3 NHEJ in prokaryotes

Prokaryotes were initially believed to repair DSBs exclusively by HR via a mechanism that is largely similar to that adopted by eukaryotic counterparts, and the NHEJ pathway was thought to confine only among eukaryotes. However, the discovery of an evolutionary related NHEJ apparatus in prokaryotes in 2001 rectified the misconception [258]. Indeed, the homologs of Ku, a 'hallmark' protein of C-NHEJ, together with an intact NHEJ system have been identified in a variety of bacterial species including *Mycobacterium tuberculosis*, *Pseudomonas aeruginosa*, and *Bacillus subtilis*. However, Ku is not ubiquitous among prokaryotes, indicating that NHEJ does not exist in all bacteria [258]. The answer as to why only select prokaryotes are endowed with NHEJ is still unclear [259]; nonetheless, it has been noticed that many of the bacterial species that possess NHEJ apparatus spend much of their life cycle in a non-replicating state [260]. Hence it might be the case that NHEJ offers protection to bacterial species during stressful conditions when only a single copy of genome is available, for example after sporulation or during stationary phase [261]. The prokaryotic NHEJ apparatus, moreover, likely possess additional biological functions that may vary in different species of bacteria [259]. For example, a recent study has extended the function of bacterial Ku protein in protecting *M. smegmatis* (a soil-dwelling mycobacterium) cells against zinc toxicity [262].

In contrast to multiple protein components that act as C-NHEJ machinery in eukaryotes, the bacterial NHEJ system is believed to comprise of only two proteins, viz., a Ku protein and a multifunctional DNA ligase D (LigD) [261]. Bacterial Ku proteins differ from the larger eukaryotic counterparts in that they are comparatively small with

molecular weight of ~30-40 kDa. Moreover, Ku homologs in prokaryotes, in general, contain only the conserved central "ring shaped" core domain but lack additional N- and C-terminal domains present in eukaryotic Ku (Figure 22). Another distinguishing feature of bacterial Ku is that it exists predominantly as a homodimer, as opposed to heterodimeric eukaryotic Ku proteins [258]. In analogous to eukaryotic Ku, however, bacterial Ku proteins bind to DSBs and bring two DNA termini in close proximity, following which the Ku-DNA complex recruits LigD to DSB ends (Figure 23) [258, 263]. Thus, functionally bacterial Ku is similar to its eukaryotic counterpart in that both proteins bind to DNA termini following which the next protein in the pathway is recruited [264]. LigD is a large protein that harbors multiple domains, viz., a polymerase domain, a 3′-phosphoesterase/nuclease domain, and an ATP-dependent ligase domain [263]. Thus, the prokaryotic DNA repair ligases, in general, are multifunctional DNA repair machines that harbor, apart from 5′→3′ exonuclease activity, all the enzymatic activities necessary to process and join incompatible DSB ends. These enzymatic domains of LigD are equivalent to multiple independent eukaryotic factors dedicated to clean, process, and ligate DNA ends. Following its recruitment, the manifold activities of LigD eventually seal the DSB. Thus, bacterial Ku and LigD form a fully functional two component NHEJ repair system in prokaryotes [258].

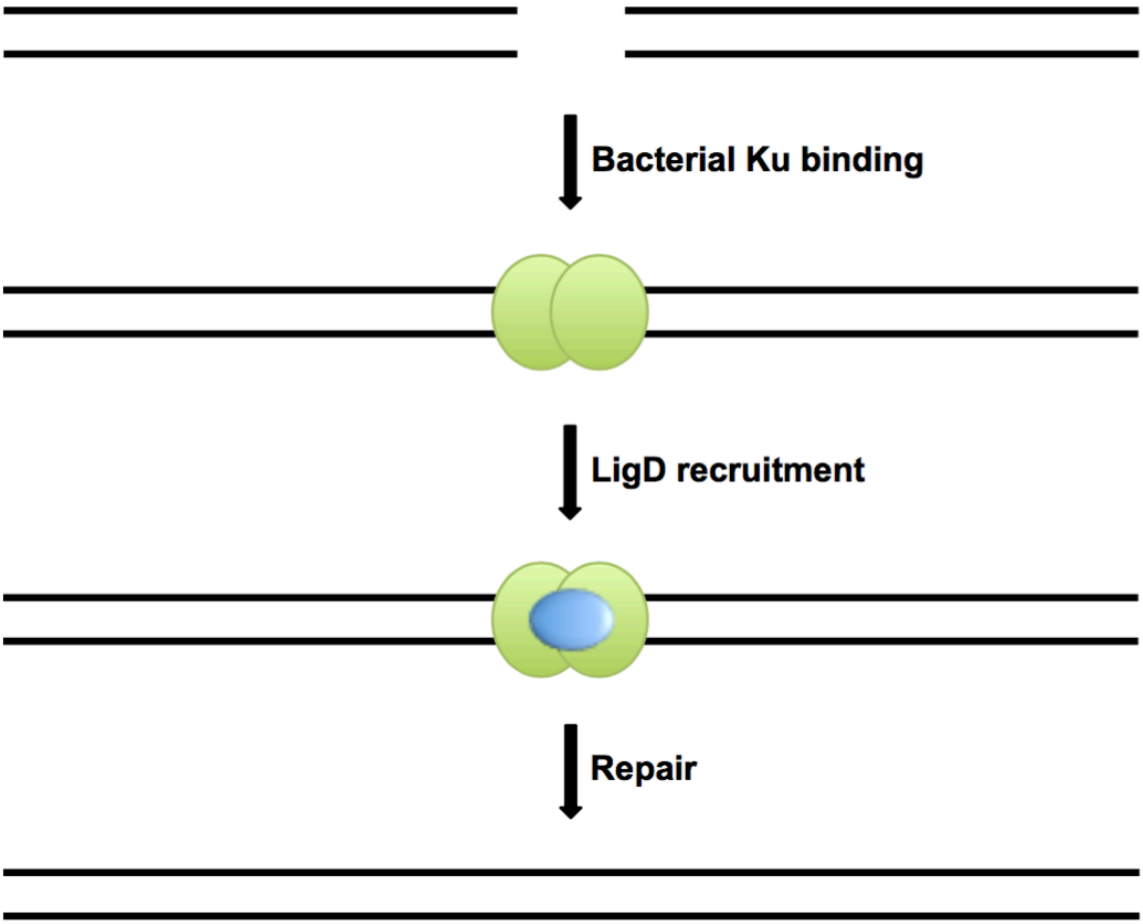

Figure 23. Two-component repair system of bacterial NHEJ. In select prokaryotes that are equipped with NHEJ machinery, the dsDNA termini are recognized and bound by bacterial Ku homodimer, which then recruits LigD to DSB ends. The multiple activities of the latter protein ultimately rejoins the DSB (Adapted from Shuman and Glickman [263]).

4.3.1 Ku proteins in *Mycobacterium tuberculosis* and *Mycobacterium marinum*

Mycobacterium tuberculosis is one of the most infectious microorganisms and causes tuberculosis in humans. In most cases, *M. tuberculosis* is transmitted through the respiratory route and after the bacteria reach the alveoli, they are phagocytosed by resident alveolar macrophages [265]. An important characteristic feature of tuberculosis is its ability to persist in an infected host for many years without exhibiting outward sign of infection, and during such periods the bacteria are in a non-replicative state [265]. Under such conditions, bacterial NHEJ is believed to provide protection to the bacteria from the host as the dormant *M. tuberculosis* cells can utilize NHEJ to repair multiple DSBs presumably instigated by genotoxins (e.g. ROS) produced from host macrophages [261]. The NHEJ apparatus in *M. tuberculosis* have been named as MtKu and MtLigD. MtKu is ~30 kDa in size that, like other prokaryotic Ku, binds DNA DSBs as a homodimer following which MtLigD is recruited to mediate DSB repair [264]. Like *M. tuberculosis*, *M. marinum* is also a pathogenic mycobacterium that primarily infects poikilotherms such as fish and frogs [266], and has mechanisms of survival and persistence inside macrophage similar to that of *M. tuberculosis* [259]. These two mycobacterial species are genetically closely related, so much so that they have ~85% amino acid sequence identity for the ~3000 orthologs. A recent study has revealed that *M. marinum* also possesses a competitive NHEJ pathway in analogous to *M. tuberculosis*. In the study, the NHEJ components of *M. marinum*, referred as MmKu and MmLigD, were expressed in *E. coli* (a model system that lacks NHEJ pathway) and it was shown that both proteins (i.e. MmKu and MmLigD) were necessary to recircularize linearized plasmid DNA in the host organism. The study also demonstrated that MtKu cooperates

with MmLigD, and similarly, MmKu can function with MtLigD to rejoin linearized plasmid DNA. As MtKu does not cooperate with all DNA ligases (e.g.T4 DNA ligase, yeast NHEJ DNA ligase, etc.) for sealing DSBs, the study provided a clear indication for substantial homology between repair proteins as well as between NHEJ repair systems in the two mycobacterial species [259].

It is interesting to note that most Ku encoding bacteria have the Ku gene organized into an operon with a gene encoding LigD on the bacterial chromosome [258, 263]. The gene arrangements for Ku and LigD on the chromosomes of *M. tuberculosis* and *M. marinum* are demonstrated in Figure 24, which reveals that genes encoding Ku and LigD are separated by 115 bp in *M. tuberculosis*. In contrast, a 1105 bp region, which also consists of a gene encoding fructokinase, separates the two NHEJ genes in *M. marinum*. Moreover, Figure 24 also demonstrates that the Ku and LigD ORF are transcribed in reverse direction in both organisms [259].

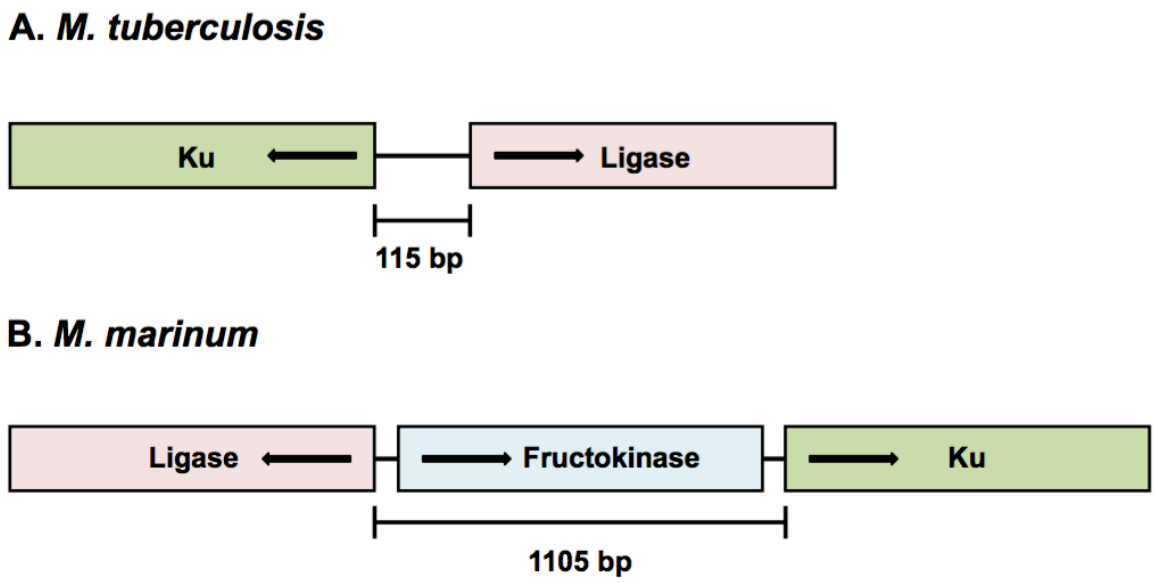

Figure 24. Operons for mycobacterial NHEJ proteins in chromosomes of *M. tuberculosis* and *M. marinum*. (**A**) In *M. tuberculosis*, the Ku and LigD genes are separated by 115 bp region, whilst in (**B**) *M. marinum*, these two genes are separated by a 1105 bp region that also harbors a gene for fructokinase. In both organisms, Ku and LigD ORF are transcribed in opposite direction (Redrawn from Wright *et al*. [259]).

Recently, the structure of bacterial Ku has been categorized into three distinct regions (Figure 25), viz., the core DNA binding domain, the minimal C-terminus, and the C-terminal extension (from amino acid 260 to the end of the protein; Figure 25) [260, 267, 268]. The minimal C-terminus is required for the interaction between Ku and LigD as well as for stimulation of LigD activity [268], whereas the functions of the C-terminal extension have been associated with the types of DNA structures that can be bound by Ku, translocation of Ku along the DNA, and Ku mediated apposition of DNA ends [260, 267, 268]. Interestingly, the sizes of core DNA-binding domains and minimal C-termini are the same for MtKu and MmKu; moreover, these proteins exhibit a high degree of sequence homology in both these regions [259]. However, MmKu possesses the C-terminal extension that consists of 32 amino acids, of which 11 residues are basic (bold letters; Figure 25). In contrast, MtKu consists of only 14 amino acids past the minimal C-terminus, of which only 3 are basic, and hence MtKu is said to be devoid of a C-terminal extension. The basic residues at the C-terminal end have been predicted to form electrostatic interactions with negatively charged DNA [267, 268]. Indeed, Ku protein from *M. smegmatis*, which possesses the C-terminal extension with multiple basic amino acid residues, has the ability to bind to supercoiled as well as DNA with free ends, a feature not exhibited by MtKu that binds only to linearized DNA [260]. Accordingly, MmKu, which also possesses a C-terminal extension with multiple basic residues, is anticipated to bind to DNA with and without free ends [259].

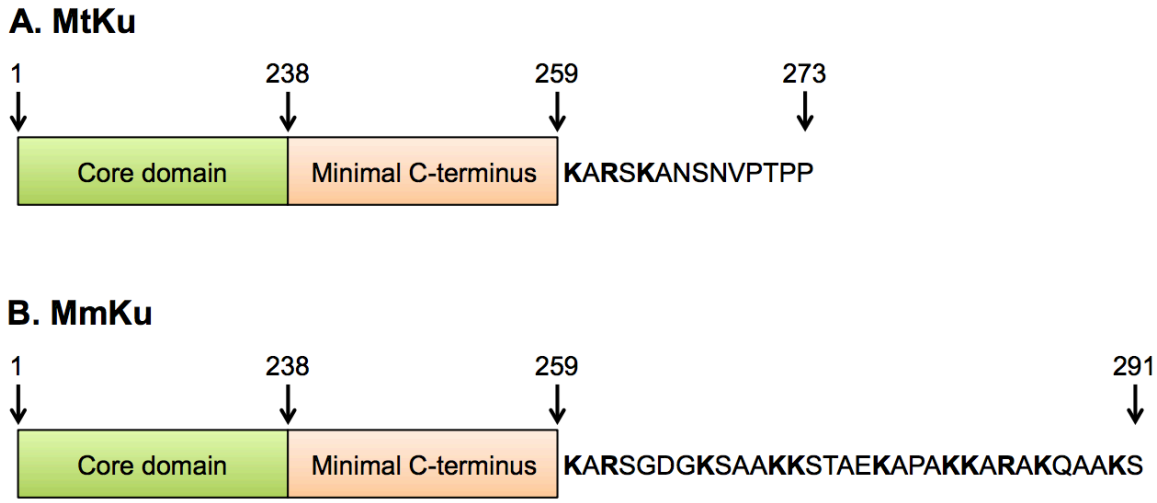

Figure 25. Regions in MtKu and MmKu proteins. Three regions of bacterial Ku proteins have been defined, viz., the core domain, the minimal C-terminus, and the C-terminal extension. In the figure, numbers above arrows denote amino acid number. In contrast to (**A**) MtKu, (**B**) MmKu possess C-terminal extension with multiple basic amino acid residues (bold letters after amino acid 259) (Adapted from Wright *et al*. [259]).

5. MTDNA REPAIR

5.1 Introduction

In a typical cell, mitochondria are the major sites for ROS generation and to deal with these metabolic byproducts, mitochondria are equipped with comprehensive defense systems (Section 1.5). However, deficiency or inefficiency of these ROS detoxifying systems could be deleterious for the integrity of the mitochondrial genome as several kinds of mtDNA damage can arise from ROS exposure (Section 3.1) [194]. As mtDNA encodes essential components of ETC and OXPHOS, failure to repair mtDNA lesions can lead to disruption of ETC and enhanced ROS generation, that can in turn result in energy depletion and ultimately cell death. Thus, an efficient mtDNA repair system is indispensible for maintaining the integrity of the mitochondrial genome and consequently for cellular homeostasis [269].

DNA repair was first reported for the nuclear compartment and was originally believed to be confined only to the nucleus. Despite the comprehension that mitochondria control a variety of crucial cellular parameters (Section 1.4), it was thought for many years that mitochondria lacked DNA repair mechanisms and the integrity of mitochondrial genome was believed to be preserved simply by degrading the damaged molecules [270]. However, a substantial body of evidence has confirmed that mitochondria are endowed with many of the same DNA repair mechanisms present in the nucleus (Sections 4.1 and 4.2), and these repair pathways, together with controlled degradation of mtDNA, help maintain the integrity of the mitochondrial genome [269-271]. The mitochondrial genome does not encode DNA repair proteins and these

organelles rely on translocation of nuclear-encoded repair enzymes, that, in general, localize to the inner membrane in the form of mitochondrial nucleoids [270]. The enzymes accountable for mtDNA repair are, in most instances, encoded by the same genes as their nuclear counterparts [272]. The basic principles of repair of nDNA and mtDNA seem to be very similar with the major difference being nDNA repair pathways involve a larger number of proteins. Moreover, our knowledge on mtDNA repair pathways is limited compared to nDNA repair pathways [241]. In sum, nucleus and mitochondria share a number of factors and processes involved in DNA repair; however, DNA repair in mitochondria also exhibits specific and original aspects (Section 5.2.2) [270].

DNA repair proteins are often mentioned to localize in the cytosol under unstressed conditions and then translocate into subcellular organelles in response to DNA damage [270]. For example, yeast cells subjected to nuclear or mitochondrial oxidative stress revealed that Ntg1, a BER enzyme with DNA glycosylase/ AP lyase activity, relocalizes dynamically to the respective subcellular compartment on which the stress was applied. By comparing ρ^+ and ρ^0 yeast cells, it was demonstrated that the localization of Ntg1 to mitochondria was triggered by mtDNA damage and not by mitochondrial ROS generated after treatment with extrinsic agents [273]. Thus, translocation of a pool of repair proteins from cytosol to the damaged compartment seems to be a major regulatory mechanism of DNA repair [270].

5.2 Types of mtDNA repair

Initially, evidence for mtDNA repair was obtained for SP-BER, and for many years, it was thought that the mtDNA repair system was limited to this pathway [269, 271]. However, the mitochondrial genome is inflicted with a wide range of complex lesions and also have potential for erroneous replication [269, 274]. Logically, just SP- BER seemed to be insufficient to handle a variety of lesions that mtDNA incur and it was speculated that additional repair pathways exist in the mitochondrial compartment. In accordance with the postulation, several studies have revealed the presence of mitochondrial LP-BER and MMR [269, 274]. Furthermore, evidences are also accumulating that support the existence of mitochondrial HR, C-NHEJ, and A-NHEJ [269, 274, 275]; however, there is a general consensus that NER does not operate in mitochondria [269, 271]. Finally, systems that remove mutagenic dNTP and degrade severely damaged mtDNA also play vital roles in preserving the integrity of mitochondrial genome [269, 274].

5.2.1 BER

Mitochondria are endowed with proficient BER, which is most likely the main mtDNA repair mechanism [194, 241, 271]. Mitochondrial expertise in this pathway is indeed logical given that mtDNA encounters a high degree of oxidative damage compared to the nuclear counterpart [271]. Evidence indicates that 8-oxoG, the most predominant oxidative base lesion, is more efficiently repaired in mitochondria compared to the nucleus [271]. Even though the molecular players in nuclear BER appear to be more diverse compared to the mitochondrial counterpart, the basic steps of BER seem to be the

same in the nucleus (Figure 16) and mitochondria [271]. Accordingly, mitochondrial BER can be divided into five steps, viz., (i) removal of damaged base; (ii) strand cleavage of the abasic site; (iii) DNA end processing; (iv) gap filling; (v) and ligation [194]. Enzymes involved in each of these steps have been identified in mitochondria making BER the only comprehensively delineated mtDNA repair pathway [194]. Like nuclear BER, two distinct BER pathways exist in mitochondria on the basis of the number of nucleotide(s) incorporated by DNA polymerase γ (pol γ): SP-BER involves addition of a single nucleotide into the gap, whereas in LP-BER multiple nucleotides are incorporated [269]. During SP-BER, a variety of mitochondrial DNA glycosylases (OGG1, UNG, MYH, NTH1, etc.) [269] recognize and eliminate damaged bases from mtDNA to generate AP sites [274]. These abasic sites then become substrate for APE1 [274], the only known mitochondrial AP endonuclease [269], that cleaves the phosphodiester backbone at the immediate 5′ position of the AP site to generate a 3′-hydroxyl and 5′-dRP residues [274]. Pol γ utilizes the 3′-hydroxyl end to prime DNA repair synthesis by inserting one nucleotide and the 5′-dRP residue is removed by the dRP lyase activity of pol γ. The final DNA nick that remains is eventually sealed by DNA ligase III to complete the SP-BER process [274].

Following strand cleavage, certain 5′-groups (e.g. 2-deoxyribonolactone) cannot be effectively eliminated by lyase activity of pol γ [271] due to which the 5′-end becomes incompatible for ligation, and under such situation, LP-BER pathway is adopted [194]. During this process, the 5′-blocking group is displaced by pol γ extending from the 3′-hydroxyl end resulting in the formation of a ‘flap’ like structure, which can be up to 6-9 nucleotides in length [271]. Evidence indicates that FEN1, an enzyme involved in nuclear

LP-BER, participates in mitochondrial BER as well [269]. This enzyme has been shown to remove short ssDNA flaps whereas long ssDNA flaps may necessitate Dna2 to first generate short flaps after which FEN1 may be involved in removing the remaining flap. Alternatively, EXOG, a mitochondrial 5′-exo/endonuclease may be involved in removing both short as well as long flaps and may be the primary 5′ flap-processing mitochondrial enzyme [194]. Finally, the nicked DNA that remains following flap removal is sealed by DNA ligase III [271].

5.2.2 MMR

Evidence indicates that mammalian mitochondria possess a novel MMR pathway [274] that is most likely distinct from the nuclear counterpart [241]. The fact that mtDNA instability in mammalian cells has been rarely associated with defects in nuclear MMR genes supports the notion that MMR machineries in the mitochondrial and nuclear compartments are independent of each other [194]. The key factor involved in human mitochondrial MMR responsible for mismatch recognition and binding has been revealed to be Y-box binding protein 1 (YB-1) [241, 274]. This mammalian mitochondrial protein detects base mismatches and small insertion/deletion loops (IDLs) and is thought to have a function analogous to MutSα (Figure 18) [194]. The involvement of YB-1 in mitochondrial MMR is underscored from the observation that mitochondrial extracts depleted of YB-1 has a substantially reduced mismatch binding and repair activity. Moreover, silencing of YB-1 is known to evoke mtDNA mutagenesis [269]. YB-1, after recognizing and binding to the mismatch, is believed to recruit the downstream mitochondrial MMR complex, the identity of which is currently unknown [194]. Thus,

the mammalian mitochondrial MMR pathway is far from being fully characterized as additional factors involved in the process are yet to be identified [274].

In regard to the mitochondrial MMR in *S. cerevisiae*, the MutS homolog (MSH1) has been identified in yeast mitochondria that can repair G:A mispairs as well as other mismatches [269, 270]. Moreover, a MutL homolog (MLH1) has also been detected in *S. cerevisiae* mitochondria [241]. Even though the MutS homolog has not been identified in mammalian mitochondria, a study has recently reported the presence of a MutL homolog (MLH1) in mitochondria of human tumor cells [269]. However, an independent study produced a conflicting result as it could not detect MLH1 in HeLa cell mitochondria [269].

5.2.3 Sanitation of premutagenic free nucleotides

Free dNTPs, which are utilized as precursors for replication and repair, are under constant exposure to oxidation and other stresses [269]. Oxidation of the mitochondrial dNTP pool represents a major threat to mtDNA integrity [269] as damaged dNTPs can substantially contribute to mismatch errors during DNA synthesis [271]. For example, 8-oxo-dGTP can be incorporated opposite to adenine (A) by pol γ, a process that can lead to A to C transversions. In order to avoid misincorporation of potentially mutagenic dNTPs into mtDNA, a number of triphosphatases sanitize the dNTP pool in the mitochondrial compartment [241]. For instance, MTH1 is known to localize to mitochondria where it hydrolyzes 8-oxodGTP to 8-oxodGMP. The latter nucleotide is not a substrate for pol γ and hence cannot be incorporated into the mtDNA [241, 274]. Moreover, MTH1 also hydrolyzes two major oxidation products of dATP, viz., 8-oxo-2′-

deoxyadenosine triphosphate and 2-hydroxy-2′-deoxyadenosine triphosphate [274]. Similarly, dUTPase is another important triphosphatase that sanitizes the mitochondrial compartment by removing dUTP from the nucleotide pool that arise via deamination of TTP [241, 269, 270]. Sanitation of the dNTP pool also occurs in the nucleus, and even though it is not a DNA repair mechanism *per se*, the process helps in maintenance of the integrity of cellular genomes by reducing DNA mismatches [271].

5.2.4 mtDNA degradation

Mitochondria, unlike the nucleus, also possess an option to selectively degrade damaged mtDNA that is beyond the scope of repair [194, 274]. Since a typical cell contains multiple copies of mtDNA, the degradation of severely damaged mtDNA molecules can be tolerated without compromising mitochondrial function [194, 271]. Indeed, by targeting site-specific restriction endonuclease into mitochondria, several studies have revealed that extensive or persistent DSBs lead to mtDNA degradation, whereas low levels of DSBs result in repair [274]. Recently, it has been shown that oxidative stress can also elicit mtDNA degradation. Moreover, inhibition of processing of abasic sites by APE1 further enhanced mtDNA degradation in response to oxidative stress, bolstering the idea that the inability to repair mtDNA may be a beacon for its degradation [269, 274]. The signal that triggers mtDNA degradation is assumed to be produced by stalled replication or transcription machineries on the damaged mtDNA template [194, 274]. As strand breaks and abasic sites lack coding information, selective degradation of severely damaged mtDNA is believed to play a crucial role in preventing mutagenesis thereby ensuring the fidelity of mitochondrial genome [274]. Endonuclease G (endoG), the most abundant and active nuclease in mitochondria, was initially hypothesized as a likely

candidate that selectively degrades irreparable mtDNA [269, 274]. However, endoG localizes exclusively in the mitochondrial IMS and its activity has neither been detected in the interior face of the MIM nor in the matrix [274]. Moreover, endoG deficient cells or endoG null mice do not exhibit accumulation of mtDNA mutation, indicating that endoG may not be the nuclease involved in mtDNA degradation [269]. Hence, it has been speculated that a novel, yet unidentified mitochondrial nuclease may be involved in degrading severely damaged mtDNA [274].

5.3 mtDNA DSB repair in mammals

Analogous to nDNA DSB repair (Section 4.2), repair of mtDNA DSBs may occur via HR, C-NHEJ, or A-NHEJ. However, owing to the presence of multiple copies of mtDNA, HR is likely to be a favorable repair system for dealing with mtDNA DSBs [241]. In this context, many nuclear HR proteins have been identified in the mitochondrial compartment [276]. For example, Rad51, a key component of nuclear HR, has been detected in human cell mitochondria where it was shown to bind to mtDNA following exposure of cells to oxidative stress [269]. Moreover, Mre11, a component of the MRN complex, has been identified in mammalian mitochondria bound to mtDNA [194, 277]. Another important component identified in mitochondria that may potentially participate in HR is Dna2 [194]. EXOG, a mitochondrial 5′-exo/endonuclease, is hypothesized to be the mitochondrial equivalent of Exo1 that may be involved in production of 3′-ssDNA tails. Thus, mammalian mitochondria appear to harbor the basic apparatus of HR [194], and in fact evidence exists in favor of HR being operative in

mammalian mitochondria [194, 241, 270, 274]. For example, mammalian mitochondrial protein extracts were shown to catalyze HR of plasmid DNA substrates and this activity was massively reduced by anti-RecA antibody, indicating that a homolog of the bacterial strand-transferase protein RecA is involved in HR activity in mammalian mitochondria [278]. Another study utilized inducible expression of mitochondrial-targeted restriction endonuclease *Sca*I in heteroplasmic cells and heteroplasmic mice to generate DSBs in mtDNA. After transient expression of the restriction endonuclease followed by a long period of recovery, both intramolecular and rare intermolecular recombination products containing large deletions were identified, indicating that induction of DSBs in mtDNA promotes recombination resulting in large deletions [279]. Similarly a separate study utilized a mouse model for expression of an inducible mitochondrial-targeted restriction enzyme *Pst*I to introduce mtDNA DSBs in adult neurons. Transient expression of the enzyme led to the generation of a family of deleted mtDNA that closely resembled naturally occurring mtDNA deletions [280]. This suggested that DSBs can act as an initiator of different types of naturally occurring mtDNA rearrangements that are observed in aging and different mitochondrial diseases [279].

Evidence also suggests that C-NHEJ exists in mammalian mitochondria [269]; however, like mitochondrial HR, our understanding of C-NHEJ is also incomplete. A study revealed that mitochondrial protein extracts prepared from a hamster cell line lacking Ku80 mRNA expression was devoid of DNA end-binding activity, which was present in similar extracts prepared from wild-type cells. Immunoblotting of mammalian mitochondrial protein extracts with a monoclonal antibody specific for an N-terminal epitope of Ku80 detected a 68 kDa protein. However, this mitochondrial protein could

not be detected by a monoclonal antibody specific for a C-terminal epitope of Ku80. The study concluded that a C-terminally truncated form of Ku80 is present in mammalian mitochondria that performs DNA end-binding activity and that Ku80 gene expression is necessary for mammalian mitochondrial DNA end-binding [281]. Another study investigated the ability of mammalian mitochondrial protein extracts to mediate repair of DNA DSBs introduced via restriction digestion following which repair products were analyzed. End joining was reported to be highly precise in the case of linearized DNA containing cohesive ends whereas blunt-ended DNA were rejoined with decreased precision and efficiency. Molecular characterization of all imprecisely repaired products showed DNA deletions spanning two direct repeats. As the deletions observed in the study were very similar to mtDNA from aged humans and patients with certain mitochondrial diseases (e.g. Kearns-Sayre syndrome, Pearson syndrome, etc.), the study concluded that that mammalian mitochondria are able to repair DSBs and the repair pathway(s) likely play(s) a role in generating mtDNA deletions seen in a number of human pathologies [282].

Interestingly, evidence is also accumulating for the presence of A-NHEJ (also referred as MMEJ) in mammalian mitochondria. A recent study revealed that CtIP, FEN1, Mre11, PARP-1 and DNA ligase III function together to efficiently repair DSBs in mammalian mitochondria via A-NHEJ. The study reported that a minimum of 5-nucleotide microhomology was essential for efficient mitochondrial A-NHEJ and the efficiency of the joining was further enhanced as the length of the microhomology was increased [275]. As A-NHEJ generates deletions, the mechanism of this pathway indeed explains the common deletions observed in human mitochondrial genome that occurs

between two 13 bp direct repeats located ~5 kb apart [194]. Moreover, A-NHEJ may also be responsible for generation of different human mtDNA deletions as the vast majority of mtDNA deletions witnessed *in vivo* span direct repeat sequences of 5-13 bp [275].

In summary, these observations clearly support the existence of mammalian mtDNA DSB repair pathways. Although the sequential molecular events and entire catalog of molecular factors involved in the repair of mtDNA DSBs are far from being discernible, aforementioned evidences suggest that HR, C-NHEJ, and A-NHEJ most likely participate in repairing mtDNA DSBs.

5.4 mtDNA DSB repair in yeast

Even though budding yeast is frequently used as a model system to elucidate various aspects of mitochondrial biology, experimental evidence regarding mtDNA DSB repair is probably present more in mammalian systems than in this unicellular eukaryote. Nonetheless, evidence does exist in support of mtDNA DSB repair in yeast [194]. In fact, recombination of the mitochondrial genome is well accepted in yeast, and it also appears to be an important mechanism for propagation of its mitochondrial genome (Section 2.3.1) [194, 271]. A variety of proteins potentially involved in recombination have been identified in yeast mitochondria [270] that include mitochondrial recombinase Mhr1, 5′→3′ DNA helicase Pif1, cruciform cutting endonuclease Cce1, and 5′→3′ exonuclease Din7 [241]. Additional proteins identified in yeast mitochondria that are likely involved in recombination include Mre11, Rad50, Rad51, and Rad59 [241, 276]. Even though the roles of Mre11 and Rad50 have not been yet characterized, yeast cells devoid of the

Mre11/Rad50/Xrs2 complex (MRX; MRN in mammals) have mtDNA rearrangements, indicating the involvement of the complex in mitochondrial DSB repair [194]. A recent study in *S. cerevisiae* mutant lacking MRX complex revealed a reduction in the rate of mtDNA deletions relative to wild-type. In contrast, the mutant lacking Yku70/Yku80 showed increased mtDNA deletion rate than wild-type strain. Apparently, the absence of the Yku complex likely favored recombination-dependent pathway for the repair of mtDNA DSBs leading to mtDNA deletions. The study supported the theory that HR is the major pathway by which mtDNA deletions occur, and emphasized the importance of the MRX and Yku complexes in the repair of mtDNA DSBs [277]. A separate study demonstrated that Rad51 and Rad59, proteins involved in nuclear HR, localize in budding yeast mitochondrial matrix and that Rad51 physically interacts with the yeast mitochondrial genome. By utilizing a mitochondrial-targeted restriction endonuclease *Kpn*I to introduce a DSB in the mitochondrial genome, the study revealed that loss of Rad51, Rad52, and Rad59 substantially reduced the rate of DSB induced mtDNA deletion. Moreover, repair of induced mtDNA DSBs was impaired as a result of loss of Rad51 and Rad59. Furthermore, absence of Rad51, Rad52, and Rad59 also decreased the rate of spontaneous mtDNA deletion events. These observation provided a clear indication these nuclear HR proteins are also involved in repair of mtDNA DSBs and such process can result in generation of mtDNA deletions [276].

6. YEAST AS A MODEL SYSTEM FOR STUDYING MTDNA METABOLISM

S. cerevisiae is an outstanding model organism to explore a myriad of basic cellular processes that are highly conserved among eukaryotes [283]. Examples of cellular pathways that have been conserved from yeast to humans include, but not limited to, DNA replication, recombination and repair, RNA transcription and translation, and mitochondrial biogenesis [284]. Many distinct features of this unicellular eukaryote render it a valuable and advantageous model system, not only for studying eukaryotic cell biology but also for unraveling the molecular details that underlie human pathophysiology. *S. cerevisiae* cells can be cultured in an economic manner and the duration of their cell cycle is short; in addition, they are easy to handle and are able to grow under a wide variety of conditions as well as in different carbon sources [284]. Above all, genome manipulation via genetic engineering is highly efficient and easy to achieve in this highly versatile model system. The simplicity of genome manipulation has made it possible for the generation of a wide range of comprehensive genomewide gene deletion libraries and gene fusion cassettes that are now available for scientific communities for systematic studies [285]. Furthermore, the availability of haploid and diploid strains and the feasibility to physically separate and identify all four haploid cells arising from a single meiotic event have made yeast an important organism for genetic manipulation [284]. Because of the ease of genome manipulation, budding yeast has been extensively exploited by cell biologists to determine if a particular gene is involved in mtDNA metabolism. For instance, by deleting a specific nuclear gene, it is possible to identify if its product is required in maintenance of the mitochondrial genome.

As a typical facultative anaerobe, *S. cerevisiae* is able to satisfy energy requirements with ATP produced via fermentation. Oxidative phosphorylation and the mitochondrial genome in this organism are dispensable provided that fermentable carbon sources (e.g. glucose) are present in the growth medium [165]. However, mitochondrial respiration and the presence of an intact mitochondrial genome become indispensible when yeast cells are cultured in non-fermentable carbon sources (e.g. glycerol) [165]. Because mutated or damaged mtDNA may result in OXPHOS dysfunction, the inability of yeast cells to grow in non-fermentable carbon sources can be used as readout for the loss of integrity of the mitochondrial genome.

Approximately 50% of mammalian mitochondrial proteins have a yeast homolog indicating that mitochondria of this single-celled organism are as complex and similar to those present in tissues of higher eukaryotes. Hence it is not surprising that the majority of our current knowledge of mitochondrial function and dysfunction comes from studies in *S. cerevisiae*. In addition to its capability of tolerating complete loss of mtDNA, this model organism is also receptive to mitochondrial genome manipulation. Mitochondrial genetic transformation can be successfully attained in budding yeast via biolistic delivery, a process that is generally used in yeast to mimic mtDNA mutations observed in patients with mitochondrial diseases. During biolistic delivery, *in vitro* designed mutated mtDNA fragments are transfected into yeast mitochondria following which mutated mtDNA gets integrated into wild-type mtDNA via homologous recombination. As yeast cells are unable to sustain a heteroplasmic state, it is relatively easy to obtain homoplasmic populations of yeast cells in which all mtDNA molecules harbor the mutation of interest. Several studies have exploited this technique to study a variety of pathogenic human

mtDNA mutations, as such mutations cannot be stably maintained in experimental mammalian systems [286]. Another example of mtDNA manipulation that can be efficiently performed in *S. cerevisiae* is the introduction of exogenous DNA reporter constructs into its mitochondrial genome, a process currently not possible in mammalian systems *in vivo* [276]. In sum, these valuable and unique features have rendered *S. cerevisiae* an excellent model for the study of mtDNA metabolism.

REFERENCES

1. Alberts, B. (2008). Molecular biology of the cell, 5th Edition, (New York: Garland Science).
2. Ernster, L., and Schatz, G. (1981). Mitochondria: a historical review. The Journal of cell biology *91*, 227s-255s.
3. Scheffler, I.E. (2008). Mitochondria, Second Edition, (Wiley-Liss).
4. Gray, M.W. (2012). Mitochondrial Evolution. Cold Spring Harbor Perspectives in Biology *4*.
5. Kühlbrandt, W. (2015). Structure and function of mitochondrial membrane protein complexes. BMC Biology *13*, 1-11.
6. Wiedemann, N., Frazier, A.E., and Pfanner, N. (2004). The Protein Import Machinery of Mitochondria. Journal of Biological Chemistry *279*, 14473-14476.
7. Schmidt, O., Pfanner, N., and Meisinger, C. (2010). Mitochondrial protein import: from proteomics to functional mechanisms. Nature Reviews Molecular Cell Biology *11*, 655-667.
8. Disentangling the origin of eukaryotes using phylogenomics and comparative genomics approaches. http://www.singek.eu/esr-5-disentangling-the-origin-of-eukaryotes-using-phylogenomics-and-comparative-genomics-approaches/ (cited on May 26, 2016).
9. Jensen, R.E., Hobbs, A.E., Cerveny, K.L., and Sesaki, H. (2000). Yeast mitochondrial dynamics: fusion, division, segregation, and shape. Microscopy research and technique *51*, 573-583.

10. Lane, N., and Martin, W. (2010). The energetics of genome complexity. Nature *467*, 929-934.

11. Westermann, B. (2010). Mitochondrial fusion and fission in cell life and death. Nature reviews. Molecular cell biology *11*, 872-884.

12. Lodish, H.F. (2013). Molecular cell biology, 7th Edition, (New York: W.H. Freeman and Co.).

13. Fawcett, D.W. (1981). The cell, 2d ed Edition, (Philadelphia: W. B. Saunders Co.).

14. Page, E., and McCallister, L.P. (1973). Quantitative electron microscopic description of heart muscle cells. Application to normal, hypertrophied and thyroxin-stimulated hearts. The American journal of cardiology *31*, 172-181.

15. Dorn, G.W., 2nd (2013). Mitochondrial dynamics in heart disease. Biochimica et biophysica acta *1833*, 233-241.

16. Boyer, T.D. (2012). Zakim and Boyer's Hepatology: A Textbook of Liver Disease, Sixth Edition, (Philadelphia, PA Saunders, an imprint of Elsevier Inc.).

17. Hoffmann, H.P., and Avers, C.J. (1973). Mitochondrion of yeast: ultrastructural evidence for one giant, branched organelle per cell. Science *181*, 749-751.

18. Stevens, B. (1977). Variation in number and volume of the mitochondria in yeast according to growth conditions. A study based on serial sectioning and computer graphics reconstitution. Journal de microscopie et de biologie cellulaire *28*, 37–56.

19. van der Laan, M., Horvath, S.E., and Pfanner, N. (2016). Mitochondrial contact site and cristae organizing system. Current Opinion in Cell Biology *41*, 33-42.

20. Walther, D.M., and Rapaport, D. (2009). Biogenesis of mitochondrial outer membrane proteins. Biochimica et Biophysica Acta (BBA) - Molecular Cell Research *1793*, 42-51.

21. Zinser, E., Sperka-Gottlieb, C.D., Fasch, E.V., Kohlwein, S.D., Paltauf, F., and Daum, G. (1991). Phospholipid synthesis and lipid composition of subcellular membranes in the unicellular eukaryote Saccharomyces cerevisiae. Journal of bacteriology *173*, 2026-2034.

22. Orientations of Proteins in Membranes (OPM) database. http://opm.phar.umich.edu/atlas.php?membrane=Mitochondrial_outer_membrane (cited on May 26, 2016).

23. Tatsuta, T., Scharwey, M., and Langer, T. (2014). Mitochondrial lipid trafficking. Trends in Cell Biology *24*, 44-52.

24. Perkins, G., Renken, C., Martone, M.E., Young, S.J., Ellisman, M., and Frey, T. (1997). Electron tomography of neuronal mitochondria: three-dimensional structure and organization of cristae and membrane contacts. Journal of structural biology *119*, 260-272.

25. Herrmann, J.M., and Riemer, J. (2010). The intermembrane space of mitochondria. Antioxidants & redox signaling *13*, 1341-1358.

26. Porcelli, A.M., Ghelli, A., Zanna, C., Pinton, P., Rizzuto, R., and Rugolo, M. (2005). pH difference across the outer mitochondrial membrane measured with a green fluorescent protein mutant. Biochemical and biophysical research communications *326*, 799-804.

27. Hu, J., Dong, L., and Outten, C.E. (2008). The redox environment in the mitochondrial intermembrane space is maintained separately from the cytosol and matrix. The Journal of biological chemistry *283*, 29126-29134.

28. Vogel, F., Bornhovd, C., Neupert, W., and Reichert, A.S. (2006). Dynamic subcompartmentalization of the mitochondrial inner membrane. The Journal of cell biology *175*, 237-247.

29. Wurm, C.A., and Jakobs, S. (2006). Differential protein distributions define two sub-compartments of the mitochondrial inner membrane in yeast. FEBS letters *580*, 5628-5634.

30. Davies, K.M., Anselmi, C., Wittig, I., Faraldo-Gomez, J.D., and Kuhlbrandt, W. (2012). Structure of the yeast F1Fo-ATP synthase dimer and its role in shaping the mitochondrial cristae. Proc Natl Acad Sci U S A *109*, 13602-13607.

31. Frey, T.G., Renken, C.W., and Perkins, G.A. (2002). Insight into mitochondrial structure and function from electron tomography. Biochimica et biophysica acta *1555*, 196-203.

32. Mannella, C.A. (2006). The relevance of mitochondrial membrane topology to mitochondrial function. Biochimica et biophysica acta *1762*, 140-147.

33. Zick, M., Rabl, R., and Reichert, A.S. (2009). Cristae formation-linking ultrastructure and function of mitochondria. Biochimica et biophysica acta *1793*, 5-19.

34. Frezza, C., Cipolat, S., Martins de Brito, O., Micaroni, M., Beznoussenko, G.V., Rudka, T., Bartoli, D., Polishuck, R.S., Danial, N.N., De Strooper, B., et al.

(2006). OPA1 controls apoptotic cristae remodeling independently from mitochondrial fusion. Cell *126*, 177-189.

35. Scorrano, L., Ashiya, M., Buttle, K., Weiler, S., Oakes, S.A., Mannella, C.A., and Korsmeyer, S.J. (2002). A distinct pathway remodels mitochondrial cristae and mobilizes cytochrome c during apoptosis. Dev Cell *2*, 55-67.

36. Yamaguchi, R., Lartigue, L., Perkins, G., Scott, R.T., Dixit, A., Kushnareva, Y., Kuwana, T., Ellisman, M.H., and Newmeyer, D.D. (2008). Opa1-mediated cristae opening is Bax/Bak and BH3 dependent, required for apoptosis, and independent of Bak oligomerization. Molecular cell *31*, 557-569.

37. Llopis, J., McCaffery, J.M., Miyawaki, A., Farquhar, M.G., and Tsien, R.Y. (1998). Measurement of cytosolic, mitochondrial, and Golgi pH in single living cells with green fluorescent proteins. Proc Natl Acad Sci U S A *95*, 6803-6808.

38. Sickmann, A., Reinders, J., Wagner, Y., Joppich, C., Zahedi, R., Meyer, H.E., Schonfisch, B., Perschil, I., Chacinska, A., Guiard, B., et al. (2003). The proteome of Saccharomyces cerevisiae mitochondria. Proc Natl Acad Sci U S A *100*, 13207-13212.

39. Reinders, J., Zahedi, R.P., Pfanner, N., Meisinger, C., and Sickmann, A. (2006). Toward the complete yeast mitochondrial proteome: multidimensional separation techniques for mitochondrial proteomics. Journal of proteome research *5*, 1543-1554.

40. Pagliarini, D.J., Calvo, S.E., Chang, B., Sheth, S.A., Vafai, S.B., Ong, S.E., Walford, G.A., Sugiana, C., Boneh, A., Chen, W.K., et al. (2008). A

mitochondrial protein compendium elucidates complex I disease biology. Cell *134*, 112-123.

41. Becker, T., Böttinger, L., and Pfanner, N. (2012). Mitochondrial protein import: from transport pathways to an integrated network. Trends in Biochemical Sciences *37*, 85-91.

42. Horvath, S.E., Rampelt, H., Oeljeklaus, S., Warscheid, B., van der Laan, M., and Pfanner, N. (2015). Role of membrane contact sites in protein import into mitochondria. Protein Science *24*, 277-297.

43. Harbauer, A.B., Zahedi, R.P., Sickmann, A., Pfanner, N., and Meisinger, C. (2014). The Protein Import Machinery of Mitochondria—A Regulatory Hub in Metabolism, Stress, and Disease. Cell Metabolism *19*, 357-372.

44. Hill, K., Model, K., Ryan, M.T., Dietmeier, K., Martin, F., Wagner, R., and Pfanner, N. (1998). Tom40 forms the hydrophilic channel of the mitochondrial import pore for preproteins [see comment]. Nature *395*, 516-521.

45. Kunkele, K.P., Heins, S., Dembowski, M., Nargang, F.E., Benz, R., Thieffry, M., Walz, J., Lill, R., Nussberger, S., and Neupert, W. (1998). The preprotein translocation channel of the outer membrane of mitochondria. Cell *93*, 1009-1019.

46. van Wilpe, S., Ryan, M.T., Hill, K., Maarse, A.C., Meisinger, C., Brix, J., Dekker, P.J., Moczko, M., Wagner, R., Meijer, M., et al. (1999). Tom22 is a multifunctional organizer of the mitochondrial preprotein translocase. Nature *401*, 485-489.

47. Abe, Y., Shodai, T., Muto, T., Mihara, K., Torii, H., Nishikawa, S., Endo, T., and Kohda, D. (2000). Structural basis of presequence recognition by the mitochondrial protein import receptor Tom20. Cell *100*, 551-560.

48. Brix, J., Dietmeier, K., and Pfanner, N. (1997). Differential recognition of preproteins by the purified cytosolic domains of the mitochondrial import receptors Tom20, Tom22, and Tom70. The Journal of biological chemistry *272*, 20730-20735.

49. Komiya, T., Rospert, S., Koehler, C., Looser, R., Schatz, G., and Mihara, K. (1998). Interaction of mitochondrial targeting signals with acidic receptor domains along the protein import pathway: evidence for the 'acid chain' hypothesis. The EMBO journal *17*, 3886-3898.

50. Meisinger, C., Ryan, M.T., Hill, K., Model, K., Lim, J.H., Sickmann, A., Muller, H., Meyer, H.E., Wagner, R., and Pfanner, N. (2001). Protein import channel of the outer mitochondrial membrane: a highly stable Tom40-Tom22 core structure differentially interacts with preproteins, small tom proteins, and import receptors. Molecular and cellular biology *21*, 2337-2348.

51. Truscott, K.N., Kovermann, P., Geissler, A., Merlin, A., Meijer, M., Driessen, A.J., Rassow, J., Pfanner, N., and Wagner, R. (2001). A presequence- and voltage-sensitive channel of the mitochondrial preprotein translocase formed by Tim23. Nature structural biology *8*, 1074-1082.

52. Meinecke, M., Wagner, R., Kovermann, P., Guiard, B., Mick, D.U., Hutu, D.P., Voos, W., Truscott, K.N., Chacinska, A., Pfanner, N., et al. (2006). Tim50

maintains the permeability barrier of the mitochondrial inner membrane. Science *312*, 1523-1526.

53. Bauer, M.F., Sirrenberg, C., Neupert, W., and Brunner, M. (1996). Role of Tim23 as voltage sensor and presequence receptor in protein import into mitochondria. Cell *87*, 33-41.

54. Martin, J., Mahlke, K., and Pfanner, N. (1991). Role of an energized inner membrane in mitochondrial protein import. Delta psi drives the movement of presequences. The Journal of biological chemistry *266*, 18051-18057.

55. Huang, S., Ratliff, K.S., and Matouschek, A. (2002). Protein unfolding by the mitochondrial membrane potential. Nature structural biology *9*, 301-307.

56. Kang, P.J., Ostermann, J., Shilling, J., Neupert, W., Craig, E.A., and Pfanner, N. (1990). Requirement for hsp70 in the mitochondrial matrix for translocation and folding of precursor proteins. Nature *348*, 137-143.

57. Matouschek, A., Azem, A., Ratliff, K., Glick, B.S., Schmid, K., and Schatz, G. (1997). Active unfolding of precursor proteins during mitochondrial protein import. The EMBO journal *16*, 6727-6736.

58. Truscott, K.N., Voos, W., Frazier, A.E., Lind, M., Li, Y., Geissler, A., Dudek, J., Muller, H., Sickmann, A., Meyer, H.E., et al. (2003). A J-protein is an essential subunit of the presequence translocase-associated protein import motor of mitochondria. The Journal of cell biology *163*, 707-713.

59. D'Silva, P.D., Schilke, B., Walter, W., Andrew, A., and Craig, E.A. (2003). J protein cochaperone of the mitochondrial inner membrane required for protein

import into the mitochondrial matrix. Proc Natl Acad Sci U S A *100*, 13839-13844.

60. Glick, B.S., Brandt, A., Cunningham, K., Muller, S., Hallberg, R.L., and Schatz, G. (1992). Cytochromes c1 and b2 are sorted to the intermembrane space of yeast mitochondria by a stop-transfer mechanism. Cell *69*, 809-822.

61. Bomer, U., Meijer, M., Guiard, B., Dietmeier, K., Pfanner, N., and Rassow, J. (1997). The sorting route of cytochrome b2 branches from the general mitochondrial import pathway at the preprotein translocase of the inner membrane. The Journal of biological chemistry *272*, 30439-30446.

62. Hawlitschek, G., Schneider, H., Schmidt, B., Tropschug, M., Hartl, F.U., and Neupert, W. (1988). Mitochondrial protein import: identification of processing peptidase and of PEP, a processing enhancing protein. Cell *53*, 795-806.

63. Taylor, A.B., Smith, B.S., Kitada, S., Kojima, K., Miyaura, H., Otwinowski, Z., Ito, A., and Deisenhofer, J. (2001). Crystal structures of mitochondrial processing peptidase reveal the mode for specific cleavage of import signal sequences. Structure (London, England : 1993) *9*, 615-625.

64. Voos, W., Gambill, B.D., Guiard, B., Pfanner, N., and Craig, E.A. (1993). Presequence and mature part of preproteins strongly influence the dependence of mitochondrial protein import on heat shock protein 70 in the matrix. The Journal of cell biology *123*, 119-126.

65. He, S., and Fox, T.D. (1997). Membrane translocation of mitochondrially coded Cox2p: distinct requirements for export of N and C termini and dependence on the conserved protein Oxa1p. Molecular biology of the cell *8*, 1449-1460.

66. Hell, K., Herrmann, J., Pratje, E., Neupert, W., and Stuart, R.A. (1997). Oxa1p mediates the export of the N- and C-termini of pCoxII from the mitochondrial matrix to the intermembrane space. FEBS letters *418*, 367-370.

67. Hell, K., Herrmann, J.M., Pratje, E., Neupert, W., and Stuart, R.A. (1998). Oxa1p, an essential component of the N-tail protein export machinery in mitochondria. Proc Natl Acad Sci U S A *95*, 2250-2255.

68. Model, K., Meisinger, C., Prinz, T., Wiedemann, N., Truscott, K.N., Pfanner, N., and Ryan, M.T. (2001). Multistep assembly of the protein import channel of the mitochondrial outer membrane. Nature structural biology *8*, 361-370.

69. Hoppins, S.C., and Nargang, F.E. (2004). The Tim8-Tim13 complex of Neurospora crassa functions in the assembly of proteins into both mitochondrial membranes. The Journal of biological chemistry *279*, 12396-12405.

70. Wiedemann, N., Truscott, K.N., Pfannschmidt, S., Guiard, B., Meisinger, C., and Pfanner, N. (2004). Biogenesis of the protein import channel Tom40 of the mitochondrial outer membrane: intermembrane space components are involved in an early stage of the assembly pathway. The Journal of biological chemistry *279*, 18188-18194.

71. Kutik, S., Stojanovski, D., Becker, L., Becker, T., Meinecke, M., Kruger, V., Prinz, C., Meisinger, C., Guiard, B., Wagner, R., et al. (2008). Dissecting membrane insertion of mitochondrial beta-barrel proteins. Cell *132*, 1011-1024.

72. Chan, N.C., and Lithgow, T. (2008). The peripheral membrane subunits of the SAM complex function codependently in mitochondrial outer membrane biogenesis. Molecular biology of the cell *19*, 126-136.

73. Popov-Celeketic, J., Waizenegger, T., and Rapaport, D. (2008). Mim1 functions in an oligomeric form to facilitate the integration of Tom20 into the mitochondrial outer membrane. Journal of molecular biology *376*, 671-680.

74. Becker, T., Pfannschmidt, S., Guiard, B., Stojanovski, D., Milenkovic, D., Kutik, S., Pfanner, N., Meisinger, C., and Wiedemann, N. (2008). Biogenesis of the mitochondrial TOM complex: Mim1 promotes insertion and assembly of signal-anchored receptors. The Journal of biological chemistry *283*, 120-127.

75. Hulett, J.M., Lueder, F., Chan, N.C., Perry, A.J., Wolynec, P., Likic, V.A., Gooley, P.R., and Lithgow, T. (2008). The transmembrane segment of Tom20 is recognized by Mim1 for docking to the mitochondrial TOM complex. Journal of molecular biology *376*, 694-704.

76. Stojanovski, D., Guiard, B., Kozjak-Pavlovic, V., Pfanner, N., and Meisinger, C. (2007). Alternative function for the mitochondrial SAM complex in biogenesis of alpha-helical TOM proteins. The Journal of cell biology *179*, 881-893.

77. Thornton, N., Stroud, D.A., Milenkovic, D., Guiard, B., Pfanner, N., and Becker, T. (2010). Two modular forms of the mitochondrial sorting and assembly machinery are involved in biogenesis of alpha-helical outer membrane proteins. Journal of molecular biology *396*, 540-549.

78. Setoguchi, K., Otera, H., and Mihara, K. (2006). Cytosolic factor- and TOM-independent import of C-tail-anchored mitochondrial outer membrane proteins. The EMBO journal *25*, 5635-5647.

79. Kemper, C., Habib, S.J., Engl, G., Heckmeyer, P., Dimmer, K.S., and Rapaport, D. (2008). Integration of tail-anchored proteins into the mitochondrial outer

membrane does not require any known import components. J Cell Sci *121*, 1990-1998.

80. Young, J.C., Hoogenraad, N.J., and Hartl, F.U. (2003). Molecular chaperones Hsp90 and Hsp70 deliver preproteins to the mitochondrial import receptor Tom70. Cell *112*, 41-50.

81. Li, J., Qian, X., Hu, J., and Sha, B. (2009). Molecular chaperone Hsp70/Hsp90 prepares the mitochondrial outer membrane translocon receptor Tom71 for preprotein loading. The Journal of biological chemistry *284*, 23852-23859.

82. Zara, V., Ferramosca, A., Robitaille-Foucher, P., Palmieri, F., and Young, J.C. (2009). Mitochondrial carrier protein biogenesis: role of the chaperones Hsc70 and Hsp90. The Biochemical journal *419*, 369-375.

83. Wiedemann, N., Pfanner, N., and Ryan, M.T. (2001). The three modules of ADP/ATP carrier cooperate in receptor recruitment and translocation into mitochondria. The EMBO journal *20*, 951-960.

84. Webb, C.T., Gorman, M.A., Lazarou, M., Ryan, M.T., and Gulbis, J.M. (2006). Crystal structure of the mitochondrial chaperone TIM9.10 reveals a six-bladed alpha-propeller. Molecular cell *21*, 123-133.

85. Curran, S.P., Leuenberger, D., Oppliger, W., and Koehler, C.M. (2002). The Tim9p-Tim10p complex binds to the transmembrane domains of the ADP/ATP carrier. The EMBO journal *21*, 942-953.

86. Davis, A.J., Alder, N.N., Jensen, R.E., and Johnson, A.E. (2007). The Tim9p/10p and Tim8p/13p complexes bind to specific sites on Tim23p during mitochondrial protein import. Molecular biology of the cell *18*, 475-486.

87. Chacinska, A., Pfannschmidt, S., Wiedemann, N., Kozjak, V., Sanjuan Szklarz, L.K., Schulze-Specking, A., Truscott, K.N., Guiard, B., Meisinger, C., and Pfanner, N. (2004). Essential role of Mia40 in import and assembly of mitochondrial intermembrane space proteins. The EMBO journal *23*, 3735-3746.

88. Naoe, M., Ohwa, Y., Ishikawa, D., Ohshima, C., Nishikawa, S., Yamamoto, H., and Endo, T. (2004). Identification of Tim40 that mediates protein sorting to the mitochondrial intermembrane space. The Journal of biological chemistry *279*, 47815-47821.

89. Terziyska, N., Lutz, T., Kozany, C., Mokranjac, D., Mesecke, N., Neupert, W., Herrmann, J.M., and Hell, K. (2005). Mia40, a novel factor for protein import into the intermembrane space of mitochondria is able to bind metal ions. FEBS letters *579*, 179-184.

90. Mesecke, N., Terziyska, N., Kozany, C., Baumann, F., Neupert, W., Hell, K., and Herrmann, J.M. (2005). A disulfide relay system in the intermembrane space of mitochondria that mediates protein import. Cell *121*, 1059-1069.

91. Rissler, M., Wiedemann, N., Pfannschmidt, S., Gabriel, K., Guiard, B., Pfanner, N., and Chacinska, A. (2005). The essential mitochondrial protein Erv1 cooperates with Mia40 in biogenesis of intermembrane space proteins. Journal of molecular biology *353*, 485-492.

92. Allen, S., Balabanidou, V., Sideris, D.P., Lisowsky, T., and Tokatlidis, K. (2005). Erv1 mediates the Mia40-dependent protein import pathway and provides a functional link to the respiratory chain by shuttling electrons to cytochrome c. Journal of molecular biology *353*, 937-944.

93. Nunnari, J., and Suomalainen, A. (2012). Mitochondria: In Sickness and in Health. Cell *148*, 1145-1159.

94. Duchen, M.R. (2004). Roles of mitochondria in health and disease. Diabetes.

95. Mayr, J.A. (2015). Lipid metabolism in mitochondrial membranes. Journal of Inherited Metabolic Disease *38*, 137-144.

96. Paradies, G., Paradies, V., Benedictis, V., Ruggiero, F.M., and Petrosillo, G. (2014). Functional role of cardiolipin in mitochondrial bioenergetics. Biochimica et Biophysica Acta (BBA) - Bioenergetics *1837*, 408-417.

97. Grisham, R.H.G.a.C.M. (2010). Biochemistry, Fourth Edition, (Boston, MA, USA: Brooks/Cole, Cengage Learning).

98. Cox, D.L.N.a.M.M. (2005). Lehninger Principles of Biochemistry, Fourth Edition, (New York: W.H. Freeman and Company).

99. Hiltunen, K.J., Autio, K.J., Schonauer, M.S., Kursu, V.A., Dieckmann, C.L., and Kastaniotis, A.J. (2010). Mitochondrial fatty acid synthesis and respiration. Biochimica et Biophysica Acta (BBA) - Bioenergetics *1797*, 1195-1202.

100. Houten, S., and Wanders, R.J.A. (2010). A general introduction to the biochemistry of mitochondrial fatty acid β-oxidation. Journal of Inherited Metabolic Disease *33*, 469-477.

101. Ferrier, R.A.H.a.D.R. (2011). Lippincott's Illustrated Reviews: Biochemistry, Fifth Edition, (Baltimore, MD, USA: Lippincott Williams & Wilkins).

102. Voet, D.V.a.J.G. (2011). Biochemistry, Fourth Edition, (Hoboken, NJ, USA: John Wiley & Sons, Inc.).

103. Synthesis of Heme. http://www.rpi.edu/dept/bcbp/molbiochem/MBWeb/mb2/part1/heme.htm.

104. Heme Synthesis. http://library.med.utah.edu/NetBiochem/hi3.htm.

105. West, A.R., and Oates, P.S. (2008). Mechanisms of heme iron absorption: current questions and controversies. World journal of gastroenterology *14*, 4101-4110.

106. Maio, N., and Rouault, T.A. (2015). Iron–sulfur cluster biogenesis in mammalian cells: New insights into the molecular mechanisms of cluster delivery. Biochimica et Biophysica Acta (BBA) - Molecular Cell Research *1853*, 1493-1512.

107. Rouault, T.A. (2012). Biogenesis of iron-sulfur clusters in mammalian cells: new insights and relevance to human disease. Disease Models & Mechanisms *5*, 155-164.

108. Lill, R., Hoffmann, B., Molik, S., Pierik, A.J., Rietzschel, N., Stehling, O., Uzarska, M.A., Webert, H., Wilbrecht, C., and Muhlenhoff, U. (2012). The role of mitochondria in cellular iron-sulfur protein biogenesis and iron metabolism. Biochimica et biophysica acta *1823*, 1491-1508.

109. Fedorenko, A., Lishko, P.V., and Kirichok, Y. (2012). Mechanism of Fatty-Acid-Dependent UCP1 Uncoupling in Brown Fat Mitochondria. Cell *151*, 400-413.

110. Harms, M., and Seale, P. (2013). Brown and beige fat: development, function and therapeutic potential. Nature Medicine *19*, 1252-1263.

111. Jacobsson, A., Cannon, B., and Nedergaard, J. (1987). Physiological activation of brown adipose tissue destabilizes thermogenin mRNA. FEBS letters *224*, 353-356.

112. Daikoku, T., Shinohara, Y., Shima, A., Yamazaki, N., and Terada, H. (2000). Specific elevation of transcript levels of particular protein subtypes induced in brown adipose tissue by cold exposure. Biochimica et biophysica acta *1457*, 263-272.

113. Vitali, A., Murano, I., Zingaretti, M.C., Frontini, A., Ricquier, D., and Cinti, S. (2012). The adipose organ of obesity-prone C57BL/6J mice is composed of mixed white and brown adipocytes. Journal of lipid research *53*, 619-629.

114. Stefani, D., Rizzuto, R., and Pozzan, T. (2014). Enjoy the Trip: Calcium in Mitochondria Back and Forth. Annual Review of Biochemistry *85*, 1-32.

115. Rutter, G.A., and Denton, R.M. (1988). Regulation of NAD+-linked isocitrate dehydrogenase and 2-oxoglutarate dehydrogenase by Ca2+ ions within toluene-permeabilized rat heart mitochondria. Interactions with regulation by adenine nucleotides and NADH/NAD+ ratios. The Biochemical journal *252*, 181-189.

116. Denton, R.M., Randle, P.J., and Martin, B.R. (1972). Stimulation by calcium ions of pyruvate dehydrogenase phosphate phosphatase. The Biochemical journal *128*, 161-163.

117. Szabo, I., and Zoratti, M. (1991). The giant channel of the inner mitochondrial membrane is inhibited by cyclosporin A. The Journal of biological chemistry *266*, 3376-3379.

118. Crompton, M. (1999). The mitochondrial permeability transition pore and its role in cell death. The Biochemical journal *341 (Pt 2)*, 233-249.

119. Seth, R.B., Sun, L., Ea, C.K., and Chen, Z.J. (2005). Identification and characterization of MAVS, a mitochondrial antiviral signaling protein that activates NF-kappaB and IRF 3. Cell *122*, 669-682.

120. Yoneyama, M., Kikuchi, M., Natsukawa, T., Shinobu, N., Imaizumi, T., Miyagishi, M., Taira, K., Akira, S., and Fujita, T. (2004). The RNA helicase RIG-I has an essential function in double-stranded RNA-induced innate antiviral responses. Nature immunology *5*, 730-737.

121. Kato, H., Takeuchi, O., Sato, S., Yoneyama, M., Yamamoto, M., Matsui, K., Uematsu, S., Jung, A., Kawai, T., Ishii, K.J., et al. (2006). Differential roles of MDA5 and RIG-I helicases in the recognition of RNA viruses. Nature *441*, 101-105.

122. Koshiba, T. (2013). Mitochondrial-mediated antiviral immunity. Biochimica et Biophysica Acta (BBA) - Molecular Cell Research *1833*, 225-232.

123. Brunelle, J.K., and Letai, A. (2009). Control of mitochondrial apoptosis by the Bcl-2 family. Journal of Cell Science *122*, 437-441.

124. Martinou, J.-C., and Youle, R.J. (2011). Mitochondria in Apoptosis: Bcl-2 Family Members and Mitochondrial Dynamics. Developmental Cell *21*, 92-101.

125. Lopez, J., and Tait, S.W.G. (2015). Mitochondrial apoptosis: killing cancer using the enemy within. British Journal of Cancer *112*, 957-962.

126. Liu, X., Kim, C.N., Yang, J., Jemmerson, R., and Wang, X. (1996). Induction of apoptotic program in cell-free extracts: requirement for dATP and cytochrome c. Cell *86*, 147-157.

127. Du, C., Fang, M., Li, Y., Li, L., and Wang, X. (2000). Smac, a mitochondrial protein that promotes cytochrome c-dependent caspase activation by eliminating IAP inhibition. Cell *102*, 33-42.

128. Hegde, R., Srinivasula, S.M., Zhang, Z., Wassell, R., Mukattash, R., Cilenti, L., DuBois, G., Lazebnik, Y., Zervos, A.S., Fernandes-Alnemri, T., et al. (2002). Identification of Omi/HtrA2 as a mitochondrial apoptotic serine protease that disrupts inhibitor of apoptosis protein-caspase interaction. The Journal of biological chemistry *277*, 432-438.

129. Susin, S.A., Lorenzo, H.K., Zamzami, N., Marzo, I., Snow, B.E., Brothers, G.M., Mangion, J., Jacotot, E., Costantini, P., Loeffler, M., et al. (1999). Molecular characterization of mitochondrial apoptosis-inducing factor. Nature *397*, 441-446.

130. Li, L.Y., Luo, X., and Wang, X. (2001). Endonuclease G is an apoptotic DNase when released from mitochondria. Nature *412*, 95-99.

131. Wang, C., and Youle, R.J. (2009). The Role of Mitochondria in Apoptosis*. Genetics *43*, 95-118.

132. Sazanov, L.A. (2015). A giant molecular proton pump: structure and mechanism of respiratory complex I. Nature Reviews Molecular Cell Biology *16*, 375-388.

133. Chaban, Y., Boekema, E.J., and Dudkina, N.V. (2014). Structures of mitochondrial oxidative phosphorylation supercomplexes and mechanisms for their stabilisation. Biochimica et biophysica acta *1837*, 418-426.

134. Schultz, B.E., and Chan, S.I. (2001). Structures and Proton-Pumping Strategies of Mitochondrial Respiratory Enzymes. Annual Review of Biophysics and Biomolecular Structure *30*, 23-65.

135. Schon, E.A., DiMauro, S., and Hirano, M. (2012). Human mitochondrial DNA: roles of inherited and somatic mutations. Nature reviews. Genetics *13*, 878-890.

136. Carroll, J., Fearnley, I.M., Skehel, J.M., Shannon, R.J., Hirst, J., and Walker, J.E. (2006). Bovine complex I is a complex of 45 different subunits. The Journal of biological chemistry *281*, 32724-32727.

137. Rich, P.R., and Maréchal, A. (2010). The mitochondrial respiratory chain. Essays In Biochemistry *47*, 1-23.

138. Jonckheere, A.I., Smeitink, J.A.M., and Rodenburg, R.J.T. (2012). Mitochondrial ATP synthase: architecture, function and pathology. Journal of Inherited Metabolic Disease *35*, 211-225.

139. Circu, M.L., and Aw, T.Y. (2010). Reactive oxygen species, cellular redox systems, and apoptosis. Free radical biology & medicine *48*, 749-762.

140. Cui, H., Kong, Y., and Zhang, H. (2012). Oxidative stress, mitochondrial dysfunction, and aging. Journal of signal transduction *2012*, 646354.

141. Sena, L.A., and Chandel, N.S. (2012). Physiological roles of mitochondrial reactive oxygen species. Molecular cell *48*, 158-167.

142. Duchen, M.R. (2004). Mitochondria in health and disease: perspectives on a new mitochondrial biology. Molecular aspects of medicine *25*, 365-451.

143. Andreyev, A.Y., Kushnareva, Y.E., and Starkov, A.A. (2005). Mitochondrial metabolism of reactive oxygen species. Biochemistry. Biokhimiia *70*, 200-214.

144. Chen, Y.R., and Zweier, J.L. (2014). Cardiac mitochondria and reactive oxygen species generation. Circulation research *114*, 524-537.

145. Bolisetty, S., and Jaimes, E.A. (2013). Mitochondria and reactive oxygen species: physiology and pathophysiology. International journal of molecular sciences *14*, 6306-6344.

146. Mailloux, R.J., and Harper, M.E. (2012). Mitochondrial proticity and ROS signaling: lessons from the uncoupling proteins. Trends in endocrinology and metabolism: TEM *23*, 451-458.

147. Prabu, S.K., Anandatheerthavarada, H.K., Raza, H., Srinivasan, S., Spear, J.F., and Avadhani, N.G. (2006). Protein kinase A-mediated phosphorylation modulates cytochrome c oxidase function and augments hypoxia and myocardial ischemia-related injury. The Journal of biological chemistry *281*, 2061-2070.

148. Rindler, P.M., Plafker, S.M., Szweda, L.I., and Kinter, M. (2013). High dietary fat selectively increases catalase expression within cardiac mitochondria. The Journal of biological chemistry *288*, 1979-1990.

149. Bakala, H., Hamelin, M., Mary, J., Borot-Laloi, C., and Friguet, B. (2012). Catalase, a target of glycation damage in rat liver mitochondria with aging. Biochimica et biophysica acta *1822*, 1527-1534.

150. Chandel, N.S., Trzyna, W.C., McClintock, D.S., and Schumacker, P.T. (2000). Role of oxidants in NF-kappa B activation and TNF-alpha gene transcription induced by hypoxia and endotoxin. Journal of immunology (Baltimore, Md. : 1950) *165*, 1013-1021.

151. Chandel, N.S., Maltepe, E., Goldwasser, E., Mathieu, C.E., Simon, M.C., and Schumacker, P.T. (1998). Mitochondrial reactive oxygen species trigger hypoxia-induced transcription. Proc Natl Acad Sci U S A *95*, 11715-11720.

152. Chandel, N.S., McClintock, D.S., Feliciano, C.E., Wood, T.M., Melendez, J.A., Rodriguez, A.M., and Schumacker, P.T. (2000). Reactive oxygen species generated at mitochondrial complex III stabilize hypoxia-inducible factor-1alpha during hypoxia: a mechanism of O2 sensing. The Journal of biological chemistry *275*, 25130-25138.

153. Bell, E.L., Klimova, T.A., Eisenbart, J., Moraes, C.T., Murphy, M.P., Budinger, G.R., and Chandel, N.S. (2007). The Qo site of the mitochondrial complex III is required for the transduction of hypoxic signaling via reactive oxygen species production. The Journal of cell biology *177*, 1029-1036.

154. Klimova, T., and Chandel, N.S. (2008). Mitochondrial complex III regulates hypoxic activation of HIF. Cell death and differentiation *15*, 660-666.

155. Nemoto, S., Takeda, K., Yu, Z.X., Ferrans, V.J., and Finkel, T. (2000). Role for mitochondrial oxidants as regulators of cellular metabolism. Molecular and cellular biology *20*, 7311-7318.

156. Chandel, N.S., Vander Heiden, M.G., Thompson, C.B., and Schumacker, P.T. (2000). Redox regulation of p53 during hypoxia. Oncogene *19*, 3840-3848.

157. Dimauro, S., and Davidzon, G. (2005). Mitochondrial DNA and disease. Annals of medicine *37*, 222-232.

158. van der Giezen, M. (2011). Mitochondria and the Rise of Eukaryotes. BioScience *63*, 594-601.

159. Burger, G., Gray, M.W., and Lang, B.F. (2003). Mitochondrial genomes: anything goes. Trends in genetics : TIG *19*, 709-716.

160. Friedman, J.R., and Nunnari, J. (2014). Mitochondrial form and function. Nature *505*, 335-343.

161. Williamson, D. (2002). The curious history of yeast mitochondrial DNA. Nature reviews. Genetics *3*, 475-481.

162. Sloan, D.B., Alverson, A.J., Chuckalovcak, J.P., Wu, M., McCauley, D.E., Palmer, J.D., and Taylor, D.R. (2012). Rapid evolution of enormous, multichromosomal genomes in flowering plant mitochondria with exceptionally high mutation rates. PLoS biology *10*, e1001241.

163. Lang, B.F., Burger, G., O'Kelly, C.J., Cedergren, R., Golding, G.B., Lemieux, C., Sankoff, D., Turmel, M., and Gray, M.W. (1997). An ancestral mitochondrial DNA resembling a eubacterial genome in miniature. Nature *387*, 493-497.

164. Lang, B.F. Reclinomonas americana - Mitochondrial genome organization, gene content, genetic code. Volume 2016.

165. Westermann, B. (2014). Mitochondrial inheritance in yeast. Biochimica et biophysica acta *1837*, 1039-1046.

166. Ling, F., Mikawa, T., and Shibata, T. (2011). Enlightenment of yeast mitochondrial homoplasmy: diversified roles of gene conversion. Genes *2*, 169-190.

167. Kaniak-Golik, A., and Skoneczna, A. (2015). Mitochondria-nucleus network for genome stability. Free radical biology & medicine *82*, 73-104.

168. Ling, F., and Shibata, T. (2002). Recombination-dependent mtDNA partitioning: in vivo role of Mhr1p to promote pairing of homologous DNA. The EMBO journal *21*, 4730-4740.

169. Lecrenier, N., and Foury, F. (2000). New features of mitochondrial DNA replication system in yeast and man. Gene *246*, 37-48.

170. Foury, F., Roganti, T., Lecrenier, N., and Purnelle, B. (1998). The complete sequence of the mitochondrial genome of Saccharomyces cerevisiae. FEBS letters *440*, 325-331.

171. Kucej, M., and Butow, R.A. (2007). Evolutionary tinkering with mitochondrial nucleoids. Trends Cell Biol *17*, 586-592.

172. Sedman, T. (2005). Characterization of the yeast *Saccharomyces Cerevisiae* mitochondrial DNA helicase Hmi1. In Department of general and microbial biochemistry, Volume PhD. (Estonia: University of Tartu), pp. 1-56.

173. Lipinski, K.A., Kaniak-Golik, A., and Golik, P. (2010). Maintenance and expression of the S. cerevisiae mitochondrial genome--from genetics to evolution and systems biology. Biochimica et biophysica acta *1797*, 1086-1098.

174. Langkjaer, R.B., Casaregola, S., Ussery, D.W., Gaillardin, C., and Piskur, J. (2003). Sequence analysis of three mitochondrial DNA molecules reveals interesting differences among Saccharomyces yeasts. Nucleic acids research *31*, 3081-3091.

175. Solieri, L. (2010). Mitochondrial inheritance in budding yeasts: towards an integrated understanding. Trends in microbiology *18*, 521-530.

176. Ricchetti, M., Fairhead, C., and Dujon, B. (1999). Mitochondrial DNA repairs double-strand breaks in yeast chromosomes. Nature *402*, 96-100.

177. Kucej, M., Kucejova, B., Subramanian, R., Chen, X.J., and Butow, R.A. (2008). Mitochondrial nucleoids undergo remodeling in response to metabolic cues. J Cell Sci *121*, 1861-1868.

178. Chen, X.J., and Butow, R.A. (2005). The organization and inheritance of the mitochondrial genome. Nature reviews. Genetics *6*, 815-825.

179. Shadel, G.S. (1999). Yeast as a model for human mtDNA replication. American journal of human genetics *65*, 1230-1237.

180. Michaelis, G., Douglass, S., Tsai, M.J., and Criddle, R.S. (1971). Mitochondrial DNA and suppressiveness of petite mutants in Saccharomyces cerevisiae. Biochemical genetics *5*, 487-495.

181. Bernardi, G. (1979). The petite mutation in yeast. Trends in Biochemical Sciences *4*, 197–201.

182. Shibata, T., and Ling, F. (2007). DNA recombination protein-dependent mechanism of homoplasmy and its proposed functions. Mitochondrion *7*, 17-23.

183. Hori, A., Yoshida, M., Shibata, T., and Ling, F. (2009). Reactive oxygen species regulate DNA copy number in isolated yeast mitochondria by triggering recombination-mediated replication. Nucleic acids research *37*, 749-761.

184. You, H.J., Swanson, R.L., and Doetsch, P.W. (1998). Saccharomyces cerevisiae possesses two functional homologues of Escherichia coli endonuclease III. Biochemistry *37*, 6033-6040.

185. Harrison, L., Brame, K.L., Geltz, L.E., and Landry, A.M. (2006). Closely opposed apurinic/apyrimidinic sites are converted to double strand breaks in Escherichia

coli even in the absence of exonuclease III, endonuclease IV, nucleotide excision repair and AP lyase cleavage. DNA repair *5*, 324-335.

186. Ling, F., Hori, A., Yoshitani, A., Niu, R., Yoshida, M., and Shibata, T. (2013). Din7 and Mhr1 expression levels regulate double-strand-break-induced replication and recombination of mtDNA at ori5 in yeast. Nucleic acids research *41*, 5799-5816.

187. Ling, F., and Shibata, T. (2004). Mhr1p-dependent concatemeric mitochondrial DNA formation for generating yeast mitochondrial homoplasmic cells. Molecular biology of the cell *15*, 310-322.

188. Ling, F., Morioka, H., Ohtsuka, E., and Shibata, T. (2000). A role for MHR1, a gene required for mitochondrial genetic recombination, in the repair of damage spontaneously introduced in yeast mtDNA. Nucleic acids research *28*, 4956-4963.

189. Ling, F., Makishima, F., Morishima, N., and Shibata, T. (1995). A nuclear mutation defective in mitochondrial recombination in yeast. The EMBO journal *14*, 4090-4101.

190. Amunts, A., Brown, A., Bai, X.C., Llacer, J.L., Hussain, T., Emsley, P., Long, F., Murshudov, G., Scheres, S.H., and Ramakrishnan, V. (2014). Structure of the yeast mitochondrial large ribosomal subunit. Science *343*, 1485-1489.

191. Tuppen, H.A., Blakely, E.L., Turnbull, D.M., and Taylor, R.W. (2010). Mitochondrial DNA mutations and human disease. Biochimica et biophysica acta *1797*, 113-128.

192. Holt, I.J., and Reyes, A. (2012). Human mitochondrial DNA replication. Cold Spring Harb Perspect Biol *4*.

193. Taanman, J.W. (1999). The mitochondrial genome: structure, transcription, translation and replication. Biochimica et biophysica acta *1410*, 103-123.

194. Kazak, L., Reyes, A., and Holt, I.J. (2012). Minimizing the damage: repair pathways keep mitochondrial DNA intact. Nature reviews. Molecular cell biology *13*, 659-671.

195. Shadel, G.S. (2008). Expression and maintenance of mitochondrial DNA: new insights into human disease pathology. The American journal of pathology *172*, 1445-1456.

196. Stewart, J.B., and Chinnery, P.F. (2015). The dynamics of mitochondrial DNA heteroplasmy: implications for human health and disease. Nature reviews. Genetics *16*, 530-542.

197. Clayton, D.A. (2003). Mitochondrial DNA replication: what we know. IUBMB life *55*, 213-217.

198. Pohjoismaki, J.L., and Goffart, S. (2011). Of circles, forks and humanity: Topological organisation and replication of mammalian mitochondrial DNA. BioEssays : news and reviews in molecular, cellular and developmental biology *33*, 290-299.

199. Pohjoismaki, J.L., Goffart, S., Tyynismaa, H., Willcox, S., Ide, T., Kang, D., Suomalainen, A., Karhunen, P.J., Griffith, J.D., Holt, I.J., et al. (2009). Human heart mitochondrial DNA is organized in complex catenated networks containing abundant four-way junctions and replication forks. The Journal of biological chemistry *284*, 21446-21457.

200. Kukat, C., and Larsson, N.G. (2013). mtDNA makes a U-turn for the mitochondrial nucleoid. Trends Cell Biol *23*, 457-463.

201. Gilkerson, R., Bravo, L., Garcia, I., Gaytan, N., Herrera, A., Maldonado, A., and Quintanilla, B. (2013). The mitochondrial nucleoid: integrating mitochondrial DNA into cellular homeostasis. Cold Spring Harb Perspect Biol *5*, a011080.

202. Gilkerson, R.W. (2009). Mitochondrial DNA nucleoids determine mitochondrial genetics and dysfunction. The international journal of biochemistry & cell biology *41*, 1899-1906.

203. Young, M.J., and Copeland, W.C. (2016). Human mitochondrial DNA replication machinery and disease. Current opinion in genetics & development *38*, 52-62.

204. Sage, J.M. (2011). Support of Mitochondrial DNA Replication by Human Rad51: A Dissertation. In Biochemistry and Molecular Pharmacology, Volume PhD Thesis. (Worcester, Massachusetts: University of Massachusetts Medical School), p. 123.

205. Hudson, G., and Chinnery, P.F. (2006). Mitochondrial DNA polymerase-gamma and human disease. Human molecular genetics *15 Spec No 2*, R244-252.

206. Vega, R.B., Horton, J.L., and Kelly, D.P. (2015). Maintaining ancient organelles: mitochondrial biogenesis and maturation. Circulation research *116*, 1820-1834.

207. Wanrooij, S., and Falkenberg, M. (2010). The human mitochondrial replication fork in health and disease. Biochimica et biophysica acta *1797*, 1378-1388.

208. Miralles Fuste, J., Shi, Y., Wanrooij, S., Zhu, X., Jemt, E., Persson, O., Sabouri, N., Gustafsson, C.M., and Falkenberg, M. (2014). In vivo occupancy of

mitochondrial single-stranded DNA binding protein supports the strand displacement mode of DNA replication. PLoS genetics *10*, e1004832.

209. Holt, I.J., and Jacobs, H.T. (2014). Unique features of DNA replication in mitochondria: a functional and evolutionary perspective. BioEssays : news and reviews in molecular, cellular and developmental biology *36*, 1024-1031.

210. Kohen, R., and Nyska, A. (2002). Oxidation of biological systems: oxidative stress phenomena, antioxidants, redox reactions, and methods for their quantification. Toxicologic pathology *30*, 620-650.

211. Jena, N.R. (2012). DNA damage by reactive species: Mechanisms, mutation and repair. Journal of biosciences *37*, 503-517.

212. Marnett, L.J. (2000). Oxyradicals and DNA damage. Carcinogenesis *21*, 361-370.

213. Wiseman, H., and Halliwell, B. (1996). Damage to DNA by reactive oxygen and nitrogen species: role in inflammatory disease and progression to cancer. The Biochemical journal *313 (Pt 1)*, 17-29.

214. Cooke, M.S., Evans, M.D., Dizdaroglu, M., and Lunec, J. (2003). Oxidative DNA damage: mechanisms, mutation, and disease. FASEB journal : official publication of the Federation of American Societies for Experimental Biology *17*, 1195-1214.

215. Soman, S. (2013). OXIDATIVE DAMAGE TO DNA IN ALZHEIMERS DISEASE. In Department of Chemistry, Volume Ph.D. (Lexington, Kentucky: University of Kentucky), pp. 1-231.

216. Rai, P. (2010). Oxidation in the nucleotide pool, the DNA damage response and cellular senescence: Defective bricks build a defective house. Mutation research *703*, 71-81.

217. Boiteux, S., and Guillet, M. (2004). Abasic sites in DNA: repair and biological consequences in Saccharomyces cerevisiae. DNA repair *3*, 1-12.

218. Shokolenko, I., Venediktova, N., Bochkareva, A., Wilson, G.L., and Alexeyev, M.F. (2009). Oxidative stress induces degradation of mitochondrial DNA. Nucleic acids research *37*, 2539-2548.

219. Yakes, F.M., and Van Houten, B. (1997). Mitochondrial DNA damage is more extensive and persists longer than nuclear DNA damage in human cells following oxidative stress. Proc Natl Acad Sci U S A *94*, 514-519.

220. Lomax, M.E., Folkes, L.K., and O'Neill, P. (2013). Biological consequences of radiation-induced DNA damage: relevance to radiotherapy. Clinical oncology *25*, 578-585.

221. Azzam, E.I., Jay-Gerin, J.P., and Pain, D. (2012). Ionizing radiation-induced metabolic oxidative stress and prolonged cell injury. Cancer letters *327*, 48-60.

222. Yu, W.H.a.K.N. (2010). Ionizing Radiation, DNA Double Strand Break and Mutation. In Advances in Genetics Research, Volume 4, K.V. Urbano, ed. (Nova Science Publishers, Inc.), pp. 97-210.

223. Kam, W.W., and Banati, R.B. (2013). Effects of ionizing radiation on mitochondria. Free radical biology & medicine *65*, 607-619.

224. Cheung-Ong, K., Giaever, G., and Nislow, C. (2013). DNA-damaging agents in cancer chemotherapy: serendipity and chemical biology. Chemistry & biology *20*, 648-659.

225. Swift, L.H., and Golsteyn, R.M. (2014). Genotoxic anti-cancer agents and their relationship to DNA damage, mitosis, and checkpoint adaptation in proliferating cancer cells. International journal of molecular sciences *15*, 3403-3431.

226. Chen, J., and Stubbe, J. (2005). Bleomycins: towards better therapeutics. Nature reviews. Cancer *5*, 102-112.

227. Cullen, K.J., Yang, Z., Schumaker, L., and Guo, Z. (2007). Mitochondria as a critical target of the chemotheraputic agent cisplatin in head and neck cancer. Journal of bioenergetics and biomembranes *39*, 43-50.

228. Garrido, N., Perez-Martos, A., Faro, M., Lou-Bonafonte, J.M., Fernandez-Silva, P., Lopez-Perez, M.J., Montoya, J., and Enriquez, J.A. (2008). Cisplatin-mediated impairment of mitochondrial DNA metabolism inversely correlates with glutathione levels. The Biochemical journal *414*, 93-102.

229. Yang, Z., Schumaker, L.M., Egorin, M.J., Zuhowski, E.G., Guo, Z., and Cullen, K.J. (2006). Cisplatin preferentially binds mitochondrial DNA and voltage-dependent anion channel protein in the mitochondrial membrane of head and neck squamous cell carcinoma: possible role in apoptosis. Clinical cancer research : an official journal of the American Association for Cancer Research *12*, 5817-5825.

230. Yeung, M., Hurren, R., Nemr, C., Wang, X., Hershenfeld, S., Gronda, M., Liyanage, S., Wu, Y., Augustine, J., Lee, E.A., et al. (2015). Mitochondrial DNA damage by bleomycin induces AML cell death. Apoptosis : an international journal on programmed cell death *20*, 811-820.

231. Brar, S.S., Meyer, J.N., Bortner, C.D., Van Houten, B., and Martin, W.J., 2nd (2012). Mitochondrial DNA-depleted A549 cells are resistant to bleomycin.

American journal of physiology. Lung cellular and molecular physiology *303*, L413-424.

232. Brooks, J.E. (1987). Properties and uses of restriction endonucleases. Methods in enzymology *152*, 113-129.

233. Pingoud, A., Wilson, G.G., and Wende, W. (2014). Type II restriction endonucleases--a historical perspective and more. Nucleic acids research *42*, 7489-7527.

234. Loenen, W.A., Dryden, D.T., Raleigh, E.A., Wilson, G.G., and Murray, N.E. (2014). Highlights of the DNA cutters: a short history of the restriction enzymes. Nucleic acids research *42*, 3-19.

235. Pingoud, A., and Jeltsch, A. (2001). Structure and function of type II restriction endonucleases. Nucleic acids research *29*, 3705-3727.

236. XhoI. (Ipswich, MA New England Biolabs).

237. Bacman, S.R., Williams, S.L., Pinto, M., and Moraes, C.T. (2014). The use of mitochondria-targeted endonucleases to manipulate mtDNA. Methods in enzymology *547*, 373-397.

238. Kukat, A., Kukat, C., Brocher, J., Schafer, I., Krohne, G., Trounce, I.A., Villani, G., and Seibel, P. (2008). Generation of rho0 cells utilizing a mitochondrially targeted restriction endonuclease and comparative analyses. Nucleic acids research *36*, e44.

239. Finn, K., Lowndes, N.F., and Grenon, M. (2012). Eukaryotic DNA damage checkpoint activation in response to double-strand breaks. Cellular and molecular life sciences : CMLS *69*, 1447-1473.

240. Dexheimer, T.S. (2013). DNA Repair Pathways and Mechanisms. In DNA Repair of Cancer Stem Cells, S.M.C. Lesley A Mathews, Elaine M. Hurt ed. (Netherlands: Springer), pp. 19-32.

241. Larsen, N.B., Rasmussen, M., and Rasmussen, L.J. (2005). Nuclear and mitochondrial DNA repair: similar pathways? Mitochondrion *5*, 89-108.

242. Liu, Y., and Wilson, S.H. (2012). DNA base excision repair: a mechanism of trinucleotide repeat expansion. Trends Biochem Sci *37*, 162-172.

243. de Laat, W.L., Jaspers, N.G., and Hoeijmakers, J.H. (1999). Molecular mechanism of nucleotide excision repair. Genes & development *13*, 768-785.

244. Bak, S.T., Sakellariou, D., and Pena-Diaz, J. (2014). The dual nature of mismatch repair as antimutator and mutator: for better or for worse. Frontiers in genetics *5*, 287.

245. Stojic, L., Brun, R., and Jiricny, J. (2004). Mismatch repair and DNA damage signalling. DNA repair *3*, 1091-1101.

246. Vilenchik, M.M., and Knudson, A.G. (2003). Endogenous DNA double-strand breaks: production, fidelity of repair, and induction of cancer. Proc Natl Acad Sci U S A *100*, 12871-12876.

247. Davis, A.J., and Chen, D.J. (2013). DNA double strand break repair via non-homologous end-joining. Translational cancer research *2*, 130-143.

248. Axelle Renodon-Cornière, P.W., Magali Le Breton and Fabrice Fleury (2013). New Potential Therapeutic Approaches by Targeting Rad51-Dependent Homologous Recombination. In New Research Directions in DNA Repair, C. Chen, ed. (InTech), pp. 467-488.

249. Emerson, C.H., and Bertuch, A.A. (2016). Consider the workhorse: Nonhomologous end-joining in budding yeast. Biochemistry and cell biology = Biochimie et biologie cellulaire, 1-11.

250. Fell, V.L., and Schild-Poulter, C. (2015). The Ku heterodimer: function in DNA repair and beyond. Mutation research. Reviews in mutation research *763*, 15-29.

251. Downs, J.A., and Jackson, S.P. (2004). A means to a DNA end: the many roles of Ku. Nature reviews. Molecular cell biology *5*, 367-378.

252. Deriano, L., and Roth, D.B. (2013). Modernizing the nonhomologous end-joining repertoire: alternative and classical NHEJ share the stage. Annual review of genetics *47*, 433-455.

253. Gelot, C., Magdalou, I., and Lopez, B.S. (2015). Replication stress in Mammalian cells and its consequences for mitosis. Genes *6*, 267-298.

254. Chiruvella, K.K., Liang, Z., and Wilson, T.E. (2013). Repair of double-strand breaks by end joining. Cold Spring Harb Perspect Biol *5*, a012757.

255. Lazzerini-Denchi, E., and Sfeir, A. (2016). Stop pulling my strings - what telomeres taught us about the DNA damage response. Nature reviews. Molecular cell biology *17*, 364-378.

256. Daley, J.M., Palmbos, P.L., Wu, D., and Wilson, T.E. (2005). Nonhomologous end joining in yeast. Annual review of genetics *39*, 431-451.

257. Matsumoto, R.P.K.a.Y. (2011). DNA Double-Strand Break Repair Through Non-Homologous End-Joining: Recruitment and Assembly of the Players. In DNA repair, I. Kruman, ed. (InTech), pp. 477-502.

258. Bowater, R., and Doherty, A.J. (2006). Making ends meet: repairing breaks in bacterial DNA by non-homologous end-joining. PLoS genetics *2*, e8.

259. Wright, D.G., Castore, R., Shi, R., Mallick, A., Ennis, D.G., and Harrison, L. (2016). Mycobacterium tuberculosis and Mycobacterium marinum non-homologous end-joining proteins can function together to join DNA ends in Escherichia coli. Mutagenesis.

260. Kushwaha, A.K., and Grove, A. (2013). Mycobacterium smegmatis Ku binds DNA without free ends. The Biochemical journal *456*, 275-282.

261. Matthews, L.A., and Simmons, L.A. (2014). Bacterial nonhomologous end joining requires teamwork. Journal of bacteriology *196*, 3363-3365.

262. Kushwaha, A.K., Deochand, D.K., and Grove, A. (2015). A moonlighting function of Mycobacterium smegmatis Ku in zinc homeostasis? Protein science : a publication of the Protein Society *24*, 253-263.

263. Shuman, S., and Glickman, M.S. (2007). Bacterial DNA repair by non-homologous end joining. Nature reviews. Microbiology *5*, 852-861.

264. Castore, R., Hughes, C., Debeaux, A., Sun, J., Zeng, C., Wang, S.Y., Tatchell, K., Shi, R., Lee, K.J., Chen, D.J., et al. (2011). Mycobacterium tuberculosis Ku can bind to nuclear DNA damage and sensitize mammalian cells to bleomycin sulfate. Mutagenesis *26*, 795-803.

265. Wright, D.G. (2010). The role of Mycobacterium tuberculosis Ku and ligase D in an Escherichia coli model of non-homologous end joining. . In Department of molecular and cellular physiology, Volume Ph.D. (Shreveport, Louisiana: Louisiana State University Health Sciences Center-Shreveport), pp. 1-171.

266. Abshire, C.F. (2014). Mycobacterium marinum in simulated microgravity: growth, survival, and gene expression. In Department of Molecular and Cellular Physiology, Volume MS. (Shreveport, LA, USA: Louisiana State University Health Sciences Center-Shreveport), p. 103.

267. Kushwaha, A.K., and Grove, A. (2013). C-terminal low-complexity sequence repeats of Mycobacterium smegmatis Ku modulate DNA binding. Bioscience reports *33*, 175-184.

268. McGovern, S., Baconnais, S., Roblin, P., Nicolas, P., Drevet, P., Simonson, H., Pietrement, O., Charbonnier, J.B., Le Cam, E., Noirot, P., et al. (2016). C-terminal region of bacterial Ku controls DNA bridging, DNA threading and recruitment of DNA ligase D for double strand breaks repair. Nucleic acids research.

269. Martin, S.A. (2011). Mitochondrial DNA Repair. In DNA Repair - On the Pathways to Fixing DNA Damage and Errors, F. Storici, ed. (InTech), pp. 313-338.

270. Boesch, P., Weber-Lotfi, F., Ibrahim, N., Tarasenko, V., Cosset, A., Paulus, F., Lightowlers, R.N., and Dietrich, A. (2011). DNA repair in organelles: Pathways, organization, regulation, relevance in disease and aging. Biochimica et biophysica acta *1813*, 186-200.

271. Alexeyev, M., Shokolenko, I., Wilson, G., and LeDoux, S. (2013). The maintenance of mitochondrial DNA integrity--critical analysis and update. Cold Spring Harb Perspect Biol *5*, a012641.

272. Kang, D., and Hamasaki, N. (2002). Maintenance of mitochondrial DNA integrity: repair and degradation. Current genetics *41*, 311-322.

273. Griffiths, L.M., Swartzlander, D., Meadows, K.L., Wilkinson, K.D., Corbett, A.H., and Doetsch, P.W. (2009). Dynamic compartmentalization of base excision repair proteins in response to nuclear and mitochondrial oxidative stress. Molecular and cellular biology *29*, 794-807.

274. Liu, P., and Demple, B. (2010). DNA repair in mammalian mitochondria: Much more than we thought? Environmental and molecular mutagenesis *51*, 417-426.

275. Tadi, S.K., Sebastian, R., Dahal, S., Babu, R.K., Choudhary, B., and Raghavan, S.C. (2016). Microhomology-mediated end joining is the principal mediator of double-strand break repair during mitochondrial DNA lesions. Molecular biology of the cell *27*, 223-235.

276. Stein, A., Kalifa, L., and Sia, E.A. (2015). Members of the RAD52 Epistasis Group Contribute to Mitochondrial Homologous Recombination and Double-Strand Break Repair in Saccharomyces cerevisiae. PLoS genetics *11*, e1005664.

277. Kalifa, L., Quintana, D.F., Schiraldi, L.K., Phadnis, N., Coles, G.L., Sia, R.A., and Sia, E.A. (2012). Mitochondrial genome maintenance: roles for nuclear nonhomologous end-joining proteins in Saccharomyces cerevisiae. Genetics *190*, 951-964.

278. Thyagarajan, B., Padua, R.A., and Campbell, C. (1996). Mammalian mitochondria possess homologous DNA recombination activity. The Journal of biological chemistry *271*, 27536-27543.

279. Bacman, S.R., Williams, S.L., and Moraes, C.T. (2009). Intra- and inter-molecular recombination of mitochondrial DNA after in vivo induction of multiple double-strand breaks. Nucleic acids research *37*, 4218-4226.

280. Fukui, H., and Moraes, C.T. (2009). Mechanisms of formation and accumulation of mitochondrial DNA deletions in aging neurons. Human molecular genetics *18*, 1028-1036.

281. Coffey, G., and Campbell, C. (2000). An alternate form of Ku80 is required for DNA end-binding activity in mammalian mitochondria. Nucleic acids research *28*, 3793-3800.

282. Lakshmipathy, U., and Campbell, C. (1999). Double strand break rejoining by mammalian mitochondrial extracts. Nucleic acids research *27*, 1198-1204.

283. The budding yeast Saccharomyces cerevisiae. Volume 2016. (Sweden).

284. Barrientos, A. (2003). Yeast models of human mitochondrial diseases. IUBMB life *55*, 83-95.

285. Altmann, K., Durr, M., and Westermann, B. (2007). Saccharomyces cerevisiae as a model organism to study mitochondrial biology: general considerations and basic procedures. Methods in molecular biology *372*, 81-90.

286. Lasserre, J.P., Dautant, A., Aiyar, R.S., Kucharczyk, R., Glatigny, A., Tribouillard-Tanvier, D., Rytka, J., Blondel, M., Skoczen, N., Reynier, P., et al. (2015). Yeast as a system for modeling mitochondrial disease mechanisms and discovering therapies. Dis Model Mech *8*, 509-526.

CHAPTER II

EVIDENCE FOR DOUBLE-STRAND BREAK MEDIATED MITOCHONDRIAL DNA REPLICATION IN *SACCHAROMYCES CEREVISIAE*

ABSTRACT

The mechanism of mitochondrial DNA (mtDNA) replication in *Saccharomyces cerevisiae* is controversial. Evidence exists for double-strand break (DSB) mediated recombination-dependent replication at mitochondrial replication origin *ori5* in hypersuppressive ρ^- cells. However, it is not clear if this replication mode operates in ρ^+ cells. To understand this, we targeted bacterial Ku (bKu), a DSB binding protein, to the mitochondria of ρ^+ cells with the hypothesis that bKu would bind persistently to mtDNA DSBs, thereby preventing mtDNA replication or repair. Here, we show that mitochondrial-targeted bKu binds to *ori5* and that inducible expression of bKu triggers petite formation preferentially in daughter cells. bKu expression also induces mtDNA depletion that eventually results in the formation of ρ^0 cells. This data supports the idea that yeast mtDNA replication is initiated by a DSB and bKu inhibits mtDNA replication by binding to a DSB at *ori5,* preventing mtDNA segregation to daughter cells. Interestingly, we find that mitochondrial-targeted bKu does not decrease mtDNA content in human MCF7 cells. This finding is in agreement with the fact that human mtDNA replication, typically, is not initiated by a DSB. Therefore, this study provides evidence that DSB-mediated replication is the predominant form of mtDNA replication in ρ^+ yeast cells.

INTRODUCTION

Mitochondria are double-membrane organelles that generally harbor multiple copies of mitochondrial DNA (mtDNA) [1], which are organized as nucleoprotein complexes called nucleoids [2]. Different eukaryotic species exhibit heterogeneity in size and physical form of their mtDNA molecules. For example, the ~16.6 kb human mtDNA, which encodes protein subunits of the oxidative phosphorylation (OXPHOS) system, typically forms double-stranded, closed circles of one genome length [1, 3]. In contrast, mtDNA in the budding yeast *Saccharomyces cerevisiae* exists predominantly as head-to-tail linear multimers (concatemers) of several genome units, with a minor proportion occurring in a circular form [4, 5]. The mtDNA monomer in *S. cerevisiae* (strain S288C) is ~85.8 kb that, like human mtDNA, encodes protein components of the OXPHOS system [[6] and references therein]. The topological variation of mtDNA between human (typically closed-circular) and *S. cerevisiae* (mainly polydisperse linear) is likely due to the differences in the mode of mtDNA replication. However, the mechanisms by which these species replicate their mitochondrial genome are only partially understood and multiple models have been proposed for human [for review see [7]] as well as for *S. cerevisiae* (discussed below).

Budding yeast mtDNA contains 8 replication origin-like sequences (*ori*s 1-8), of which at least three are believed to be active origins (*ori*s 2, 3, and 5) [6]. The active *ori*s contain 3 GC clusters (A-C), each separated by stretches of AT sequence. A transcription promoter (*r*) is present upstream of the GC cluster C that contains the consensus sequence for mitochondrial RNA polymerase (Rpo41) binding [6, 8, 9]. Two distinct mechanisms for mtDNA replication have been proposed in *S. cerevisiae*: transcription-dependent

replication and recombination-dependent replication [10]. According to the transcription-dependent model, Rpo41 recognizes transcriptional promoters at the active *ori*s and produces RNA transcripts, which are further processed to generate primers for mtDNA replication [for review see [9]]. However, the transcription-dependent replication is largely hypothetical and evidence supporting this model is limited only to the initiation steps [11-13]. Furthermore, Rpo41 is not essential for mtDNA maintenance [14, 15], clearly indicating the existence of a transcription-independent mtDNA replication mechanism.

Recombinant-dependent replication is the more popular mtDNA replication model in yeast. This model was proposed to explain the observation that the major form of mtDNA in mother cells is concatemers, whereas circular monomers prevail in growing buds [16]. According to this model, recombination-dependent rolling circle replication (RDR) initiates at *ori5*. This replication origin has a bubble-like structure and bases on the opposite strands of *ori5* are preferentially damaged by reactive oxygen species (ROS). These base damages are eventually converted into a double-strand break (DSB) by the base-excision repair enzyme Ntg1. The DSB is then processed to generate a 3'-tail, which is bound by the mitochondrial homologous recombinase (Mhr1). The nucleoprotein filament then invades a template circular mtDNA molecule to form a heteroduplex joint and initiation of rolling circle replication ensues. This process can generate mtDNA concatemers of multiple genome units that are selectively transmitted to growing buds, where concatemers are circularized into monomers [16-21]. In addition to explaining the existence of mtDNA in different topologies (linear and circular), this model also accounts for a characteristic feature of the *S. cerevisiae* mitochondrial system:

its tendency to maintain the state of homoplasmy [22]. The evidence for ROS-instigated DSB at *ori5* and its involvement in mtDNA replication was obtained from the hypersuppressive (HS) ρ^- mitochondrial genomes [18, 19] [for review of ρ^+, ρ^-, HS ρ^-, and ρ^0 see [23]]. Even though exposure of ρ^+ cells to low levels of ROS increases mtDNA copy number in an Ntg1- and Mhr1-dependent manner [19], it remains to be determined whether a DSB at *ori5* is also involved in mtDNA replication in ρ^+ cells. Uncertainty also exists as to which mode(s) of replication is/are primarily utilized by ρ^+ cells. To gain insight into these issues, we targeted a DSB DNA binding protein (bacterial Ku) to the mitochondria of ρ^+ cells.

Ku is a protein involved in non-homologous end joining (NHEJ) DSB repair [for review see [24, 25]] and exists predominantly as a heterodimeric Ku70-Ku80 complex in eukaryotes. Each eukaryotic Ku subunit is composed of three distinct regions: an N-terminal domain, a central 'core' domain, and a C-terminal domain. While the 'core' domain is required for dimerization as well as for the formation of a ring-like structure that wraps around DNA ends, the N- and C-terminal domains are involved in recruiting and interacting with downstream NHEJ factors to mediate DSB repair [24, 25]. Analogous to eukaryotes, homologs of Ku and an intact NHEJ system have been identified in certain bacteria including multiple species of mycobacterium [for review see [26]]. Bacterial Ku (bKu) proteins form small homodimers that possess an evolutionarily conserved 'core' domain but lack the additional N- and C-terminal domains present in eukaryotes [27-29]. Because these terminal domains are required for communication with eukaryotic NHEJ proteins, expression of bKu in eukaryotic cells should, in theory, bind to DNA DSBs and prevent repair due to lack of communication between bKu and

eukaryotic repair proteins. Indeed, we showed previously that nuclear-targeted *Mycobacterium tuberculosis* Ku (MtKu) binds to laser-induced DSBs and increases sensitivity of human cancer cells to bleomycin sulfate, a DSB inducing agent [30]. Nuclear-targeted MtKu also attenuates homologous recombination in mammalian cells [31]. Analogous to *M. tuberculosis*, *M. marinum* was recently shown to possess a proficient NHEJ system [32]. We have determined that *M. marinum* Ku (MmKu) is expressed at a higher level than MtKu in bacterial [32] and mammalian cells (this study). Hence, we selected mitochondrial-targeted MmKu as a molecular tool to bind to DSBs in ρ^+ mtDNA to test the hypothesis that DSB-bound MmKu could prevent mtDNA replication or repair.

Here we report that expression of mitochondrial-targeted MmKu induces petite formation, which occurs selectively in daughter cells. We show that MmKu binds to *ori5* in the yeast mtDNA and that MmKu expression triggers mtDNA depletion. Since MmKu possesses a DSB-binding domain but lacks domains to communicate with eukaryotic repair factors, we conclude that binding of MmKu to *ori5* inhibits mtDNA RDR, thereby preventing transmission of mtDNA from mother cells to daughter cells. We also demonstrate that mitochondrial-targeted MmKu does not decrease mtDNA content in human MCF7 cells. This observation is in agreement with the current knowledge on human mtDNA replication, which typically does not involve DSBs [7, 33]. These findings indicate that mitochondrial-targeted MmKu impairs mtDNA homeostasis only when DSBs are involved in the perpetuation of the mtDNA. Finally, our data suggest that DSB-mediated replication is the predominant form of mtDNA replication in the ρ^+ yeast cells since binding of MmKu to *ori5* can result in the complete loss of mtDNA.

MATERIALS AND METHODS

Oligodeoxyribonucleotides

Oligodeoxyribonucleotides (oligonucleotides) were purchased from Operon Technologies Inc. (Alameda, CA, USA), the DNA Facility at Iowa State University (Ames, IA, USA) or the DNA Sequence/Synthesis Facility at University of Wisconsin Biotechnology Center (Madison, WI, USA). The sequences of the oligonucleotides used in this study are listed in Table 1.

Table 1. Oligonucleotides used in this study

Name	Sequence (5'-3')	Purpose	Reference
MM26	AAAAAGCGGCCGCGGACTTGGCAGCTTGTTTG	Plasmid generation	This study
MM27	AAAAAGTCGACCGCTCCATCTGGAAGGGTTC	Plasmid generation	This study
Flag6	GGCCGCAGACTACAAGGACGATGACGACAAGG-ACTACAAGGACGATGACGACAAGTGACC	Plasmid generation	This study
Flag7	GGCCGGTCACTTGTCGTCATCGTCCTTGTAGTCC-TTGTCGTCATCGTCCTTGTAGTCTGC	Plasmid generation	This study
Ku40	AAAAAGCTAGCATGTCCGTCCTGACGCCGCTG	Plasmid generation	This study
Ku41	AAAAAAAGCTTCTATGCGGCCCCATTCAGATCCTCTTCTG	Plasmid generation	This study
KE1	AAAAACTGCAGCGAGCCATTTGGACGGGTTCG	Plasmid generation	This study
Ku30	AAAAAGCGGCCGCCGGAGGCGTTGGGACGTTTG	Plasmid generation	This study
Su9-Nterm	AAAAAACTGCAGATCTATGGCCTCCACTCGTGTCCTCG	Plasmid generation	This study
RFP-Cterm	AAAAAAAGATCTCTACAGGAACAGGTGGTGGCGGCCC	Plasmid generation	This study
BamMmKu	AAAAAAGGATCCCGCTCCATCTGGAAGGGT	Plasmid generation	This study
SalFlag	AAAAAAGTCGACTCACTTGTCGTCATCGTCC	Plasmid generation	This study
Gal2	AAAAAAACTAGTATCACGAGGCCCTTTCGTCTTC	Plasmid generation	This study
Gal3	AAAAAACTCGAGCGTATATATACCAATCTAAGTCTGTGC	Plasmid generation	This study
RFP1	TCGATCTCGAACTCGTG	Plasmid sequencing	This study
MM9	TCCAGGAAGTAGCTGCGG	Plasmid sequencing	This study
MM10	GTCATGGTGGTGCATACCC	Plasmid sequencing	This study
RS1	ATACGACTCACTATAGG	Plasmid sequencing	This study
RS2	ACAGGAAACAGCTATGAC	Plasmid sequencing	This study
NTG1F	CACTGTCTCAGTCTATTGGGAGG	KT1112/Δ*ntg1* generation	This study
NTG1R	GCCCGTGGTATCGTTAGATGTCG	KT1112/Δ*ntg1* generation	This study
deltaNTG1R	GAGGCAACCGTTACAGGAATGG	*NTG1* deletion verification	This study
Y2Oli2	CATGACCCATAGCTTCC	End-point PCR	This study
Y2Oli7	GCTGCACTATAAGATAGG	End-point PCR	This study
XhoIF	TGATGGTTCATTTGTAAAAGG	End-point PCR	This study
XhoIR	AATCATTACTGATCTCATTGG	End-point PCR	This study
ORI5AcrF	GGTATATAATGAAGATCTATTAGAACC	End-point PCR	This study
XhoIUpInF	CAGGACCTAGTGTAGATTTAG	End-point PCR	This study
XhoIUpInR	CTCGTATAAGATTGGGTCAC	End-point PCR	This study
ACT1F	GTATGTGTAAAGCCGGTTTTG	Real-time qPCR	[34]
ACT1R	CATGATACCTTGGTGTCTTGG	Real-time qPCR	[34]
COX1F	CTACAGATACAGCATTTCCAAGA	Real-time qPCR	[34]
COX1R	GTGCCTGAATAGATGATAATGGT	Real-time qPCR	[34]
ORI5F	CAGAGCACACATTTGTTAATATTTAATAA	Real-time qPCR	[35]
ORI5R	CCCGGATATCTTCTTGTTTATC	Real-time qPCR	[35]
Human18SF	AGCCATGCATGTCTAAGTACGCACG	Real-time qPCR	[36]
Human18SR	CAAGTAGGAGAGGAGCGAGCGACCA	Real-time qPCR	[36]
Human-mtDNAF	CAGGAGTAGGAGAGAGGGAGGTAAG	Real-time qPCR	[36]
Human-mtDNAR	TACCCATCATAATCGGAGGCTTTGG	Real-time qPCR	[36]

DNA manipulation and plasmid construction

All plasmid amplification was performed in *Escherichia coli* strain TOP 10 (Life Technologies, Carlsbad, CA, USA). For selection of plasmids, bacteria were grown in LB media containing carbenicillin (100 μg/ml; Life Technologies, Carlsbad, CA, USA). Plasmids were harvested from bacteria and purified using the QIAfilter Plasmid Maxi Kit (QIAGEN GmbH, Hilden, Germany). Restriction enzymes (NEB, Ipswich, MA, USA), T4 DNA ligase (Promega Corporation, Madison, WI, USA) and Phusion High-Fidelity DNA Polymerase (NEB) were used as per the manufacturer's recommendations. Plasmids generated for this work were sequenced by the DNA Facility at Iowa State University.

The pTRE-Tight vector system (Clontech, Mountain View, CA, USA) was used to express the MmKu and MtKu in MCF7 Tet-On cells (Clontech, Mountain View, CA, USA). PCR with primers MM26 and MM27, Phusion High-Fidelity DNA Polymerase and pDUBmKu [32] was performed according to manufacturer's recommendations using an annealing temperature of 70°C. This produced a DNA fragment containing the MmKu coding sequence, minus the ATG translational start codon and the translational stop codon, with a SalI restriction site at the 5′ end and a NotI restriction site at the 3′ end. The DNA was digested with SalI and NotI and ligated into the SalI-NotI sites of the pCMV/myc/mito pShooter vector (Invitrogen, ThermoFisher Scientific) to generate pcmKu. This positioned the mitochondrial targeting sequence from human cytochrome C oxidase subunit VIII in-frame and upstream of the MmKu coding sequence. To tag the MmKu protein with two Flag epitopes, the Flag6 and Flag7 oligonucleotides were annealed by heating to >90°C and cooling slowly to room temperature, prior to ligation

into the NotI site of pcmKu to generate pcmKuFlag. The coding sequence for the mitochondrial-targeted MmKu Flag-tagged protein was then amplified using primers Ku40 and Ku41, Phusion High-Fidelity DNA Polymerase, pcmKuFlag and an annealing temperature of 65°C. The generated DNA fragment was then digested with NheI and HindIII, and ligated into the NheI-HindIII sites of pTRE-Tight to generate pTREcmKuFlag.

The MtKu coding sequence was amplified in Phusion High-Fidelity DNA Polymerase PCR reaction using KE1 and Ku30 primers, pKuEnls [30] and an annealing temperature of 70°C. The MtKu DNA fragment was digested with PstI and NotI and ligated into the PstI-NotI sites of pCMV/myc/mito pShooter to generate pcKumyc. This positioned MtKu downstream of the mitochondrial targeting sequence. The Flag tag was added to the 3′ terminus of the MtKu coding sequence by ligating the Flag6-Flag7 double-stranded DNA molecule into the NotI site of pcKumyc to generate pcKuFlag1-1. PCR with Phusion High-Fidelity DNA Polymerase, Ku40 and Ku41 primers and pcKuFlag1-1 generated a DNA fragment that was digested with NheI and HindIII and ligated into the NheI-HindIII sites of pTRE-Tight to generate pTREctKuFlag.

The pGal plasmid (originally called pJB9) is a low copy number plasmid constructed by incorporating the *GAL1* promoter directly into a yeast centromere-containing shuttle plasmid YCp50 [37] (Figure 26A). The *GAL1* promoter in the plasmid allows expression of a downstream coding region in the presence of galactose. Expression is repressed by glucose, and growth in raffinose medium neither induces nor represses the promoter. The mitochondrial targeting sequence of F_0-ATPase subunit 9 (Su9) of *Neurospora crassa* was used to target proteins to yeast mitochondria [38]. To

express mitochondrial-targeted red fluorescent protein (RFP), the Su9-RFP coding sequence was amplified from B1642 [[39]; a generous gift from Dr. Paul W. Doetsch, Emory University, Atlanta, GA, USA] using Su9-Nterm and RFP-Cterm primers. The fragment was digested with BglII and introduced into the pGal plasmid at the BamHI site to generate pGalSu9RFP.

For yeast expression of mitochondrial-targeted MmKu containing two Flag epitopes, pGalSu9RFP was digested with BamHI and SalI to remove the RFP coding sequence, resulting in the generation of pGalSu9. The MmKuFlag coding region from pcmKuFlag was amplified using BamMmKu and SalFlag primers. The product was digested with BamHI and SalI, and ligated to pGalSu9 to generate pGalSu9MmKu.

A yeast integrating plasmid for expression of mitochondrial-targeted MmKu was constructed by amplifying the sequence *GAL1*P-Su9-MmKu-Flag from pGalSu9MmKu using Gal2 and Gal3 primers. The product was digested with SpeI and XhoI, and ligated to SpeI and XhoI digested pRS305 [40] to generate pRS305MmKu.

The coding sequence in each plasmid was sequenced by the DNA Facility at Iowa State University to ensure correct reading frame and correct orientation of inserts.

Yeast strains, media, and transformation

Yeast strains used in this study were congenic to strain KT1112 [nuclear genotype: *MAT***a** *leu2 ura3 his3*; mitochondrial genotype: ρ^+] [41], unless stated otherwise. The *ntg1* null mutant (KT1112/Δ*ntg1*) was constructed by amplifying the G418 cassette from the *ntg1* deletion panel strain [42] with NTG1F and NTG1R primers. Purified PCR products were introduced into KT1112 and mutants were selected in medium containing G418 (200

μg/ml; Life Technologies, Grand Island, NY, USA). Positive clones were confirmed for the absence of the *NTG1* gene by PCR using NTG1F and deltaNTG1R primers.

Strain KT1112 pRS305MmKu (nuclear genotype: *MAT***a** *leu2*:pRS305MmKu:*LEU2 ura3 his3*; mitochondrial genotype: ρ^+) was constructed by transforming KT1112 with pRS305MmKu linearized with EcoRV within *LEU2*. Transformants were selected in medium lacking leucine (–Leu).

Strain KT1177 (nuclear genotype: *bar1::LEU2 ura3 his4*; mitochondrial genotype: ρ^0), was engineered as described previously [43].

Yeast transformation was performed by a LiAc procedure as described previously [44] with the following modifications: (i) cells were grown in YPD to OD_{600} of 0.6-0.9, and (ii) carrier DNA was from salmon testes (Sigma, Saint Louis, MO, USA). Yeast transformed with pGalSu9RFP or pGalSu9MmKu were selected and grown in medium lacking uracil (–Ura).

YPD, YPGal, and YPRaff contained 1% yeast extract and 2% bacto peptone with 2% glucose, galactose, and raffinose, respectively. YPEG medium contained 1% yeast extract, 2% bacto peptone, 2% ethanol, and 3% glycerol. Selective media were prepared by combining complete supplement mixture lacking uracil (–Ura) or leucine (–Leu) with yeast nitrogen base (Sunrise Science Products, San Diego, CA, USA) and this was supplemented with 2% carbon source (–Ura D or Gal or Raff, –Leu D or Gal or Raff). Synthetic complete medium contained complete supplement mixture (Sunrise Science Products) and yeast nitrogen base (Sunrise Science Products) with 2% carbon source.

Human cell culture

MCF7 Tet-On cells were co-transfected with pTK-Hyg (Clontech, Mountain View, CA, USA) and pTRE-Tight, pTREcmKuFlag or pTREctKuFlag using Lipofectamine (Invitrogen, ThermoFisher Scientific) and selected with hygromycin B (200 μg/ml; Sigma, Saint Louis, MO, USA) as well as G418 (200 μg/ml). The hygromycin B selection was removed after the individual colonies were isolated for expansion into cell lines. Cell lines containing pTRE-Tight, pTREcmKuFlag or pTREctKuFlag (named MCF7 TreTight, MCF7 cMmKu, and MCF7 cMtKu, respectively) were identified by PCR. Doxycycline (0.5 μg/ml; Sigma, Saint Louis, MO, USA) dependent expression of MmKu and MtKu was confirmed by western analyses. All MCF7 Tet-On cell lines were grown in DMEM containing stable glutamine and sodium pyruvate (Corning Life Sciences, Manassas, VA, USA) supplemented with 10% fetal bovine serum (Gemini Bio-Products, West Sacramento, CA, USA) and G418 (200 μg/ml) at 37°C and 10% CO_2. The medium was further supplemented with 50 μg/ml uridine (Sigma, Saint Louis, MO, USA) to make it suitable for growth of respiratory deficient and/or ρ^0 human cells.

Spot dilution analysis

Stationary phase yeast cultures pre-grown in –Ura Raff liquid medium were 25-fold serially diluted using sterile water and 6 μl of each dilution was applied to a –Ura Gal plate. Cells were grown at 30°C for 48 h, following which colonies were replica-plated to YPEG and grown at 30°C for 36 h.

Microscopy

A mid-log phase culture of KT1112 harboring pGalSu9RFP was grown in Gal for 6 h, following which cells were incubated with MitoTracker® Green FM (Molecular Probes, Eugene, OR, USA) according to the manufacturer's instructions. Cells were then examined by fluorescence microscopy using the TRITC filter set (for RFP) and GFP filter set (for MitoTracker® Green FM). For mtDNA visualization, live yeast cells treated with DAPI (0.2 μg/ml; Sigma, Saint Louis, MO, USA) were incubated at 30°C for 30 minutes and imaged for DAPI. Fluorescence images (TRITC, GFP, and DAPI filter sets; Olympus, Japan) and DIC images were acquired using SlideBook Digital Microscopy Imaging Software (Intelligent Imaging Innovations, Denver, CO, USA).

Determination of percentage of ρ^+ colonies

Determination of percentage of ρ^+ colonies was performed as described below, unless stated otherwise. Stationary phase yeast cultures harboring pGalSu9MmKu or pRS305MmKu were pre-grown in –Ura Raff or –Leu Raff, respectively, and diluted to a final concentration of OD_{600} of 0.04. The cultures were grown at 30°C for 3 h on a rotary shaker (200 rpm), following which 2% Gal or 2% Raff was added. The experimental procedure up to this stage is referred to as the initial culture set up. The cultures were then returned to the rotary shaker, and aliquots were removed at the indicated time points. Aliquots were then serially diluted in sterile water to plate ~200 cells on –Ura D or –Leu D agar plates and grown to obtain colonies at 30°C for 72 h. The colonies were counted, replica-plated to YPEG and incubated at 30°C for 36 h, before counting YPEG-positive colonies. The percentage of ρ^+ colonies was calculated using the following formula:

% ρ^+ colonies = (number of colonies on YPEG/ number of colonies on –Ura D or –Leu D) × 100.

Immunoblot analysis

Yeast total protein extracts were prepared by lysing yeast with glass beads in trichloroacetic acid as described previously [45]. Yeast mitochondrial extract (Mito) was prepared from cells using the Yeast Mitochondria Isolation Kit according to manufacturer's instruction (Bio Vision, Milpitas, CA, USA). Protein extracts were subjected to SDS-PAGE and transferred to nitrocellulose (Bio-Rad Laboratories, Inc., Germany). Membranes were probed with the indicated primary antibodies: for anti-Flag M2 antibody (1:2000; Sigma, Saint Louis, MO, USA), a sheep anti-mouse secondary horseradish peroxidase antibody (1:8000; Amersham Biosciences, Buckinghamshire, UK) was used, whereas for anti-Cox4 (1:2000; MitoSciences, Eugene, OR, USA) and anti-Pgk1 (1:30000; Invitrogen, Frederick, MD, USA) antibodies, a goat anti-mouse secondary horseradish peroxidase antibody (1:20000 and 1:31250, respectively; Bio-rad, Hercules, CA, USA) was used.

Human total protein extract was prepared as previously described [46]. Mitochondrial and cytosolic extracts were obtained using the Mitochondria Isolation Kit for Mammalian Cells according to the manufacturer's instructions (Thermo Scientific, Rockford, IL, USA). Protein extracts were subjected to SDS-PAGE and transferred to nitrocellulose. Membranes were probed with the following antibodies: for anti-Flag M2 (1:4000) and anti-Actin (1:4000; BD Biosciences Pharmingen, San Diego, CA) antibodies, a sheep anti-mouse secondary horseradish peroxidase antibody (1:5000) was

used, whereas for anti-SDHB antibody (1:2000; Santa Cruz Biotechnology Inc., Santa Cruz, CA, USA), an anti-rabbit secondary horseradish peroxidase antibody (1:2000; Jackson ImmunoResearch Laboratories, Inc., West Grove, PA, USA) was used.

For all immunoblots, antibody binding was detected by enhanced chemiluminescence (ECL-Prime; GE Healthcare, Buckinghamshire, UK) and visualized using autoradiography and/or a Chemi Doc MP Imaging System (Bio-Rad, USA). Image Lab Software 5.2 (Bio-Rad, USA) was used to quantitate the signal on immunoblots.

Total DNA isolation

Isolation of yeast total DNA was performed as described previously [47]. Briefly, yeast cells were lysed with glass beads for 5 min in lysis buffer and phenol/chloroform/isoamylalcohol (25:24:1; Fisher Scientific, Fair Lawn, NJ, USA). The pellet obtained after ethanol precipitation was resuspended in TE and treated with DNase-free RNase (Sigma, Saint Louis, MO, USA) for 1 h at 37°C. A final DNA precipitation was performed with ice-cold absolute ethanol in the presence of ammonium acetate. The DNA pellet was dried and resuspended in TE. Total DNA from human cells was isolated using the QIAamp DNA Mini Kit according to the manufacturer's instructions (QIAGEN GmbH, Hilden, Germany). DNA was quantitated using a Nanodrop ND-1000 spectrophotometer (Wilmington, DE, USA).

End-point PCR and real-time quantitative PCR (qPCR)

End-point PCR was performed with 250 nM of each primer, 20 ng template DNA, 3 mM $MgCl_2$, 200 µM (each) dATP, dGTP, dCTP and dTTP, and 0.5 U Go Taq Flexi DNA

polymerase (Promega, Madison, WI, USA) in a MyCycler Thermal Cycler (Bio-Rad, USA). To determine mtDNA content, mtDNA amplification was performed using XhoIF and XhoIR primers for 25 cycles with an annealing temperature of 50°C, whereas nuclear DNA (nDNA) amplification was performed using Y2Oli2 and Y2Oli7 primers for 20 cycles with an annealing temperature of 42°C. To examine the PCR product generated across *ori5*, mtDNA amplification was performed using ORI5AcrF and ORI5R for 23 cycles, and XhoIUpInF and XhoIUpInR for 18 cycles. Both primer sets used an annealing temperature of 53.5°C. PCR products were subjected to electrophoresis, visualized using a Chemi Doc MP Imaging System, and quantitated with Image Lab Software 5.2.

For real-time qPCR, Power SYBR Master Mix (Applied Biosystems, Warrington, UK), 300 nM of each primer and 1 ng of DNA template were mixed in a 15 µL reaction. All qPCR was performed in a 7500 Fast Real-Time PCR systems (Applied Biosystems) using the following cycling conditions: 50°C for 2 minutes, 95°C for 10 minutes, and 40 cycles of 95°C for 15 seconds and 60°C for 1 minute, followed by a dissociation curve analysis to ascertain amplicon specificity. Nuclease-free water was substituted for template in negative control reactions. mtDNA amplification was performed using COX1F and COX1R primers (amplicon length 147 bp) for yeast cells, and Human-mtDNAF and Human-mtDNAR primers (amplicon length 125 bp) for human cells. Similarly, nDNA amplification was performed using ACT1F and ACT1R primers (amplicon length 89 bp) for yeast cells, and Human18SF and Human18SR primers (amplicon length 100 bp) for human cells. Relative DNA (mtDNA and nDNA) levels were determined by using a standard curve, which was generated with serially diluted

total DNA (ranging from 10,000 pg to 1 pg) obtained from KT1112 (for yeast) or MCF7 (for human cells). Primer efficiencies were established from the slope of the standard curve and hence the efficiencies were taken into account in the determination of the relative amounts of DNA. mtDNA amplification was normalized to nDNA amplification to obtain the relative mtDNA copy number.

Determination of ρ^0 formation

Following the initial culture set up, KT1112 cells containing pGalSu9MmKu were grown in Raff or Gal for 8 h and ~200 cells were plated on –Ura D to obtain colonies. The 8 h cultures were diluted to OD_{600} of 0.04 and grown for another 24 h so that the total growth period in the indicated sugar was 32 h. ~200 cells were then plated on –Ura D to obtain colonies. Colonies were then replica-plated to YPEG and –Ura D. Petite colonies were identified as those unable to grow on YPEG. At each time point, 5 ρ^+ colonies from the Raff culture and 12 petite colonies from the Gal culture were randomly selected and used to initiate cultures in –Ura D medium. Total DNA was isolated from each culture and relative mtDNA copy number was determined by real-time qPCR. Genomic DNA from KT1177 (ρ^0 strain) was used in negative control reactions for mtDNA amplification. The mtDNA status in petite colonies that showed no mtDNA amplification was verified with DAPI.

mtDNA Immunoprecipitation (mtDNA IP)

The procedure for mtDNA IP was adapted from a protocol described originally for chromatin immunoprecipitation [48]. Briefly, following the initial culture set up, yeast

cells containing pGalSu9MmKu were grown in Gal for 5 h. DNA was crosslinked to proteins by the addition of formaldehyde to a final concentration of 1%. Cells were harvested, resuspended in lysis buffer and lysed with glass beads by vigorous shaking. The sample was sonicated to obtain a mean DNA length of ~0.3 kb. After centrifugation at 4°C, the supernatant containing soluble DNA-protein complexes was precleared with Dynabeads protein G (45 µl; Life Technologies, Oslo, Norway) for 16 h at 4°C with mixing. The supernatant obtained from the preclearing step was treated with 1.5 µg of anti-Flag M2 antibody or mouse IgG1 (Sigma, Saint Louis, MO, USA) for 16 h at 4°C. Dynabeads (40 µl) were then added to the DNA-protein-antibody complex and mixed for 16 h at 4°C. The mixture of Dynabeads and DNA-protein-antibody complexes were washed, in succession, with lysis buffer, high salt lysis buffer, wash buffer, and TE. DNA-protein complexes were eluted from the Dynabeads twice with elution buffer at 65°C for 30 min. Crosslinks were reversed at 65°C for 16 h in the presence of proteinase K (50 µg/ml; Roche diagnostics, Indianapolis, IN, USA). The solution containing the DNA was extracted twice with phenol/chloroform/isoamylalcohol (25:24:1; Amresco LLC, Solon, OH, USA) and the DNA precipitated with ice-cold absolute ethanol in the presence of glycogen (20 µg; Affymetrix, Santa Clara, CA, USA). The purified immunoprecipitated DNA was dissolved in 60 µl TE, of which 2 µl was subjected to real-time qPCR using *ori5* specific primers (ORI5F and ORI5R) and *COX1* specific primers. A standard curve specific for each amplicon was used to determine the amount of mtDNA present in each immunoprecipitate and background signal obtained from the IgG1 control was subtracted. The net immunoprecipitate obtained was used to calculate the percentage of input immunoprecipitated using the following formula:

% Input immunoprecipitated = (Amount of mtDNA in net IP/ Amount of mtDNA in total input) x 100

Total input represents total amount of DNA-protein complex used in the immunoprecipitation.

End-point PCR across the *ori5* DSB region

Cultures of KT1112 and KT1112/Δ*ntg1* were grown as described for the mtDNA IP assay. End-point PCR was performed from total cellular DNA as described above using primers ORI5AcrF and ORI5R to amplify a 562 bp region that encompassed the *ori5* DSB region, and XhoIUpInF and XhoIUpInR to amplify a 281 bp segment of mtDNA that lies >24 kb away from *ori5* and is a control region on mtDNA. PCR products were subjected to electrophoresis, visualized using a Chemi Doc MP Imaging System, and quantitated with Image Lab Software 5.2. A ratio of the amount of PCR product across the *ori5* DSB region/PCR product from the control region was calculated.

Pedigree analysis

Pedigree analysis was adapted from [49]. Briefly, pedigree plates consisted of two segments of agar containing YPGal and YPD separated by ~5 mm. Early log phase yeast cells grown in YPRaff were streaked on the YPGal segment, from which unbudded cells were transferred to discrete positions on YPGal by micromanipulation. These cells were designated as mother cells for the pedigree. After cell division, the daughter cell from each mother cell was transferred from YPGal to YPD. This process was continued for three daughter generations from each mother cell, following which the mother cell was

placed on YPD. During transfer, each pedigree was observed regularly such that the interval of observation was always less than 1 h. After completion of cell transfer, cells were incubated at 30°C for 72 h. The colonies were replica plated to YPEG and incubated at 30°C for 36 h. The percentage of ρ^+ colonies for each daughter generation and the mother generation was calculated as follows:

% of ρ^+ colonies = (number of colonies on YPEG/number of colonies on YPD) × 100.

Statistical analysis

Data are presented as mean ± standard deviation (SD) of three independent experiments, unless stated otherwise. Statistical comparisons were performed either with Student's *t*-test (between two groups) or with ANOVA (for more than two groups) followed by *post hoc* analysis using Tukey's multiple comparison test. Differences are considered statistically significant at $P < 0.05$.

RESULTS

Expression of mitochondrial-targeted proteins from pGal plasmids

To express mitochondrial-targeted proteins in yeast cells, we used the presequence of the F_0-ATPase subunit 9 (Su9) of *Neurospora crassa* as a mitochondrial targeting sequence [38]. pGalSu9RFP contains the Su9 in frame with RFP. Induction of the promoter with Gal produces a fusion protein in which the Su9 sequence is linked to the N-terminus of RFP (Figure 26B, upper panel). Induction of pGalSu9MmKu with Gal results in expression of a fusion protein in which MmKu has the Su9 sequence at the N-terminus and two Flag epitopes at the C-terminus (Figure 26B, lower panel). Su9 contains 69 amino acid residues and possesses a mitochondrial matrix processing peptidase site at the interface between the 66^{th} and 67^{th} amino acids, hence the last three amino acids at the C-terminus of Su9 remain attached to the N-terminus of downstream proteins following the activity of the mitochondrial matrix processing peptidase [50, 51]. To confirm the ability of Su9 to deliver proteins into yeast mitochondria, KT1112 harboring pGalSu9RFP was grown in the presence of Gal for 6 h, following which cells were treated with MitoTracker® Green. Visualization of cells using fluorescence microscopy revealed that the RFP and the MitoTracker® Green localized to the same mitochondrial structures (Figure 26C). To assess expression of MmKu, total cell extracts and mitochondrial extracts from KT1112 carrying pGalSu9MmKu were subjected to western analysis. Growth of cells in Gal for 8 h triggered expression of MmKu, which localized to yeast mitochondria (Figure 26D).

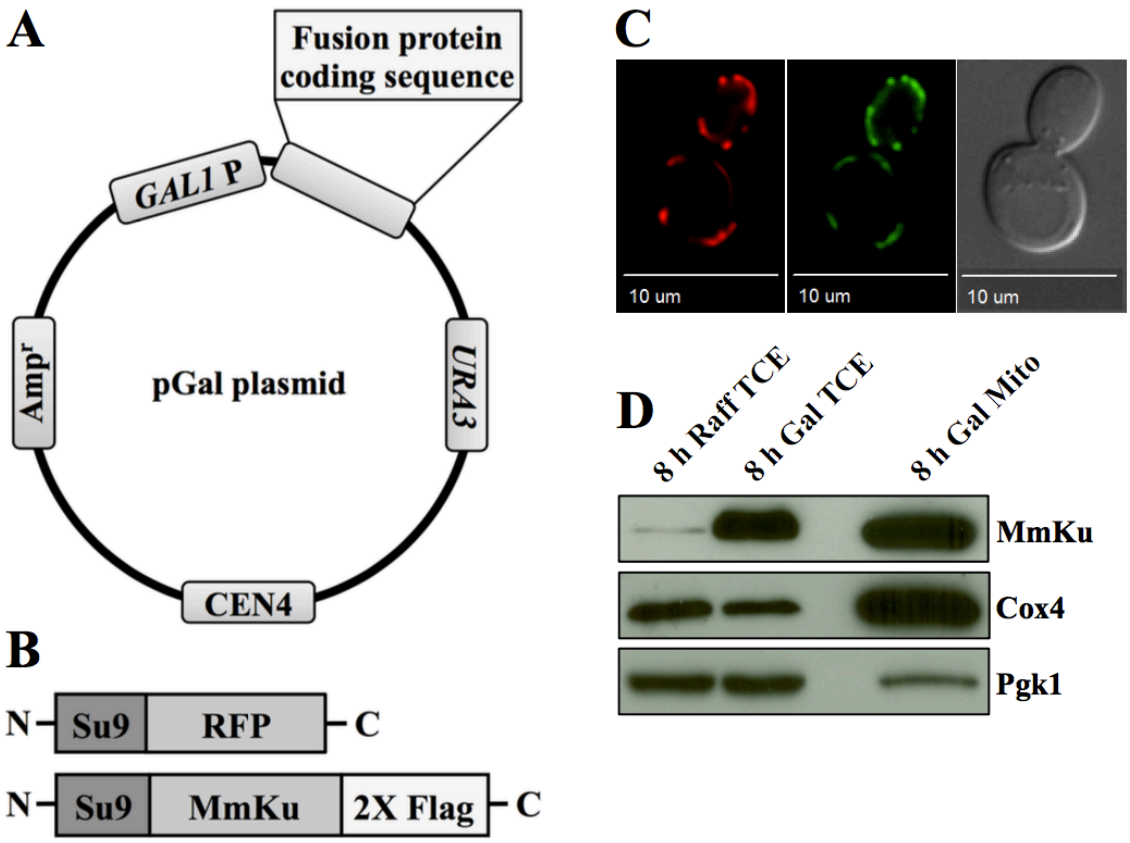

Figure 26. Galactose-inducible expression of mitochondrial-targeted proteins. (**A**) Schematic representation of pGal plasmid. *GAL1*P: Gal-inducible promoter; Amp^r: ampicillin/carbenicillin resistance gene; *URA3*: gene encoding orotidine-5'-phosphate decarboxylase; CEN4: centromere from chromosome IV. (**B**) Schematic representations of fusion proteins expressed from two pGal plasmids: Su9 is fused to the N-terminus of both RFP and MmKu; MmKu also has 2 Flag epitopes at the C-terminus. (**C**) pGalSu9RFP was introduced into KT1112, and RFP expressed in the presence of Gal was visualized using fluorescence microscopy (left panel). Mitochondria in live cells were stained with MitoTracker® Green FM and visualized under the fluorescence microscope (middle panel). The red and green fluorescence signal in the same cell localized to the same mitochondrial structures. While images were being captured by microscopy the yeast cells moved and this prevented a merged image from the same yeast cell. The corresponding image to the right is DIC. Images shown are representative of 3 independent experiments. (**D**) Mitochondrial extracts (Mito) were obtained from cells carrying pGalSu9MmKu grown in the presence of Gal for 8 h, and total cell extracts (TCEs) were prepared from cells harboring the same plasmid grown either in raffinose (Raff) or Gal for 8 h. The extracts were probed with anti-Flag, anti-Cox4, or anti-Pgk1 antibody. An image representative of 2 independent experiments is shown. Cox4, cytochrome C oxidase subunit 4, is a mitochondrial marker. Pgk1, phosphoglycerate kinase, is used as a cytosolic marker for mitochondrial extracts and as a loading control for TCEs. The presence of a faint band of Pgk1 in the lane containing mitochondrial extracts shows a low level of cytosolic contamination.

Mitochondrial-targeted MmKu triggers petite formation

Petite formation was determined by the ability of yeast cells to perform mitochondrial respiration. KT1112 cells carrying pGalSu9MmKu or pGalSu9RFP were serially diluted and applied to Gal medium to induce expression of the mitochondrial-targeted proteins. Cells carrying pGalSu9RFP grew normally on the medium, whereas cells harboring pGalSu9MmKu grew slowly (Figure 27A, upper panel). The colonies were then replica plated to YPEG, a medium on which only respiratory competent yeast cells can grow. Although cells expressing RFP grew well on YPEG, cells harboring pGalSu9MmKu formed small or no colonies (Figure 27A, lower panel), indicating a compromised mitochondrial electron transport chain. To quantitate the respiration defect, yeast cells transformed with MmKu or RFP expression plasmid were grown in Raff or Gal liquid medium for increasing time intervals, following which cells were plated on solid medium containing glucose. The colonies were then replica plated to YPEG and the percentage of ρ^+ colonies was determined. The percentage of ρ^+ colonies in cells expressing MmKu decreased with time; only ~26% and ~19% of colonies were ρ^+ at 8 h and 24 h, respectively (Figure 27B). In contrast, colonies obtained from control cultures maintained the ρ^+ phenotype. The percentage of ρ^+ colonies for cells expressing MmKu plateaus after 8 h, and this corresponded to the time that the yeast culture exited exponential growth (Figure 27C). When the 8 h Gal culture was diluted with medium containing Gal and grown for another 24 h, the percentage of ρ^+ colonies further decreased (Figure 28C). Western analysis detected MmKu within 30 min of Gal treatment, and expression was maximal at ~6-8 h (Figure 27D). These results indicate that mitochondrial-targeted MmKu impairs mitochondrial respiration and induces petite formation.

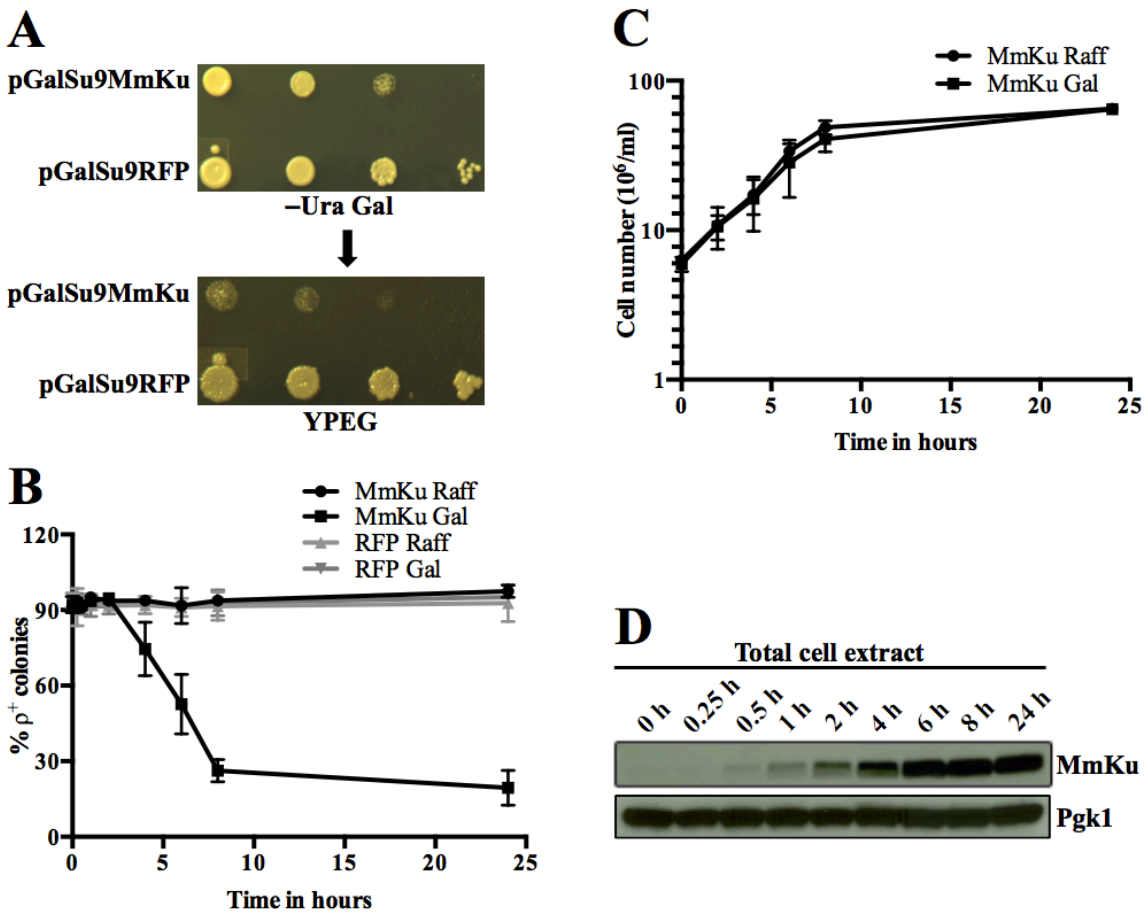

Figure 27. Mitochondrial-targeted MmKu impairs mitochondrial respiration. (**A**) Following serial dilution, cells containing pGalSu9MmKu or pGalSu9RFP were spotted on –Ura Gal, and imaged after 48 h (upper panel). The colonies were replica-plated to YPEG and imaged after 36 h (lower panel). Images are representative of at least three independent experiments. (**B**) For determination of the percentage of ρ^+ colonies, the procedure for the initial culture set up (see the Materials and Methods) was modified slightly such that the stationary phase yeast cultures carrying MmKu or RFP expression plasmid pre-grown in –Ura Raff were diluted 20-fold in the same medium. After addition of Raff or Gal for the indicated time periods, cells were plated on –Ura D. Colonies were replica-plated to YPEG and the percentage of ρ^+ colonies was calculated. Each curve depicts average measurements from three independent experiments. (**C**) Growth of cultures containing pGalSu9MmKu was followed over the indicated time period. Each curve represents average measurements from two independent experiments. (**D**) Cells carrying pGalSu9MmKu were grown in Gal and samples were taken at indicated time points to obtain total cell extracts, which were probed with anti-Flag or anti-Pgk1 antibody. The immunoblot shown is representative of two independent experiments. Pgk1, phosphoglycerate kinase, is used as a loading control.

Mitochondrial-targeted MmKu induces mtDNA depletion

As MmKu possesses a DSB DNA binding domain, we hypothesized that mitochondrial-targeted MmKu triggers petite formation by disturbing mtDNA homeostasis. To test this, we determined the approximate mtDNA content of pGalSu9MmKu-containing cells by examining the mtDNA/nDNA ratio using end-point PCR (Figure 28A). Total DNA isolated from cells grown in Raff or Gal for 8 h was used as the template for PCR. Quantitation of EtBr-stained amplicons revealed ~4-fold decrease in the mtDNA/nDNA ratio for cells grown in Gal compared to Raff (data not shown). To verify this effect of MmKu, we assessed the relative mtDNA copy number using real-time qPCR. As shown in Figure 28B, there was ~3 fold decrease in relative mtDNA copy number in cells grown in Gal for 8 h. The 8 h cultures were diluted and grown for another 24 h in Gal or Raff such that the total period of growth was 32 h. After 32 h, there was further decrease in the relative mtDNA copy number in Gal-grown cells compared to Raff-grown cells. The respiratory competence of these cells was also tested and only ~22% and ~1% of colonies from cells grown in Gal maintained ρ^+ phenotype at 8 h and 32 h, respectively (Figure 28C). In contrast, the percentage of ρ^+ colonies for Raff-grown cells was ~94% at 8 h and 32 h. The expression of MmKu at 8 h and 32 h was confirmed by western analysis (Figure 28D).

As a control, we determined the relative mtDNA copy number from total DNA obtained from cells containing pGalSu9RFP grown in Raff or Gal for 8 h or 32 h (Figure 29A). The relative mtDNA copy number did not vary between the 8 h treatment groups and there was only an ~9% reduction in the relative mtDNA copy number in 32 h Gal-grown cells compared to 32 h Raff control. This indicates expression of a foreign

mitochondrial-targeted protein alone or growth in Gal does not dramatically reduce the mtDNA copy number.

To visualize the mtDNA, cells containing pGalSu9RFP or pGalSu9MmKu grown in Raff or Gal for 32 h were stained with DAPI. Whereas bright punctate mtDNA nucleoids were observed towards the cell periphery in 32 h Raff-grown cells and 32 h Gal-grown pGalSu9RFP-containing cells, the punctate staining was markedly reduced in 32 h Gal-grown pGalSu9MmKu-containing cells (Figures 29 and 30). The loss of punctate staining therefore confirmed the reduction in mtDNA in the Gal-grown pGalSu9MmKu-containing cells.

Further examination of the western analysis in Figure 28D revealed there was a relatively low Cox4 signal in Gal samples compared to Raff samples. Quantitation of Cox4 relative to the loading control Pgk1 revealed a significantly decreased level of Cox4 in 32 h Gal-grown cells compared to cells grown in Raff for the same period (Table 2). A small reduction in Cox4 level was also observed for cells grown in Gal for 8 h compared to the 8 h Raff control (Table 2). We therefore examined the Cox4 levels in other western analyses performed during these studies using strains carrying the pGalSu9MmKu and pRS305MmKu after 8 h of Gal treatment (Figures 26D and 35A). A 9-12% reduction of Cox4 was also detected in these experiments in Gal-grown compared to Raff-grown cells. This suggests MmKu resulted in a reduction of expression of nuclear-encoded Cox4.

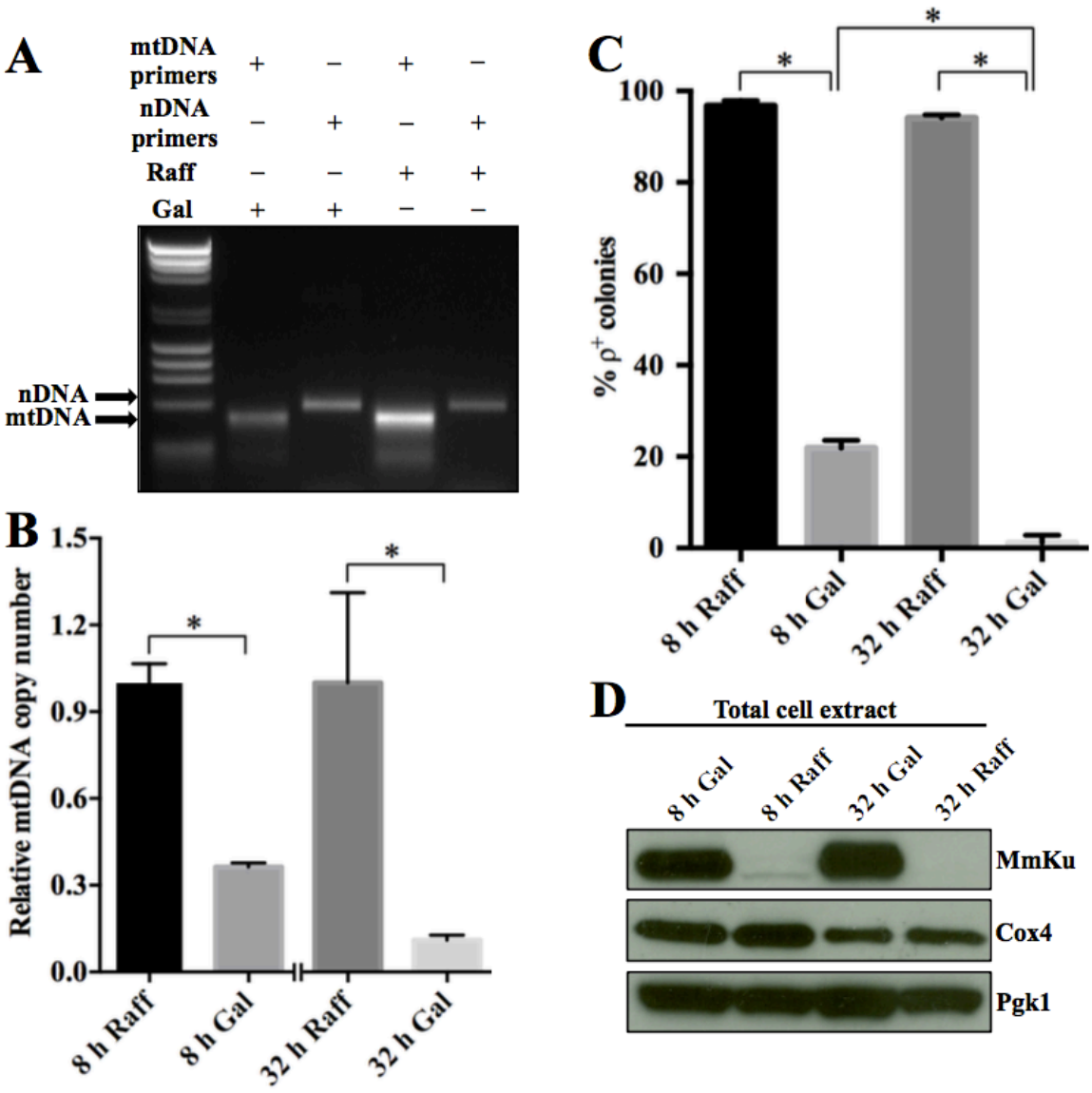

Figure 28. Mitochondrial-targeted MmKu decreases mtDNA content in yeast cells. Total DNA was isolated from KT1112 harboring pGalSu9MmKu grown in Raff or Gal for 8 h or 32 h and end-point PCR (**A**) or real-time qPCR (**B**) was performed to amplify segments of mtDNA and nDNA. An image (**A**) representative of at least three independent end-point PCR experiments is shown. For real-time qPCR (**B**), data are represented graphically as the mean ± SD from three independent experiments. * represents $P < 0.05$. (**C**) Part of the cultures used for DNA isolation were used to quantitate the percentage of ρ^+ colonies, and the averages are shown graphically. Error bars represent SD and * represents $P < 0.05$. (**D**) MmKu, Cox4 and Pgk1 expression in KT1112 carrying pGalSu9MmKu grown in Raff or Gal for 8 h and 32 h. An immunoblot representative of three independent experiments is shown. Cox4, cytochrome C oxidase subunit 4, is a mitochondrial protein.

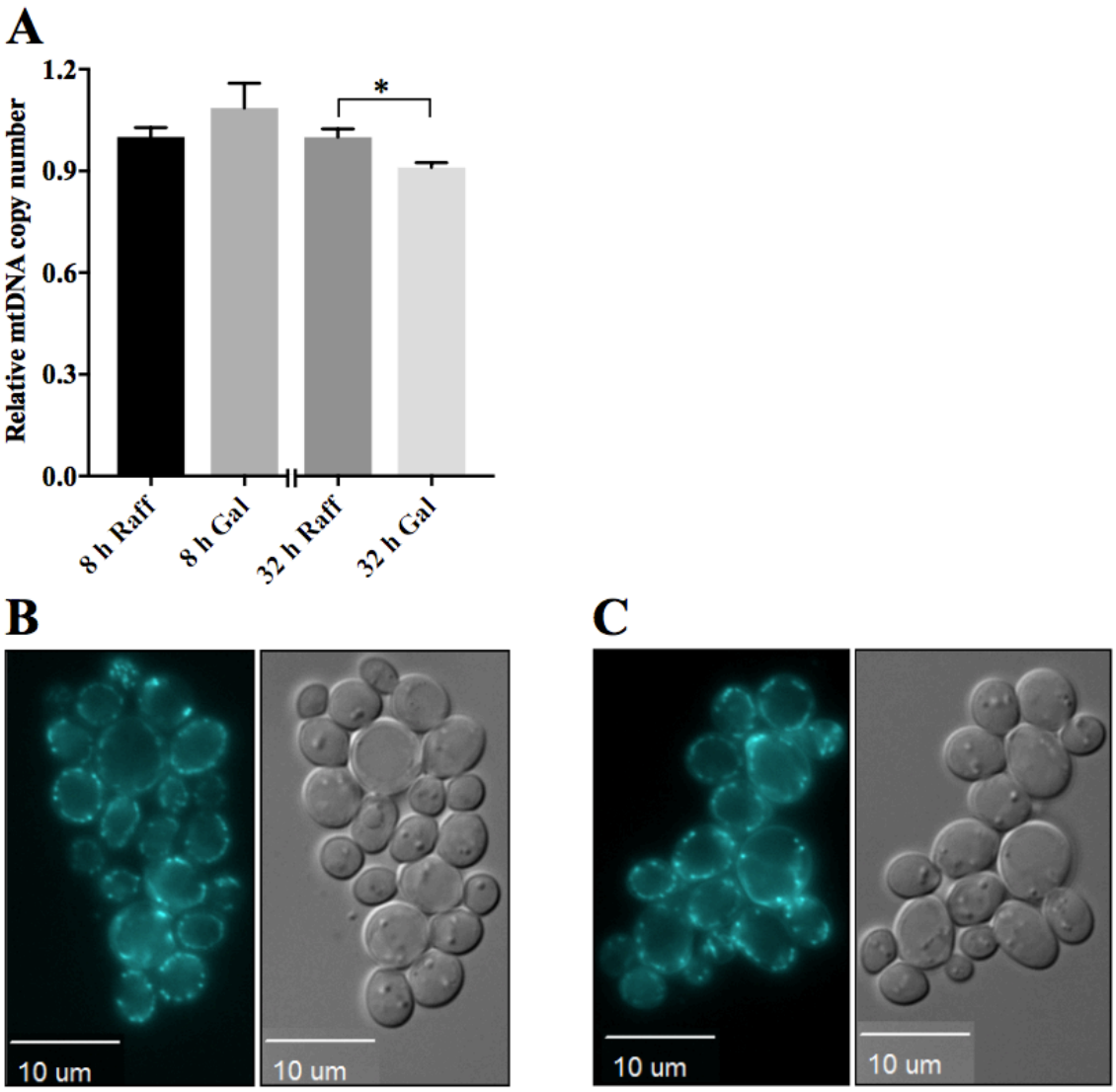

Figure 29. Comparison of mtDNA content in cells containing pGalSu9RFP grown in Raff or Gal. (**A**) Total DNA was isolated from KT1112 carrying pGalSu9RFP grown in Raff or Gal for 8 h or 32 h, following which real-time qPCR was performed to determine the relative mtDNA copy number. Data are represented graphically as mean ± SD from three independent experiments. * represents $P < 0.05$. (**B**) Cells containing pGalSu9RFP were grown in Raff for 32 h, treated with DAPI at 30°C for 30 min, and visualized using fluorescence microscopy. The corresponding image to the right is DIC. (**C**) Cells carrying pGalSu9RFP grown in Gal for 32 h underwent the same procedure as described in Figure 29B. Images shown are representative of three independent experiments. DAPI staining experiments were performed on live yeast cells. During such vital staining procedure, localization of DAPI into the nucleus is somewhat restricted [52]. The preferential mtDNA staining by DAPI could be due to: (i) the negative mitochondrial membrane potential towards the matrix side, which may electrophoretically pull positively charged DAPI to make it readily available for binding to mtDNA; (ii) DAPI preferentially binds to AT regions of DNA and yeast mtDNA has high AT content (GC content of yeast mtDNA is 17.1% [6]).

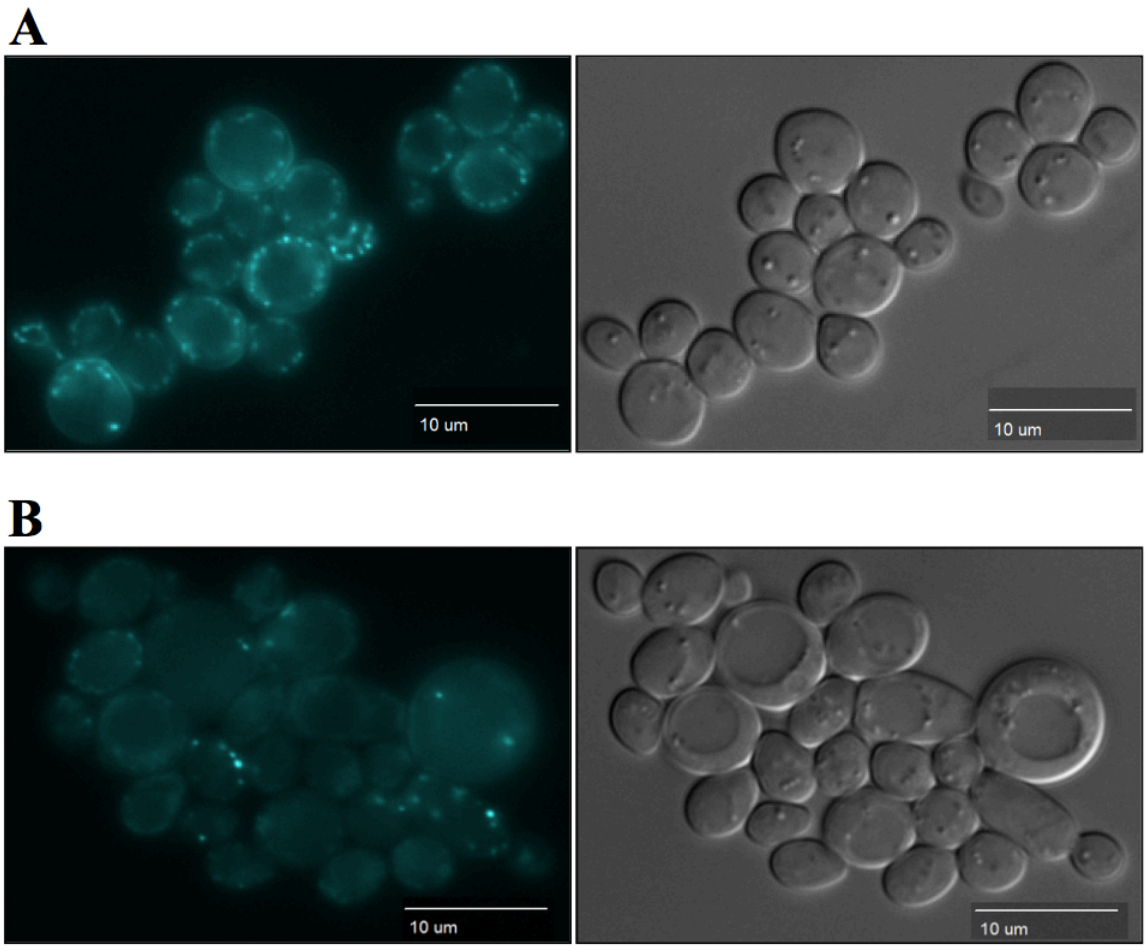

Figure 30. Mitochondrial-targeted MmKu triggers mtDNA depletion. (**A**) Cells containing pGalSu9MmKu were grown in Raff for 32 h. Following treatment with DAPI at 30°C for 30 min, cells were visualized using a fluorescence microscope (left panel). The corresponding image to the right is DIC. (**B**) Cells containing pGalSu9MmKu grown in Gal for 32 h underwent the same procedure as described in Figure 30A. Images shown are representative of three independent experiments.

Table 2. Quantitation of MmKu and Cox4 in total cell extracts

Time and treatment	MmKu/Pgk1	Cox4/Pgk1
8 h Raff	0.004 ± 0.001	0.449 ± 0.031
8 h Gal	0.852 ± 0.181*	0.348 ± 0.155
32 h Raff	0.001 ± 0.003	0.264 ± 0.095
32 h Gal	0.765 ± 0.102**	0.051 ± 0.033**

Levels of MmKu and Cox4 from immunoblots (Figure 28D) were quantitated. The levels were normalized to Pgk1 and represented as mean ± SD. * and ** denote $P < 0.05$ for protein level in Gal culture compared to Raff culture at 8 h and 32 h, respectively.

Mitochondrial-targeted MmKu triggers ρ^0 formation

To determine if MmKu induces complete loss of mtDNA, we used real-time qPCR to analyze the mtDNA/nDNA ratio for individual ρ^+ colonies obtained from Raff cultures and petite colonies from Gal cultures. As shown in Table 3, the mtDNA/nDNA ratio was greater than 1 for almost all colonies from the Raff culture. In contrast, 33% of the colonies from the 8 h Gal culture and 50% of the colonies from the 32 h Gal culture had undetectable levels of mtDNA. These colonies with undetectable levels of mtDNA were verified for the complete loss of mtDNA by DAPI staining (Figure 31).

MmKu binds to the mtDNA replication origin *ori5*

A DSB at yeast mitochondrial replication origin *ori5* (Figure 32A) has been implicated in initiation of mtDNA RDR [18, 19]. As MmKu possesses a DSB binding domain, we hypothesized that MmKu binds to DSBs at *ori5* and inhibits mtDNA replication, thereby decreasing total mtDNA content. To test this, mtDNA IP assays were performed using Flag-tagged MmKu expressed in KT1112. An anti-Flag antibody or an IgG1 control antibody was used for the IP. Real-time qPCR with purified immunoprecipitated DNA was performed using *ori5*-specific primers or *COX1*-specific primers. The *COX1* mitochondrial gene was used as a control because this gene is situated at least 23 kb away from *ori5* region. As shown in Figure 32B, binding of MmKu was significantly higher to *ori5* compared to the *COX1* region, which supports the idea of MmKu binding to DSBs at *ori5*.

Table 3. Mitochondrial-targeted MmKu induces ρ^0 formation

Culture in Raff	mtDNA/nDNA ratio in 5 randomly chosen ρ^+ colonies			
	< x - 0.005	0.0051 - 0.8	0.81 - 1.0	1.01 - 1.25
8 h	0	0	0	5 (100%)
32 h	0	0	1 (20%)	4 (80%)
Culture in Gal	mtDNA/nDNA ratio in 12 randomly chosen petite colonies			
	< x	> x and < 0.005	0.005-0.8	0.81-1.0
8 h	4 (33%)	4 (33%)	3 (25%)	1 (8%)
32 h	6 (50%)	6 (50%)	0	0

KT1112 harboring pGalSu9MmKu were grown in Raff or Gal for 8 h and cells were plated on –Ura D. 8 h cultures were then diluted and grown for another 24 h, following which cells were plated on –Ura D. The colonies were replica plated to YPEG and –Ura D. After identifying ρ^+ and petite colonies, total DNA was isolated from randomly selected ρ^+ and petite colonies to determine the mtDNA/nDNA ratio. In Table 3, x is the ratio for the border between the undetectable level and the least detectable level.

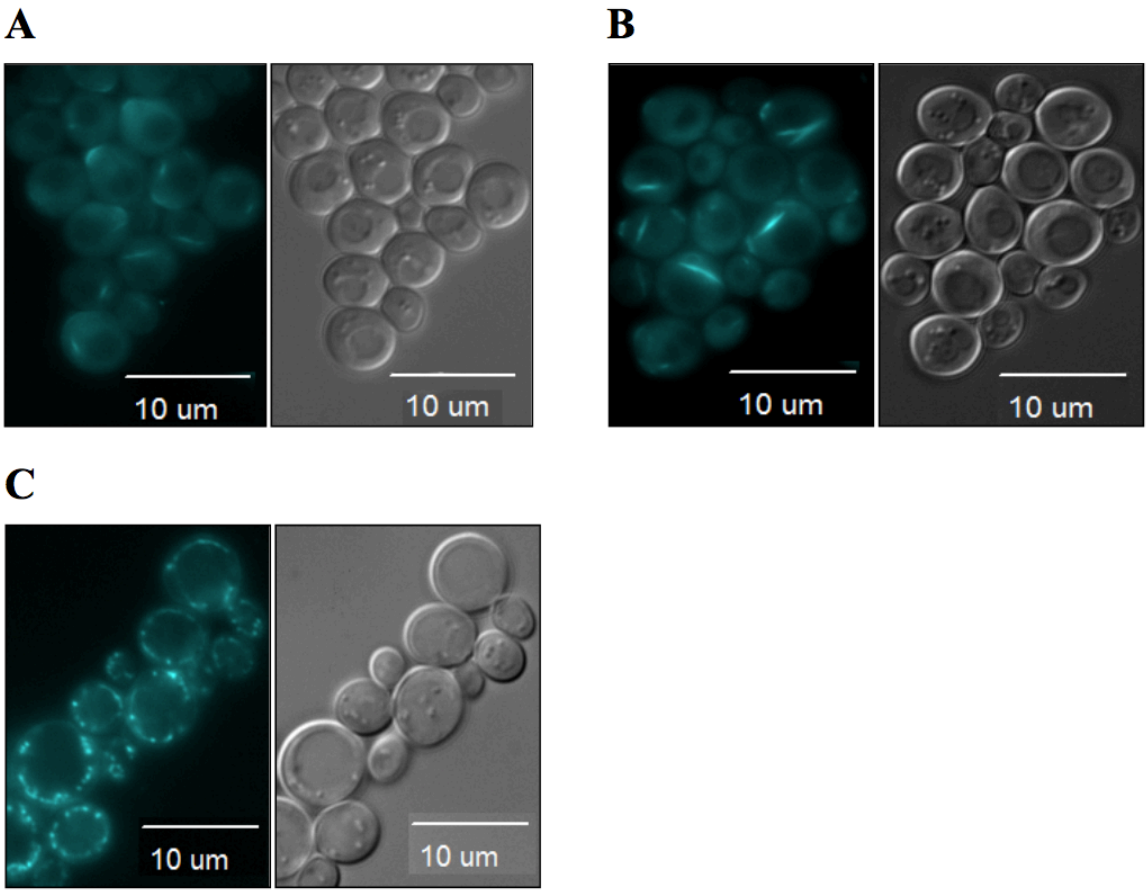

Figure 31. Verification for the lack of mtDNA in ρ^0 cells generated following MmKu expression. (**A**) ρ^0 colonies obtained by expressing mitochondrial-targeted MmKu (Table 3) were grown in synthetic complete medium containing Raff. After treating with DAPI at 30°C for 30 min, cells were visualized using a fluorescence microscope (left panel). The corresponding image to the right is DIC. Representative images from an MmKu-induced ρ^0 colony are shown. (**B**) KT1177 (ρ^0 strain) and (**C**) KT1112 (ρ^+ strain) following the same DAPI staining procedure as described in Figure 31A. Images shown are representative of two independent experiments.

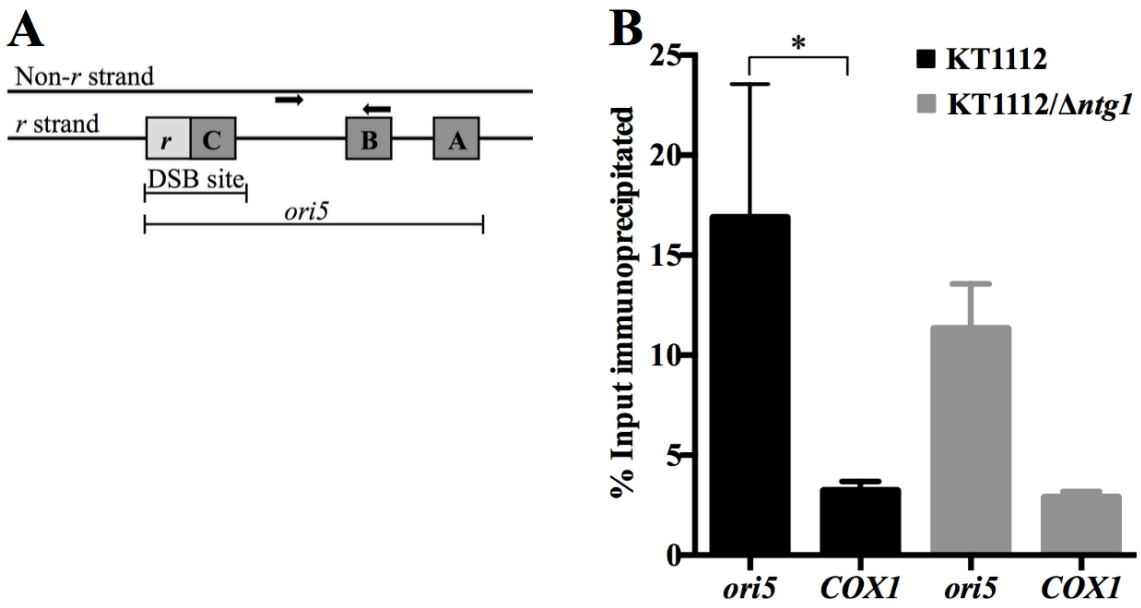

Figure 32. MmKu binds preferentially to *ori5* in the yeast mitochondrial genome. (**A**) Schematic representation of *ori5*. The replication origin consists of 3 GC clusters (A, B, and C) and a transcriptional promoter *r*. A DSB at *ori5* can occur in a region that spans the promoter *r* and ~5 bp downstream of GC cluster C [18]. The *ori5*-specific primers (bold arrows) amplify a region of *ori5* that is downstream of the DSB-occurring region. Figure 32A is adapted from [9] and [18]. (**B**) The indicated strains harboring pGalSu9MmKu were grown in Gal for 5 h, following which DNA-protein complexes were crosslinked with formaldehyde, sheared by sonication and immunoprecipitated with either anti-Flag antibody or IgG1 control. Crosslinks were reversed and purified immunoprecipitated DNA samples were quantitated by real-time qPCR using *ori5*-specific primers and *COX1*-specific primers. The graph shows mean ± SD from three independent experiments. *P* values are as follows: for KT1112 *ori5* vs. KT1112 *COX1* $P = 0.0064$; for KT1112/Δ*ntg1 ori5* vs. KT1112/Δ*ntg1 COX1* $P = 0.0741$; and for KT1112 *ori5* vs. KT1112/Δ*ntg1 ori5* $P = 0.2892$.

MmKu expression in an *ntg1* null mutant

Ntg1 has been shown to play a role in instigating DSBs at *ori5*. In the absence of Ntg1 in hypersuppressive ρ^- yeast, the extent of DSBs at *ori5* decreases [18, 19] and hence MmKu binding at *ori5* would be expected to be reduced in a strain deleted in *ntg1*. The mtDNA IP was therefore repeated in an *ntg1* null mutant (KT1112/Δ*ntg1*). Binding of MmKu to *ori5* was not significantly different from the *COX1* region in this strain, which suggests reduced binding to *ori5* in the absence of Ntg1-induced DSBs. However, when the results from independent experiments were compared for KT1112/Δ*ntg1* and KT1112, even though the average MmKu binding to *ori5* was lower in KT1112/Δ*ntg1*, the difference was not statistically significant (Figure 32B). The binding of MmKu to the *COX1* control region in the two strains was comparable and also not statistically significant (Figure 32B).

The effect of MmKu expression on mitochondrial respiration was also examined in KT1112/Δ*ntg1* and KT1112. In both strains, the percentage of ρ^+ colonies was dramatically decreased by growth in Gal (Figure 33). There was also a trend for decreased formation of ρ^+ colonies in KT1112/Δ*ntg1* compared to KT1112 when the strains were grown in Gal for 8 h, but there was no statistical difference. At 32 h in Gal, the percentage of ρ^+ formation was comparable between the two strains.

Since our data indicated that binding of MmKu to *ori5* was not dramatically different in the absence of Ntg1, end-point PCR across the *ori5* DSB region (Figure 32A) was used to compare the induction of DSBs at *ori5* in KT1112/Δ*ntg1* and KT1112. An increase in PCR product was used as the indicator of a decrease in DSB induction. In each of three independent experiments, there was a small increase in product generated

from PCR across the *ori5* DSB region in KT1112/Δ*ntg1* compared to KT1112 (Figure 34A). Even though this suggests there was reduced DSB formation at *ori5* in KT1112/Δ*ntg1*, there was no statistical difference between the average amounts of PCR product from the three experiments (Figure 34B).

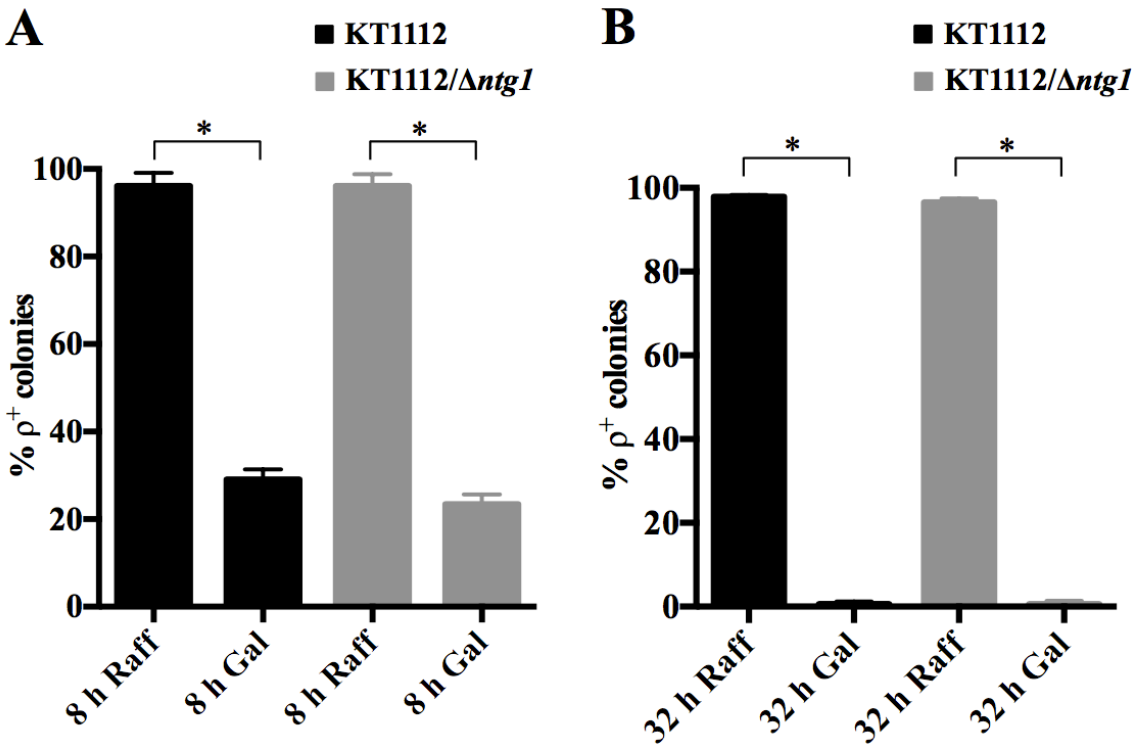

Figure 33. Comparison of the percentage of ρ^+ colonies between KT1112 and KT1112/Δ*ntg1*. (**A**) KT1112 and KT1112/Δ*ntg1* containing pGalSu9MmKu were grown at the same time in media containing Raff or Gal for 8 h and plated on –Ura glucose (–Ura D). (**B**) The cultures were then diluted at 8 h and grown for another 24 h after which the cells were plated on –Ura D. Colonies on –Ura D were replica-plated to YPEG and the percentage of ρ^+ colonies was calculated. The average percentage of ρ^+ colonies from three independent experiments are represented graphically. Error bars represent SD and * denotes $P < 0.05$.

A

Experiment number	Normalized signal across the DSB region at *ori5*	
	KT1112	KT1112/Δ*ntg1*
1	2.34	2.7
2	2.41	2.65
3	1.75	1.95

B

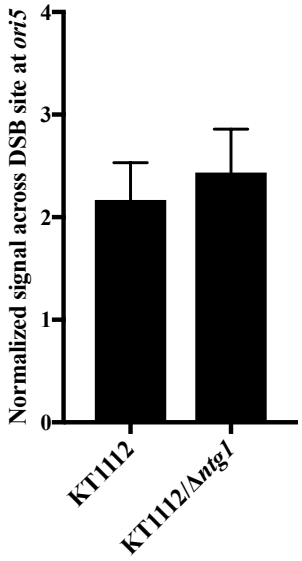

Figure 34. PCR from KT1112 and KT1112/Δ*ntg1* DNA using primers encompassing the region where DSBs are induced in *ori5*. KT1112 and KT1112/Δ*ntg1* were grown in media containing Gal for 5 h following which cells were harvested to isolate total DNA. End-point PCR was performed from total DNA using ORI5AcrF/ORI5R primer set and XhoIUpInF/R primer set. The signal of the PCR product obtained from ORI5AcrF/ORI5R primer set was normalized with that obtained from XhoIUpInF/R primer set. The values for the normalized signal across the DSB region of *ori5* from three independent experiments are presented in a table (**A**) and the mean ± SD of the three experiments are shown graphically (**B**).

MmKu triggers petite formation preferentially in daughter cells

Since the products of mtDNA RDR are selectively transmitted to the daughter cells [17], we reasoned that mtDNA depletion and accompanying petite formation due to MmKu expression occurs preferentially in daughter cells. To test this, we constructed a yeast strain (KT1112 pRS305MmKu) with a nuclear-integrated Gal-inducible MmKu expression plasmid. Following confirmation of expression and the petite generating activity of mitochondrial-targeted MmKu (Figure 35), pedigree analyses were performed on KT1112 pRS305MmKu on plates containing YPGal and YPD agar segments. Yeast cells were first placed on YPGal and after cell division, daughter cells were transferred to YPD. Following transfer of three successive daughters, the respective mother was transferred to YPD. It should be noted that each mother cell was exposed to the YPGal medium for ~7 h, whereas daughter cells were transferred immediately to YPD after cell division. As shown in Figure 36A, petite formation was observed particularly from the second daughter generation. We analyzed a total of 42 colonies for each generation and determined the percentage of ρ^+ formation (Figure 36B). We found that ~45% of colonies from the third daughter (D3) generation were petites, in contrast to ~7% petite colonies from the mother (M) generation. As a control, we repeated the procedure to analyze the pedigree of the parental strain KT1112 and observed that colonies from all three daughter generations and the mother generation essentially maintained the ρ^+ phenotype (Figures 36C and 36D). These data reveal that MmKu induces petite formation preferentially in daughter generations, which is indicative of mtDNA loss selectively in daughter cells.

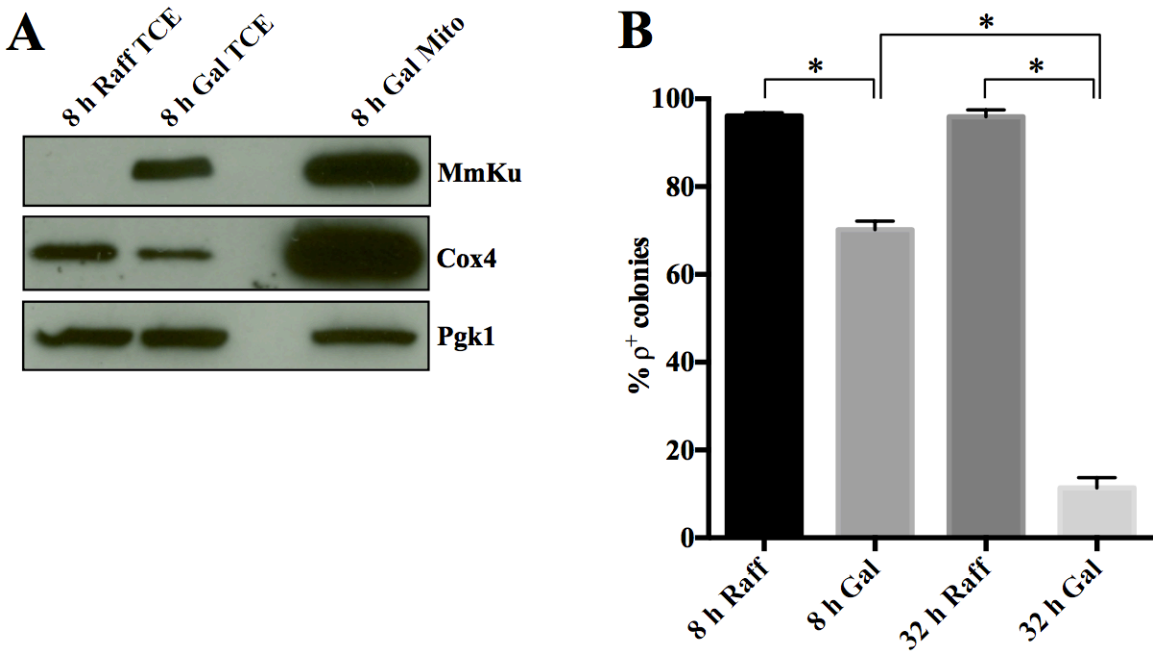

Figure 35. Expression and activity of mitochondrial-targeted MmKu from KT1112 pRS305MmKu. (**A**) Mitochondrial extracts (Mito) were obtained from KT1112 pRS305MmKu grown in Gal for 8 h, and total cell extracts (TCE) were obtained from the same strain grown in Raff or Gal for 8 h. The extracts were subjected to immunoblot analysis, following which the blot was probed with anti-Flag, anti-Cox4 or anti-Pgk1 antibody. An image representative of two independent experiments is shown. (**B**) The same yeast strain was grown in media containing Raff or Gal for 8 h and cells were plated on –Leu D. The cultures were then diluted at 8 h and grown for another 24 h following which the cells were plated on –Leu D. Colonies on –Leu D were replica-plated to YPEG and the percentage of ρ^+ colonies was determined. The average percentage of ρ^+ colonies from three independent experiments is represented graphically. Error bars represent SD and * denotes $P < 0.05$.

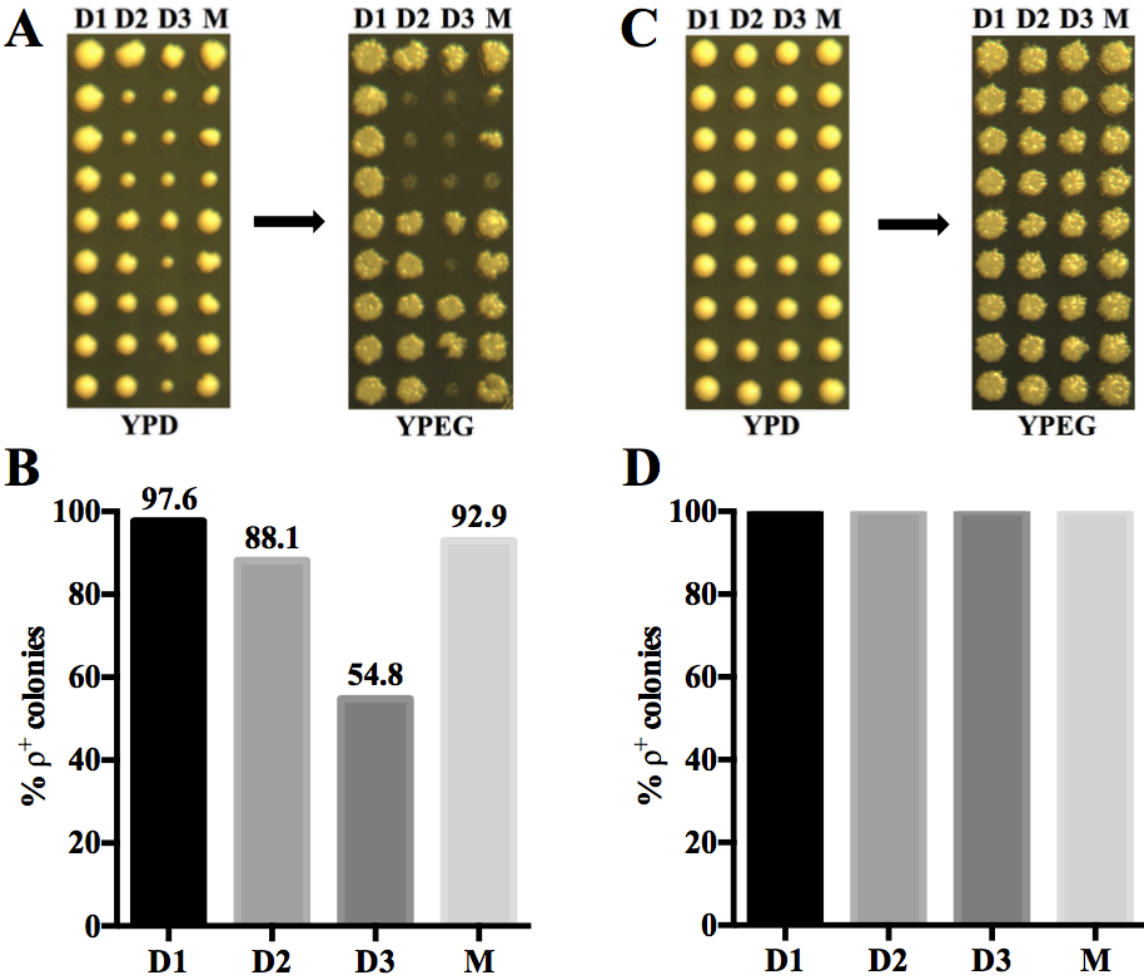

Figure 36. Pedigree analyses indicate that MmKu expression inhibits mtDNA segregation into daughter cells. (**A**) Unbudded early log phase yeast cells were streaked on YPGal segment of a plate. After cell division, a daughter cell from each mother cell was transferred from YPGal to YPD segment of the plate. This process was continued for 3 daughter generations, following which the mother cell was transferred to YPD. The colonies were replica-plated to YPEG to determine the percentage of ρ^+ colonies. D1, D2, and D3 represent first, second and third daughter generations, respectively, from the mother M. (**B**) The data from 5 independent experiments for KT1112 pRS305MmKu pedigree were pooled to determine the percentage of ρ^+ colonies for each daughter generation and the mother generation. (**C**) The procedure described for KT1112 pRS305MmKu pedigree (Figure 36A) was repeated for KT1112. (**D**) The data from 4 independent experiments for KT1112 pedigree were pooled to determine the percentage of ρ^+ colonies for each daughter generation and the mother generation.

Mitochondrial-targeted bKu proteins do not decrease mtDNA content in human cells

To understand if bKu affects mtDNA metabolism in human cells, MCF7 Tet-On cell lines were generated that expressed mitochondrial-targeted MmKu or MtKu under doxycycline (Dox) control. These cell lines, together with the vector control cell line, MCF7 TreTight, were grown in the presence or absence of Dox for 48 h, following which total cell extracts were isolated. Western analysis revealed Dox-dependent expression of bKu proteins (Figure 37A). To confirm the subcellular localization of bKu in human cells, mitochondrial and cytosolic extracts were obtained from MCF7 cMtKu and MCF7 cMmKu cells. Because the expression level of MtKu was small compared to MmKu, 35 μg of MCF7 cMtKu extracts and 3.5 μg of MCF7 cMmKu extracts were used for immunoblot analysis. Both MtKu and MmKu localized to cytosolic as well as mitochondrial fractions in human cells (Figure 37B).

To understand if mitochondrial-targeted bKu depletes human mtDNA content, the relative mtDNA copy number was determined in the MCF7 Tet-On cell lines. As illustrated in Figure 38A, cells were harvested after 4 days of growth in culture medium. From half of the harvested cells, total DNA (pretreatment) was isolated, whereas the other half was used to passage cells in the presence or absence of Dox for 2 weeks. After the 2-week period, cells were harvested to obtain total DNA and total cell extracts. Western analysis demonstrated expression of bKu after growth for 2 weeks only in cells treated with Dox (Figure 38B). However, the relative mtDNA copy number in cells expressing bKu did not change compared to Dox-untreated controls (Figure 38C). Human ρ^0 cells require uridine and pyruvate for normal growth [53]. To exclude the possibility

that we were losing respiratory deficient and/or ρ^0 MCF7 cells following bKu expression, we repeated the experiment by growing MCF7 TreTight and MCF7 cMmKu in medium containing uridine and pyruvate. Analogous to Figure 38C, the relative mtDNA copy number in cells treated with Dox did not vary compared to Dox-untreated control (Figure 39). Hence, mitochondrial-targeted bKu does not decrease mtDNA copy number in human MCF7 cells.

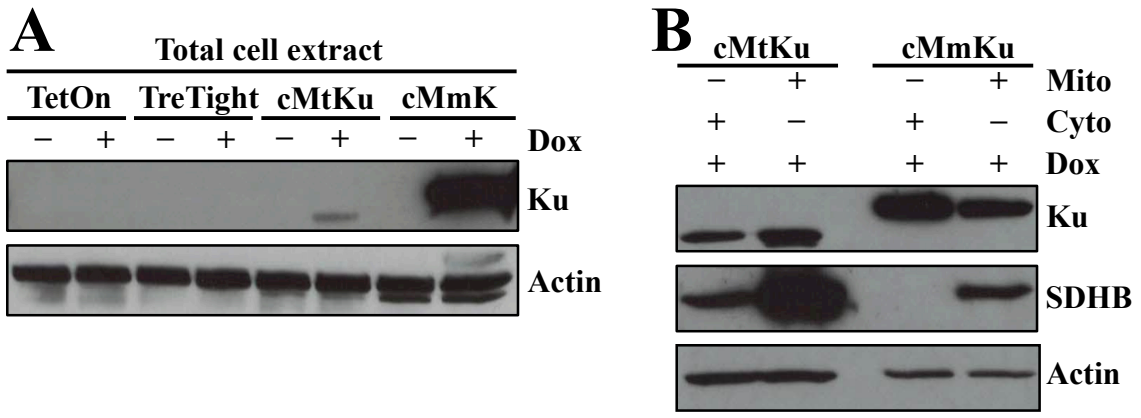

Figure 37. Expression of mitochondrial-targeted bKu proteins in human MCF7 cell lines. (**A**) MCF7 cell lines were incubated in the presence or absence of Dox for 48 h, following which total cell extracts were isolated. The extracts were probed with anti-Flag or anti-Actin antibody. An image representative of two independent experiments is shown. TetOn: MCF7 Tet-On; TreTight: MCF7 TreTight; cMtKu: MCF7 cMtKu; cMmKu: MCF7 cMmKu. (**B**) Mitochondrial extracts (Mito) and cytosolic extracts (Cyto) and were obtained from cMtKu and cMmKu cell lines following treatment with Dox for 48 h. 35 μg of each extract from cMtKu and 3.5 μg of each extract from cMmKu were used for western analysis and the membranes were probed with anti-Flag, anti-SDHB or anti-Actin antibody. An image representative of two independent experiments is shown. SDHB, succinate dehydrogenase complex iron sulfur subunit B, is a mitochondrial marker. A part of the cytosolic bKu signal may be accounted for by mitochondrial contamination of the cytosolic fraction, as evident from the presence of SDHB in the MtKu cytosolic extract. The presence of actin in the mitochondrial fractions was expected, as actin has been identified in human mitochondrial nucleoids [54, 55].

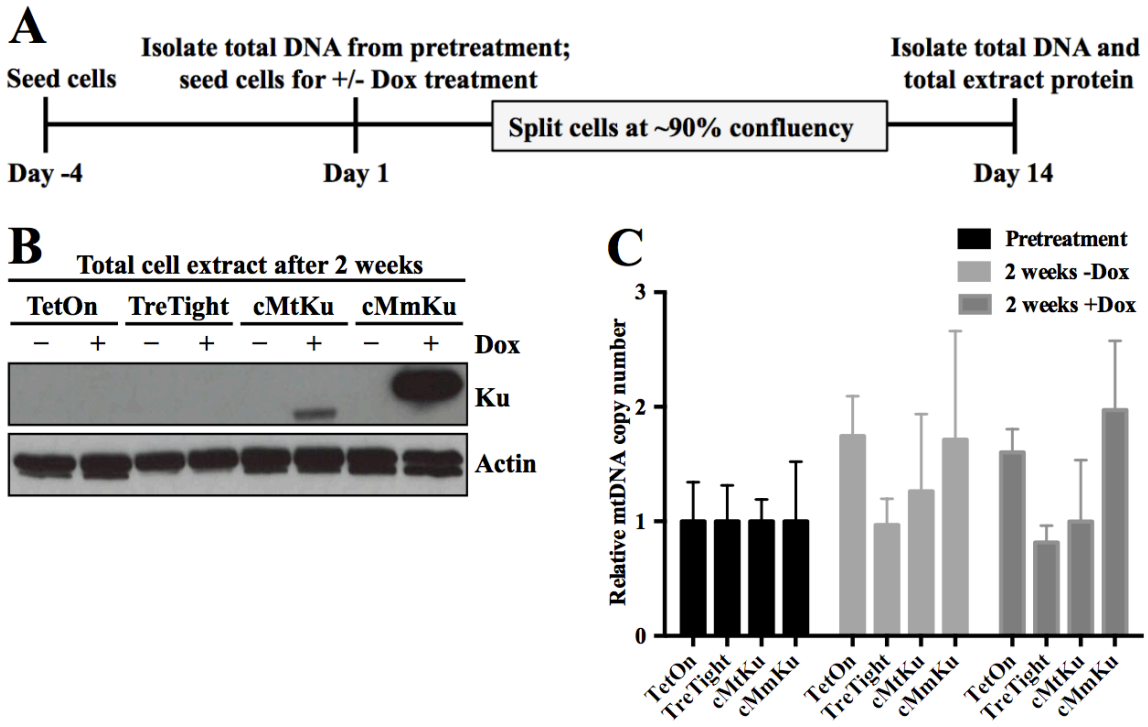

Figure 38. Mitochondrial-targeted bKu proteins do not induce mtDNA depletion in human MCF7 cells. (**A**) MCF7 cell lines were grown for 4 days prior to treatment with Dox (pretreatment) and then harvested. Total DNA was isolated from a portion of the cells, and the remaining cells were propagated in the presence or absence of Dox for 2 weeks. During the 2-week period, each cell line was passaged after reaching ~90% confluency. At the end of 2 weeks, cells were harvested to obtain total DNA and total cell extract (TCE). (**B**) Western analysis of TCEs was performed and the membranes were probed with anti-Flag or anti-actin antibody. An immunoblot representative of two independent experiments is shown. TetOn: MCF7 Tet-On; TreTight: MCF7 TreTight; cMtKu: MCF7 cMtKu; cMmKu: MCF7 cMmKu. (**C**) From total cell DNA, the relative mtDNA copy number was determined for each cell line in each group. The relative mtDNA copy number of each cell line in the treatment groups (+ and −Dox) was normalized to the respective cell line in the pretreatment group. Data are represented graphically as mean ± SD from three independent experiments.

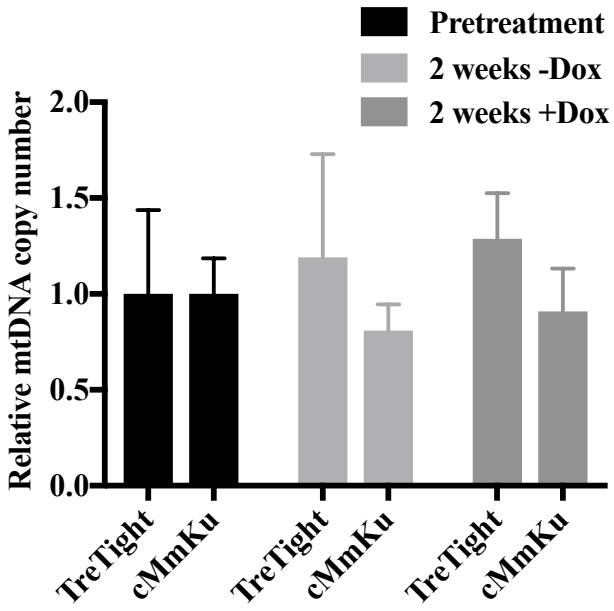

Figure 39. Determination of relative mtDNA copy number of human MCF7 cells grown in ρ^0 medium. MCF7 TreTight and MCF7 cMmKu cells lines were grown in ρ^0 medium (medium containing pyruvate and supplemented with uridine) according to the timeline shown in Figure 38A. Total DNA was then isolated to determine the relative mtDNA copy number. The relative mtDNA copy number of each cell line in the treatment group (– or +Dox) was normalized to the respective cell line in the pretreatment group. Data are represented graphically as mean ± SD from three independent experiments.

DISCUSSION

In this study, we have utilized the DSB binding property of bacterial Ku to probe for DSB-mediated mtDNA replication in yeast and human cells. The work presented here provides evidence for DSB-mediated mtDNA replication in ρ^+ yeast cells but not in human MCF7 cells.

Ori5 has been frequently studied as a model replication origin in yeast mtDNA [11, 13, 18, 19] and evidence indicates that *ori5* initiates mtDNA replication in a DSB-induced manner in HS ρ^- cells [18, 19]. Previously, it was not clear whether such DSB-mediated mtDNA replication also operates in ρ^+ cells. Here, we show that MmKu binds preferentially to *ori5* compared to a control region (*COX1*) in ρ^+ mtDNA, indicating that DSBs are present at *ori5*. This finding is in agreement with studies that showed the presence of DSBs at *ori5* in HS ρ^- mtDNA [18, 19]. The low level of MmKu binding to the *COX1* region could be due to MmKu binding to undamaged mtDNA. A recent study found that *M. smegmatis* Ku can bind to DNA without free ends and this property was attributed to its lysine-rich C-terminal extension [56]. MmKu has a similar C-terminal extension [32, 57].

Ntg1 has been shown to play an important role in generating DSBs at *ori5* [18, 19] as seen from the observation that *ntg1* null HS ρ^- mutants have about half the level of DSBs at *ori5* compared to the isogenic *NTG1* HS ρ^- cells [19]. Although we see a small decrease in binding of MmKu to *ori5* in KT1112/Δ*ntg1*, no statistical difference was found compared to KT1112 for the mtDNA IP assay and for the end-point PCR assay used to determine whether less DSBs were induced in normal growing ρ^+ *ntg1* null cultures. This suggests there is also an Ntg1-independent mechanism for DSB generation

at *ori5*. The DSBs at *ori5* could be generated via the action of an unidentified mitochondrial enzyme, as previously suggested [19]. Alternatively, ROS could abstract a hydrogen atom from any of the carbons of the deoxyribose in the DNA backbone, subsequently leading to the formation of a single-strand break [58-61]. This could occur on both strands of the damage-prone bubble-like *ori5* DNA structure resulting in the formation of a DSB.

The observation that MmKu expression triggers mtDNA depletion supports our proposal that binding of MmKu to DSBs at *ori5* inhibits mtDNA RDR. Mhr1 is regarded as a central molecule in mtDNA RDR and evidence indicates that Mhr1 facilitates heteroduplex joint formation between a linearized mtDNA molecule and its complementary region in a template circular mtDNA for the initiation of RDR [16, 17, 19] (Figure 40A). A study with *mhr1* temperature-sensitive mutants showed that growth of *mhr1* mutants at the non-permissive temperature induces mtDNA loss as well as petite formation [62]. In addition, the degree of mtDNA loss and the extent of petite formation in *mhr1* mutants increased progressively with time at the non-permissive temperature [62]. Analogous to that study, we observe that MmKu expression induces mtDNA loss and petite formation in yeast cells. In addition, the degree of mtDNA depletion and the frequency of petite formation increased progressively with the duration of MmKu expression. The extent of mtDNA depletion was such that ρ^0 yeast colonies were obtained from MmKu-expressing cells grown in Gal for 8 h; after 32 h in Gal, the percentage of ρ^0 formation further increased. MmKu-triggered mtDNA depletion also accompanied reduction in the level of Cox4, a nuclear-encoded mitochondrial protein that forms a subunit of complex IV of the mitochondrial respiratory chain [63]. The reduced level of

Cox4 could be due to diminished *COX4* gene transcription, a phenomenon that has been documented previously in ρ^0 yeast cells [64].

The products of mtDNA RDR are concatemers, which occur predominantly in mother cells, and these multi-genome units are segregated into growing buds where they are processed into genome size monomers [16, 17]. With this knowledge, we hypothesized that MmKu-induced mtDNA depletion and petite formation occur preferentially in daughter cells. As predicted, we observed that MmKu triggers petite formation preferentially in daughter generations indicating loss of mtDNA in daughter cells. The extent of petite formation was such that ~45% of colonies from the third daughter (D3) generation formed petites. This is indicative of improper mtDNA segregation to almost half of the D3 generation. Even though mother cells spent more time than any daughter cell of the same pedigree in the Gal medium that induced MmKu expression, only ~7% of colonies from the mother generation (M) formed petites. This observation supports our proposal that MmKu inhibits mtDNA replication, thereby preventing transmission of mtDNA from mother cells into the daughter cells. To account for the effect of MmKu on yeast mtDNA content, we propose a model (Figure 40B) in which the DSB binding domain of MmKu binds to DSBs at *ori5* in the yeast mitochondrial genome. Since it lacks domains to communicate with eukaryotic proteins, MmKu persistently occupies *ori5*. This results in inhibition of mtDNA RDR, thereby preventing the formation of concatemers. As a consequence, there is reduced/no mtDNA segregation into the daughter cells, which eventually form ρ^0.

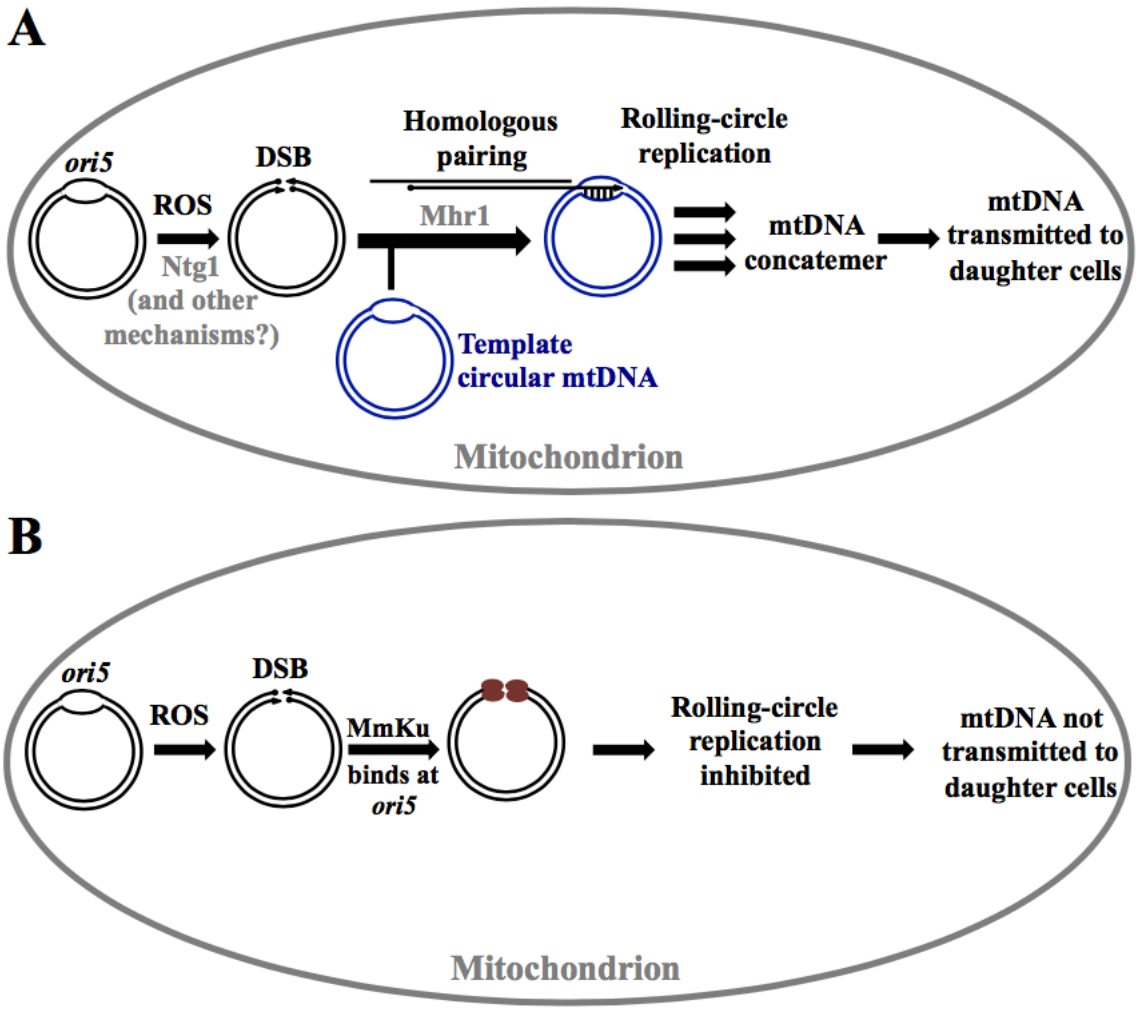

Figure 40. A model explaining the effect of MmKu on *S. cerevisiae* mtDNA. (**A**) Under normal physiological conditions, ROS oxidizes yeast mtDNA at *ori5*. Ntg1 recognizes these modifications and introduces a DSB. Other unidentified mechanisms can also account for DSB at *ori5*. A 3' single-stranded tail is generated, to which Mhr1 binds. This nucleoprotein filament invades a template circular mtDNA to mediate the initiation of mtDNA RDR. This results in formation of mtDNA concatemers, which are selectively transmitted to daughter cells. Figure 40A is adapted from [19]. (**B**) Yeast cells expressing mitochondrial-targeted MmKu have the Ku protein bound to the DSB at *ori5*. This inhibits mtDNA RDR, so new mtDNA molecules are not synthesized. As a consequence, mtDNA molecules are not segregated to daughter cells.

Evidence for transcription-dependent mtDNA replication also exists for yeast cells [11-13]; however, those studies were performed either in hypersuppressive ρ^- mtDNA [11, 13] or with cloned replication origins examined *in vitro* [12]. It is currently not known if such transcription-dependent mechanisms actually operate in ρ^+ cells. Instead, transcription-independent mtDNA replication seems more probable because of the observation that yeast cells with disrupted *RPO41* gene can still maintain mtDNA [14, 15]. In addition, yeast cells that completely lack *ori* sequences also propagate their mitochondrial genomes [65]. The DSB-mediated mtDNA RDR has gained increased attention over the last few years and this mechanism can explain many conundrums, including: (i) a mechanism for maintenance of mtDNA in Rpo41 deficient cells and cells lacking any replication origin; (ii) a mechanism for maintenance of the state of homoplasmy; (iii) a mechanism by which mtDNA concatemers and circular monomers co-exist in yeast cells.

The exact mode of human mtDNA replication is still vigorously debated and multiple replication models have been proposed. These replication modes appear to occur by a transcription-dependent mechanism and do not seem to involve DSBs [7, 33]. In agreement with this, we find that expression of mitochondrial-targeted bKu proteins (MmKu and MtKu) do not decrease mtDNA content in human MCF7 cells. This observation supports the idea that MmKu impairs mtDNA homeostasis only when DSBs are involved in the perpetuation of the mitochondrial genome. Even though DSBs and other DNA damages are generally considered deleterious for cellular health, studies have indicated that controlled damage of mtDNA is important for its maintenance, both in yeast [18, 19] as well as in mammalian cells [66]. Recently, oxidative damage to the

mtDNA regulatory region (D-loop) under hypoxic conditions has been correlated with an increase in mtDNA copy number in mammalian cells [66]. Another study has revealed that exposure of MELAS patient-derived primary fibroblasts to exogenous ROS triggers the formation of mtDNA concatemers via rolling circle replication, likely initiated from ROS-induced DSBs [67]. Although beyond the scope of this study, it would be interesting to determine if the expression of mitochondrial-targeted MmKu in ROS-treated MELAS patient-derived fibroblasts inhibits mtDNA replication and concatemer formation. Given the complex diversity of cells in mammals, it is possible that multiple mtDNA replication mechanisms coexist in higher organisms and that certain cell types utilize particular replication mechanisms. With respect to a single-celled *S. cerevisiae*, however, DSB-mediated mtDNA replication appears to be the prime mode. In this regard, we consider *ori5* as a hot spot for DSB-mediated recombination. The concept of DSB-mediated replication is not new and was originally proposed for yeast mtDNA in 1991 by Maleszka *et al* [4] and for *E. coli* DNA replication in 1994 by Asai *et al* [68]. It is currently not known if other replication origins in yeast mtDNA initiate replication in a DSB-mediated manner and our system could be used to address this in future studies. At present, our study provides crucial evidence that ρ^+ yeast cells rely on DSB-induced mtDNA replication for propagation of mtDNA, as perturbation of this pathway can result in the complete loss of their mitochondrial genome.

ACKNOWLEDGEMENTS

We thank Dr. David S. Gross (LSUHSC-Shreveport) and Dr. Anandhakumar Jayamani (LSUHSC-Shreveport) for technical assistance with mtDNA IP. We thank Reneau Castore (LSUHSC-Shreveport) for her help with MCF7 cell lines. We acknowledge Feist-Weiller Cancer Center (LSUHSC-Shreveport) for providing a Carroll Feist Predoctoral Fellowship to KP. This study was supported by the National Institutes of Health R21 grant (grant 1R21 CA167796) to LH.

REFERENCES

1. Taanman, J.W. (1999). The mitochondrial genome: structure, transcription, translation and replication. Biochimica et biophysica acta *1410*, 103-123.
2. Kucej, M., and Butow, R.A. (2007). Evolutionary tinkering with mitochondrial nucleoids. Trends in cell biology *17*, 586-592.
3. Anderson, S., Bankier, A.T., Barrell, B.G., de Bruijn, M.H., Coulson, A.R., Drouin, J., Eperon, I.C., Nierlich, D.P., Roe, B.A., Sanger, F., et al. (1981). Sequence and organization of the human mitochondrial genome. Nature *290*, 457-465.
4. Maleszka, R., Skelly, P.J., and Clark-Walker, G.D. (1991). Rolling circle replication of DNA in yeast mitochondria. The EMBO journal *10*, 3923-3929.
5. Bendich, A.J. (1996). Structural analysis of mitochondrial DNA molecules from fungi and plants using moving pictures and pulsed-field gel electrophoresis. Journal of molecular biology *255*, 564-588.
6. Foury, F., Roganti, T., Lecrenier, N., and Purnelle, B. (1998). The complete sequence of the mitochondrial genome of Saccharomyces cerevisiae. FEBS letters *440*, 325-331.
7. Holt, I.J., and Reyes, A. (2012). Human mitochondrial DNA replication. Cold Spring Harbor perspectives in biology *4*.
8. Baldacci, G., and Bernardi, G. (1982). Replication origins are associated with transcription initiation sequences in the mitochondrial genome of yeast. The EMBO journal *1*, 987-994.

9. Lecrenier, N., and Foury, F. (2000). New features of mitochondrial DNA replication system in yeast and man. Gene *246*, 37-48.

10. Kaniak-Golik, A., and Skoneczna, A. (2015). Mitochondria-nucleus network for genome stability. Free radical biology & medicine *82*, 73-104.

11. Baldacci, G., Cherif-Zahar, B., and Bernardi, G. (1984). The initiation of DNA replication in the mitochondrial genome of yeast. The EMBO journal *3*, 2115-2120.

12. Xu, B., and Clayton, D.A. (1995). A persistent RNA-DNA hybrid is formed during transcription at a phylogenetically conserved mitochondrial DNA sequence. Molecular and cellular biology *15*, 580-589.

13. Graves, T., Dante, M., Eisenhour, L., and Christianson, T.W. (1998). Precise mapping and characterization of the RNA primers of DNA replication for a yeast hypersuppressive petite by in vitro capping with guanylyltransferase. Nucleic acids research *26*, 1309-1316.

14. Fangman, W.L., Henly, J.W., and Brewer, B.J. (1990). RPO41-independent maintenance of [rho-] mitochondrial DNA in Saccharomyces cerevisiae. Molecular and cellular biology *10*, 10-15.

15. Lorimer, H.E., Brewer, B.J., and Fangman, W.L. (1995). A test of the transcription model for biased inheritance of yeast mitochondrial DNA. Molecular and cellular biology *15*, 4803-4809.

16. Ling, F., and Shibata, T. (2002). Recombination-dependent mtDNA partitioning: in vivo role of Mhr1p to promote pairing of homologous DNA. The EMBO journal *21*, 4730-4740.

17. Ling, F., and Shibata, T. (2004). Mhr1p-dependent concatemeric mitochondrial DNA formation for generating yeast mitochondrial homoplasmic cells. Molecular biology of the cell *15*, 310-322.

18. Ling, F., Hori, A., and Shibata, T. (2007). DNA recombination-initiation plays a role in the extremely biased inheritance of yeast [rho-] mitochondrial DNA that contains the replication origin ori5. Molecular and cellular biology *27*, 1133-1145.

19. Hori, A., Yoshida, M., Shibata, T., and Ling, F. (2009). Reactive oxygen species regulate DNA copy number in isolated yeast mitochondria by triggering recombination-mediated replication. Nucleic acids research *37*, 749-761.

20. Ling, F., Hori, A., Yoshitani, A., Niu, R., Yoshida, M., and Shibata, T. (2013). Din7 and Mhr1 expression levels regulate double-strand-break-induced replication and recombination of mtDNA at ori5 in yeast. Nucleic acids research *41*, 5799-5816.

21. Shibata, T., and Ling, F. (2007). DNA recombination protein-dependent mechanism of homoplasmy and its proposed functions. Mitochondrion *7*, 17-23.

22. Dujon, B. (1981). Mitochondrial Genetics and Functions. In The Molecular Biology of the Yeast Saccharomyces: Life Cycle and Inheritance, E.W.J. Jeffrey N. Strathern, James R. Broach ed. (New York: Cold Spring Harbor Laboratory Press), pp. 505-635.

23. Williamson, D. (2002). The curious history of yeast mitochondrial DNA. Nature reviews. Genetics *3*, 475-481.

24. Downs, J.A., and Jackson, S.P. (2004). A means to a DNA end: the many roles of Ku. Nature reviews. Molecular cell biology *5*, 367-378.

25. Lieber, M.R. (2010). The mechanism of double-strand DNA break repair by the nonhomologous DNA end-joining pathway. Annual review of biochemistry *79*, 181-211.

26. Shuman, S., and Glickman, M.S. (2007). Bacterial DNA repair by non-homologous end joining. Nature reviews. Microbiology *5*, 852-861.

27. Doherty, A.J., Jackson, S.P., and Weller, G.R. (2001). Identification of bacterial homologues of the Ku DNA repair proteins. FEBS letters *500*, 186-188.

28. Weller, G.R., Kysela, B., Roy, R., Tonkin, L.M., Scanlan, E., Della, M., Devine, S.K., Day, J.P., Wilkinson, A., d'Adda di Fagagna, F., et al. (2002). Identification of a DNA nonhomologous end-joining complex in bacteria. Science *297*, 1686-1689.

29. Aravind, L., and Koonin, E.V. (2001). Prokaryotic homologs of the eukaryotic DNA-end-binding protein Ku, novel domains in the Ku protein and prediction of a prokaryotic double-strand break repair system. Genome research *11*, 1365-1374.

30. Castore, R., Hughes, C., Debeaux, A., Sun, J., Zeng, C., Wang, S.Y., Tatchell, K., Shi, R., Lee, K.J., Chen, D.J., et al. (2011). Mycobacterium tuberculosis Ku can bind to nuclear DNA damage and sensitize mammalian cells to bleomycin sulfate. Mutagenesis *26*, 795-803.

31. Shao, Z., Davis, A.J., Fattah, K.R., So, S., Sun, J., Lee, K.J., Harrison, L., Yang, J., and Chen, D.J. (2012). Persistently bound Ku at DNA ends attenuates DNA end resection and homologous recombination. DNA repair *11*, 310-316.

32. Wright, D.G., Castore, R., Shi, R., Mallick, A., Ennis, D.G., and Harrison, L. (2016). Mycobacterium tuberculosis and Mycobacterium marinum non-homologous end-joining proteins can function together to join DNA ends in Escherichia coli. Mutagenesis.

33. Vega, R.B., Horton, J.L., and Kelly, D.P. (2015). Maintaining ancient organelles: mitochondrial biogenesis and maturation. Circulation research *116*, 1820-1834.

34. Taylor, S.D., Zhang, H., Eaton, J.S., Rodeheffer, M.S., Lebedeva, M.A., O'Rourke T, W., Siede, W., and Shadel, G.S. (2005). The conserved Mec1/Rad53 nuclear checkpoint pathway regulates mitochondrial DNA copy number in Saccharomyces cerevisiae. Molecular biology of the cell *16*, 3010-3018.

35. Guo, X.E., Chen, C.F., Wang, D.D., Modrek, A.S., Phan, V.H., Lee, W.H., and Chen, P.L. (2011). Uncoupling the roles of the SUV3 helicase in maintenance of mitochondrial genome stability and RNA degradation. The Journal of biological chemistry *286*, 38783-38794.

36. Sage, J.M., Gildemeister, O.S., and Knight, K.L. (2010). Discovery of a novel function for human Rad51: maintenance of the mitochondrial genome. The Journal of biological chemistry *285*, 18984-18990.

37. Babu, P., Bryan, J.D., Panek, H.R., Jordan, S.L., Forbrich, B.M., Kelley, S.C., Colvin, R.T., and Robinson, L.C. (2002). Plasma membrane localization of the Yck2p yeast casein kinase 1 isoform requires the C-terminal extension and secretory pathway function. Journal of cell science *115*, 4957-4968.

38. Rapaport, D., Brunner, M., Neupert, W., and Westermann, B. (1998). Fzo1p is a mitochondrial outer membrane protein essential for the biogenesis of functional

mitochondria in Saccharomyces cerevisiae. The Journal of biological chemistry *273*, 20150-20155.

39. Frederick, R.L., McCaffery, J.M., Cunningham, K.W., Okamoto, K., and Shaw, J.M. (2004). Yeast Miro GTPase, Gem1p, regulates mitochondrial morphology via a novel pathway. The Journal of cell biology *167*, 87-98.

40. Sikorski, R.S., and Hieter, P. (1989). A system of shuttle vectors and yeast host strains designed for efficient manipulation of DNA in Saccharomyces cerevisiae. Genetics *122*, 19-27.

41. Stuart, J.S., Frederick, D.L., Varner, C.M., and Tatchell, K. (1994). The mutant type 1 protein phosphatase encoded by glc7-1 from Saccharomyces cerevisiae fails to interact productively with the GAC1-encoded regulatory subunit. Molecular and cellular biology *14*, 896-905.

42. Winzeler, E.A., Shoemaker, D.D., Astromoff, A., Liang, H., Anderson, K., Andre, B., Bangham, R., Benito, R., Boeke, J.D., Bussey, H., et al. (1999). Functional characterization of the S. cerevisiae genome by gene deletion and parallel analysis. Science *285*, 901-906.

43. Goldring, E.S., Grossman, L.I., Krupnick, D., Cryer, D.R., and Marmur, J. (1970). The petite mutation in yeast. Loss of mitochondrial deoxyribonucleic acid during induction of petites with ethidium bromide. Journal of molecular biology *52*, 323-335.

44. Gietz, D., St Jean, A., Woods, R.A., and Schiestl, R.H. (1992). Improved method for high efficiency transformation of intact yeast cells. Nucleic acids research *20*, 1425.

45. Davis, N.G., Horecka, J.L., and Sprague, G.F., Jr. (1993). Cis- and trans-acting functions required for endocytosis of the yeast pheromone receptors. The Journal of cell biology *122*, 53-65.

46. Malyarchuk, S., Castore, R., and Harrison, L. (2008). DNA repair of clustered lesions in mammalian cells: involvement of non-homologous end-joining. Nucleic acids research *36*, 4872-4882.

47. Hoffman, C.S., and Winston, F. (1987). A ten-minute DNA preparation from yeast efficiently releases autonomous plasmids for transformation of Escherichia coli. Gene *57*, 267-272.

48. Anandhakumar, J., Moustafa, Y.W., Chowdhary, S., Kainth, A.S., and Gross, D.S. (2016). Evidence for Multiple Mediator Complexes in Yeast Independently Recruited by Activated Heat Shock Factor. Molecular and cellular biology *36*, 1943-1960.

49. Wells, W.A., and Murray, A.W. (1996). Aberrantly segregating centromeres activate the spindle assembly checkpoint in budding yeast. The Journal of cell biology *133*, 75-84.

50. Hartl, F.U., Pfanner, N., Nicholson, D.W., and Neupert, W. (1989). Mitochondrial protein import. Biochimica et biophysica acta *988*, 1-45.

51. Westermann, B., and Neupert, W. (2000). Mitochondria-targeted green fluorescent proteins: convenient tools for the study of organelle biogenesis in Saccharomyces cerevisiae. Yeast (Chichester, England) *16*, 1421-1427.

52. Williamson, D.H., and Fennell, D.J. (1979). Visualization of yeast mitochondrial DNA with the fluorescent stain "DAPI". Methods in enzymology *56*, 728-733.

53. King, M.P., and Attardi, G. (1996). Isolation of human cell lines lacking mitochondrial DNA. Methods in enzymology *264*, 304-313.

54. Kanki, T., Nakayama, H., Sasaki, N., Takio, K., Alam, T.I., Hamasaki, N., and Kang, D. (2004). Mitochondrial nucleoid and transcription factor A. Annals of the New York Academy of Sciences *1011*, 61-68.

55. Wang, Y., and Bogenhagen, D.F. (2006). Human mitochondrial DNA nucleoids are linked to protein folding machinery and metabolic enzymes at the mitochondrial inner membrane. The Journal of biological chemistry *281*, 25791-25802.

56. Kushwaha, A.K., and Grove, A. (2013). Mycobacterium smegmatis Ku binds DNA without free ends. The Biochemical journal *456*, 275-282.

57. Kushwaha, A.K., and Grove, A. (2013). C-terminal low-complexity sequence repeats of Mycobacterium smegmatis Ku modulate DNA binding. Bioscience reports *33*, 175-184.

58. Giloni, L., Takeshita, M., Johnson, F., Iden, C., and Grollman, A.P. (1981). Bleomycin-induced strand-scission of DNA. Mechanism of deoxyribose cleavage. The Journal of biological chemistry *256*, 8608-8615.

59. Frank, B.L., Worth, L., Christner, D.F., Kozarich, J.W., Stubbe, J., Kappen, L.S., and Goldberg, I.H. (1991). Isotope effects on the sequence-specific cleavage of DNA by neocarzinostatin: kinetic partitioning between 4'- and 5'-hydrogen abstraction at unique thymidine sites. Journal of the American Chemical Society *113*, 2271-2275.

60. Sitlani, A., Long, E.C., Pyle, A.M., and Barton, J.K. (1992). DNA photocleavage by phenanthrenequinone diimine complexes of rhodium(III): shape-selective recognition and reaction. Journal of the American Chemical Society *114*, 2303-2312.

61. Sugiyama, H., Tsutsumi, Y., Fujimoto, K., and Saito, I. (1993). Photoinduced deoxyribose C2' oxidation in DNA. Alkali-dependent cleavage of erythrose-containing sites via a retroaldol reaction. Journal of the American Chemical Society *115*, 4443-4448.

62. Ling, F., Makishima F Fau - Morishima, N., Morishima N Fau - Shibata, T., and Shibata, T. (1995). A nuclear mutation defective in mitochondrial recombination in yeast. The EMBO journal *14*, 4090-4101.

63. Power, S.D., Lochrie, M.A., Sevarino, K.A., Patterson, T.E., and Poyton, R.O. (1984). The nuclear-coded subunits of yeast cytochrome c oxidase. I. Fractionation of the holoenzyme into chemically pure polypeptides and the identification of two new subunits using solvent extraction and reversed phase high performance liquid chromatography. The Journal of biological chemistry *259*, 6564-6570.

64. Dagsgaard, C., Taylor, L.E., O'Brien, K.M., and Poyton, R.O. (2001). Effects of anoxia and the mitochondrion on expression of aerobic nuclear COX genes in yeast: evidence for a signaling pathway from the mitochondrial genome to the nucleus. The Journal of biological chemistry *276*, 7593-7601.

65. Fangman, W.L., Henly, J.W., Churchill, G., and Brewer, B.J. (1989). Stable maintenance of a 35-base-pair yeast mitochondrial genome. Molecular and cellular biology *9*, 1917-1921.

66. Pastukh, V.M., Gorodnya, O.M., Gillespie, M.N., and Ruchko, M.V. (2016). Regulation of mitochondrial genome replication by hypoxia: The role of DNA oxidation in D-loop region. Free radical biology & medicine *96*, 78-88.

67. Ling, F., Niu, R., Hatakeyama, H., Goto, Y., Shibata, T., and Yoshida, M. (2016). Reactive oxygen species stimulate mitochondrial allele segregation toward homoplasmy in human cells. Molecular biology of the cell *27*, 1684-1693.

68. Asai, T., Bates, D.B., and Kogoma, T. (1994). DNA replication triggered by double-stranded breaks in E. coli: dependence on homologous recombination functions. Cell *78*, 1051-1061.

CHAPTER III

IN VIVO EVIDENCE FOR MHR1, BUT NOT YKU80, AS A GENERAL MITOCHONDRIAL DNA DOUBLE-STRAND BREAK REPAIR FACTOR IN *SACCHAROMYCES CEREVISIAE*

ABSTRACT

Mitochondrial DNA (mtDNA) double-strand break (DSB) repair is essential for maintaining mtDNA integrity, but little is known about the proteins involved in mtDNA DSB repair. Here, we utilize *Saccharomyces cerevisiae* as a eukaryotic model to identify proteins involved in mtDNA DSB repair. We show that Mhr1, a protein known to possess homologous DNA pairing activity *in vitro*, binds to mtDNA DSBs *in vivo*, indicating its involvement in mtDNA DSB repair. Our data also indicate that Yku80, a protein previously implicated in mtDNA DSB repair, does not compete with Mhr1 for binding to mtDNA DSBs. In fact, C-terminally tagged Yku80 could not be detected in yeast mitochondrial extracts. Therefore, we conclude that Mhr1, but not Yku80, is a general mtDNA DSB repair factor in yeast.

INTRODUCTION

Mitochondria are essential eukaryotic organelles that harbor multiple copies of their own genetic material and mitochondrial DNA (mtDNA) is organized in nucleoprotein complexes called nucleoids [1]. Typically, mtDNA encodes a small number of protein subunits of the oxidative phosphorylation (OXPHOS) system as well as the tRNAs and rRNAs that are required for mitochondrial protein synthesis [2]. The mtDNA-derived OXPHOS subunits assemble with those encoded by the nuclear DNA (nDNA) to form functional mitochondrial ATP synthesizing machinery dedicated to the production of the majority of a cell's ATP [3]. During the process, however, reactive oxygen species (ROS) are generated as byproducts, and these ROS have the potential to damage vital cellular constituents, including DNA, proteins, and lipids [4, 5]. Because of its close proximity to the site of ROS generation, mtDNA is highly susceptible to oxidative damage. Such ROS-induced mtDNA damage includes strand breaks, base loss, and base modifications [6]. Progressive accumulation of damaged mtDNA molecules can cause respiratory chain dysfunction that can escalate ROS production, leading to further mtDNA damage. Such a 'vicious cycle' has been associated not only with aging but also with a variety of pathological conditions including diabetes, atherosclerosis, and cancer [7]. To prevent the detrimental outcomes of mtDNA damage, mitochondria have multiple mtDNA repair pathways, primarily base excision repair, mismatch repair, and double-strand break repair (for review see [8]).

DNA double-strand breaks (DSBs) are considered the most deleterious DNA lesions. DSBs can be generated by reaction with endogenous ROS and exogenous agents like ionizing radiation, as well as from biological processes like DNA replication fork

arrest [9]. DSBs in the nuclear genome are repaired primarily by two major DSB repair pathways: homologous recombination (HR) and classical non-homologous end joining (C-NHEJ). HR involves resection of the damaged DNA molecule in the 5′-3′ direction and formation of a 3′ single-stranded tail that eventually becomes substrate for a family of recombinases (for review see [10]). The nucleoprotein filament then catalyzes strand invasion and homologous pairing with an undamaged sister chromatid to form a heteroduplex joint. Finally, the undamaged sister chromatid is utilized as a template for restoring the genetic information in the damaged DNA molecule. C-NHEJ on the other hand, repairs DSBs by direct ligation of broken DNA ends and hence does not require a homologous DNA template (for review see [11]). The Ku70/Ku80 heterodimer (Ku complex) is regarded as the hallmark C-NHEJ component that binds DNA ends. The binding of the Ku complex not only protects the DNA from resection/degradation, but also anchors the broken DNA ends in close proximity for ligation. The DNA-bound Ku complex then facilitates recruitment of downstream C-NHEJ factors that modify the DNA termini and mediate rejoining of the fragmented DNA molecule. In addition to these predominant nDNA DSB repair pathways, evidence also exists for a minor nDNA DSB repair pathway called alternative non-homologous end joining (A-NHEJ; also known as microhomology-mediated end joining or MMEJ) (for review see [12]). This Ku-independent end joining pathway involves alignment of complementary microhomologous sequences located internal to the original DSB. Such microhomologies are revealed by end resection from the DSBs; hence, the process is associated with deletions at the repair junctions. MtDNA DSB repair activities and repair products have been identified in several eukaryotic systems [13-17]. However, unlike the large number

of proteins involved in nDNA DSB repair, the factors mediating mtDNA DSB repair are not well characterized and only a handful of proteins have been designated as *bona fide* mtDNA DSB repair factors in the entire Eukaryota domain [18, 19].

The purpose of this study was to identify proteins that are involved in mtDNA DSB repair. We employed the budding yeast *Saccharomyces cerevisiae* as a eukaryotic model system because: (i) genome manipulation is simple and feasible; (ii) mtDNA is not essential for cell viability; and (iii) DNA repair systems are highly conserved from yeast to humans. In this study, we focused on two potential mtDNA DSB repair factors: yeast Ku80 (Yku80) and Mhr1 (mitochondrial homologous recombinase). Yku80 is a component of the yeast Ku (Yku) complex, which functions as a stable Yku70/Yku80 heterodimer during nuclear C-NHEJ [20]. Even though the components of the Yku complex have not been demonstrated to localize to the mitochondrial compartment, genetic evidence has indicated the involvement of the Yku complex in mtDNA DSB repair. The rate of mtDNA deletions, which are considered as products of DSB repair, was reported to be higher in *yku70/yku80* null mutants compared to wild-type cells [21]. This therefore suggests a role for Yku in mtDNA repair [21]. Another potential mtDNA DSB repair candidate is Mhr1, which has been demonstrated to localize to the mitochondrial inner membrane and matrix subcompartments [22]. *In vitro*, Mhr1 promotes heteroduplex joint formation between single-stranded DNA and homologous double-stranded DNA [22]. This recombinase activity of Mhr1 has been extensively studied with respect to its involvement in recombination dependent rolling-circle mtDNA replication at the mitochondrial replication origin *ori5* (for review see [23]). However, the role of Mhr1 in repairing general mtDNA DSBs generated in different regions of the

mitochondrial genome has not been explored. An important characteristic of a DSB repair protein is its ability to bind at or near the DSBs and it has not been shown that Mhr1 does bind to mtDNA DSBs *in vivo*. To address this, we employed a mitochondrial-targeted restriction endonuclease XhoI (mitoXhoI) to introduce DSBs into the yeast mtDNA. After verifying the presence of Mhr1 in yeast mitochondrial extracts, we determined the ability of Mhr1 to bind to mitoXhoI-induced DSBs. In addition, we examined the localization of Yku80 to yeast mitochondria and compared the degree of Mhr1 binding to mitoXhoI-induced DSBs in a wild-type strain versus isogenic *yku80* null mutant.

MATERIALS AND METHODS

Oligodeoxyribonucleotides

Oligodeoxyribonucleotides (oligonucleotides) were purchased from Eurofins (Louisville, KY, USA) or the DNA Facility at Iowa State University (Ames, IA, USA). The sequences of the oligonucleotides used in this study are listed in Table 4.

Table 4. Oligonucleotides used in this study

Name	Sequence (5′-3′)	Purpose	Reference
BamXhoI	AAAAAAGGATCCGCATTGGATCTAGCCGAATACG	Plasmid construction	This study
SalFlag	AAAAAAGTCGACTCACTTGTCGTCATCGTCC	Plasmid construction	[24]
NtermXhoI	AAAAAACTGCAGGCATTGGATCTAGCCGAA-TACGACCGC	Plasmid construction	This study
CtermXhoI	AAAAAAGCGGCCGCACGCGGATGCGACTCTGC	Plasmid construction	This study
COX2F	AAAGTTGATGCTACTCCTGGTAGA	Real-time qPCR	[25]
COX2R	CATGACCTGTCCCACACAAC	Real-time qPCR	This study
ACT1F	GTATGTGTAAAGCCGGTTTTG	Real-time qPCR	[26]
ACT1R	CATGATACCTTGGTGTCTTGG	Real-time qPCR	[26]
XhoIupF	GAGTAGAATCTGTTAAAAGATTATTTCC	Real-time qPCR	This study
XhoIupR	TTAGTTCGACGGTTGTCATATAATT	Real-time qPCR	This study
XhoIdownF	ATATGGGGTTATGGATTTCGTTC	Real-time qPCR	This study
XhoIdownR	AAATAGGTATGAACCTCGAGTA	Real-time qPCR	This study
RegionIF	TTTATAATGGTAGAGTAAAAATTGTACC	Real-time qPCR	This study
RegionIR	CACCTTTTACAAATGAACCATCAC	Real-time qPCR	This study
RegionIIF	AGACGCCTCTGGTTATCTAAG	Real-time qPCR	This study
RegionIIR	TACTGATCTCATTGGATTATACC	Real-time qPCR	This study
RegionIIIF	TATTACTTCATATGGGGTTATGG	Real-time qPCR	This study
RegionIIIR	AAATAGAGGTAGGAGGGAGGA	Real-time qPCR	This study
ProbeXhoIupF	CCATTATCATCTATTCAGGCAC	Southern analysis	This study
ProbeXhoIupR	TTTCTTGTAGTCTCTGAGGATC	Southern analysis	This study
ProbeCOX2F	ATAACTCCTTGCTTCATACC	Southern analysis	This study
ProbeCOX2R	AAGGTGTTGGTACATCATTC	Southern analysis	This study
YKU80DelF	CAAAGATTAGCAGTTGGAGGG	*YKU80* deletion	This study
YKU80DelR	CTTCACCGAGCCTAAGTTGG	*YKU80* deletion	This study
DeltaYKU80R	GCTTAATTCTTCCGTTAGCAGG	Deletion verification	This study
MHR1Myc9F	CGAATCACATCCTACAGAGCAGACGGAAG TGTCTTCCCAGTCCGGTTCTGCTGCTAG	*MHR1-MYCX9* tagging	This study
MHR1Myc9R	GTTTTTTTTTCTACCTGCATTTGTATATCTAA TGACGAAGCGTTCCTCGAGGCCAGAAGAC	*MHR1-MYCX9* tagging	This study
MHR1F	GGTGACAAGGACAAACATTGG	*MHR1-MYCX9* verification	This study
MHR1R	AAGGTGAGGAGGATAAAACG	*MHR1-MYCX9* verification	This study
Yku80Myc9F	TGAAGCGCGGTGAACAACACAGTAGGGGAAGTC-CAAACAATAGCAATAATTCCGGTTCTGCTGCTAG	*YKU80-MYCX9* tagging	This study
Yku80Myc9R	CTCTTTAACTGTGGTGACGAAAACATAACTCAAA-GGATGTTAGACCTTTTCCTCGAGGCCAGAAGAC	*YKU80-MYCX9* tagging	This study
Yku80F	CATAGGCGAAGTAACAACAG	*YKU80-MYCX9* verification	This study
Yku80R	GGTGTAAAGGAGGAAAAGC	*YKU80-MYCX9* verification	This study

DNA manipulation and plasmid construction

Plasmid amplification was performed in *Escherichia coli* strain TOP 10 (Life Technologies, Carlsbad, CA, USA). For selection of plasmids, bacteria were grown in LB media containing carbenicillin (100 μg/ml; Life Technologies, Carlsbad, CA, USA). Plasmids were harvested from bacteria and purified using the QIAfilter Plasmid Maxi Kit (QIAGEN GmbH, Hilden, Germany). Restriction enzymes (NEB, Ipswich, MA, USA), T4 DNA ligase (Promega Corporation, Madison, WI, USA) and Phusion High-Fidelity DNA Polymerase (NEB, Ipswich, MA, USA) were used as per the manufacturer's recommendations. Plasmids generated for this work were sequenced by the DNA Facility at Iowa State University to ensure correct reading frame and correct orientation of inserts.

The XhoI coding sequence was amplified from pXhoRM3.OB (provided by New England Biolabs) using the NtermXhoI and CtermXhoI primers, Phusion High-Fidelity DNA Polymerase, and an annealing temperature of 71°C. The insert was purified and digested with PstI and NotI. The plasmid pcKuFlag1-1 [24] was digested with PstI and NotI to remove the *Mycobacterium tuberculosis* Ku coding sequence and the resulting linear vector DNA was ligated with the PstI-NotI digested XhoI coding sequence to generate pMTSXhoIFlag. The XhoI-Flag sequence from pMTSXhoIFlag was amplified with BamXhoI and SalFlag primers using Phusion High-Fidelity DNA Polymerase and an annealing temperature of 65°C. The insert was digested with BamHI and SalI and ligated to the mitochondrial targeting sequence of F_0-ATPase subunit 9 (Su9) of *Neurospora crassa* [27] in the pGAL plasmid. This was done by BamHI and SalI digestion of pGalSu9RFP [24], which removed the red fluorescent protein (RFP) coding sequence, and ligation of this linearized vector to the BamHI-SalI-digested XhoI-Flag

DNA fragment generated pGalSu9XhoI. The plasmids pGalSu9RFP and pGalSu9XhoI contain the *GAL1* promoter and hence the expression of mitochondrial-targeted proteins (RFP and XhoI, respectively) is driven in a galactose-inducible manner. Glucose represses the promoter, while raffinose has no effect on expression.

Yeast strains, media, and transformation

S. cerevisiae strains used in this study are listed in Table 5 and are congenic to KT1357 [28].

Table 5. Yeast strains used in this study

Name	Genotype	Reference
KT1357	*MAT***a** *ura3 leu2 his3 trp1*; mitochondrial genotype: ρ^+	[28]
KT1358	*MATα ura3 leu2 his3 trp1*; mitochondrial genotype: ρ^+	[29]
KJP1976	*MAT***a** *ura3 leu2 his3 trp1 MHR1-MYCX9*:*TRP1*; mitochondrial genotype: ρ^+	This study
KJP2011	*MAT***a** *ura3 leu2 his3 trp1 YKU80-MYCX9*:*TRP1*; mitochondrial genotype: ρ^+	This study
KJP2038	*MAT***a** *ura3 leu2 his3 trp1 MHR1-MYCX9*:*TRP1 yku80*::*KAN-MX*; mitochondrial genotype: ρ^+	This study

To generate KJP1976, a strain capable of expressing C-terminally Myc-tagged Mhr1 from the endogenous *MHR1* locus, the Myc9 tag and the *klTRP1* selectable marker from plasmid pWZV87 ([30]; a gift from Dr. David S. Gross) were amplified using MHR1Myc9F and MHR1Myc9R primers, Phusion High-Fidelity DNA Polymerase, and an annealing temperature of 70°C. Seventeen nucleotides at the 3′ end of the primers (MHR1Myc9F and MHR1Myc9R; Table 4) were complementary to the regions upstream or downstream of the *MYCx9-klTRP1* cassette in pWZV87. The remaining nucleotide

sequences in the MHR1Myc9F and MHR1Myc9R primers were homologous to ~40 bp immediately 5′ and 3′ to the *MHR1* stop codon, respectively. These regions of homology were used to direct integration of *MYCX9-klTRP1* cassette to the 3′ end of the MHR1 gene, eliminating the Mhr1 stop codon and generating a coding region to produce a Mhr1-Myc tagged fusion protein. The PCR product was purified and introduced into the *trp1* mutant strain KT1358 [29]. Transformants containing *MYCX9-klTRP1* cassette were selected in medium lacking tryptophan. Positive transformants were then screened by PCR using MHR1F and MHR1R primers. A positive transformant was mated with KT1357, following which the diploid strain was sporulated and haploid meiotic segregants were isolated by tetrad analysis to obtain KJP1976. The expression of Myc-tagged Mhr1 from KJP1976 was verified by western analysis.

The yeast strain KJP2011 expressing C-terminally Myc-tagged Yku80 from the endogenous *YKU80* locus was engineered as described for KJP1976 except that Yku80Myc9F and Yku80Myc9R primers were used to amplify the Myc9 tag and *klTRP1* selectable marker from pWZV87. Yku80Myc9F and Yku80Myc9R primers also contained nucleotide sequences that were homologous to ~50 bp immediately 5′ and 3′ to the *YKU80* stop codon, respectively. The purified PCR product was introduced into KT1357 and transformants were selected in medium lacking tryptophan, following which positive transformants were screened by PCR using Yku80F and Yku80R primers. A positive transformant was mated with KT1358 and the diploid strain was sporulated, following which KJP2011 was obtained by tetrad analysis. The expression of Myc-tagged Yku80 from KJP2011 was verified by western analysis.

The *yku80* null mutant (KJP2038) was constructed by amplifying the G418 cassette from the *yku80* deletion panel strain [31] with YKU80DelF and YKU80DelR primers, Phusion High-Fidelity DNA Polymerase, and an annealing temperature of 61.5°C. The purified PCR product was introduced into KJP1976 and *yku80* null mutants were selected by their ability to grow in G418 (200 μg/ml; Life Technologies, Grand Island, NY, USA). KJP2038 was confirmed for the absence of the *YKU80* gene by PCR using YKU80DelF and DeltaYKU80R primers.

YPD and YPEG contained 1% yeast extract and 2% bacto peptone with 2% glucose or 2% ethanol and 3% glycerol, respectively. Selective media were prepared by combining complete supplement mixture lacking uracil (–Ura) or tryptophan (-Trp; Sunrise Science Products, San Diego, CA, USA) with yeast nitrogen base (Sunrise Science Products) and 2% carbon source.

Yeast transformation was performed by a LiAc procedure as described previously [32] with the following modifications: (i) cells were grown in YPD to OD_{600} of 0.6-0.9, and (ii) the carrier DNA was from salmon testes (Sigma, Saint Louis, MO, USA).

Spot dilution analysis

Stationary phase yeast cultures containing pGalSu9RFP or pGalSu9XhoI pre-grown in –Ura raffinose liquid medium were 25-fold serially diluted using sterile water. 6 μl of each dilution was applied to a –Ura galactose plate and cells were grown at 30°C for 48 h. The colonies were then replica-plated to YPEG and grown at 30°C for 36 h.

Determination of percentage of ρ^+ colonies

Determination of the percentage of ρ^+ colonies was performed as described previously [24]. Briefly, stationary phase KT1357 cultures harboring pGalSu9XhoI pre-grown in –Ura raffinose were diluted in fresh –Ura raffinose liquid medium to a final concentration of OD_{600} of 0.04. The cultures were grown at 30°C for 3 h on a rotary shaker (200 rpm), after which 2% galactose or 2% raffinose was added. The cultures were then returned to the rotary shaker and aliquots were removed at the indicated time points. Cells were counted using a hemocytometer and serially diluted in sterile water to plate ~200 cells on –Ura glucose agar plates. The colonies were counted and replica-plated to YPEG, following which YPEG-positive colonies were counted and the percentage of ρ^+ colonies was calculated using the following formula:

% of ρ^+ colonies = (number of colonies on YPEG/ number of colonies on –Ura glucose) × 100

Immunoblot analysis

Total cell extracts were prepared by lysing yeast cells with glass beads in trichloroacetic acid as described previously [33]. Mitochondrial extracts were prepared from yeast cells using the Yeast Mitochondria Isolation Kit according to manufacturer's instructions (Bio Vision, Milpitas, CA, USA). Protein extracts were subjected to electrophoresis through 4-20% tris-glycine gradient gels (Life Technologies, Carlsbad, CA, USA) and transferred to 0.2 μm nitrocellulose membrane (Bio-Rad Laboratories, Inc., Germany). Membranes were probed with the following antibodies: (i) anti-Flag M2 primary antibody (1:2000; Sigma, Saint Louis, MO, USA) and a sheep anti-mouse secondary horseradish peroxidase

antibody (1:8000; Amersham Biosciences, Buckinghamshire, UK); (ii) anti-Cox4 (1:2000; MitoSciences, Eugene, OR, USA) primary antibody or anti-Pgk1 (1:30000; Invitrogen, Frederick, MD, USA) primary antibody and a goat anti-mouse secondary horseradish peroxidase antibody (1:20000 and 1:31250, respectively; Bio-rad, Hercules, CA, USA); and (iii) anti-cMyc primary antibody (1:6000; Santa Cruz Biotechnology, Inc., Dallas, TX, USA) and a goat anti-mouse secondary horseradish peroxidase antibody (1:30000; Santa Cruz Biotechnology, Inc., Dallas, TX, USA).

For all immunoblots, antibody binding was detected by incubation with chemiluminescent substrate (ECL-Prime; GE Healthcare, Buckinghamshire, UK) and visualized using autoradiography. Bound antibody was removed from blots with stripping buffer (Thermo Scientific, Rockford, IL, USA) prior to subsequent re-probing.

Total DNA isolation

Isolation of yeast total DNA was performed as described previously [34] with slight modifications. Briefly, cells aliquoted at indicated time points were lysed with glass beads for 5 min in lysis buffer and phenol/chloroform/isoamylalcohol (25:24:1; Fisher Scientific, Fair Lawn, NJ, USA). The pellet obtained after ethanol precipitation was resuspended in TE and treated with DNase-free RNase for 1 h at 37°C. A final DNA precipitation was performed with ice-cold absolute ethanol in the presence of ammonium acetate. The DNA pellet was resuspended in TE and quantitated using a Nanodrop ND-1000 spectrophotometer (Wilmington, DE, USA).

Real-time quantitative PCR (qPCR)

Real-time qPCR was performed as described previously [24]. The monomeric form of the budding yeast mitochondrial genome contains two XhoI restriction sites, located at 23224 bp (upstream XhoI site) and 51370 bp (downstream XhoI site). Amplification across the upstream and downstream XhoI sites was performed using XhoIupF/R and XhoIdownF/R primer sets, respectively. The COX2F/R primer set was used to amplify a region of *COX2* in the mtDNA, and the ACT1F/R primer set was utilized to amplify a region of *ACTIN* in the nDNA.

Southern analysis

Southern analysis was performed to demonstrate mtDNA fragmentation by sonication. The sonicated DNA-protein complex (see Section 2.10) was treated with proteinase K (50 μg/ml; Roche Diagnostics, Indianapolis, IN, USA) at 65°C for 16 h. DNA was then extracted twice with phenol/chloroform/isoamylalcohol (25:24:1; Amresco LLC, Solon, OH, USA) and precipitated with ice-cold absolute ethanol in the presence of sodium acetate. The purified DNA was dissolved in TE, electrophoresed through a 1% agarose gel, and transferred by capillary action [35] to a nylon membrane (Hybond-N; Amersham Biosciences, Buckinghamshire, UK). The membrane was hybridized with two ^{32}P-labeled mtDNA probes. ^{32}P-labeled mtDNA probes were generated by PCR with [α-^{32}P] dCTP and mtDNA specific primer sets: ProbeXhoIupF/R primer set amplified a 548 bp mtDNA segment located ~2 kb 5′ to the upstream XhoI site, whereas ProbeCOX2F/R primer set amplified a 511 bp mtDNA segment that includes part of the *COX2* gene. Hybridization was performed overnight in 50X Denhardt's solution, 20X SSC (SSC is 0.15 M NaCl,

0.015 M sodium citrate, pH 7), 0.5% SDS, 10% dextran sulfate, and 0.1 mg/ml salmon testes single-stranded DNA. The membrane was washed twice with 6X SSC and 0.1% SDS for 15 min at 65°C, once with 2X SSC and 0.1% SDS for 15 min at 65°C, once with 2X SSC and 0.5% SDS for 30 min at 50°C, and once with 0.5X SSC and 0.5% SDS for 30 min at 50°C, following which the ^{32}P signal was visualized by autoradiography using Konica SRX-101A Medical Film Processor (Tokyo, Japan).

mtDNA immunoprecipitation (mtDNA IP)

mtDNA IP was performed as described previously [24] with minor modifications. Briefly, yeast cells containing pGalSu9XhoI were grown in raffinose or galactose for 2 h. DNA was crosslinked to proteins by the addition of formaldehyde (1% final concentration). Cells were harvested, resuspended in lysis buffer and lysed with glass beads by vigorous shaking. The sample was sonicated to obtain a mean DNA length of ~0.3 kb. After centrifugation at 4°C, the supernatant containing soluble DNA-protein complexes was mixed with 1.5 µg of anti-cMyc antibody or mouse IgG1 (Sigma, Saint Louis, MO, USA) for 16 h at 4°C. Dynabeads protein G (50 µl; Life Technologies, Oslo, Norway) was added to the DNA-protein-antibody complex and mixed for 16 h at 4°C. DNA-protein complexes were eluted and the immunoprecipitated DNA was purified. The purified immunoprecipitated DNA was dissolved in TE and subjected to real-time qPCR using RegionIF/R, RegionIIF/R, RegionIIIF/R, and COX2F/R primer sets. A standard curve specific for each amplicon was used to determine the amount of mtDNA present in each immunoprecipitate and background signal obtained from IgG1 control was subtracted. The net immunoprecipitate so obtained was used to calculate percentage of

input immunoprecipitated using the following formula: % Input immunoprecipitated = (Amount of mtDNA in net IP/ Amount of mtDNA in total input) x 100; where total input represents total amount of DNA-protein complex used in the immunoprecipitation.

Statistics

Data are presented as mean ± standard deviation (SD) of three independent experiments. Statistical comparisons were performed with ANOVA followed by *post hoc* analysis using Tukey's multiple comparison test. Differences are considered significant at $P < 0.05$.

RESULTS

Galactose-inducible system for expression of mitochondrial-targeted proteins

To deliver proteins to yeast mitochondria, we utilized the N-terminal 69 amino acids of F_0-ATPase subunit 9 (Su9) of *Neurospora crassa* as a mitochondrial targeting sequence (MTS). This sequence has previously been used to target proteins to yeast mitochondria [24, 27]. The plasmid pGalSu9RFP [24] contains the Su9 MTS in frame with RFP (Figure 41A), and induction of the *GAL1* promoter with galactose results in the expression of a fusion protein in which the C-terminus of Su9 is linked to the N-terminus of RFP. We have previously demonstrated that induction of pGalSu9RFP with galactose results in localization of RFP to yeast mitochondria [24]. Similarly, galactose-mediated induction of pGalSu9XhoI (Figure 41B) results in expression of a fusion protein in which the N-terminus of XhoI is connected to Su9, while its C-terminus is tagged with two Flag epitopes.

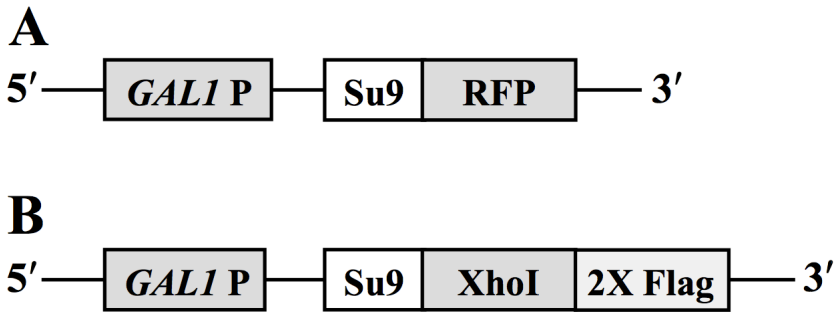

Figure 41. Schematic representation of the galactose-inducible system for expression of mitochondrial-targeted proteins. The expression cassettes of pGalSu9RFP (**A**) or pGalSu9XhoI (**B**) containing the galactose inducible promoter (*GAL1* P) and downstream fusion protein coding sequence is shown. Su9: F_0-ATPase subunit 9 of *N. crassa.*

Mitochondrial-targeted XhoI (mitoXhoI) cleaves mtDNA and decreases mitochondrial respiration

The ~85.8 kb monomeric form of yeast mtDNA [36] contains two XhoI restriction sites, which are located at 23224 bp and 51370 bp, respectively (Figure 42A). To determine expression of mitoXhoI, KT1357 containing pGalSu9XhoI were grown in the presence of galactose and aliquots were taken at increasing time intervals to isolate total cell extracts. The extracts were subjected to western analysis using anti-Flag antibody to detect expression of mitoXhoI. As shown in Figure 42B, mitoXhoI was expressed within 1 h of galactose treatment and expression increased over 8 h.

Next, the mtDNA-cleaving activity of mitoXhoI was assessed using PCR. Introduction of a DSB at the XhoI sites decreases the amount of PCR product generated using XhoIupF/R and XhoIdownF/R primer sets, which amplify across the upstream and downstream XhoI sites, respectively. K1357 containing pGalSu9XhoI was grown in the presence of galactose for up to 8 h, during which cells were harvested to obtain total DNA. Real-time qPCR was performed to amplify across the upstream and downstream XhoI sites. The mitochondrial gene *COX2* and the nuclear gene *ACT1* were used as controls for mtDNA and nDNA amplifications, respectively. The *COX2* mitochondrial gene was selected because it is situated > 20 kb away from either XhoI site. As shown in Figure 42C, the normalized mtDNA/nDNA ratio across both XhoI restriction sites decreased substantially within 1 h of galactose treatment, indicating that digestion of both restriction sites occurred within 1 h of plasmid induction. The degree of cleavage increased with time such that after 2 h, ~80% of both XhoI sites were cleaved. In contrast, amplification across a region of *COX2* did not fluctuate significantly over the 8h

time period. Therefore cleavage of mitoXhoI was specific for the XhoI sites in the mtDNA.

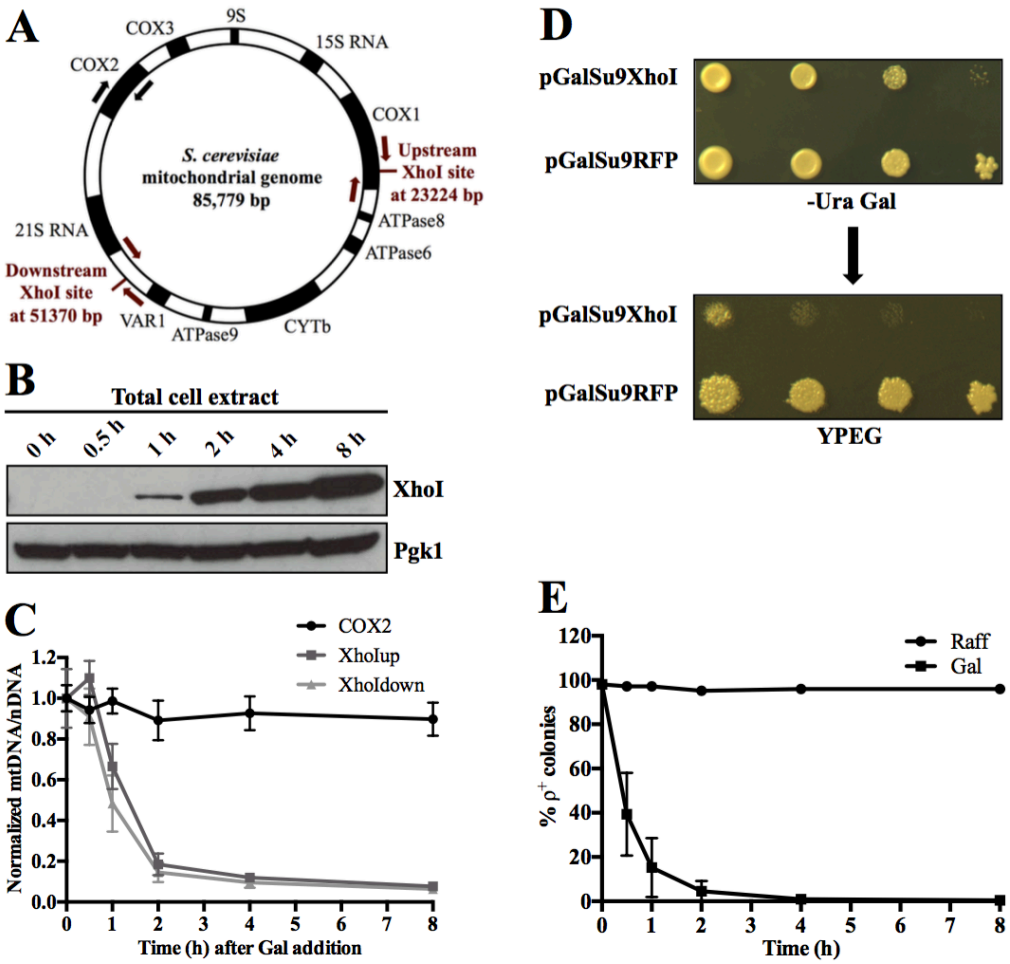

Figure 42. Expression and activity of mitoXhoI in KT1357. (**A**) The ~85.8 kb budding yeast mtDNA monomer has two XhoI restriction sites, located at ~23.2 kb and ~51.4 kb, respectively. Brown arrows flanking the XhoI restriction sites represent qPCR primers that amplify across the sites. Arrows represent qPCR primers that amplify a region of *COX2*. (**B**) KT1357 carrying pGalSu9XhoI was grown in galactose for the indicated time points to obtain total cell extracts, which were subjected to Western analysis and probed with anti-Flag (to detect mitoXhoI) or anti-Pgk1 antibody. The immunoblot shown is representative of three independent experiments. Pgk1, phosphoglycerate kinase, was used as a loading control. (**C**) KT1357 containing pGalSu9XhoI was grown in galactose (Gal) for the indicated times, following which total DNA was isolated and the mtDNA/nDNA ratio was determined using real-time qPCR for specific mtDNA regions. The mtDNA/nDNA ratio obtained at different time points for each mtDNA region was normalized to the 0 h galactose sample. Data are represented graphically as mean ± SD from three independent experiments. (**D**) KT1357 containing pGalSu9XhoI or pGalSu9RFP were serially diluted and applied to a –Ura galactose plate, following which cells were grown for 48 h and the colonies were imaged (top panel). The colonies were then replica plated to YPEG and imaged after ~36 h (bottom panel). (**E**) Cells harboring pGalSu9XhoI were grown in media containing raffinose (Raff) or galactose (Gal) for the indicated times, following which cells were plated on –Ura glucose media. The colonies were then replica plated to YPEG and the percentage of ρ^+ colonies was determined. Data are represented graphically as mean ± SD from three independent experiments.

Cleavage at both XhoI restriction sites in the mtDNA can result in the loss of an ~28.1 kb mtDNA fragment that contains genes encoding essential components of the OXPHOS machinery. To determine if expression of mitoXhoI compromises mitochondrial respiration, KT1357 containing pGalSu9XhoI or pGalSu9RFP were serially diluted and spotted on galactose agar medium to induce expression of the mitochondrial-targeted proteins. Cells carrying pGalSu9XhoI grew slowly on galactose medium, whereas cells containing pGalSu9RFP grew normally (Figure 42D, top panel). The colonies were then replica plated to YPEG, a medium containing ethanol and glycerol that requires functional electron transport chain activity for metabolism; hence, only respiratory competent yeast cells can grow on the medium. Although cells carrying pGalSu9RFP grew well on YPEG, cells containing pGalSu9XhoI formed small or no colonies (Figure 42D, lower panel), indicating a loss of mitochondrial respiratory activity. The mitoXhoI-induced respiration defect was quantitated by growing cells containing pGalSu9XhoI in raffinose or galactose liquid medium for increasing time intervals. Cells were then plated on solid medium containing glucose, following which the colonies were replica plated to YPEG to determine the percentage of ρ^+ colonies. We observed ~60% decrease in the percentage of ρ^+ colonies after 30 min of growth in galactose (Figure 42E). Even though expression of mitoXhoI and its mtDNA-cleaving activity was not detectable during the first 30 minutes of galactose induction (Figures 42B and 42C), it should be noted that during total cell extract and total DNA isolation procedures, cells and cell pellets were processed in ice-cold conditions, which is expected to stop further protein production and mtDNA cleavage. However, during the ρ^+ colony formation assay cells were processed (counted, serially diluted, and plated) at room

temperature, which took ~10-15 min. In addition, glucose repression of the *GAL1* promoter takes time [37] following cell plating. Therefore it is likely that during the processing time the cells were continuing to produce mitoXhoI protein and the mitoXhoI was able to catalyze mtDNA cleavage and hence petite formation. As shown in Figure 42E, the degree of petite formation increased progressively with time such that by 4 h, almost all colonies were respiratory deficient. In contrast, colonies obtained from cells grown with the raffinose control sugar essentially maintained a ρ^+ phenotype. Subsequent experiments were performed following a 2 h galactose induction of pGalSu9XhoI since ~80% cleavage of the XhoI sites was observed at this time point.

MitoXhoI and Mhr1, unlike Yku80, localize to mitochondria.

KT1357 was genetically manipulated to generate KJP1976, which expresses Myc-tagged Mhr1 (Mhr1-9XMyc) from the *MHR1* genetic locus. Following transformation with pGalSu9XhoI, KJP1976 was grown in medium containing raffinose or galactose for 2 h, and total cell extracts were prepared. Mitochondrial extracts were also prepared from 2 h galactose treated cells. Western analysis not only confirmed localization of Myc-tagged Mhr1 and Flag-tagged mitoXhoI to yeast mitochondria, but also verified galactose-dependent expression of mitoXhoI (Figure 43A).

To determine if Yku80 localizes to yeast mitochondria, we engineered a yeast strain (KJP2011) capable of expressing Myc-tagged Yku80 (Yku80-9XMyc) from the *YKU80* genetic locus. KJP2011 containing pGalSu9XhoI was grown in raffinose or galactose for 2 h, following which total cell extracts and mitochondrial extracts were prepared. Western analysis revealed galactose-dependent expression of mitoXhoI, which

localized to mitochondria (Figure 43B). Interestingly, we could only detect Yku80 in the total cell extracts; Yku80 was not seen in the mitochondrial extracts.

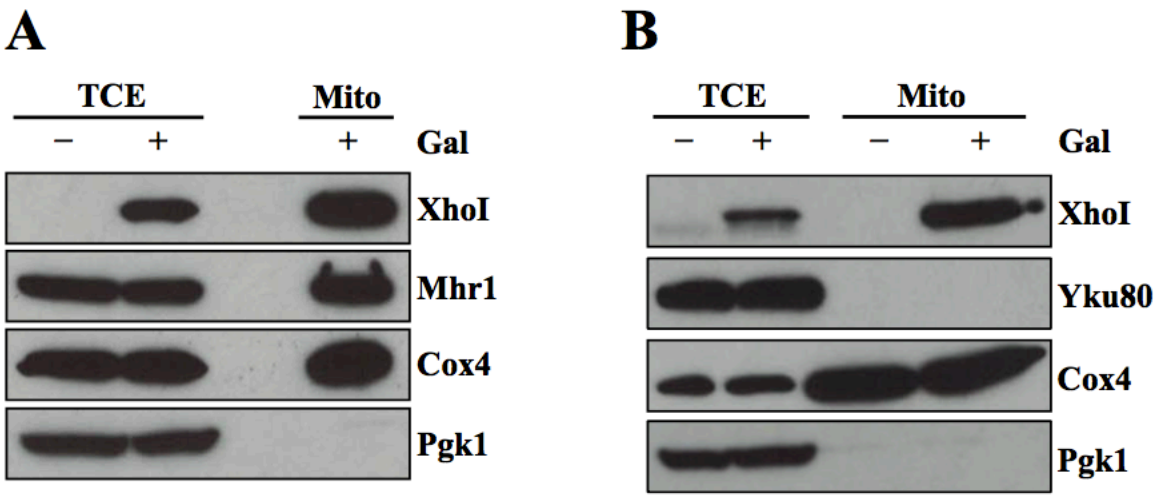

Figure 43. Expression of mitoXhoI in KJP1976 and KJP2011. (**A**) Mitochondrial extracts (Mito) were prepared from KJP1976 carrying pGalSu9XhoI grown in the presence of galactose (Gal) for 2 h, and total cell extracts (TCE) were prepared after growth in either raffinose or galactose for 2 h. The extracts were probed with anti-Flag (to detect mitoXhoI), anti-cMyc (to detect Mhr1), anti-Cox4, or anti-Pgk1 antibody. An image representative of three independent experiments is shown. Cox4, cytochrome C oxidase subunit 4, is a mitochondrial protein. Pgk1 is used as a cytosolic marker and is a loading control for total cell extracts. (**B**) KJP2011 carrying pGalSu9XhoI was grown in the presence of raffinose or galactose for 2 h to obtain total cell extracts (TCE) and mitochondrial extracts (Mito). The extracts were subjected to Western analysis and probed with anti-Flag (to detect mitoXhoI), anti-cMyc (to detect Yku80), anti-Cox4 or anti-Pgk1 antibody. An image representative of three independent experiments is shown.

mtDNA cleaving activity of mitoXhoI in KJP1976 and KJP2038

Mammalian mitochondria contain a truncated form of Ku80, which is absent in a cell line that lacks Ku80 mRNA expression [38]. Evidence has also shown that nuclear NHEJ competes with HR, and loss of Ku80 or Ku70 in mammalian cells increases nuclear HR [39, 40]. Even though western analysis of strain KJP2011 provided no evidence that Yku80 is present in mitochondria, we wanted to ensure that the *YKU80* gene product is not competing with Mhr1 during mtDNA DSB repair. Therefore, we deleted the *YKU80* gene in KJP1976, and the resulting *yku80* null strain, KJP2038, as well as KJP1976 was transformed with the XhoI expression plasmid.

Strains KJP1976 and KJP2038 were grown in raffinose or galactose for 2 h, following which cells were harvested to isolate total DNA. To confirm that cleavage of the XhoI restriction sites occurred only following mitoXhoI expression in these strains, real-time qPCR was performed. As shown in Figures 44A and 44B, the amplification of a region of *COX2* was similar when the strains were grown in raffinose or galactose. However, decreased PCR amplification across both XhoI sites was only found in DNA from galactose treated cultures. This indicates the XhoI sites were cleaved and the degree of mtDNA cleavage at both restriction sites was comparable in strains KJP1976 and KJP2038.

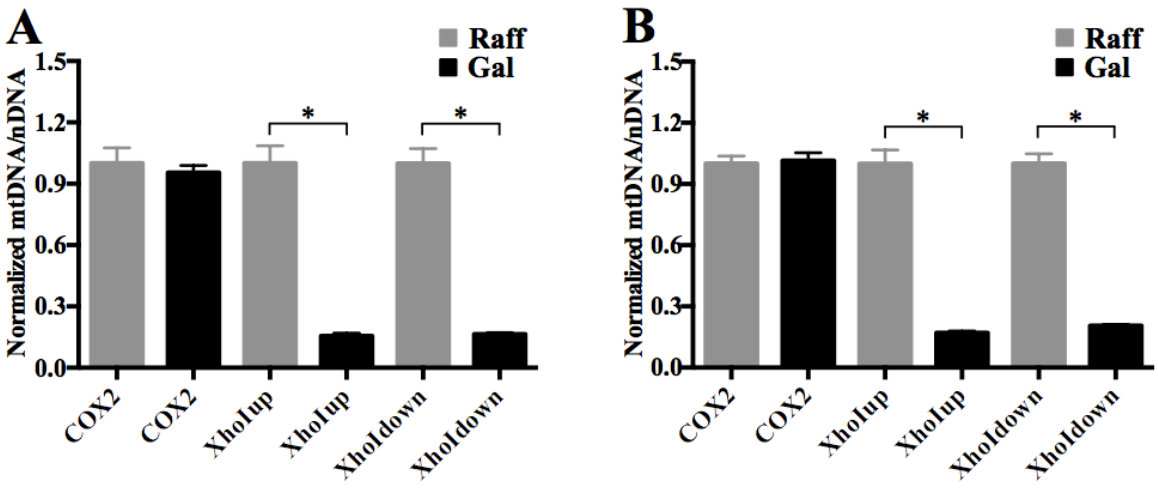

Figure 44. XhoI restriction sites in KJP1976 and KJP2038 are cleaved only following induction of mitoXhoI expression. Total DNA was isolated from KJP1976 (**A**) or KJP2038 (**B**) carrying pGalSu9XhoI grown in raffinose (Raff) or galactose (Gal) for 2 h and the mtDNA/nDNA ratio was determined at the indicated mtDNA regions. The mtDNA/nDNA ratio obtained from the 2 h galactose sample was normalized with respect to the 2 h raffinose sample. Data are represented graphically as mean ± SD from three independent experiments and * represents $P < 0.05$ between the indicated samples.

Mhr1 binds near mitoXhoI-induced DSBs

The restriction endonuclease XhoI recognizes the palindromic sequence 5′-CTCGAG-3′ in double-stranded DNA (Figure 45A) and cleaves after the first cytosine, resulting in the production of 5′ 4-nucleotide single-stranded complementary ends. To determine if Mhr1 binds near mitoXhoI-induced DSBs and to determine whether Yku80 alters Mhr1 binding to mtDNA DSBs, we performed an mtDNA immunoprecipitation (IP) assay. KJP1976 and KJP2038 containing pGalSu9XhoI grown in raffinose or galactose for 2 h were treated with formaldehyde, following which the DNA crosslinked to protein was sonicated. Southern analysis of sonicated DNA with mtDNA specific probes revealed that the average length of mtDNA fragments was ~0.3 kb (Figure 45B). The immunoprecipitation of DNA-protein complexes was carried out either with anti-cMyc antibody or the IgG1 control. Real-time qPCR of purified immunoprecipitated DNA was performed using *COX2*, region I-, region II-, or region III-specific primer sets (Figure 45A). The distance of the amplicons from the upstream XhoI site at regions I and II is 404 bp and 169 bp, respectively, whereas the distance of the region III amplicon is 105 bp from the downstream XhoI site. The nucleotide sequence in region IV near the downstream XhoI site (Figure 45A) consists of extensive stretches of adenine and thymine. This prevented design of qPCR primers within 900 bp of the downstream XhoI site at region IV. As shown in Figure 45C, Mhr1 binds to *COX2* sequences in KJP1976 and KJP2038, and this interaction occurred irrespective of the status of mitoXhoI expression in either strain. However, there was a significant increase in the degree of Mhr1 binding to regions I, II and III following growth in galactose compared to growth in

raffinose for KJP1976 and KJP2038 (Figures 45D-F). Binding to regions I-III was comparable in both strains.

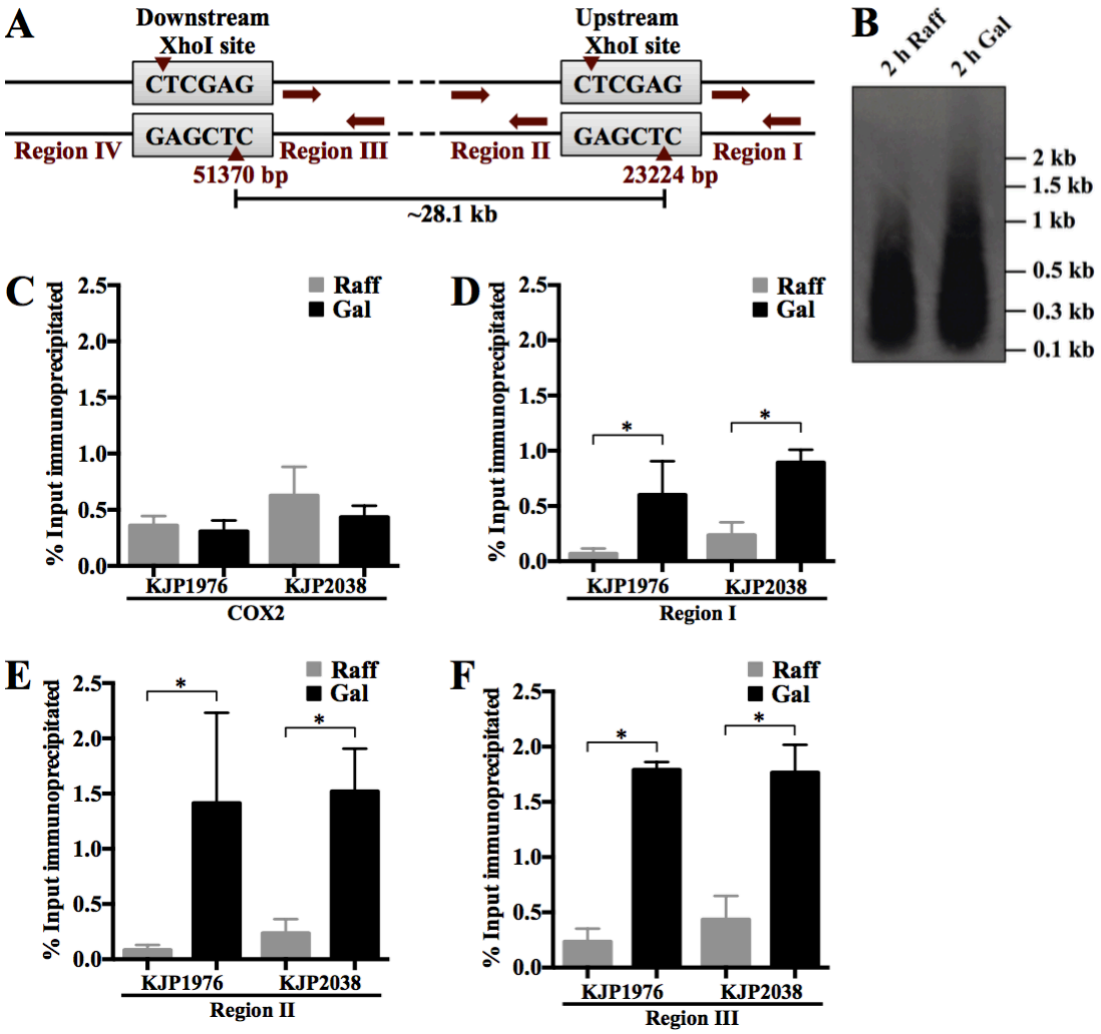

Figure 45. Following induction of mitoXhoI expression, Mhr1 has increased binding to mtDNA near the XhoI restriction sites. (**A**) Schematic representation of upstream and downstream XhoI sites depicting the location of qPCR primers (arrows) used for quantitating immunoprecipitated mtDNA. XhoI cleaves the palindromic sequence 5′-CTCGAG-3′ after the first cytosine (site represented by closed triangles) resulting in a staggered break containing 4 base overhang. Cleavage of both XhoI sites results in the removal of ~28.1 kb mtDNA segment. (**B**) KJP1976 carrying pGalSu9XhoI was grown in medium containing raffinose (Raff) or galactose (Gal) for 2 hours, following which formaldehyde crosslinked DNA-protein complexes were sonicated to shear cellular DNA. DNA-protein crosslinks were reversed and the purified DNA was subjected to southern analysis. Binding of mtDNA-specific radioactive probes to the sonicated DNA samples was visualized by autoradiography. (**C-F**) KJP1976 and KJP2038 harboring pGalSu9XhoI were grown in raffinose or galactose for 2 h, following which DNA-protein complexes were crosslinked with formaldehyde, sheared by sonication and immunoprecipitated with either anti-Myc antibody or IgG1 control. Crosslinks were reversed and purified immunoprecipitated DNA samples were quantitated by real-time qPCR using primers specific for the indicated mtDNA region. Each graph represents data as mean ± SD from three independent experiments. * denotes $P < 0.05$ between the indicated samples.

DISCUSSION

MHR1 was first identified as a gene required for mitochondrial recombination that occurs after mating between yeast cells [41]. The finding that Mhr1 promotes heteroduplex joint formation between single- and homologous double-stranded DNA *in vitro* [22] supports its *in vivo* role in mtDNA recombination. Several studies have explored the recombinase activity of Mhr1 in mediating recombination-dependent rolling circle replication [22, 42, 43] at *ori5*, an active mtDNA origin of replication possessing inherent DSBs [44, 45]. However, a potential role of Mhr1 as a 'common' mtDNA DSB repair factor has not been thoroughly investigated. Because of its abundance in the mitochondrial fraction and its ability to mediate homologous pairing *in vitro* [22], we hypothesized that Mhr1 is a general mtDNA DSB repair factor. In this study, we have provided evidence in support of this hypothesis.

DSBs can be lethal. Following their occurrence, DSBs are recognized and bound by DSB repair proteins in order to restore genomic integrity. Indeed, one of the hallmarks of a classical DSB repair protein is its ability to bind at or near DNA ends. To understand if Mhr1 possesses this characteristic, we explored its ability to bind to mtDNA DSBs. For this, we employed a mitochondrial-targeted XhoI (mitoXhoI) to generate DSBs in the mitochondrial genome. Expression of mitoXhoI was achieved from a galactose-inducible expression system. After confirming expression and mtDNA cleaving activity of mitoXhoI, we determined the binding ability of Mhr1 to mitoXhoI-induced DSBs. Results from mtDNA IP revealed that Mhr1 binds near the XhoI restriction sites at a significantly higher level following induction of mitoXhoI expression compared to the uninduced condition. In contrast, the binding of Mhr1 to the control region *COX2* was

comparable between galactose and raffinose treatment groups. The basal binding of Mhr1 to *COX2* gene occurs presumably because Mhr1 is a component of mitochondrial nucleoids [46], which are nucleoprotein complexes consisting of mtDNA molecule(s) and a diverse set of proteins involved in mtDNA maintenance [1]. Taken together, these results clearly demonstrate that Mhr1 binds preferentially at or near the sites where the mtDNA DSBs occur.

Yku80 is a *bona fide* mammalian Ku80 homolog [47]. The essential nature of Yku80 in C-NHEJ has been previously demonstrated. Using an *in vivo* plasmid rejoining assay, it was shown that *yku80* null mutants were as defective as *yku70*, *yku80* double mutants in repairing restriction endonuclease (EcoRI, XhoI, or PstI) induced DSBs [47]. Following association of Yku80 with Yku70, the Yku heterodimer binds DNA ends [48] to mediate nDNA DSB repair via C-NHEJ, particularly in G1-phase haploid yeast cells when a homologous DNA template is unavailable for recombinational repair [49]. With regard to its role in mtDNA DSB repair, indirect evidence exists for the involvement of the Yku complex in suppressing mtDNA deletions [21]. It is, however, not known if the components of the Yku complex are present in yeast mitochondria. To determine if Yku80 localizes to the mitochondrial compartment, we isolated the mitochondrial fraction from a yeast strain capable of expressing C-terminally Myc-tagged Yku80 from the endogenous *YKU80* locus. Western analyses revealed the presence of Yku80 in total cell extracts but not in mitochondrial extracts, indicating that C-terminally Myc-tagged Yku80 does not significantly localize to yeast mitochondria.

In mammalian cells, a C-terminally truncated version of Ku80 has been shown to localize to mammalian mitochondria [38]. Since we have added Myc epitope to the C-

terminus of Yku80, a C-terminally truncated form of Yku80 would not have been detected in this study. It should, however, be noted that the C-terminus of Yku80 is required for C-NHEJ in *S. cerevisiae* [50]; hence, the presence of a C-terminally truncated form of Yku80 in yeast mitochondria would not likely assist in mtDNA DSB repair. Nonetheless, there is still the possibility that an alternate version of Yku80 may localize to yeast mitochondria. To understand if any form of Yku80 is involved in mtDNA DSB repair, we deleted the *YKU80* gene and compared the degree of Mhr1 binding to mitoXhoI-induced DSBs in *yku80* null mutants versus wild-type cells. Previous studies [51, 52] have demonstrated competition between the HR and C-NHEJ pathway for nuclear DNA DSBs. Therefore, we hypothesized that if the *YKU80* gene product participates in mtDNA DSB repair, deletion of the *YKU80* gene would increase the availability of mtDNA DSBs and hence increase Mhr1 binding to mtDNA DSBs. Data from the mtDNA IP assay revealed a comparable amount of Mhr1 binding near mtDNA DSBs between the wild-type strain and the *yku80* null mutant, which suggests that the *YKU80* gene product does not compete with Mhr1 for binding to mtDNA DSBs *in vivo*. This observation, together with the lack of Yku80 in yeast mitochondrial extracts, suggests that Yku80 is likely not involved in mtDNA DSB repair under normal growth conditions.

CONCLUSIONS

To our knowledge, this is the first study in which Mhr1 has been shown to bind to mtDNA DSBs *in vivo*. This property of Mhr1, together with its homologous pairing activity *in vitro* [22], supports the hypothesis that Mhr1 is a general mtDNA DSB repair factor. Our results also indicate that Yku80 does not compete with Mhr1 for binding to mtDNA DSBs and cannot be significantly detected in yeast mitochondrial extracts. Taken together, we conclude that Mhr1, but not Yku80, is a general mtDNA DSB repair factor in yeast and propose that Mhr1-mediated HR is likely the predominant pathway by which yeast cells repair mtDNA DSBs.

ACKNOWLEDGEMENTS

We thank Dr. Rona Scott (LSUHSC-Shreveport) for her help with the qPCR assays. We thank Dr. David S. Gross (LSUHSC-Shreveport) and Dr. Anandhakumar Jayamani (LSUHSC-Shreveport) for technical assistance with mtDNA IP and gene-tagging experiments, and to New England Biolabs for providing the coding sequence for XhoI. We acknowledge Feist-Weiller Cancer Center (LSUHSC-Shreveport) for providing a Carroll Feist Predoctoral Fellowship to KP. This study was supported by the National Institutes of Health R21 grant (grant 1R21 CA167796) to LH. The funding agencies had no input on design of this study.

REFERENCES

1. Kucej, M., and Butow, R.A. (2007). Evolutionary tinkering with mitochondrial nucleoids. Trends in cell biology *17*, 586-592.
2. Taanman, J.W. (1999). The mitochondrial genome: structure, transcription, translation and replication. Biochimica et biophysica acta *1410*, 103-123.
3. Schon, E.A., DiMauro, S., and Hirano, M. (2012). Human mitochondrial DNA: roles of inherited and somatic mutations. Nature reviews. Genetics *13*, 878-890.
4. Andreyev, A.Y., Kushnareva, Y.E., and Starkov, A.A. (2005). Mitochondrial metabolism of reactive oxygen species. Biochemistry. Biokhimiia *70*, 200-214.
5. Bolisetty, S., and Jaimes, E.A. (2013). Mitochondria and reactive oxygen species: physiology and pathophysiology. International journal of molecular sciences *14*, 6306-6344.
6. Shokolenko, I., Venediktova, N., Bochkareva, A., Wilson, G.L., and Alexeyev, M.F. (2009). Oxidative stress induces degradation of mitochondrial DNA. Nucleic acids research *37*, 2539-2548.
7. Pieczenik, S.R., and Neustadt, J. (2007). Mitochondrial dysfunction and molecular pathways of disease. Experimental and molecular pathology *83*, 84-92.
8. Kazak, L., Reyes, A., and Holt, I.J. (2012). Minimizing the damage: repair pathways keep mitochondrial DNA intact. Nature reviews. Molecular cell biology *13*, 659-671.
9. Van Houten, B., Hunter, S.E., and Meyer, J.N. (2016). Mitochondrial DNA damage induced autophagy, cell death, and disease. Frontiers in bioscience (Landmark edition) *21*, 42-54.

10. San Filippo, J., Sung, P., and Klein, H. (2008). Mechanism of eukaryotic homologous recombination. Annual review of biochemistry *77*, 229-257.

11. Lieber, M.R. (2010). The mechanism of double-strand DNA break repair by the nonhomologous DNA end-joining pathway. Annual review of biochemistry *79*, 181-211.

12. Sfeir, A., and Symington, L.S. (2015). Microhomology-Mediated End Joining: A Back-up Survival Mechanism or Dedicated Pathway? Trends in biochemical sciences *40*, 701-714.

13. Thyagarajan, B., Padua, R.A., and Campbell, C. (1996). Mammalian mitochondria possess homologous DNA recombination activity. The Journal of biological chemistry *271*, 27536-27543.

14. Lakshmipathy, U., and Campbell, C. (1999). Double strand break rejoining by mammalian mitochondrial extracts. Nucleic acids research *27*, 1198-1204.

15. D'Aurelio, M., Gajewski, C.D., Lin, M.T., Mauck, W.M., Shao, L.Z., Lenaz, G., Moraes, C.T., and Manfredi, G. (2004). Heterologous mitochondrial DNA recombination in human cells. Human molecular genetics *13*, 3171-3179.

16. Morel, F., Renoux, M., Lachaume, P., and Alziari, S. (2008). Bleomycin-induced double-strand breaks in mitochondrial DNA of Drosophila cells are repaired. Mutation research *637*, 111-117.

17. Bacman, S.R., Williams, S.L., and Moraes, C.T. (2009). Intra- and inter-molecular recombination of mitochondrial DNA after in vivo induction of multiple double-strand breaks. Nucleic acids research *37*, 4218-4226.

18. Tadi, S.K., Sebastian, R., Dahal, S., Babu, R.K., Choudhary, B., and Raghavan, S.C. (2016). Microhomology-mediated end joining is the principal mediator of double-strand break repair during mitochondrial DNA lesions. Molecular biology of the cell *27*, 223-235.

19. Wisnovsky, S., Jean, S.R., and Kelley, S.O. (2016). Mitochondrial DNA repair and replication proteins revealed by targeted chemical probes. Nature chemical biology *12*, 567-573.

20. Daley, J.M., Palmbos, P.L., Wu, D., and Wilson, T.E. (2005). Nonhomologous end joining in yeast. Annual review of genetics *39*, 431-451.

21. Kalifa, L., Quintana, D.F., Schiraldi, L.K., Phadnis, N., Coles, G.L., Sia, R.A., and Sia, E.A. (2012). Mitochondrial genome maintenance: roles for nuclear nonhomologous end-joining proteins in Saccharomyces cerevisiae. Genetics *190*, 951-964.

22. Ling, F., and Shibata, T. (2002). Recombination-dependent mtDNA partitioning: in vivo role of Mhr1p to promote pairing of homologous DNA. The EMBO journal *21*, 4730-4740.

23. Ling, F., Mikawa, T., and Shibata, T. (2011). Enlightenment of yeast mitochondrial homoplasmy: diversified roles of gene conversion. Genes *2*, 169-190.

24. Prasai, K., Robinson, L.C., Scott, R., Tatchell, K., and Harrison, L. (2017). Evidence for double-strand break mediated mitochondrial DNA replication in Saccharomyces cerevisiae. Nucleic Acids Research (accepted for publication).

25. Sedman, T., Gaidutsik, I., Villemson, K., Hou, Y., and Sedman, J. (2014). Double-stranded DNA-dependent ATPase Irc3p is directly involved in mitochondrial genome maintenance. Nucleic acids research *42*, 13214-13227.

26. Taylor, S.D., Zhang, H., Eaton, J.S., Rodeheffer, M.S., Lebedeva, M.A., O'Rourke T, W., Siede, W., and Shadel, G.S. (2005). The conserved Mec1/Rad53 nuclear checkpoint pathway regulates mitochondrial DNA copy number in Saccharomyces cerevisiae. Molecular biology of the cell *16*, 3010-3018.

27. Rapaport, D., Brunner, M., Neupert, W., and Westermann, B. (1998). Fzo1p is a mitochondrial outer membrane protein essential for the biogenesis of functional mitochondria in Saccharomyces cerevisiae. The Journal of biological chemistry *273*, 20150-20155.

28. Frederick, D.L., and Tatchell, K. (1996). The REG2 gene of Saccharomyces cerevisiae encodes a type 1 protein phosphatase-binding protein that functions with Reg1p and the Snf1 protein kinase to regulate growth. Molecular and cellular biology *16*, 2922-2931.

29. Venturi, G.M., Bloecher, A., Williams-Hart, T., and Tatchell, K. (2000). Genetic interactions between GLC7, PPZ1 and PPZ2 in saccharomyces cerevisiae. Genetics *155*, 69-83.

30. Knop, M., Siegers, K., Pereira, G., Zachariae, W., Winsor, B., Nasmyth, K., and Schiebel, E. (1999). Epitope tagging of yeast genes using a PCR-based strategy: more tags and improved practical routines. Yeast (Chichester, England) *15*, 963-972.

31. Winzeler, E.A., Shoemaker, D.D., Astromoff, A., Liang, H., Anderson, K., Andre, B., Bangham, R., Benito, R., Boeke, J.D., Bussey, H., et al. (1999). Functional characterization of the S. cerevisiae genome by gene deletion and parallel analysis. Science *285*, 901-906.

32. Gietz, D., St Jean, A., Woods, R.A., and Schiestl, R.H. (1992). Improved method for high efficiency transformation of intact yeast cells. Nucleic acids research *20*, 1425.

33. Davis, N.G., Horecka, J.L., and Sprague, G.F., Jr. (1993). Cis- and trans-acting functions required for endocytosis of the yeast pheromone receptors. The Journal of cell biology *122*, 53-65.

34. Hoffman, C.S., and Winston, F. (1987). A ten-minute DNA preparation from yeast efficiently releases autonomous plasmids for transformation of Escherichia coli. Gene *57*, 267-272.

35. J. Sambrook, E.F.F., T. Maniatis (1989). Molecular Cloning: A Laboratory Handbook, 2nd Edition, (Cold Spring Harbor Laboratory Press).

36. Foury, F., Roganti, T., Lecrenier, N., and Purnelle, B. (1998). The complete sequence of the mitochondrial genome of Saccharomyces cerevisiae. FEBS letters *440*, 325-331.

37. Johnston, M., Flick, J.S., and Pexton, T. (1994). Multiple mechanisms provide rapid and stringent glucose repression of GAL gene expression in Saccharomyces cerevisiae. Molecular and cellular biology *14*, 3834-3841.

38. Coffey, G., and Campbell, C. (2000). An alternate form of Ku80 is required for DNA end-binding activity in mammalian mitochondria. Nucleic acids research *28*, 3793-3800.

39. Shao, Z., Davis, A.J., Fattah, K.R., So, S., Sun, J., Lee, K.J., Harrison, L., Yang, J., and Chen, D.J. (2012). Persistently bound Ku at DNA ends attenuates DNA end resection and homologous recombination. DNA repair *11*, 310-316.

40. Pierce, A.J., Hu, P., Han, M., Ellis, N., and Jasin, M. (2001). Ku DNA end-binding protein modulates homologous repair of double-strand breaks in mammalian cells. Genes & development *15*, 3237-3242.

41. Ling, F., Makishima, F., Morishima, N., and Shibata, T. (1995). A nuclear mutation defective in mitochondrial recombination in yeast. The EMBO journal *14*, 4090-4101.

42. Ling, F., and Shibata, T. (2004). Mhr1p-dependent concatemeric mitochondrial DNA formation for generating yeast mitochondrial homoplasmic cells. Molecular biology of the cell *15*, 310-322.

43. Ling, F., Hori, A., Yoshitani, A., Niu, R., Yoshida, M., and Shibata, T. (2013). Din7 and Mhr1 expression levels regulate double-strand-break-induced replication and recombination of mtDNA at ori5 in yeast. Nucleic acids research *41*, 5799-5816.

44. Ling, F., Hori, A., and Shibata, T. (2007). DNA recombination-initiation plays a role in the extremely biased inheritance of yeast [rho-] mitochondrial DNA that contains the replication origin ori5. Molecular and cellular biology *27*, 1133-1145.

45. Hori, A., Yoshida, M., Shibata, T., and Ling, F. (2009). Reactive oxygen species regulate DNA copy number in isolated yeast mitochondria by triggering recombination-mediated replication. Nucleic acids research *37*, 749-761.

46. Shibata, T., and Ling, F. (2007). DNA recombination protein-dependent mechanism of homoplasmy and its proposed functions. Mitochondrion *7*, 17-23.

47. Boulton, S.J., and Jackson, S.P. (1996). Identification of a Saccharomyces cerevisiae Ku80 homologue: roles in DNA double strand break rejoining and in telomeric maintenance. Nucleic acids research *24*, 4639-4648.

48. Milne, G.T., Jin, S., Shannon, K.B., and Weaver, D.T. (1996). Mutations in two Ku homologs define a DNA end-joining repair pathway in Saccharomyces cerevisiae. Molecular and cellular biology *16*, 4189-4198.

49. Gao, S., Honey, S., Futcher, B., and Grollman, A.P. (2016). The non-homologous end-joining pathway of S. cerevisiae works effectively in G1-phase cells, and religates cognate ends correctly and non-randomly. DNA repair *42*, 1-10.

50. Palmbos, P.L., Daley, J.M., and Wilson, T.E. (2005). Mutations of the Yku80 C terminus and Xrs2 FHA domain specifically block yeast nonhomologous end joining. Molecular and cellular biology *25*, 10782-10790.

51. Zhang, Y., Hefferin, M.L., Chen, L., Shim, E.Y., Tseng, H.M., Kwon, Y., Sung, P., Lee, S.E., and Tomkinson, A.E. (2007). Role of Dnl4-Lif1 in nonhomologous end-joining repair complex assembly and suppression of homologous recombination. Nature structural & molecular biology *14*, 639-646.

52. Clerici, M., Mantiero, D., Guerini, I., Lucchini, G., and Longhese, M.P. (2008). The Yku70-Yku80 complex contributes to regulate double-strand break

processing and checkpoint activation during the cell cycle. EMBO reports *9*, 810-818.

SUMMARY AND FUTURE PROSPECTS

DSBs, in general, are considered deleterious for cellular health. However, mtDNA DSBs can be also be beneficial depending on the type of eukaryotic cell under consideration. In the budding yeast *S. cerevisiae*, mtDNA DSB at the replication origin *ori5* has been demonstrated to initiate mtDNA recombination dependent rolling circle replication (RDR) in the hypersuppressive (HS) ρ^- mutants [1, 2]. However, it was unclear if such DSB-mediated mtDNA replication mechanism existed in ρ^+ yeast cells. To address this, the DSB binding property of *Mycobacterium marinum* Ku (MmKu) was utilized. MmKu, owing to its evolutionarily conserved DSB DNA binding domain, binds to DSBs, but lacks domains to interact with eukaryotic repair proteins. Hence, I hypothesized that the binding of MmKu to mtDNA DSB in ρ^+ yeast cells could prevent mtDNA replication or repair. Results from chapter two demonstrated that mitochondrial-targeted MmKu bound to *ori5* in ρ^+ mtDNA and that inducible expression of MmKu triggered petite formation preferentially in daughter cells. MmKu expression also induced mtDNA depletion that eventually resulted in the formation of ρ^0 cells. As MmKu possesses a DSB-binding domain but is devoid of additional domains required to communicate with eukaryotic repair factors, we concluded that binding of MmKu to DSBs at *ori5* inhibited mtDNA RDR, thereby preventing mtDNA segregation into daughter cells. Our data also suggested that DSB-mediated replication is the predominant from of mtDNA replication in the ρ^+ yeast cells since binding of MmKu to *ori5* can result in the total loss of mtDNA. To date, other *ori*s in the yeast mitochondrial genome have not been demonstrated to possess inherent DSBs; hence, it is not known if other *ori*s in yeast mtDNA can initiate

replication in a DSB-mediated manner. To address this, future studies could be directed in determining the level of MmKu binding to other mtDNA *ori*s.

Data in chapter two also revealed that MmKu bound moderately to *COX1*, a gene in the yeast mtDNA that is not known to possess inherent DSBs under normal physiological conditions. This was indicative of basal interaction of MmKu with mtDNA. As discussed in chapter two, the binding of MmKu to *COX1* could be due to its lysine rich C-terminal extension because such C-terminal extension in *M. smegmatis* Ku has been demonstrated to bind to DNA without free ends [3]. To ascertain this postulation, mitochondrial-targeted *M. tuberculosis* Ku (MtKu), which lacks C-terminal extension [4], could be employed in future studies.

Analogous to their role in HS ρ^- mutants, the 5′-3′ exonuclease activity of Din7 [5] and the homologous pairing activity of Mhr1 [6] are believed to be critically involved in initiating DSB-mediated mtDNA replication at *ori5* in ρ^+ yeast cells. Therefore, it would be interesting to determine and compare the degree of Din7 and Mhr1 binding to *ori5* in ρ^+ cells expressing mitochondrial-targeted MmKu versus those lacking MmKu expression. Such experiments could reveal if competition exists between Din7/Mhr1 and MmKu for binding to *ori5*, and if MmKu expression inhibits mtDNA replication by preventing the binding of Din7 and/or Mhr1.

With regard to human cells, expression of mitochondrial-targeted MmKu did not decrease mtDNA content in MCF7 cells. This observation is in agreement with the current knowledge on human mtDNA replication, which typically does not involve DSBs. Interestingly, however, a recent study has identified mtDNA concatemer in MELAS patient-derived primary fibroblasts [7]. Other tissues in the human body also

possess unorthodox mtDNA structures. For example, the adult human heart contains multimeric networks of mtDNA molecules linked by abundant recombination junctions and catenations [8]. Such observations led to the hypothesis that mammalian cells, at least in some cases, can utilize DSB-mediated RDR for initiation of mtDNA replication [9]. To address this hypothesis, the DSB binding-and-blocking property of mitochondrial-targeted MmKu could be employed in future studies. In such an experimental setting, human cells that employ DSB-mediated mtDNA replication would be expected to lose their mtDNA following expression of mitochondrial-targeted MmKu. Given the complexity of a human body and diversity of its tissues, it may well be the case that certain human tissues employ DSB-mediated mechanism of mtDNA replication. The understanding of the exact mode of mtDNA replication in different human tissues is important as the knowledge can be utilized to increase the mtDNA copy number, for example in tissues of patients with mtDNA depletion syndrome. Apart from the possibility of understanding the mechanism of human mtDNA replication, the DSB binding-and-blocking property of MmKu could also be explored as a potential mechanism for sensitizing human cancer cells to DSB inducing agents. Chemotherapeutic agents like cisplatin represent a major cancer treatment regimen and are known to induce DSBs in the mitochondrial genome. Cancer cells can become resistant to chemotherapy overtime, and one of the main bases of such resistance has been ascribed to increased DNA repair activity. As cancer cell survival and proliferation requires electron transport chain activity, which in turn is dependent on mtDNA integrity, mitochondrial-targeted MmKu could be used to block repair of mtDNA DSBs potentially formed following administration of chemotherapeutic drugs. If explored, such strategy

could prevent cancer cell survival/proliferation and hence could provide an important complementary approach to eradicate cancer cells.

In a typical cell, mitochondria are the major sources of ROS. The close proximity of mtDNA to the site of ROS generation renders mtDNA molecules highly susceptible to oxidative damage. Because mtDNA integrity is essential for electron transport chain activity, progressive accumulation of damaged mtDNA molecules can cause respiratory chain failure. In order to prevent this from happening, cells have evolved mtDNA repair pathways, which include mtDNA DSB repair. Despite the identification of mtDNA DSB repair activities and repair products in several eukaryotic systems, the factors involved in mtDNA DSB repair are not well characterized and only a few proteins have been identified as genuine mtDNA DSB repair factors in the entire Eukaryota domain. Chapter three of this thesis was dedicated to identify putative proteins involved in mtDNA DSB repair. In the study, *S. cerevisiae* was utilized as a eukaryotic model system in which Mhr1 and Yku80 were selected as putative mtDNA DSB repair factors. Utilizing mitochondrial-targeted restriction endonuclease XhoI (mitoXhoI), it was demonstrated that Mhr1 bound to mitoXhoI-induced DSBs *in vivo*. This, together with the knowledge on its homologous pairing activity *in vitro*, supported the hypothesis that Mhr1 is a general mtDNA DSB repair factor. On the other hand, Yku80 was found less likely to be involved in repairing mtDNA DSBs, as indicated by the following observations: (i) C-terminally Myc-tagged Yku80 did not localize to yeast mitochondria; and (ii) the level of Mhr1 binding to mitoXhoI-induced DSBs were comparable between wild-type strain and *yku80* null mutant, suggesting that the product of *YKU80* gene did not compete with Mhr1 for binding to mtDNA DSBs.

In the study, Yku80 was tagged at the C-terminus with Myc epitope. As discussed in chapter three, C-terminally truncated version of Ku80 has been identified in mammalian mitochondria. Hence, there is a possibility for an alternate form of Yku80 to reside in yeast mitochondria. Future studies, therefore, could be directed to identify if other form(s) of Yku80 exist(s) in yeast mitochondria. N-terminal tagging could be a way to address this issue. However, N-terminal tagging is considerably more complex than C-terminal tagging and can prove daunting because insertion of a selectable marker in the 5′ region of a gene can disrupt gene expression [10]. In addition, it is not known if Yku80 possesses a putative mitochondrial-targeting sequence (MTS). Generally, proteins destined to the mitochondrial matrix contain an MTS, which is typically located in the N-terminus of the protein. After localizing into the mitochondrial matrix, the N-terminal MTS is cleaved from the protein. Hence, if the putative MTS in Yku80 lies downstream of the N-terminal epitope tag, the latter can be lost during MTS processing. This could also make it difficult to interpret the result. If encountered with such situations, tagging epitopes internal to the coding region of Yku80 could be an option.

A recent study has revealed that Rad51, a recombinase involved in nDNA DSB repair via homologous recombination (HR), localizes to the yeast mitochondrial matrix [11]. The study utilized mitochondrial-targeted restriction endonuclease KpnI to induce a site-specific DSB in the yeast mitochondrial genome. Even though Rad51 was not shown to bind to KpnI-induced mtDNA DSBs, the study revealed that wild-type cells have significantly higher mtDNA deletion compared to *rad51* null mutants following KpnI induction [11]. This indicated a role of Rad51 in mtDNA DSB repair. In future, our inducible mitoXhoI system could be used to determine if Rad51 binds to mitoXhoI-

induced DSBs. By comparing the degree of binding of Rad51 and Mhr1 to mitoXhoI-induced DSBs, it could be possible to determine which, between the two recombinases, predominantly binds to mtDNA DSBs *in vivo*. Competition between the two recombinases for binding to mtDNA DSBs could also be determined by deleting *RAD51* gene and comparing the level of Mhr1 binding to mitoXhoI-induced DSBs in wild-type cells versus isogenic *rad51* null mutants.

Clearly, much remains to be learned about the mechanisms of mtDNA replication and mtDNA DSB repair. Nonetheless, the work presented in this thesis has contributed to the understanding of mtDNA DSBs in replication and in repair. In sum, this dissertation has revealed that DSB-mediated replication is the predominant, and probably the only, form of mtDNA replication in ρ^+ yeast cells. With regard to mtDNA DSB repair, evidence indicates that Mhr1, but not Yku80, is a general mtDNA DSB repair factor in the budding yeast *S. cerevisiae*.

REFERENCES

1. Ling, F., Hori, A., and Shibata, T. (2007). DNA recombination-initiation plays a role in the extremely biased inheritance of yeast [rho-] mitochondrial DNA that contains the replication origin ori5. Molecular and cellular biology *27*, 1133-1145.
2. Hori, A., Yoshida, M., Shibata, T., and Ling, F. (2009). Reactive oxygen species regulate DNA copy number in isolated yeast mitochondria by triggering recombination-mediated replication. Nucleic acids research *37*, 749-761.
3. Kushwaha, A.K., and Grove, A. (2013). Mycobacterium smegmatis Ku binds DNA without free ends. The Biochemical journal *456*, 275-282.
4. Kushwaha, A.K., and Grove, A. (2013). C-terminal low-complexity sequence repeats of Mycobacterium smegmatis Ku modulate DNA binding. Bioscience reports *33*, 175-184.
5. Ling, F., Hori, A., Yoshitani, A., Niu, R., Yoshida, M., and Shibata, T. (2013). Din7 and Mhr1 expression levels regulate double-strand-break-induced replication and recombination of mtDNA at ori5 in yeast. Nucleic acids research *41*, 5799-5816.
6. Ling, F., and Shibata, T. (2002). Recombination-dependent mtDNA partitioning: in vivo role of Mhr1p to promote pairing of homologous DNA. The EMBO journal *21*, 4730-4740.
7. Ling, F., Niu, R., Hatakeyama, H., Goto, Y., Shibata, T., and Yoshida, M. (2016). Reactive oxygen species stimulate mitochondrial allele segregation toward homoplasmy in human cells. Molecular biology of the cell *27*, 1684-1693.

8. Pohjoismaki, J.L., Goffart, S., Tyynismaa, H., Willcox, S., Ide, T., Kang, D., Suomalainen, A., Karhunen, P.J., Griffith, J.D., Holt, I.J., et al. (2009). Human heart mitochondrial DNA is organized in complex catenated networks containing abundant four-way junctions and replication forks. The Journal of biological chemistry *284*, 21446-21457.

9. Pohjoismaki, J.L., and Goffart, S. (2011). Of circles, forks and humanity: Topological organisation and replication of mammalian mitochondrial DNA. BioEssays : news and reviews in molecular, cellular and developmental biology *33*, 290-299.

10. Gardner, J.M., and Jaspersen, S.L. (2014). Manipulating the yeast genome: deletion, mutation, and tagging by PCR. Methods in molecular biology (Clifton, N.J.) *1205*, 45-78.

11. Stein, A., Kalifa, L., and Sia, E.A. (2015). Members of the RAD52 Epistasis Group Contribute to Mitochondrial Homologous Recombination and Double-Strand Break Repair in Saccharomyces cerevisiae. PLoS genetics *11*, e1005664.

CURRICULUM VITAE

Name Kanchanjunga Prasai

Place of Birth and Nationality Kathmandu, Nepal, Nepali citizen

Academic Degrees

2017 Ph.D. in Molecular and Cellular Physiology, LSU Health Sciences Center-Shreveport, Louisiana, USA (GPA 4.0)

2007 M.Sc. in Biochemistry, Hemwati Nandan Bahuguna Garhwal University, India (First Class)

2005 B.Sc. in Biochemistry, University of Madras, India (First Class)

Previous Academic Position

2008-11 Assistant Professor, Department of Biochemistry, Institute of Medicine, Tribhuvan University Teaching Hospital (TUTH), Kathmandu, Nepal

Teaching Experience

2013-16 Lectures on endocrinology to the first year graduate class of Allied Health Professionals, LSUHSC-Shreveport, LA, USA

2008-11 Lectures on biochemistry to the undergraduate class of Medical, Nursing, and Allied Health Professionals, TUTH, Nepal

Oral Presentations/Talks

2015 Exploring mitochondrial DNA double-strand break repair disruption as a novel approach to inhibit eukaryotic cell proliferation. Feist-Weiller Cancer Center (FWCC) Spring Seminar Series, LSUHSC-Shreveport

2014 Exploring mitochondrial DNA double-strand break repair disruption as a novel approach to inhibit eukaryotic cell proliferation: A study in *Saccharomyces cerevisiae*. 13th International Workshop on Radiation Damage to DNA, Massachusetts Institute of Technology, Cambridge, Massachusetts

2014 Exploring mitochondrial DNA double-strand break repair disruption as a novel approach to inhibit eukaryotic cell proliferation: A study in *Saccharomyces cerevisiae*. Graduate Research Day, LSUHSC-Shreveport

2013 Mitochondrial DNA metabolism and eukaryotic cell survival: An unwinding story. Fall Seminar Series, Department of Molecular and Cellular Physiology, LSUHSC-Shreveport

Poster Presentations/Abstracts

2016	Mitochondrial homologous recombinase (Mhr1) is a potential mitochondrial DNA double-strand break repair factor. Graduate Research Day, LSUHSC-Shreveport
2016	Mitochondrial homologous recombinase (Mhr1) is a potential mitochondrial DNA double-strand break repair factor. Keystone Symposia-Mitochondrial Dynamics, Steamboat Springs, Colorado
2015	Mitochondrial-targeted bacterial Ku inhibits mitochondrial DNA replication in *Saccharomyces cerevisiae* but not in human cells. Ray A. Barlow Scientific Symposium, FWCC, LSUHSC-Shreveport
2015	Mitochondrial-targeted bacterial Ku inhibits mitochondrial DNA replication in *Saccharomyces cerevisiae* but not in human cells. Graduate Research Day, LSUHSC-Shreveport
2015	Mitochondrial-targeted bacterial Ku inhibits mitochondrial DNA replication in *Saccharomyces cerevisiae* but not in human cells. Emerging Topics on Genome Instability, Oklahoma Medical Research Foundation, Oklahoma City, Oklahoma
2014	Exploring mitochondrial DNA double-strand break repair disruption as a novel approach to inhibit eukaryotic cell proliferation: A study in *Saccharomyces cerevisiae*. 13th International Workshop on Radiation Damage to DNA, Massachusetts Institute of Technology, Cambridge, Massachusetts
2014	Exploring mitochondrial DNA double-strand break repair disruption as a novel approach to inhibit eukaryotic cell proliferation: A study in *Saccharomyces cerevisiae*. Ray A. Barlow Scientific Symposium, FWCC, LSUHSC-Shreveport
2014	Exploring mitochondrial DNA double-strand break repair disruption as a novel approach to inhibit eukaryotic cell proliferation: A study in *Saccharomyces cerevisiae*. Graduate Research Day, LSUHSC-Shreveport
2013	Expression of bacterial Ku in the mitochondria to sensitize eukaryote cells to reactive oxygen species. 59th Annual International Meeting of the Radiation Research Society, New Orleans

Committee Member

2015	Allen A. Copping Excellence in Teaching Awards Selection Committee, LSUHSC-Shreveport

Awards and Honors

2013-16	Carroll Feist Predoctoral Fellowship, FWCC, LSUHSC-Shreveport
2015	Jason A. Cardelli Award for Excellence in Cancer Research, Ray A. Barlow Scientific Symposium, FWCC, LSUHSC-Shreveport
2015	Travel Award, Emerging Topics on Genome Instability, Oklahoma Medical Research Foundation, Oklahoma
2015	Honorary Mention, Poster Presentation (post-proposal graduate students), Graduate Research Day, LSUHSC-Shreveport
2014	Young Investigator Award, 13th International Workshop on Radiation Damage to DNA, Massachusetts Institute of Technology, Massachusetts
2014	First Place in Student Talks, Graduate Research Day, LSUHSC-Shreveport

Publications

Prasai K, Robinson LC, Scott R, Tatchell K, Harrison L. Evidence for double-strand break mediated mitochondrial DNA replication in *Saccharomyces cerevisiae*. *Nucleic Acids Research* 2017 (Accepted for publication).

Prasai K. Regulation of mitochondrial structure and function by protein import: A current review. *Pathophysiology* 2017, dx.doi.org/10.1016/j.pathophys.2017.03.001.

Abshire C, **Prasai K**, Soto I, Shi R, Concha M, Baddoo M, Flemington E, Ennis D, Scott R, Harrison L. Exposure of *Mycobacterium marinum* to low shear modeled microgravity: Effect on growth, the transcriptome and survival under stress. *npj Microgravity* 2016; 2: 16038.

Carter PR, Watts MN, Kosloski-Davidson M, **Prasai K**, Grisham MB, Harris NR. Iron status, anemia, and plasma erythropoietin levels in acute and chronic mouse models of colitis. *Inflammatory Bowel Diseases* 2013; 19: 1260-5.

Prasai K. Excessive fatness can show the way to darkness. *Annual Report* 2009-2010, B.P. Koirala Lions Centre For Ophthalmic Studies (TUTH, Nepal): 18-19.

Prasai K. Obesity: A big, fat global threat. *SCI-MET* (TUTH, Nepal) 2010; 10: 3-5.

Manuscript Under Revision

Prasai K, Robinson LC, Tatchell K, Harrison L. *In vivo* Evidence for Mhr1, but not Yku80, as a general mitochondrial DNA double-strand break repair factor in *Saccharomyces cerevisiae*.